Structural network degeneration in the frontotemporal lobar degenerations

Dr. Colin J. Mahoney BMedSci MRCPI

A thesis submitted to

University College London for the degree of

Doctor of Philosophy

2015

Signed declaration

I, Colin John Mahoney confirm that the work presented in this thesis is my own. Where information has been derived from other sources or derived in collaboration with other researchers this is indicated in the thesis. All participants gave informed consent and the subsequent research was carried out with approval of the University College London/University College London Hospitals NHS Foundation Trust joint research ethics committee and in accordance with the Declaration of Helsinki.

Dr Colin J. Mahoney

1st November 2015, London.

Abstract

Frontotemporal lobar degenerations (FTLD) represent a group of neurodegenerative conditions characterised by their often overlapping but yet diverse clinical, radiological and pathological features. Clinically they may manifest as either a behavioural syndrome, termed behavioural variant frontotemporal dementia (bvFTD) or as a language led dementia, termed primary progressive aphasia (PPA).

The same protein can cause multiple disease phenotypes, whilst the same clinical phenotype may result from any of several different proteinopathies. Our understanding of this apparent divergence (or indeed convergence) remains poor. The concept of network-led neurodegeneration may offer an explanation. This suggests that specific brain networks are vulnerable to certain proteins and an attack on certain brain networks may result in a certain disease phenotype, and may also facilitate disease propagation, through network connections.

The advent of diffusion tensor imaging (DTI) now allows us to explore the microstructure of white matter and as it is white matter that binds functional networks together, understanding the changes in white matter across the spectrum of FTLD may provide insights into its disease biology. Specifically DTI may allow us to establish the profiles of structural network degeneration in FTLD and enable us to relate these changes to known functional networks, which govern key aspects of cognition affected in FTLD.

This thesis will investigate white matter microstructural changes across the spectrum of FTLD and will examine both cross-sectional and longitudinal white matter changes. The initial chapters will set out to establish these changes in both clinically and molecularly defined individuals affected with bvFTD and the subsequent chapters will study those with PPA.

The primary aim of this thesis is to establish the profiles of white matter pathology across the spectrum of FTLD using advanced imaging methods. Secondary aims include establishing the role of DTI as a potential imaging biomarker for future clinical trials in FTLD, and exploring differences in sensitivity and specificity of each DTI metric, establishing optimal metrics for studying white matter tract pathology in FTLD.

Table of contents

List of tables and figures

Tables

4. Longitudinal profiles of white matter disease in behavioural variant frontotemporal dementia

4.1. Study participant's clinical and imaging characteristics. *Linear regression comparing controls with all bvFTD subjects (n=23), § Fisher's exact test, ^ Wilcoxon rank-sum test.

4.2 Study participant's neuropsychological performance at baseline and follow up. Scores shown are raw scores for each test with maximum scores shown in parentheses. * and ** denotes p-values of <0.05 and <0.001 respectively comparing behavioural scores (raw score at baseline and change from baseline over time) of all bvFTD (n=23) participants with control participants after adjustment for age, gender and disease duration. ^ Total scores on the TASIT are scaled scores.

4.3 bvFTD subgroup neuropsychological performances at baseline and follow up. * and ** denotes p-values of <0.05 and <0.001 respectively comparing behavioural scores (raw score at baseline and change from baseline over time) of all bvFTD (n=23) participants with control participants after adjustment for age, gender and disease duration. ^ Total scores on the TASIT are scaled scores.

4.4 Baseline FA for individual white matter regions of interest for control participants and patients. *Linear regression comparing bvFTD (n=19) with controls after adjusting for age, gender and disease duration. Data is uncorrected for multiple comparisons.

4.5 Baseline MD for individual white matter regions of interest for control participants and patients. *Linear regression comparing bvFTD (n=19) with controls after adjusting for age, gender and disease duration. Data is uncorrected for multiple comparisons.

4.6 Baseline RD for individual white matter regions of interest for control participants and patients. *Linear regression comparing bvFTD (n=19) with controls after adjusting for age, gender and disease duration. Data is uncorrected for multiple comparisons.

4.7 Baseline AX for individual white matter regions of interest for control participants and patients. *Linear regression comparing bvFTD (n=19) with controls after adjusting for age, gender and disease duration. Data is uncorrected for multiple comparisons.

4.8 Estimated percentages per year difference in the rate of change of FA for bvFTD patients and bvFTD subgroups, by region, compared with controls. Data is uncorrected for multiple comparisons.

4.9 Estimated percentages per year difference in the rate of change of MD for bvFTD patients and bvFTD subgroups, by region, compared with controls. Data is uncorrected for multiple comparisons.

4.10 Estimated percentages per year difference in the rate of change of RD for bvFTD patients and bvFTD subgroups, by region, compared with controls. Data is uncorrected for multiple comparisons.

4.11 Estimated percentage per year difference in the rate of change of AX for bvFTD patients and bvFTD subgroups, by region, compared with controls. Data is uncorrected for multiple comparisons.

4.12. Sample Size Estimates per treatment arm of a putative clinical trial comparing 3 different outcome measures to detect a 20 to 50% reduction in rates of change. $\beta = 80\%$, $\alpha = 0.05$.

5. Cross-sectional signatures of white matter disease in the primary progressive aphasias

5.1 Comparison of FA changes in DTI studies of PPA. Results reported reflect most statistically robust findings (for present study, only significance values p<0.01 are included here; see also Table 5.2 to 5.5). *=only left hemispheric tracts reported. ^=Results reported based on authors figures. nt = data not reported/tested, - indicates no significant result found. 1=Arcuate and fronto-parietal SLF, 2=Genu, 3=Posterior ILF, 4=Anterior SLF, 5= Bilateral anterior ILF and left medial ILF, 6=SLF temporo-parietal fibres, 7=Arcuate and SLF temporo-parietal, 8=Inferior fronto-occipital fasciculus.

5.2 Summary of demographics, neuropsychological and CSF data for PPA groups, AD patients and healthy controls. Statistical significance of between group comparisons is displayed in the legend at the bottom of the table.

5.3. Profiles of changes in FA in each PPA groups compared with healthy controls. Results are FWE corrected p <0.05. Results are ordered by % of tract involvement.

5.4. Profiles of changes in AX in each PPA groups compared with healthy controls. Results are FWE corrected p <0.05. Results are ordered by % of tract involvement.

5.5. Profiles of changes in RD in each PPA group compared with healthy controls. Results are FWE corrected p <0.05. Results are ordered by % of tract involvement.

5.6. Profiles of changes in TR in each PPA group compared with healthy controls. Results are FWE corrected p <0.05. Results are ordered by % of tract involvement.

5.7. Profiles of DTI metric change in PPA groups compared with AD patients. Results are FWE corrected p <0.05. Results are ordered by % of tract involvement.

5.8 White matter tract comparisons between PPA groups. All results are FWE corrected p <0.05 and ordered by p-value. %, percentage of altered voxels within each tract.

6. Longitudinal profiles of white matter pathology in the primary progressive aphasias

6.1. Study participants' clinical and imaging characteristics. Linear regression comparing controls with each PPA sub-group, § Fisher's exact test. * BBSI is only available for 8 patients with nvPPA due to significant motion artefact in either baseline or follow-up scan.

6.2. Neuropsychological performance at baseline and longitudinally displayed as estimated mean difference from controls with change expressed as a percentage per year. *Indicates baseline values signifantly (p<0.05) different from controls. Bold values indicate significant (p<0.05) change over time.

6.4 Baseline FA values and estimated mean differences within white matter regions of interest comparing control participants and PPA syndromic groups. * p-value following linear regression comparing PPA syndromic group with controls adjusting for age, gender and disease duration. Data is uncorrected for multiple comparisons.

6.5 Baseline MD values and estimated mean differences within white matter regions of interest comparing control participants and PPA syndromic groups. * p-value following linear regression comparing PPA syndromic groups with controls adjusting for age, gender and disease duration. Data is uncorrected for multiple comparisons.

6.6 Baseline RD values and estimated mean differences within white matter regions of interest comparing control participants and PPA syndromic groups. * p-value following linear regression comparing PPA syndromic groups with controls adjusting for age, gender and disease duration. Data is uncorrected for multiple comparisons.

6.7 Baseline AX values and estimated mean differences within white matter regions of interest comparing control participants and PPA syndromic groups. * p-value following linear regression comparing PPA syndromic group with controls adjusting for age, gender and disease duration. Data is uncorrected for multiple comparisons.

6.8 Estimated percentage per year difference in the rate of change for each DTI metric for non-fluent/agrammatic PPA patients (nvPPA), by region, compared with controls. Data is uncorrected for multiple comparisons.

6.9 Estimated percentage per year difference in the rate of change for each DTI metric for semantic PPA patients (svPPA), by region, compared with controls. Data is uncorrected for multiple comparisons.

6.10 Estimated percentage per year difference in the rate of change for each DTI metric for logopenic PPA patients (lvPPA), by region, compared with controls. Data is uncorrected for multiple comparisons.

6.11 Sample size estimates per treatment arm of a clinical trial comparing 2 DTI metrics (FA and RD) and whole brain atrophy (BBSI) to detect a 20%, 30% and 40% reduction in rates of change. $\beta = 80\%$, $\alpha = 0.05$.

7. Conclusions

7.1 Overview of WM tract involvement in bvFTD cross-sectionally and longitudinally based on FA data. Cross-sectional data: ++++ >50% tract involved, +++ 25-50%, ++ 10-25%, + 5-10%, blank minimal/no involvement. Longitudinal data: +++ >10%/year change, ++ 5-10%/year change +, 2.5-5%/year change, blank <2.5%/year change.

7.2 Overview of WM tract involvement in PPA cross-sectionally and longitudinally based on FA data. Cross-sectional data: ++++ >50% tract involved, +++ 25-50%, ++ 10-25%, + 5-10%, blank minimal/no involvement. Longitudinal data: +++ >10%/year change, ++ 5-10%/year change +, 2.5-5%/year change, blank <2.5%/year change. Key: ns, not studied longitudinally.

7.3 Overview of individual DTI metrics performance reflecting potential as a disease biomarker. Table constructed using data obtained from ROC curve analysis to determine sensitivity and specificty. Increasing number of + signs denotes increasing performance as a biomarker and is based on quantative AUC values. Key: +++ AUC>0.9, ++ AUC=0.8-0.9, + AUC=0.7-0.8, - AUC<0.7.

Figures

1. Introduction

1.1 Genetic, histopathological and clinical spectrum of FTLD demonstrating their complex interrelationships. Long multi-coloured rectangles represent the syndromic continuum of FTLD. Position along this scale relates to their likely correlation with a specific pathological protein (indicated by single coloured circles) and genetic mutation (indicated by red rectangles), i.e. syndromes directly below circles indicate a strong correlation, if halfway between circles indicates histopathogy may be either protein. Size of circles and rectanges is indicative of their relative prevalence in FTLD.

1.2 A), Schematic representation of an axon indicating axonal barriers (myelin), major and minor diffusion gradients. B), Diffusion ellipsoid characterised by its three eigenvalues (λ1, λ2 and λ3), representing the direction of diffusion in each direction. The ellipsoid is shown in relationship to the normal geometry within the scanner (x, y and z).

1.3 Representation of major brain networks/brain regions and the white matter connections that link them. Green circles represent the Salience network (ACC, anterior cingulate cortex; FrIns, Front-insular cortex); orange circles represent the default mode network (PCC, posterior cingulate cortex; Prec, precuneus); blue circles represents the fronto-parietal control network (DLPFC, dorsolateral prefrontal cortex; TPJ, temporo-parietal junction) and red circle represents the executive control network (DMPFC, dorso-medial prefrontal cortex). Lines represent white matter connections between functional networks/regions; solid lines represent major projection and commissural tracts, dashed lines represent shorter-range projection and association fibres.

1.4 Chronological progression of atrophy in a MAPT mutation carrier visualised using fluid registration. Baseline scan was acquired 7 years prior to symptom onset. Colour bar signifies % volume change per voxel from baseline scan. Blue/green=contraction, red/yellow=expansion.

2. Material and methods

2.1. Overview of DTI imaging methods used.

2.2. Overview of processing pipeline for longitudinal DTI analysis.

3. Cross-sectional profiles of white matter pathology in behavioural variant frontotemporal dementia

3.1 Comparison of customised 'group-wise' TBSS image pipeline (left) with standard TBSS pipeline (right) performed on the same single participant. Images reflect single participant fractional anisotropy volume registered to the group-wise template on left and FMRIB58 template on right. The participant's white matter skeleton is overlaid (red-yellow) on right of each panel. Spatial coordinates of the plane of each section are indicated on the left of the figure.

3.2 Unadjusted white matter tract data: Patterns of white matter alteration in the bvFTD group compared with healthy participants. Right (R) hemisphere is shown on the left. The colour scale indexes p-values after family-wise error correction for multiple comparisons over the whole brain.

3.3 Unadjusted white matter tract data: Patterns of white matter alteration in the bvFTD group compared with the AD group. Right hemisphere is shown on the left. The colour scale indexes p-values after family-wise error correction for multiple comparisons over the whole brain.

3.4 Adjusted white matter tract data: Patterns of white matter alteration in the bvFTD group compared with the healthy control group after correction for mean global diffusivity value. Results for particular DTI metrics (AX, FA, RD, TR) are shown separately. The colour scale indexes P values after family-wise error correction for multiple comparisons over the whole brain

3.5 Adjusted white matter tract data: Patterns of white matter alteration in the bvFTD group compared with the healthy control group after correction for mean global diffusivity value. Results for particular DTI metrics (AX, FA, RD, TR) are shown separately. The colour scale indexes P values after family-wise error correction for multiple comparisons over the whole brain.

3.6 Patterns of white matter alteration in the MAPT and C9ORF72 mutation groups compared with the healthy control group and the AD group, after correction for mean global diffusivity value. The colour scale indexes P values after family-wise error correction for multiple comparisons over the whole brain.

3.7 ROC curves for classification of individuals to the bvFTD group and healthy control group (left) or AD group (right), based on each participant's global mean diffusivity data (above) and each participant's unadjusted mean diffusivity data within a tract region of interest (below). ROC curves for particular DTI metrics (AX, FA, RD, TR) and white matter tracts of interest (CB, CC, UF) are shown separately; area-under-curve is displayed for each curve (area-under-curve = 1 corresponds to ideal separation of groups).

3.8 Maps of grey matter (GM) atrophy (light blue) and regions of intersection of all four white matter DTI metrics (adjusted for mean global diffusivity value) in the bvFTD group compared with the healthy control group. Maps are overlaid on representative coronal sections of the MNI152 template brain; the right hemisphere (R) is shown on the left. The diffusivity tensor (DT) metric data intersection colour scale indexes the extent of overlap between metrics, i.e. dark blue indicates change in only one metric whereas red indicates change in all four metrics; the GM colour scale indexes P values after family-wise error correction for multiple comparisons over the whole brain.

4. Longitudinal profiles of white matter pathology in behavioural variant frontotemporal dementia

4.1 Individual trajectories of change in FA over time within right and left paracallosal cingulum bundles. The red dashed line indicates mean trajectory.

4.2 Individual trajectories of change in FA over time within right and left uncinate fasciculus. The red dashed line indicates mean trajectory.

4.3 Individual trajectories of change in FA over time within the body of the corpus callosum. The red dashed line indicates mean trajectory.

5. Cross-sectional profiles of white matter pathology in the primary progressive aphasias.

5.1. Patterns of decreased FA in PPA groups compared with controls. Results are overlaid on representative sections derived from the FA skeleton. For coronal and axial sections, the right hemisphere is shown on the left. The colour scale indexes P values after family-wise error correction for multiple comparisons over the whole brain.

5.2. Patterns of increased AX and RD in PPA groups compared with controls. For each panel, the AX map (green) is displayed on the top and the RD map (blue) on the bottom. Results are overlaid on representative sections derived from the average FA skeleton. For coronal and axial sections, the right hemisphere is shown on the left. The colour scale indexes P values after family-wise error correction for multiple comparisons over the whole brain.

5.3. Patterns of increased TR in PPA groups compared with controls. Results are overlaid on representative sections derived from the FA skeleton. For coronal and axial sections, the right hemisphere is shown on the left. The colour scale indexes P values after family-wise error correction for multiple comparisons over the whole brain.

5.4. Top panel shows areas of altered white matter in svPPA compared with AD patients; indicating profiles of increased AX (top), RD (middle) and TR (bottom). Results are overlaid on representative sections (MNI co-ordinates shown on left) derived from the average FA skeleton. For coronal and axial sections, the right hemisphere is shown on the left. The colour bar (bottom) codes significance (FWE corrected p-value).

5.5. Patterns of altered diffusivity (decreased FA and increased AX/RD/TR) in AD compared with healthy controls. Results are overlaid on representative sections derived from the average FA skeleton. For coronal and axial sections, the right hemisphere is shown on the left. The colour bar (bottom) codes significance (FWE corrected p-value).

5.6. Comparison of WM tract degeneration between PPA syndromic groups. Each tile shows significant WM tract (FWE corrected $p < 0.05$) differences between groups as measured by increased AX (green) and RD (blue). The colour bar (bottom) codes significance (FWE corrected p-value).

5.7. Maps of grey matter (GM) atrophy (blue-green) and reduced white matter fractional anisotropy (FA) (orange-yellow) in PPA syndromic groups compared to healthy controls overlaid on a MNI152 template brain. GM and FA maps are thresholded at $p < 0.05$ after family-wise error correction with threshold-free cluster enhancement. MNI co-ordinates are displayed. R=right. Colour bars (bottom) code FWE corrected p-values (blue-green) for GM atrophy and FA change (red-yellow).

6. Longitudinal profiles of white matter pathology in the primary progressive aphasias.

6.1 Individual trajectories of change in FA (y-axis) over time (x-axis in years) within body of the corpus callosum in each PPA syndrome. The red dashed line indicates mean trajectory.

6.2 Individual trajectories of change in FA (y-axis) over time (x-axis in years) within the ILF in each PPA syndrome. The red dashed line indicates mean trajectory.

6.3 Individual trajectories of change in FA (y-axis) over time (x-axis in years) within the SLF in each PPA syndrome. The red dashed line indicates mean trajectory.

6.4 Individual trajectories of change in FA (y-axis) over time (x-axis in years) within the uncinate fasciculus in each PPA syndrome. The red dashed line indicates mean trajectory.

7. Conclusions.

7.1. Overview of pathology across distributed brain networks in each syndromic group based on findings from the current study. Black lines with diamond caps indicate tracts with prominent white matter pathology (based on FA). Grey circles indicate regions with grey matter atrophy. Compare these patterns of structural and functional network change with patterns of normal connectivity in figure 1.3.

Glossary of abbreviations

AD	Alzheimer's disease
AF	Arcuate Fasciculus
ANCOVA	Analysis of covariance
AUC	Area under the curve
ATR	Anterior thalamic radiation
AX	Axial diffusivity
B	Bilateral
BPVS	British picture vocabulary test
BSI	Boundary shift integral
bvFTD	Behavioural variant frontotemporal dementia
C9ORF72	Chromosome 9 open reading frame 72
CB	Cingulum bundle
CBD	Corticobasal degeneration
CBS	Corticobasal syndrome
CC	Corpus callosum
CSF	Cerebrospinal fluid
CST	Corticospinal tract
DARTEL	Diffeomorphic anatomical registration through lie algebra
DKEFS	Delis-Kaplan executive function system
DIR	Direcetions (i.e. number of diffusion gradients)
DTI	Diffusion tensor imaging
DTI-TK	Diffusion tensor imaging toolkit
FA	Fractional anisotropy
FLIRT	FMRIB Linear image registration tool
FM	Forceps Major
FMRIB	Functional MRI brain software library
FSL	FMRIB software library
FTD	Frontotemporal dementia (cf. bvFTD)

FTLD	Frontotemporal lobar degeneration
GDA	Graded difficulty arithmetic test
GM	Grey matter
GNT	Graded naming test
GRN	Progranulin
GW	Group-wise
IFOF	Inferior fronto-occipital fasciculus
ILF	Inferior longitudinal fasciculus
L	Left
lvPPA	Logopenic variant primary progressive aphasia
MANCOVA	Multivariate analysis of varience
MAPT	Microtubule associated protein tau
MD	Mean diffusivity
MMSE	Mini-mental state examination
MNI	Montreal neuroimaging institute (brain template)
MRI	Magnetic resonance imaging
nvPPA	Non-Fluent/17Agrammatic variant primary progressive aphasia
PIQ	Performance intelligence quotient
PPA	Primary progressive aphasia
PRIDE	Philips Research Integrated Device Environment
PSP	Progressive supranuclear palsy
R	Right
RD	Radial diffusivity
RMT	Recognition memory test
ROC	Receiver operating characteristic
ROI	Region of interest
SCP	Superior cerebellar peduncle
SLF	Superior longitudinal fasciculus
SPM	Statistical parametric mapping
svPPA	Semantic variant Primary Progressive Aphasia

TASIT	The awareness of social inference test
TBSS	Tract based spatial statistics
TDP-43	Transactive response DNA-binding protein 43
TFCE	Threshold free cluster enhancement
TIV	Total intracranial volume
TR	Trace diffusivity
UF	Uncinate fasciculus
VBM	Voxel-based morphometry
VCP	Valosin containing protein
VIQ	Verbal intelligence quotient
VOSP	Visual object space perception
WASI	Wechsler abbreviated scale of intelligence

1. Introduction

1.1 Background

The fontotemporal lobar degenerations (FTLD) are a diverse group of neurodegenerative disorders which have an insidious clinical course with variability in their clinical, molecular and neuroimaging phenotypes. FTLD, whilst relatively uncommon, results in a devastating clinical syndrome causing a progressive dementia, affecting particularly those under the age of sixty-five (Ratnavalli et al., 2002), and is increasingly recognized as a cause of dementia in older age groups. Over the last two decades a substantial body of clinical, genetic, imaging and pathological data has been amassed, improving our understanding of these disorders. Despite this limited data exisits on the role of white matter pathology in FTLD. Understanding the profiles of white matter pathology is important in further unravelling the complex neurobiology of these disorders and may help link clinical phenotypes with molecular alterations in the brains of patients with FTLD. The principle aim of this Thesis is to provide a detailed characterization of white matter tract pathology across the spectrum of FTLD using both cross-sectional and longitudinal diffusion tensor imaging (DTI). This introductory chapter will provide an overview of the clinical syndromes of FTLD and outline previous major neuroimaging studies. It will also discuss how DTI can be used to examine WM in vivo and thus provide an understanding of changes to structural brain connectivity in neurodegenerative disorders. A methodology chapter will outline the inclusion criteria for the subsequent experiments along with detailed methods on imaging data acquisition and analysis. Chapters 3 and 5 will examine cross-sectional white matter pathology, first in the behavioural variant of frontotemporal dementia (bvFTD) and then in the primary

progressive aphasias (PPA). Chapter 4 and 6 will examine longitudinal white matter pathology in bvFTD and PPA.

1.2 Historical overview of FTLD

Some of the earliest descriptions of focal neuropathology and behavioural and language disturbance were repoted by Arnold Pick in 1892 and 1904 respectively (Pick, 1904, 1892). This was the first attempt to distinguish relatively focal patterns of brain atrophy from the more generalised brain atrophy of senile dementia. Whilst these reports of focal neurodegeneration are over 100 years old we still do not understand the mechanisms that lead to such focal patterns of brain degeneration. Over the subsequent decades the pathology of these conditions was differentiated from Alzheimer's disease (AD), with the characteristic spongiosis and Pick bodies being identified in 1922 (Gans, 1922), which in fact turned out to be just one pathological subtype of this diverse group of diseases. In the following decades psychologists and behavioural neurologists continued to refine the clinical phenotype of these disorders. In 1975 a dementia with a core feature of semantic impairment was defined in 4 patients, which would later become known as semantic dementia (Snowden et al., 1994; Warrington, 1975). In 1982 Mesulam followed several patients with characteristic patterns of effortful speech and associated left peri-sylvian atrophy, coining the term primary progressive aphasia (Mesulam, 1982). Further clinical characterisation of bvFTD led to the first consensus criteria (Neary et al., 1998), which aimed to improve diagnosis and allowing a more standardised approach to performing research in this area. Also around this time the familial aspect of FTLD came under close scrutiny with several families identified as having dementia with

parkinsonism, with affected family members having linkage on chromosome 17 (Lynch et al., 1994). These individuals would latter be identified as having a mutation in the *microtubule associated protein tau (MAPT)* (Hutton et al., 1998). It was also becoming clear that many patients, who had the same clinical features, had different underlying pathologies. This in stark contrast to the vast majority of patients who presented with episodic memory problems, who at autopsy had the hallmarks of AD, namely beta-amyloid plaques and tau tangles (Braak and Braak, 1996). Whilst Pick's bodies and tau deposition was seen in many patients with clinical syndromes of bvFTD and PPA a large proportion had an alternate, more non-specific proteinopathy, termed ubiquitin. This included patients with apparently sporadic and familial disease, as well as patients with different phenotypes of either a behavioural led (bvFTD) or language lead (PPA) dementia.

With the increasing availability of magnetic resonance imaging (MRI) in the 1990's the neuroimaging phenotype of FTLD associated syndromes began to emerge, with specific profiles of brain atrophy emerging at both clinical and pathological levels, which will be discussed in the subsequent section. In 2006 ubiquitin was identified as the protein Transactive Repeat DNA binding protein 43 *(TDP-43)* (Neumann et al., 2006). It was also found to be the pathological hallmark of the second major genetic cause of FTLD, *Progranulin (GRN),* identified around the same time and found to occupy a locus also on chromosome 17 (Baker et al., 2006). Over the last decade work on the heritability of FTLD suggested that up to 40% of patients with bvFTD might have inherited the condition in an autosomal dominant fashion (Rohrer et al., 2009), in addition this data suggested that

other genes causing FTLD were to still to be identified (Vance et al., 2006). Most recently the third major genetic cause of FTLD has been identified, which is a hexanucleotide repeat expansion located on chromosome 9 open reading frame 72, the *C9ORF72* mutation (Dejesus-Hernandez et al., 2011; Renton et al., 2011). This genetic discovery has also provided molecular validity for the overlap commonly seen between motor neurone disease and frontotemporal dementia (FTD). The degree to which FTLD might be inherited is significant, as presymptomatic mutation carriers provide a population in which to characterise the diseases natural history. This may allow the identification of preclinical disease states through the identification of clinical, chemical or radiological biomarkers, with potential therapeutic implications for both presymptomatic and affected individuals. More recently the clinico-pathological criteria for FTLD have been updated to reflect these refinements in clinical, imaging and pathology (Cairns et al., 2007; Gorno-Tempini et al., 2011; Mackenzie et al., 2010; Rascovsky et al., 2011). With this emerging genetic and molecular knowledge future goals are likely to be focused on how genetic and other molecular alterations result in neurodegeneration, and how initial focal patterns of disease, both clinically and radiologically, evolve over time.

1.3 Biomarkers in neurodegeneration

Throughout subsequent chapters the term biomarker will be used, it is therefore important to provide some background and guidance as to what constitutes an appropriate biomarker. The term biomarker, or biological marker, has become commonplace in medical literature and it broadly relates to a means with which one can detect and monitor a response to a treatment or detect a particular disease state. Prior to a

discussion on the role of potential novel biomarkers in FTLD it is important to provide further details on what constitutes a biomarker, and indeed what makes for a useful biomarker. Early definitions of a biomarker tended to focus on areas of drug safety and drug discovery. Over time the concept of what constitutes a biomarker has broadened. In 1993 The World Health Organisation provided a definition of a biomarker as “any substance, structure, or process that can be measured in the body or its products and influence or predict the incidence of outcome or disease” and more broadly “almost any measurement reflecting an interaction between a biological system and a potential hazard” (WHO, 1993). More recently in 2001, a framework for the development of biomarkers was proposed (“Biomarkers and surrogate endpoints,” 2001). This framework provided a further expansion of the concept of biomarkers and defined a biomarker as “a characteristic that is objectively measured and evaluated as an indicator of normal biological processes, pathogenic processes, or pharmacologic responses to a therapeutic intervention.” In addition the role of biomarkers as a diagnostic tools, as a means to stage and provide prognostic information on a disease state, and as means of assessing disease response to a particular intervention has also been emphasised. From a pragmatic standpoint a biomarker should be clinically relevant, reflecting how a patient feels or functions, it should be reproducible and it should be reasonably and safely accessible. With regards to neurodegenerative diseases biomarkers should reflect the clinical changes reported by patients and/or careers. Biomarkers should be able to reflect clinical endpoints, which characterised in the most finite terms would be reflect either a patient being either cured or dying from a particular disease. In many diseases, particular in the area of neurodegeneration, these clinical end-points may be deemed unreasonable. The natural

history of most neurodegenerative diseases is one of insidious progression over the course of many years, making some clinical endpoints unreasonable to access. Whilst curative or restorative treatments for neurodegenerative disorders are the ultimate aspiration, it is not unreasonable to develop interventions that may exert a disease modifying affect. Therefore in lieu of the above clinical end-points, a surrogate endpoint, which is reflected by change in a particular biomarker, may be considered. Surrogate endpoints may be defined as being a biomarker, which substitutes for a clinical endpoint, but which is expected to predict a clinical response, based on robust scientific data. Over time it is import to validate the sensitivity and specificity of a particular biomarker in predicting a clinical endpoint. More recently the use of biomarkers has been proposed to enrich clinical populations to provide more optimum outcome measures, particular when dealing with smaller sample size or diseases with multiple sub-types.

Across neurodegenerative conditions a range of biomarkers are either in use clinically or have been proposed on a research basis (Ahmed et al., 2014; Hampel et al., 2010). Neuroimaging biomarkers are perhaps the most well established surrogate endpoints for trials, with structural MRI accounting for the majority of studies reported (Noel-Storr et al., 2013). CSF biomarkers are also in common use with protein levels such as beta-amyloid, tau, phosphoralyted tau and 14-3-3 protein having good sensitivity and specificity for Alzheimer's disease and Prion disease respectively. As mentioned previously validation of individual biomarkers is important. Pathological confirmation of a predictive biomarker is key, with one meta-analysis of known biomarkers (neuroimaging and CSF) finding an average sensitivity of 85% and specificity of 78% across studies with pathological confirmation of AD (Sandrine et al., 2014). Future biomarkers will need to offer at least

similar levels of sensitivity and specific if not higher, in order to be adopted. Future biomarkers in neurodegeneration may include blood and urine measures, as well as additional CSF markers such as TDP-43 and neurofilament light in FTD and β-site APP-cleaving enzyme 1 in AD. New imaging techniques such as tau PET imaging and DTI, which is proposed as a potential biomarker in this thesis, may also hold promise.

A key issue in the development of biomarkers for frontotemporal dementias is the heterogeneity of the disease. Putative cognitive biomarkers, such as neuropsychological testing, have been shown to be unreliable with poor pathological specificity, which may be due to issues as diverse as anatomical overlap between pathologies resulting in common profiles of cognitive demise, the disease stage the patient was tested at, or the patient's ability to engage in a particular task. Of course this does not limit the potential role of a cognitive biomarker in the future, particular as with improved understanding of the brain networks that are preferentially targeted in FTLD, it is likely that novel cognitive paradigms could be applied to more robustly probe the functionality of these regions (Agustus et al., 2015; Henley et al., 2014).

Diagnosis of FTLD syndromes is aided by macroscopic patterns of brain atrophy and is incorporated in the most recent consensus criteria; as such neuroimaging would seem to be a good candidate as a disease biomarker. Previously proposed imaging biomarkers, such rates of whole brain and lobar atrophy are compelling, not least because of their ease of measurement and widespread availability. However a number of studies have shown poor sensitivity using routine MRI in the diagnosis of FTLD, which may be explained by patients with either slowly progressive forms of bvFTD or patients with more generalised patterns of brain atrophy (Suarez et al., 2009). Indeed the role of neuroimaging as a biomarker is often

based on patterns of brain atrophy seen at a group level across a particular clinical syndrome, however it is worth noting the hetereogenetity of syndromes (see figure 1.1). This may result in large inter-subject variablitiy within a particular group, for example patients with *C9ORF72* mutations have hugely variable patterns of brain atrophy (Mahoney et al., 2012a). In the development of biomarkers for FTLD it seems increasing likely that there will be a need to use sophisticated methodologies. Potential biomarkers will need to target brain changes that either cut across the clinicopathological spectrum or that adopt a multimodal approach, combining multiple pieces of data (clinical, biochemical and neuroimaging), to create a personalised biomarker reflecting disease changes, which map onto a clinically defined end-point thus enabling their use as surrogate end-points for trials.

1.4 Current clinical and imaging features of FTLD

The most recent clinical criteria for bvFTD and PPA were published in 2010 and 2011 respectively (Gorno-Tempini et al., 2011; Rascovsky et al., 2011). The current pathological criteria were published in 2007 and updated in 2010. These criteria form the basis for inclusion of participants within the current study. The hallmark of bvFTD is a progressive change in social cognition and personality, underpinned by any one of the multiple pathologies seen across the FTLD spectrum. The full clinical criteria for bvFTD are listed in Table 1. Clinically the distinction between what is normal behaviour, psychiatric behaviour and neurodegenerative related behavioural change is often difficult to make. The recent consensus criteria attempted to adopt a flexible approach in describing the clinical features of bvFTD, in the knowledge that some patients can display rather discrepant clinical features: for example some patients may suffer with severe apathy and inertia,

whilst others may have more florid disinhibition. In addition these criteria adopt a hierarchy of certainty in classifying individuals, with the main rationale for this being a way of including cases, which may have early disease, this being the group most likely to benefit from disease modifying treatments.

Patients with possible bvFTD are classified based on clinical features solely, resulting in 86% sensitivity. Patients with probable bvFTD are those with neuroimaging features, such as focal atrophy or hypometabolism, for which the current criteria claim a lower sensitivity of 76%, although these individuals will have a greater specificity (i.e. certainty of underlying FTLD pathology). Finally those with definite bvFTD are clinically affected with a known genetic mutation or have had pathologically confirmed disease.

I. Neurodegenerative disease
Shows progressive deterioration in behaviour/cognition by observation or history (must be present)
II. Possible bvFTD (>3 must be recurrently present)
A) Early behavioural disinhibition (≥ 1 must be present) 1) Socially inappropriate behaviour 2) Loss of decorum 3) Impulsive, rash or careless actions B) Early apathy or inertia (≥ 1 must be present) 1) Apathy 2) Inertia C) Early loss of sympathy or empathy (≥ 1 must be present) 1) Diminished response to others needs or feelings 2) Diminished social interest, interrelatedness or personal warmth D) Early perseverative, stereotyped, compulsive or ritualistic behaviour (≥ 1 must be present) 1) Simple repetitive movements 2) Complex, compulsive or ritualized behaviours 3) Stereotyped speech E) Hyperorality and dietary changes (≥ 1 must be present) 1) Altered food preferences 2) Binge eating, increased consumption of alcohol or cigarettes 3) Oral exploration, consumption of inedible objects F) Neuropsychological profile shows executive deficits with relative sparing of memory and visuospatial function (all must be present) 1) Deficits in executive tasks 2) Relative sparing of episodic memory 3) Relative sparing of visuospatial skills
III Probable bvFTD (A-C must all be present)
A) Meets criteria for possible bvFTD B) Exhibits significant functional decline C) Neuroimaging is consistent with bvFTD (≥ 1 must be present) 1) Frontal and/or anterior temporal atrophy on MRI or CT 2) Frontal and/or anterior temporal hypoperfusion on PET or SPECT
IV Definite bvFTD (A and B and/or C must be present
A) Meets criteria for possible or probable bvFTD B) Histopathological evidence of FTLD on biopsy or at post-mortem C) Presence of a known pathogenic mutation
V. Exclusionary criteria (A and B must be answered negatively all diagnosis if bvFTD, C can be positive for possible bvFTD only)
A) Pattern of deficits is better accounted for by another non-degenerative medical condition B) Behavioural disturbance is better accounted for by a psychiatric diagnosis C) Biomarkers strongly indicative of Alzheimer's or other neurodegenerative process

Table 1.1 Current consensus criteria for a diagnosis of bvFTD (Rascovsky et al., 2011)

The PPAs represent a clinically and pathologically heterogeneous group of language-led dementias, which, prior to the current consensus criteria, were not bound together through a single classification framework. The majority of these syndromes overlap with FTLD pathologically, however AD pathology is not uncommon, most notably within the

logopenic variant (lvPPA). The authors stress that PPA is a clinical entity and to distinguish it from other neurodegenerative syndromes they exclude patients with prominent early behavioural or amnestic features. Additionally they stress the use of appropriate bedside clinical tools to identify if patients have compatible clinical features of PPA: examination of spontaneous speech through a picture description task, assessing confrontational naming and comprehension with a word-picture matching task. As in the bvFTD criteria the authors recognize the need to identify patients with early signs of PPA, assuming that these individuals may benefit the most from disease modifying treatments. The current criteria recognise that some patients have clinical features *sui generis,* and as such could not be readily classified, leading to the category of PPA unclassifiable.

As with the bvFTD criteria, the authors also developed a category likely to have greater specificity for neurodegenerative histopathology, an image-supported diagnosis of PPA. However, unlike the bvFTD criteria, the authors did not state that the presence of biomarkers (e.g. CSF Beta Amyloid levels) consistent with AD or another non-FTLD pathology was reason to exclude individuals. As the primary aim of this Thesis is to analyse the variation of white matter pathology in the syndromic cohorts indivudals with AD pathology may also therefore be included.

<table>
<tr><td colspan="4">Primary Progressive Aphasia</td></tr>
<tr><td colspan="4">Inclusion criteria (a, b and c must be present)</td></tr>
<tr><td colspan="2">a) Language most prominent clinical feature</td><td colspan="2">b) Language deficits are the principle cause of impaired activities of daily living</td><td>c) Aphasia the most prominent feature at symptom onset</td></tr>
<tr><td colspan="4">Exclusion criteria (a-d must all be answered negatively)</td></tr>
<tr><td>a) Pattern of deficits better accounted for by another non-degenerative or medical disorder</td><td>b) Cognitive disturbance better accounted for by a psychiatric disturbance</td><td>c) Prominent initial episodic memory, visual memory and visuoperceptual impairments</td><td>d) Prominent initial behavioural disturbance</td></tr>
<tr><td colspan="4">If meets criteria for PPA than classify sub-type</td></tr>
<tr><td colspan="4">Clinical diagnosis (Possible)</td></tr>
<tr><td>Semantic Variant</td><td colspan="2">Non-Fluent Agrammatic Variant</td><td>Logopenic Variant</td></tr>
<tr><td>Both of
A. Impaired confrontation naming
B. Impaired single-word comprehension</td><td colspan="2">One or more of
A. Agrammatism in language production
B. Effortful, halting speech with speech sound errors (apraxia of speech)</td><td>Both of
A. Impaired single-word retrieval during speech
B. Impaired repetition of sentences and phrases</td></tr>
<tr><td>Three or more of
A. Impaired object knowledge
B. Surface dyslexia or dysgraphia
C. Spared repetition
D. Spared speech production</td><td colspan="2">Two or more of
A. Impaired comprehension of syntactically complex sentences
B. Spared single word comprehension
C. Spared object knowledge</td><td>Three or more of
A. Speech (phonological) errors during speech and naming
B. Spared single-word comprehension and object knowledge
C. Spared motor speech
D. No frank agrammatisim</td></tr>
<tr><td colspan="4">Imaging Supported Diagnosis (Probable)</td></tr>
<tr><td>Semantic Variant</td><td colspan="2">Non-Fluent Agrammatic Variant</td><td>Logopenic Variant</td></tr>
<tr><td>Both of
A. Clinical diagnosis of svPPA
B. Imaging shows (either)
a. Anterior temporal lobe atrophy
b. Anterior temporal hypometabolism on PET or SPECT</td><td colspan="2">Both of
A. Clinical diagnosis of nvPPA
B. Imaging shows (either)
a. Left posterior fronto-insular atrophy
b. Left posterior fronto-insular hypometabolism on PET or SPECT</td><td>Both of
A. Clinical diagnosis of lvPPA
B. Imaging shows (either)
a. Left posterior perisylvian-parietal atrophy
b. Left posterior perisylvian/parietal hypometabolism on PET or SPECT</td></tr>
<tr><td colspan="4">Pathological Diagnosis (All must meet clinical diagnosis and either A or B)</td></tr>
<tr><td>Semantic Variant</td><td colspan="2">Non-Fluent Agrammatic Variant</td><td>Logopenic Variant</td></tr>
<tr><td>A. Histopathological evidence of neurodegeneration (can include Alzheimer's)
B. Presence of a known pathogenic mutation</td><td colspan="2">A. Histopathological evidence of neurodegeneration (can include Alzheimer's)
B. Presence of a known pathogenic mutation</td><td>A. Histopathological evidence of neurodegeneration (can include Alzheimer's)
B. Presence of a known pathogenic mutation</td></tr>
</table>

Table 1.2 Current consensus criteria for a diagnosis of PPA (Gorno-Tempini et al., 2004)

1.5 The histopathology of FTLD

The current neuropathological classification of FTLD is defined in large part by two major proteins; tau (FTLD-tau), the normal function of which is to help stabilize microtubules, maintaining cell structure and aiding intracellular transport, and TDP-43 (FTLD-TDP-43), the major role of which is thought to be in RNA regulation and managing intracellular stresses (Lee et al., 2011). Approximately 10% of FTLD is made up of uncommon pathological subtypes, such as the protein fused in sarcoma (FTLD-FUS) characterized by neuronal cytoplasmic inclusions which stain for FUS and ubiquitin proteasome system (FTLD-UPS), which stain for ubiquitin or p62 but not for FUS, and are almost exclusively associated with a rare mutations in the *CHMP2B* gene (Cairns et al., 2007; Mackenzie et al., 2010). Within the group FTLD-tau further pathological subdivisions are recognised, based on the number of repeats of particular tau isoforms. In normal individuals the six isoforms of tau are equally balanced however in FTLD-tau particular isoforms dominate; 3 repeat tau results in the classical Pick bodies of Pick's disease; 4 repeat tau lesions within the cortical and striatal regions, along with astrocytic plaques and ballooned neurons are typical of corticobasal degeneration (CBD); 4 repeat tau neurofibrillary tangles mainly constrained to the basal ganglia are typical of progressive supranuclear palsy (PSP); and 4 repeat tau with spindle shaped lesions within limbic regions are typical of agyrophillic grain disease. A combination of widespread 3 and 4 repeat tau lesions are the hallmark of FTLD due to mutations in the *MAPT* gene. Within the FTLD-TDP-43 category four subtypes of TDP-43 (types A-D) are recognized based on the morphology and anatomical distribution of TDP-43 cortical inclusions (Mackenzie et al., 2011). Many studies have reported that patients have specific clinical and radiological features which can help

predict the underlying neuropathological syndrome (Grossman, 2010; Knibb et al., 2006; Pereira et al., 2009a; Rohrer et al., 2011). Semantic variant primary progressive aphasia (svPPA) has a strong association with TDP-43 type C pathology; patients with bvFTD and features of motor neuron disease most typically have TDP type B pathology and patients with *GRN* mutations typically have TDP-43 type A pathology. These associations are important, as it is likely that future treatments will target specific molecular pathologies and identifying clinical and radiological signals in individual patients will be necessary for study inclusion. However it is also true that many syndromes within the FTLD spectrum overlap in terms of clinical and histopathological features. Figure 1.1 provides an illustration of the incidence and overlap of clinical syndromes with neuropathology and gene mutations based on previously published data relating to clinicopathological correlations and pathological frequency (Grossman, 2010; Lashley et al., 2011; Rohrer et al., 2011; Rohrer et al., 2010; Snowden et al., 2011); for example this figure illustrates the fact that patients with bvFTD can have either tau, TDP-43 or AD pathology at post-mortem. Therefore current clinical metrics are not sufficient at readily discriminating histopathological subtypes and indeed there is a limitation in our understanding of why the same clinical syndrome can be underpinned by different pathologies.

A major theme of this study is to identify profiles of white matter pathology in FTLD. At present little is known about associations between white matter pathology and the clinical syndromes associated with FTLD. Despite the lack of neuroimaging data on this subject there is a substantial amount of histopathological data implicating white matter structures in FTLD, and this was a major impetus for the subsequent studies. With

regards to the tauopathies in those with CBD pathology a hallmark of the diagnosis is the presence of 4-repeat tau containing astrocytic plaques at post-mortem. These plaques area present in grey and white matter in similar proportions (Forman et al., 2002). Some studies have also suggested that white matter pathology in CBD may be more manifest in white matter as compared with grey matter, with the presence of significant quantities of 4-repeat tau fibrillary structures and coiled bodies throughout subcortical frontal white matter (Piao et al., 2005; Sakai et al., 2006). In PSP oligodendroglial inclusions are commonly reported within frontal, tegmental and cerebellar white matter tracts (Armstrong and Cairns, 2013). One report in PSP patients suggests that 70% of subjects have a greater burden of tau inclusions within frontal white matter compared with grey matter, as measured using a quantitative western blot technique (Zhukareva et al., 2006). More recently a set of tauopathies with prominent white matter pathology, termed globular glial tauopathies, have also been reported. These are characterised by the presence of globular oligodendroglial inclusions and encompass a wide clinical spectrum from PSP and CBS to bvFTD and even a motor-neuron phenotype (Ahmed et al., 2013).

The other major pathological protein in FTLD is TDP-43. The number of publications documenting the profiles of white matter pathology in this proteinopathy is fewer compared to tau, perhaps owing to its more recent identification, however there remains substantial evidence that this protein is implicated in white matter degeneration. Neumann and colleagues first noted this association in 2007, shortly after this protein was identified, identifying TDP-43 positive inclusions within oligodendrocytes in 38 consecutive patients, with similar levels of hyperphorylated TDP-43 detectable in white

matter as seen in grey matter (Neumann et al., 2007). Whole brain pathological studies have also identified widespread TDP-43 deposition in white matter, with glial pathology including "coiled body-like comma shaped" inclusions, astrocytic inclusions and axonal swellings. Sub-cortical deposition was extensive with only visual cortex, cerebellum and anterior and posterior spinal roots spared (Brandmeir et al., 2008). Further pathological studies by Hiji and colleagues in patients within the FTLD-MND spectrum identified numerous thread-like white matter inclusions, which were found to be TDP-43 positive. In fact these inclusions were comparatively different to inclusions seen in grey matter, which were ubiquitinated, whilst white matter inclusions were not (Hiji et al., 2008). The finding of such widespread TDP-43 pathology in FTLD is perhaps unsurprising given that it is so abundantly expressed in the normal brain. TDP-43 binds mRNA and DNA and has a key role in the regulation of mRNA levels with increasing evidence that it has an important role in stress responses (Liu-Yesucevitz et al., 2010).

A number of other clinical observations provide further evidence for the role of white matter pathology in FTLD. For example severe white matter hyper-intensities on MRI has been reported in patients with *GRN* mutations (Caroppo et al., 2014), increased expression of glial fibrillary acidic protein, which is thought to be important in maintaining normal astrocyte function, has been also reported in FTLD (Herskowitz et al., 2010), and in bvFTD patients polymorphisms in myelin-associated basic protein have been associated with more aggressive clinical courses (Irwin et al., 2014).

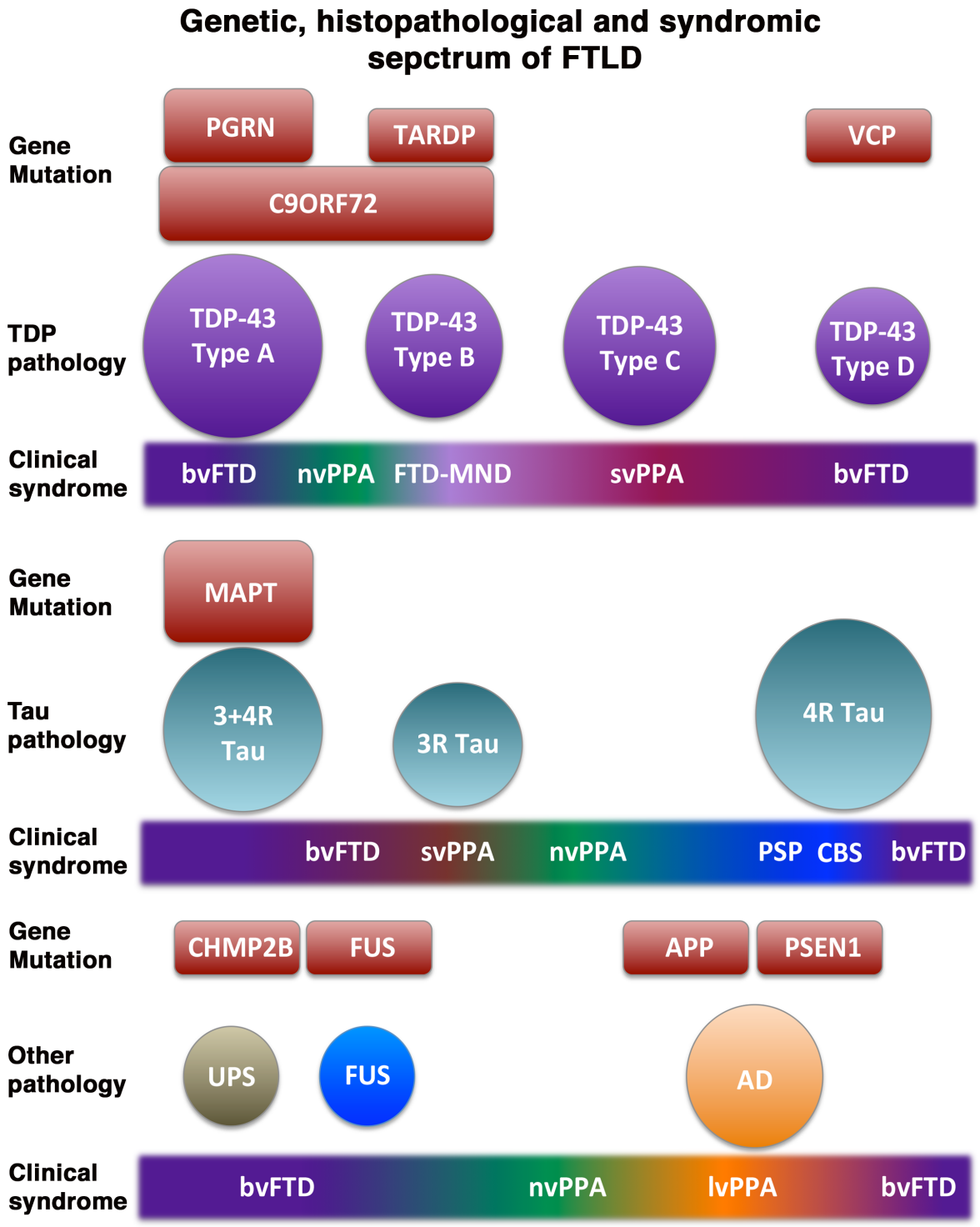

Figure 1.1 Genetic, histopathological and clinical spectrum of FTLD demonstrating their complex interrelationships. Long multi-coloured rectangles represent the syndromic continuum of FTLD. Position along this scale relates to their likely correlation with a specific pathological protein (indicated by single coloured circles) and genetic mutation (indicated by red rectangles), i.e. syndromes directly below circles indicate a strong correlation, if halfway between circles indicates histopathogy may be either protein. Size of circles and rectanges is indicative of their relative prevalence in FTLD.

1.6 Previous neuroimaging studies in FTLD

Since the 1990s MRI and metabolic imaging have been used to help better define the neuroanatomical features of FTLD as well as differentiating the patterns of brain atrophy and hypometabolism from AD. Indeed it is noteworthy that assessment of brain atrophy remains an important tool both diagnostically in the clinic, with incorporation into clinical criteria, and also within clinical trials, with rates of brain atrophy commonly used as an outcome measure owing to its wide availability and relative ease of use. The earliest neuroimaging studies involved calculation of changes in whole brain and regional volumes by drawing around brain structures. More recently, techniques including voxel-based morphometry (VBM) have emerged allowing the study of alterations in grey matter (GM) in larger patient groups by using automated brain segmentation and registration techniques. Two recent meta-analysis utilizing data from structural and metabolic imaging suggest that frontomedian and anterior cingulate brain atrophy is a consistent finding in bvFTD (Schroeter et al., 2008, 2007). These regions have long been thought to be important in tasks relating to social cognition such as theory of mind and self-monitoring (Carrington and Bailey, 2009). In addition subcortical atrophy within the thalamus was a finding of these studies, which is perhaps unsurprising given the extent of connections between thalamus and frontal lobes (Barbas, 2000). Despite these relatively specific anatomical findings it is clear from other individual studies that the patterns of atrophy in bvFTD are quite variable and may even include involvement of structures, outside regions of atrophy considered 'typical' for bvFTD, such as parietal and occipital lobes and cerebellum (Grossman et al., 2007; Hartikainen et al., 2012; Mahoney et al., 2012a). Other recent studies have attempted to characterise profiles of atrophy

along clinical grounds. One such study examined cases of bvFTD with prominent right temporal lobe and suggested that these individuals had specific clinical features including prosopagnosia, memory impairment and visual and somatic hallucinosis (Chan et al., 2009). Another study identified multiple subtypes of bvFTD on imaging grounds using a cluster analysis of MRI data from sixty-six subjects (Whitwell et al., 2009). These data suggest a frontal dominant subtype with predominant executive and behavioural dysfunction; a frontotemporal subtype with additional memory and language dysfunction; a temporo-fronto-parietal subtype with more global cognitive dysfunction and a temporal dominant subtype with mainly memory and language deficits. More recent imaging techniques including postitron emission tomography (PET) and resting state functional MRI (fMRI) have continued to support the notion of greatest disease burden being located in frontotemporal brain regions in bvFTD. In addition these techniques allow us to better understand dynamic brain changes, *in vivo,* through the use of activation paradigms and resting state fMRI. A significant finding has been the identification of dysfunction within a so-called 'Salience Network', comprising ventral frontal, insular and anterior cingulate cortex, areas important in external event monitoring and other aspects of social cognition (Seeley et al., 2009; Zhou et al., 2010). It has been suggested that this finding may be useful biomarker in distinguishing bvFTD from AD, were activity within this network appears increased in AD and decreased in bvFTD (Zhou et al., 2010).

Whilst there have been fewer neuroimaging studies of the PPA subtypes the results from metabolic and structural imaging studies have shown relative concordance. SvPPA is

consistently associated with atrophy and hypometabolism of the anterior temporal lobe, most typically on the left side, including the fusiform gyrus and amygdala (Acosta-Cabronero et al., 2011; Mummery et al., 2000). Longitudinally there is progressive atrophy in these regions as well as within the contralateral anterior temporal lobe and orbitofrontal cortex (Rohrer et al., 2008). In those with nvPPA a largely consistent pattern of atrophy and hypometabolism within the frontal lobe, typically the left side, involving Broca's area, insular and premotor cortex has been reported across studies (Grossman, 2010; Nestor et al., 2003; Rohrer et al., 2009). Longitudinally atrophy progresses superiorly and medially to further involve frontal lobe and temporal lobe structures. Atrophy also appears to track posteriorly along the Sylvian fissure to include the parietal lobe (Rogalski et al., 2011). Finally those with lvPPA have a pattern of atrophy involving more posterior temporal lobe and parietal regions, and again like svPPA and nvPPA this tends to be asymmetric, with greater involvement of the left hemisphere (Henry and Gorno-Tempini, 2010). Longitudinally those with lvPPA have progressive atrophy of these regions as well as right-sided temporo-parietal frontal and subcortical atrophy (Rohrer et al., 2013).

Beyond defining the neuroimaging signatures for clinical syndromes more recent attempts have been made to identify molecular neuroimaging signatures, by using histopathological and genetic data. This is important given that future drug treatments are likely to target specific molecular disorders. Much like the clinical heterogeneity of FTLD, there is also substantial pathologically heterogeneity. The most common proteinopathies relate to tau and TDP pathology. Pathological Pick's disease has been

associated with marked and quite generalised atrophy of bilateral prefrontal cortex and anterior temporal lobes (Lieberman et al., 1998; Rohrer et al., 2011; Whitwell et al., 2005). *MAPT* mutations are associated with mainly temporal lobe atrophy, and often striking bilateral medial temporal lobe atrophy (Janssen et al., 2002; Rohrer et al., 2011), additionally there may be inferior temporal lobe and orbitofrontal cortex atrophy. In cases of CBD and PSP, most commonly presenting as either nvPPA or bvFTD clinically, atrophy can be quite focal; in CBD atrophy is perhaps somewhat more widespread and more apparent on individual imaging with focal atrophy often reported in the parietal lobes (Josephs et al., 2008). Other studies have reported relatively symmetrical dorsolateral frontal lobe atrophy (Rohrer et al., 2011). In PSP atrophy of the superior cerebellar peduncle and midbrain are common (Josephs et al., 2008; Paviour et al., 2006). It should be pointed out that whilst these pathologies can present as bvFTD or nvPPA clinically, they typically present as corticobasal syndrome or clinical PSP and as such the neuroimaging hallmarks of these pathologies presenting as bvFTD or nvPPA are relatively unknown. In the case of TDP pathology there have been several studies attempting to identify profiles of atrophy specific to TDP subtypes (Rohrer et al., 2011; Rohrer et al., 2010; Whitwell and Josephs, 2012). TDP type A pathology has a rather heterogeneous profile of brain atrophy often involving frontal, temporal and parietal lobes. The degree of atrophy can be significant and highly asymmetric as in cases associated with *GRN* mutations (Beck et al., 2008). However in those with *C9ORF72* mutations there appears to be significant variation in the patterns of atrophy despite individuals having the same molecular lesion (Mahoney et al., 2012a). For example cases have been reported with striking fronto-temporal atrophy, whilst some cases have resembled "phenocopies" with

very slow disease progression (Devenney et al., 2014). At a group level *C9ORF72* appears to be associated with subcortical and cerebellar atrophy (Boxer et al., 2011; Mahoney et al., 2012a, 2012b; Whitwell et al., 2012), with p62 cerebellar pathology being characteristic (Al-Sarraj et al., 2011; Mahoney et al., 2012a). TDP type B overlaps with *C9ORF72* and motor neuron disease and has been associated with relatively less severe symmetrical atrophy of prefrontal cortex and antero-medial temporal lobe (Rohrer et al., 2010). TDP type C is perhaps the strongest clinicopathological correlation. Clinically this molecular subtype is highly correlated with svPPA and antero-inferior temporal lobe atrophy. TDP type D is rare and no clear imaging correlate has been identified.

More recently neuroimaging studies have adopted newer imaging techniques to identify clinical and molecular signatures. fMRI has recently emerged as a way of assessing functional connectivity between brain regions using resting state protocols. This has lead to the identification of a number of clinically defined dysfunctional brain networks across the spectrum of neurodegeneration (Barkhof et al., 2014). Perhaps the most well known examples are in AD where reduced activity is observed in the 'default mode network' (Greicius et al., 2004), and more recently in bvFTD where reduced connectivity is observed within the 'salience network'. These findings have been repeated by others and also show a divergence in functional connectivity between bvFTD and patients with Alzheimer's disease, making fMRI a potentially useful clinical biomarker (Filippi et al., 2013). fMRI studies in those with PPA are fewer and typically involve activation paradigms aimed at better understanding the neural basis of semantic categorization, language and memory (Binney et al., 2010; Goll et al., 2012; Wilson et al., 2011).

Other techniques to image neuropathology *in vivo* show promise with amyloid imaging now readily available to detect AD pathology (Klunk et al., 2004), and several tau based ligands in development and showing early promise (Maruyama et al., 2013). These techniques provide additional tools for understanding the neurobiology of FTLD and will be of particular interest in longitudinal studies and in combination with other imaging modalities to more fully explain the evolution of neurodegeneration.

1.7 Diffusion Tensor Imaging

1.7.1 An overview

The previously discussed imaging methodologies have heavily relied on identification of either macroscopic patterns of lobar atrophy or often seemingly disconnected areas of functional alteration, and whilst these forms of imaging remain important, they are associated with a number of limitations. Firstly techniques such as whole brain atrophy or fMRI may lack in either sensitivity or practicality to detected the earliest disease related changes. Secondly grey matter analysis tends to indirectly assess network breakdown often making inferences about associations between atrophy, reduced functional activity and clinical syndromes. This limits a full appreciation of the *in vivo* neurobiological changes occurring in the brains of patents with FTLD.

Analysis of microstructural change of white matter connections between brain regions *in vivo* has become possible with more advanced neuroimaging such as DTI, whilst still maintaining the practicalities and convenience of MRI. This has allowed researchers to provide more detailed maps of changes to white matter architecture in many

neurological diseases (Ciccarelli et al., 2008). Diffusion weighted imaging (DWI) utilises the principle of Brownian motion, to detect the movement (or restriction) of water molecules within brain structures and has been an invaluable tool in the detection of acute cerebral ischaemia for many years. DTI is a further advance on DWI, applying diffusion gradients in multiple (six or more) directions. The study of cerebral white matter is particularly well suited to DTI as it displays high anisotropy due to myelinated axons. In healthy white matter water tends to diffuse along a parallel gradient with limited diffusion perpendicularly (Figure 1.2A). This normal gradient of diffusion tends to alter in many neurological diseases. A mathematical model to describe this process was introduced by Basser and colleagues, termed the diffusion tensor (Basser et al., 1994). This model, a 3 x 3 matrix, describes the degree and direction of diffusion displacement over time. From the diffusion tensor matrix three eigenvalues ($\lambda 1$, $\lambda 2$ and $\lambda 3$) and their eigenvectors ($\varepsilon 1$, $\varepsilon 2$ and $\varepsilon 3$) are derived. Within each brain voxel the tensor is imagined as an ellipsoid with the eigenvectors defining the principal direction of diffusion along the axis of the ellipsoid and the eigenvalues defining the radius of the ellipsoid (Figure 1.2B).

A. Schematic of diffusion characteristics within an axon

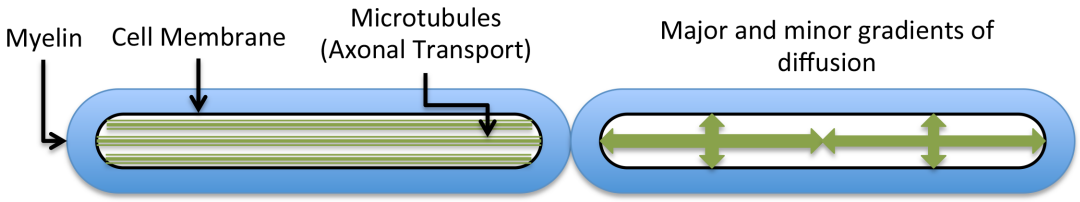

B. Diffusion ellipsoid and its eigenvalues

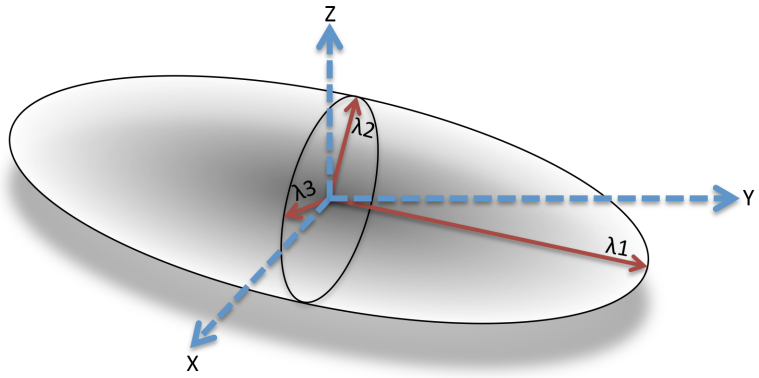

Figure 1.2 A), Schematic representation of an axon indicating axonal barriers (myelin), major and minor diffusion gradients. B), Diffusion ellipsoid characterised by its three eigenvalues (λ1, λ2 and λ3), representing the direction of diffusion in each direction. The ellipsoid is shown in relationship to the normal geometry within the scanner (x, y and z).

When a property is highly isotropic (e.g. in water), each eigenvalue will be similar to one another (i.e. $\lambda 1 \approx \lambda 2 \approx \lambda 3$); when an object is highly anisotropic (e.g. a white matter tract) each eigenvalue will differ in order of magnitude (i.e. $\lambda 1 > \lambda 2 > \lambda 3$). It is change in these properties, which allow us to probe for pathology in white matter using DTI. To allow us to understand complex 3-D changes in both the magnitude and directionality of diffusion a number of simpler scalars have been derived. The most common quoted is fractional

anisotropy (FA), which describes the degree of directionality of diffusion and is calculated as follows:

$$FA = \frac{1}{\sqrt{2}}\left(\frac{(\lambda_1 - \lambda_2)^2 + (\lambda_2 - \lambda_3)^2 + (\lambda_1 - \lambda_3)^2}{\lambda_1^2 + \lambda_2^2 + \lambda_3^2}\right)$$

Other scalars better represent the magnitude of diffusion and include trace diffusivity (TR) and its average mean diffusivity (MD):

$$TR = \lambda_1 + \lambda_2 + \lambda_3$$

$$MD = \frac{(\lambda_1 + \lambda_2 + \lambda_3)}{3}$$

Axial diffusivity (AX) is a measure of the magnitude of diffusion parallel to the orientation of the white matter tract being studied, which should be the dominate direction, as diffusion of water in this direction should be relatively unimpeded given the orientation of the structure:

$$AX = \lambda_1$$

Radial diffusivity RD, which is a measure of the magnitude of diffusion perpendicular to the orientation of the white matter tract being studied, should detect only minor diffusion, as the movement of water molecules in this direction is more impeded by tract fibres:

$$RD = \frac{(\lambda_2 + \lambda_3)}{2}$$

It is possible to obtain measurements for each DTI metric (FA, MD, AX and RD) within each brain voxel during one scan, yielding large amounts of data for each subject. At present, FA remains the most commonly reported metric within the literature. It is a useful metric, which reflects the overall integrity of a white matter tract by reporting the degree of isotropy within it, whereby a value approaching one signifies highly anisotropic diffusion of water, often associated with a tract being more structurally intact, whilst values approaching zero signify isotropic diffusion, which tends to be associated with tract pathology. One of the benefits of DTI is being able to acquire data on multiple DTI metrics in one session and it is therefore important to consider each DTI metric, not least because FA cannot fully explain all the changes within the diffusion tensor, in particular the magnitude of change. Reviewing the equation for FA above we note that increases of similar magnitudes in each eigenvalue can result in no change to FA. For this reason it is important to also consider the absolute changes in diffusion as measured by AX, RD and MD.

1.7.2 DTI Metrics

The neurobiological basis for each of the DTI metrics mentioned above continues to be established. However a number of observations have been made, in particular relating to FA, the most widely reported DTI metric, with lower FA values being associated with a range of neurological and psychiatric conditions (Ciccarelli et al., 2008; Thomason and Thompson, 2011). However as alluded to changes in FA are driven by changes in either AX or RD and the interpretation of these metrics remains somewhat controversial, for example when white matter structures are not in uniform alignment and in regions were

there is a high amount of crossing fibres (Wheeler-Kingshott and Cercignani, 2009). Work in mouse models of demyelination has shown that RD was higher in animals with no myelin whilst AX was unchanged (Song et al., 2002), suggesting that RD may be a useful measure of demyelination but not axonal loss, and in fact this has been repeated by others (Harsan et al., 2006; Tyszka et al., 2006). Change in AX has been reported in the context of axonal damage, with decreased AX reported following an acute axonal injury (Liu et al., 2013; Sun et al., 2006). However changes in the magnitude of diffusion also appear to be variable and dynamic with initial decreases in AX and RD reported in the context of acute injury, such as nerve transection or acute inflammation, followed by an increase in both these metrics, felt to be compatible with more chronic neuropathological processes (Acosta-Cabronero et al., 2012; Brennan et al., 2013; Fox et al., 2010; Liu et al., 2013). These dynamic changes may be explained by multiple phases of change within the milieu of the white matter axon, with an initial phase of dysmyelination-remyelination and cellular oedema as part of an acute inflammatory processes, followed by a more chronic process of demyelination, failure of axonal transport, axonal degeneration and neuronal death. This is certainly plausible given that most of the variability in these metrics have been reported in conditions associated with inflammation, such as multiple sclerosis. Whilst some variability has been reported in some neurodegenerative conditions, there appears to be relatively more consistency in the direction of change for each metric, particular FA, RD and MD (Acosta-Cabronero et al., 2012, 2010), most likely due to these processes being a more insidious and unidirectional process of neuronal decline. In one recent study in AD, AX and MD were reported to be a more sensitive metric cross-sectionally, whilst FA was better at

detecting longitudinally change (Acosta-Cabronero et al., 2012). Overall however the tracking of pathological change in neurodegenerative diseases may be well suited to DTI, given that most neurodegenerative process are associated with mainly monodirectional changes in axonal pathology and therefore interpretation of DTI metric data will be less influenced by acute inflammatory processes.

1.7.3 Limitations of DTI

Whilst DTI offers many benefits in terms of measuring white matter microstructure there are also a number of limitations with DTI in the areas such as scan acquisition, data analysis and interpretation (Jones et al., 2013). From a technical point of view the resolution used to acquire data is typically quite large in comparison to the size of an individual axon, with a typical voxel sizes being 2-3mm in size. This relatively low spatial resolution limits are ability to capture changes in smaller white matter structures, particularly as they interface with cortex. This may also result in partial volume effects, with may result in a combination of mis-registration between white matter structures and contamination between white and grey matter, and cerebrospinal fluid (CSF). With improvements in scanner field strength it is possible to improve the resolution, however this must be balanced with scan time and safety, a particular issue for patients with behavioural problems. Other issues such as artefacts due to eddy currents, head movement and susceptibility, particularly at air/brain boundaries can be a problem, although improved algorithms for pre-processing of diffusion-weighted data have reduced these problems somewhat. Having good anatomical specificity for particular white matter structures can be problematic due to close proximity of tracts to one

another or due to crossing fibres. For example a structure like the cingulum bundle, which runs antero-posteriorly in near isolation from other tracts, is relatively easy to isolate for region-of-interest (ROI) analysis, whilst the superior longitudinal fasciculus crosses or neighbours many white matter tracts. Much of the processing of DTI data is based on certain mathematical and physical assumptions of water diffusion, for example an ellipsoid is viewed as the best way of characterizing diffusion in the healthy brain. It may be true to say that many of these assumptions are valid in healthy individuals but changes to the microstructures of individuals with neurodegenerative conditions may cause some of these assumptions to become less valid. One extreme example may occur during the registration of DTI images to one another. Current registration techniques tend to rely on a process that involves warping a diseased brain to one of a young healthy individual, which can result in misalignment and excessive warping of the patient's brain. In addition registration and analysis techniques in DTI are often multistage processes that are both labour and time intensive, resulting in a further potential source of noise. Finally, as mentioned in the preceding paragraph, considerable debate exists on the interpretation of DTI data. Indeed many questions remain on which DTI metric is 'best'; this may well depend on the structure being studied, along with the type of study i.e. cross-sectional versus longitudinal and the particular disease under study.

1.8 From axonal degeneration to clinical syndrome

Previous sections have highlighted the substantial evidence amassed regarding the prevalence of white matter histopathology in FTLD. Further, the potential of DTI in assessing the microstructural changes within white matter, by measuring alterations in diffusion within axons, has been discussed. Whilst accumulation of potentially toxic proteins has been observed within cells at post-mortem it is likely that a number of steps precede this; for example firstly failures in axonal transport and axonal degeneration leading to some of the changes which DTI may be detecting.

Axonal degeneration occurs in health and is a tightly regulated and efficient process that contributes to the development of the normal brain, ensuring that healthy functional neural circuits develop (Chevalier-Larsen and Holzbaur, 2006; Saxena and Caroni, 2007). As the brain develops, axons undergo targeted degeneration, termed pruning, mostly through neuronal apotosis. A variety of genes and proteins both guide this process, and prevent unwanted axonal degeneration. These include *MAPT*, a gene of high importance in the emergence of FTLD. A multitude of other proteins such as tubulin, acetylating and de-acetylating proteins such as HDAC6, filament severing proteins such as Katanin, and protective proteins such as slow Wallerian degeneration protein guide the process of axonal degeneration (Saxena and Caroni, 2007). Pathological axonal degeneration has been implicated in a range of neurodegenerative disorders; mutations in Amyloid precursor protein, causing AD, are known to cause axonal blockage; whilst mutant huntingtin, causing Huntington's disease, induces axonal swelling and disruption of both anterograde and retrograde axoplasmic transport (Chevalier-Larsen and Holzbaur, 2006).

Tau is a key pathological constituent in FTLD and a key intra-axonal constituent. A recent study has examined how pathological tau pathology my influence axonal function. Using a mutant P301S tau transgenic mouse model axonal swellings were observed which contained neurofilament, which occurred prior to the development of neurofibrillary tangles. The same study also identified that these neurofilament containing axonal swellings were also present in post-mortem brains of patients with FTLD-tau (van Eersel et al., 2015). Neurofilament in its normal state provides structural support for axons, and it would be reasonable to conclude that abnormal aggregations of neurofilament may contribute to axonal degeneration. Indeed it is possible to measure abnormal forms in CSF. Termed neurofilament light, these proteins have been associated with neurodegenerative pathologies as well as white matter lesion load on MRI (Sjögren et al., 2001). The role of the other major pathology in FTLD, TDP-43, in contributing to axonal degeneration has been studied mainly in motor-neruon disease. A number of mouse models of motor-neuron disease utilising the *SOD1* mutation have identified early axonal degeneration as a feature of motor neuron disease (Clement, 2003; Jaarsma et al., 2000). More recent studies have shown that TDP-43 supports anterograde axonal transport of mRNA from the cell body. Inducing a mutation in TDP-43, a rare cause of FTD and motor-neruon disease, impairs axonal transport of mRNA and may contribute to the emergence of FTLD (Alami et al., 2014). Several other disease models, although rare, provide further mechanistic evidence of axonal degeneration in FTLD. Valosin containing protein (VCP) regulates the ubiquitin-proteasome system, which in turn provides a mechanism for ordered cell degeneration (Kimonis et al., 2008). Mutations in this gene results in bvFTD, inclusion body myositis and Paget's disease. Slow Wallerian degeneration protein is an

important regulator in protecting against axonal degeneration and in animal models VCP has been shown to be an important regulator of this protein, suggesting that mutations may directly contribute to axonal degeneration (Beirowski et al., 2010). Another rare syndrome, which may present as bvFTD, along with respiratory failure and Parkinsonism, is Perry syndrome. This syndrome is a result of mutations in the Dynactin gene, a gene which codes for dynactin, a protein which is a constituent of the dynenin-dynactin complex which drives retrograde axonal transport, transporting key neurotrophic growth factors (Chevalier-Larsen and Holzbaur, 2006). Perry syndrome, associated with TDP-43 pathology, provides further evidence for the role of axonal degeneration in TDP-43 related neurodegeneration (Wider et al., 2010).

It is plausible that through a combination of failures in normal axonal transport processes along with deposition of toxic protein species within axons that a process of axonal degeneration is initiated with a subsequent gradual 'dying-back' process whereby more proximal neurons and synapses become dysfunctional (Chevalier-Larsen and Holzbaur, 2006; Simons et al., 2014). Beyond just axonal degeneration the extensive histopathological suggest that axonal degeneration and failures in myelination combine, perhaps in a synergic way, to induce neurodegeneration, and with loss of a sufficient neurons and synapses certain clinical syndromes emerge (Simons et al., 2014). The time course and temporal ordering of events continue to be established, and additionally the role of certain abnormal proteins is also unclear, are they directly toxic to cells or merely by-products in a more complex chain of events?

Whilst direct *in vivo* histopathological studies are not possible in humans a number of relatively 'pure' white matter diseases can be used to understand the influence of white matter pathology on cognition. Perhaps the most closely related to FTLD is adult onset leukodystrophy with neuroaxonal spheroids, which has recently been associated with a mutation in colony stimulating factor 1 R (CSF1R) gene (Rademakers et al., 2012), and most commonly presents with a clinical phenotype of bvFTD. Whilst the neuropathology of this disease does show occasional ballooned neurons within the cortex, the vast bulk of pathology is within white matter, particularly within frontal white matter and corpus callosum, often with complete absence of myelin, extensive axonal damage and the presence of axonal spheroids (Freeman et al., 2009). Beyond FTLD large epidemiological studies of the aging population, such as the Rotterdam Study, also provide robust evidence that progression in white matter lesion load, in this case presumed to be due to vascular disease, correlates strongly with deteriorating memory and speed of information processing (Cees De Groot et al., 2000). Indeed some studies suggest that the degree of white matter pathology in small vessel disease may directly influence the profiles of cortical atrophy (Du et al., 2005). Multiple sclerosis is perhaps the most widely studied disease of white matter, and whilst commonly referred to as a demyelinating disorder it is clear that substantial axonal degeneration also occurs (Lassmann et al., 2012; Newcombe et al., 1991). MS lesion load has also been consistently associated with cognitive deficits, and in particular total brain lesion load seems to have a marked impact on fronto-executive systems (Rovaris et al., 1998).

Scaling intra-axonal pathophysiology up to explain clinical syndromes is a more challenging concept, particularly given that neurodegeneration encompasses both white and grey matter, making examination of changes in isolation difficult. A number of animal models and human disease processes highlight that relatively selective white matter pathology can induce clinical deficits. In aged non-human primates a linear decline in the density of myelinated axons and increasing axonal degeneration is observed in structures such as the anterior commissure, with a direct correlation between the number of healthy of nerve fibres and cognitive performance (Sandell and Peters, 2003). A number of selective white matter lesion studies have also shown that monkeys develop syndromes compatible with bvFTD (Horel and Misantone, 1974), whilst lesions of amygdalofugal tracts result in severe impairment of visual memory (Bachevalier et al., 1985). Lesion studies have also provided insights on the trajectory of axonal degeneration, for example targeted lesions within tracts connecting the fornix and fimbria identified subsequent downstream trans-neuronal degeneration within the medial mammillary nucleus (Ginsberg and Martin, 2002). There is direct evidence of the importance of intra-axonal pathology in neurodegeneration however new concepts, such as network-led degeneration (discussed below), are needed to understand how relatively axonal pathology can lead to more wide-spread neurodegenerative syndromes, and how initial focal cognitive defects evolve towards syndromes of global cognitive failure.

1.9 Network-led degeneration

Classical neuro-anatomists believed that brain functions were compartmentalised to particular brain regions and gyri and whilst this can be said to be true for certain primary

functions such as the motor cortex, it is increasingly recognised that many higher cognitive functions are a result of anatomically distributed brain regions working in synchrony as a functional network. Early ideas on how higher cognitive functions were distributed are exemplified in the work of Geschwind, who gave a detiled account of disconnection syndromes, for example the interruption of the structural connections between two cortical language regions resulted in the clinical syndrome of conduction aphasia (Benson et al., 1973). With new techniques to study structural connections the concept of hodology – the pattern of white matter connections between cortical regions, has once again become an important concept in integrating function with anatomy (Catani and ffytche, 2005). Beyond these 'direct' structural brain connections it has also been established, mainly through the use of fMRI, that brain regions can work in synchrony through both direct and indirect connections, for example via subcortical structures such as the thalamus. Examples of functional brain networks include the default mode network, which includes ventromedial prefrontal cortex and posterior cingulate cortex and is active during internally orientated tasks (Buckner et al., 2008); Salience network, composed of anterior cingulate and insular cortex and activated during detection of external and internal salient events and important in modulating behavioural responses to these stimuli (Seeley et al., 2007); Fronto-parietal control network, composed of lateral prefrontal and inferior parietal cortex and activated when performing a goal directed task (Vincent et al., 2008); linguistic networks composed of mainly left side fronto-temporo-parietal regions for speech generation (Geranmayeh et al., 2014), and ventral prefrontal and temporal regions for semantic processing (Noonan et al., 2013). These large scale cognitive networks are distributed across brain regions

with both functional and structural components, individual functional components are viewable as activation maps, reflecting intrinsic connectivity between brain regions using fMRI; structural connections are viewable as structural connectivity maps, reflecting the relative strength of white matter connections between brain regions, as measured using DTI.

These functional and structural brain networks work in synchrony to execute complex cognitive tasks. However multiple smaller scale networks, termed *modules*, exist within these networks. Whilst each module executes different cognitive processes, they work synergistically towards a more complex final output. Beyond this again there are smaller nework components, which in an imaging terms may be comparable to a voxel, termed *nodes*, which carry out even more sub-ordinate tasks. Advances in imaging the physiology of brain networks, through the use of technologies such as the use of optogenetics, allows us to resolve the basic constituents of brain networks down to small groups of neurons synapsing with one another (Bock et al., 2011). However it is clear that in order to carry out complex cognitive tasks these small-scale networks must communicate with one another either through connections, viz-a-viz white matter fibres, which are mathematical termed *edges*. *Edges* may operate over a short distance between *nodes* or over longer range between *modules*. In addition some nodes may be highly interconnected to allow rapid integration of information across multiple modules, so-called *rich-club nodes* (van den Heuvel and Sporns, 2011). Some nodes may have high numbers of *edges,* indicating a high degree of connectivity to other brain regions, and may be termed a *hub* (Park and Friston, 2013). Examples of hubs in the human brain may

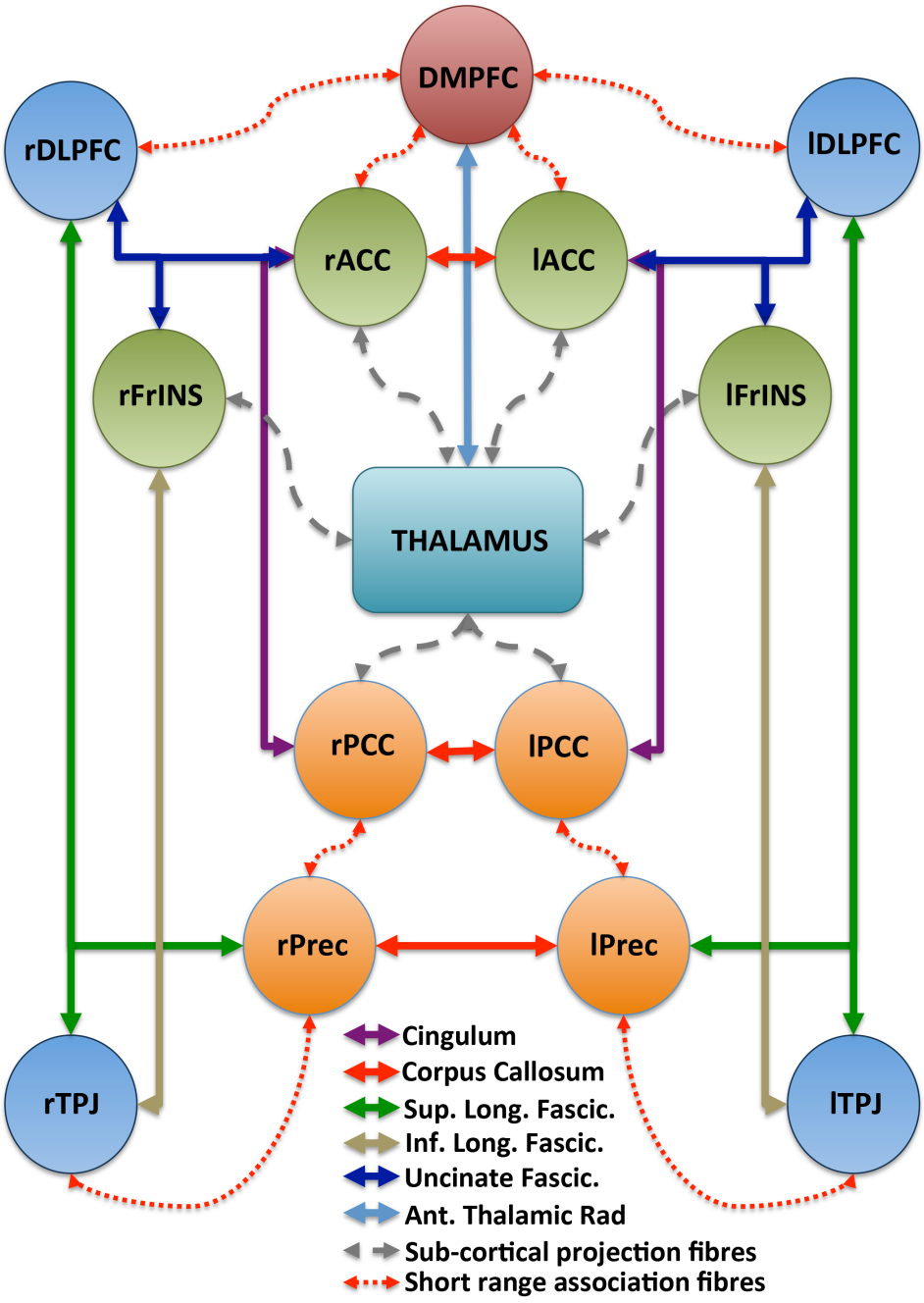

Figure 1.3 Representation of major brain networks/brain regions and the white matter connections that link them. Green circles represent the Salience network (ACC, anterior cingulate cortex; FrIns, Front-insular cortex); orange circles represent the default mode network (PCC, posterior cingulate cortex; Prec, precuneus); blue circles represents the fronto-parietal control network (DLPFC, dorsolateral prefrontal cortex; TPJ, temporo-parietal junction) and red circle represents the executive control network (DMPFC, dorso-medial prefrontal cortex). Lines represent white matter connections between functional networks/regions; solid lines represent major projection and commissural tracts, dashed lines represent shorter-range projection and association fibres.

include the temporo-parietal junction as it overlaps the default mode, control and ventral attention networks.

A schematic of major brain networks can be seen in figure 1.3, with functional networks (modules) represented by coloured circles and structural connections (edges) represented by filled and dashed lines.

With improvements in neuroimaging we can now image many of the components of these brain networks *in vivo*, whilst acknowledging the lack the resolution to fully resolve sub-voxel components of brain networks. The availability of these techniques was a major motivation for the current undertaking, coupled with the increasing recognition that neurodegenerative conditions may target specific aspects of both functional and structural brain networks. This concept of neurodegeneration across specific brain networks, *network-led degeneration,* may provide a common framework for understanding and potentially tracking the disease neurobiology across the FTLD spectrum.

The terminology of *network-led degeneration* is perhaps a recent development but it has been known for some time that specific brain networks and their components are vulnerable in neurodegenerative diseases. For example reduced intrinsic connectivity within the default-mode network has been repeatedly demonstrated in Alzheimer's disease, and not just in symptomatic individuals but also in pre-symptomatic familial Alzheimer's disease mutation carriers (Chhatwal et al., 2013). More recently changes to structural connections have also been shown in presymptomatic frontotemporal dementia patients who harbour both *PGRN* and *MAPT* mutations (Borroni et al., 2008;

Dopper et al., 2013). As mentioned previously the *Salience network* has shown selective vulnerability in patients with frontotemporal dementia (Zhou et al., 2010). One can imagine that there are specific features of these networks, which make them particularly vulnerable to degeneration (Pievani et al., 2011). This could be one of, or a combination of the following: abnormal development, exposures to specific environmental triggers, genetic modifiers conferring greater risks of degeneration to specific networks. With a network in a vulnerable state a second hit with a toxic protein, for example *tau*, may instigate further damage to the network resulting in nodal stress with downstream loss of synapses and more widespread network failure due to loss of trophic support, perhaps through failure of axonal transport (Goedert et al., 2014). The speed and propagation of network degeneration may depend upon the configuration of the network under attack, with a more focal contiguous degeneration within networks with composed of short-range connections between nodes and modules, and large-scale degeneration in network with higher numbers of *rich-club* nodes or with long-range connections. Reviewing figure 1.3 we can hypothesise how a disease might evolve depending on which network is affected, for example a molecular insult to the *Salience network* (green) may result in an initially relative anatomically constrained degeneration, targeting mainly short-range or local connections within this network, clinically resulting in quite focal cognitive deficits. However over time other networks may also become affected, noting the long-range association fibres linking the salience network with other brain networks. Alternatively if a highly interconnected network, such as the subcortical/thalamic (turquoise) network, is affected this may lead to pan-network degeneration, clinically manifesting as more global cognitive impairment.

To further support the notion of selective network vulnerability it is worth nothing that in those with genetic forms of bvFTD, despite every neuron harbouring a pathogenic mutation, global simultaneous brain degeneration does not occur, instead a specific, almost programmed, pattern of degeneration occurs. For example in figure 1.4 an individual who was initially clinically unaffected with bvFTD had serial volumetric MRI scans over a ten-year period. This individual harboured a *MAPT* mutation (exon 10 +16) and exhibits the commonly reported radiological findings of focal medial temporal lobe atrophy with subsequent orbitofrontal atrophy. This pattern suggests that these brain regions have a selective vulnerability. These important genetic cases also suggest that specific proteins may also determine how network degeneration proceeds. Increasing evidence suggests that tau exhibits prion-like properties with intracellular, transynaptic and transaxonal spread of this protein observed in cell and animal models of tauopathy (Clavaguera et al., 2013; Goedert et al., 2014; Nussbaum et al., 2012) and it has been postulated that brain networks are the vehicle through which tau species (and perhaps other proteins) preferentially disperse. Brain networks may also be targets for deficiencies in normal cell repair and metabolism. For example in *GRN* mutations, a haploinsufficeny resulting in 50% less granulin - an important cell repair protein, may result in damage to key functional nodes with downstream damage to distant nodes due to loss of trophic support provided via long-range association fibres. This is plausible given that *GRN* mutations are associated with a widespread intrahemispheric pattern of atrophy.

In summary there is growing evidence that neurodegenerative diseases target specific brain networks (Warren et al., 2013). Elements of these networks, such as their structural connections can be visualized *in vivo* using DTI. Identification of both common and syndrome specific profiles of structural network breakdown may provide a more uniform way of understanding disease biology and tracking disease progression over time.

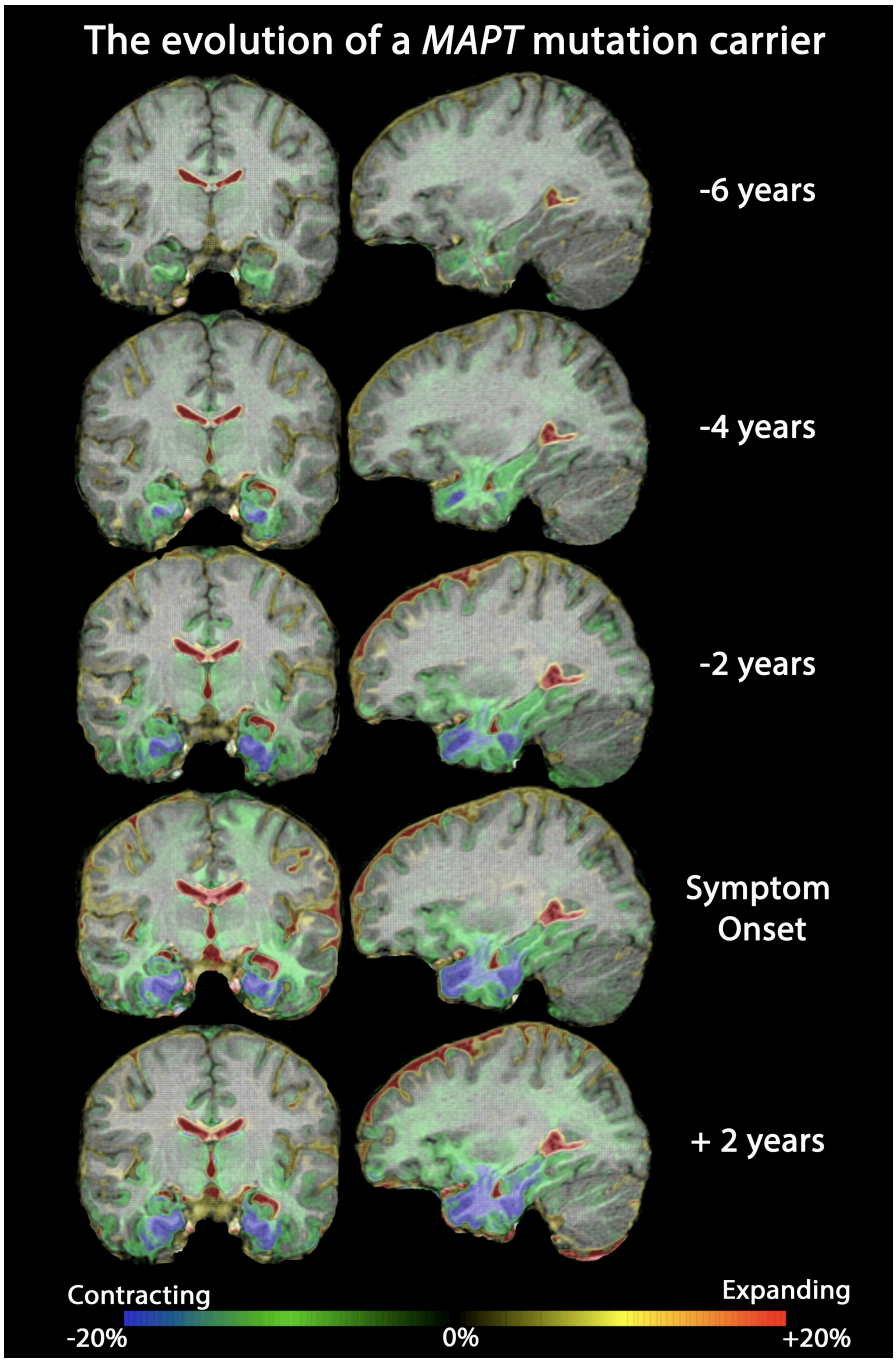

Figure 1.4 Chronological progression of atrophy in a *MAPT* mutation carrier visualised using fluid registration. Baseline scan was acquired 7 years prior to symptom onset. Colour bar signifies % volume change per voxel from baseline scan. Blue/green=contraction, red/yellow=expansion.

1.10 Chapter summary

Whilst our knowledge of non-Alzheimer's dementia, originally described by Pick, stretches back over one hundred years, it is in the last two decades that real progress has been made in refining the clinical, radiological and neuropathological phenotype of the non-Alzheimer's dementia, or specifically in FTLD. There has been multiple imaging studies performed to establish the patterns of grey matter atrophy in FTLD, however these studies, alone, have a number of limitations. Firstly, increasing evidence suggests that macroscopic brain atrophy is a terminal process in the evolution of FTLD, and therefore may not be sufficiently sensitive to capture the earliest features. Secondly, grey matter studies cannot fully explain the variability on both imaging and clinical grounds seen in FTLD, in particular it does not explain why some individuals with little atrophy have florid clinical syndromes or vice-versa, or indeed why the same clinical syndrome is associated with different imaging phenotypes and pathologies.

This thesis aims to build on previous neuroimaging studies and will exploit novel imaging techniques, in this case DTI as the imaging modality best suited to capture changes in structural pathway connections that bind networks together. Increasing evidence suggests that certain brain networks may exhibit specific vulnerabilities and it has been suggested that these vulnerable networks may be a conduit through which neurodegenerative proteins spreads. This concept, along with the increased availability of DTI, has provided much of the hypothetical impetus for the subsequent studies.

This Thesis attempts to address a number of issues relevant to understanding the disease biology of FTLD:

1 Establish the profiles of white matter tract pathology in bvFTD and PPA by examining clinically, and were possible genetically, defined phenotypes using both cross-sectional and longitudinal DTI.

2 Establish the relationship of white matter and grey matter pathology to one another.

3 Establish the usefulness of DTI as a potential disease biomarker, with which FTLD can be monitored.

4 Establish the sensitivity and specificity of individual DTI metrics in the monitoring of FTLD.

Chapter 2 sets out the clinical assessments and imaging techniques used in the subsequent chapters.

Chapter 3 will test the hypothesis that there are clinically and moleculary defined profiles of white matter pathology in bvFTD. Using a a well defined patient cohort key white matter tracts are examined cross-sectionally, using a number of DTI metrics, to establish the extent of white matter tract pathology. DTI metrics are also compared with one another to establish optimal DTI metrics. Grey matter is also studied using VBM and compared with the profiles of white matter tract pathology.

Chapter 4 will test the hyptothesis that longitudinal DTI can be applied to study white matter tract changes in bvFTD. Previously longitudinal DTI has been a technically challenging methodlogy to apply. This chapter aims to establish it as a useful measure of disease pathology. Furhtermore this chapter will test the hyptothesis that functionally

relevant white matter tracts show evidence of progressive disease pathology in line with the syndromic evolution. Patients with bvFTD will undergo serial clinical and imaging assessments, approximately one year apart. Key white matter tracts are studied and change in each DTI metric over time is calculated, identifying both spatial and temporal profiles of disease propagation. DTI metrics are compared with one another to establish optimal longitudinal DTI metrics. Clinical and imaging outcome measures are compared with one another and estimated sample sizes for clinical trials are calculated.

Chapter 5 will test that hypothesis that there are syndromically defined profiles of white matter pathology in PPA. Using a clinically defined cohort of patients with svPPA, nvPPA and lvPPA key white matter tracts are examined using a number of DTI metrics to establish the extent of white matter tract pathology. DTI metrics are compared with one another to establish optimal DTI metrics. Grey matter is also studied using VBM and compared with profiles of white matter tract pathology.

Chapter 6 sets out to establish the longitudinal profiles of white matter tract pathology in PPA. Patients with PPA will undergo the same serial assessments and analysis as those with bvFTD in chapter 4.

2. Methods

2.1 Study participants.

2.1.1 Subject ascertainment and inclusion criteria.

Patients were recruited via the Specialist Cognitive Disorders Clinic, National Hospital for Neurology and Neurosurgery, London, UK, as part of longitudinal clinical study of FTLD. Study participants clinical features were assessed against current consensus criteria for bvFTD and PPA (see Table 1.1 and 1.2) and an experienced cognitive neurologist validated inclusion decisions. Patients with a diagnosis of probable or definite bvFTD or PPA were recruited to participate in the studies herein. Patients were not included in the event they had a clinical diagnosis, which was only *possibly* consistent with bvFTD, i.e. potential phenocopies, or if their PPA syndrome was unclassifiable. Patients were also excluded if they were unable to tolerate MRI scanning, had white matter pathology consistent with ≥ 2 on the Fazekas scale (Fazekas et al., 1987) for deep and/or periventricular white matter signal changes (i.e. consistent with moderate or severe small vessel disease) or had other structural lesions on MRI which may interfere with image analysis. Cognitively normal participants (hereafter called controls) were recruited to match age and gender of recruited patients. Were possible spouses/partners were recruited. Controls were included only after completing a detailed clinical assessment and neurological examination to ensure they did not have a diagnosis of a neurodegenerative or psychiatric disorder, or excessive vascular risk factors (e.g. poorly controlled hypertension, diabetes or known cardio- or cerebrovascular disease).

Ethical approval for the all studies contained in this Thesis was obtained from the local institutional ethics committee and all participants gave written informed consent to participate in accordance with the Declaration of Helsinki.

2.1.2 Clinical and neuropsychological assessment

Clinical assessment was completed using the same standardized clinical questionnaire for patients and healthy participants. This captured basic demographics such as age, handedness, occupation and years of education; clinical history including, first symptoms, estimated year of disease onset, current symptoms, prior medical history and current medications. A standardized physical and neurological examination was carried out which included bedside assessment of praxis. All patients and controls underwent a mini-mental state examination (MMSE). Blood samples where obtained for DNA analysis, with additional blood samples archived, were consent was given. In addition a subset of patients had cerebrospinal fluid (CSF) analysed for total tau and beta-amyloid 1-42, where clinically indicated to determine the likelihood of AD pathology. Total CSF tau (a measure of neuronal loss, as a non-specific accompaniment of neurodegeneration) and CSF amyloid-beta$_{1-42}$ (Aß$_{1-42}$); a measure of amyloid deposition specific for AD pathology) were measured (Innotest platforms, Innogenetics, Ghent, Belgium). Local reference ranges for tau and Aß$_{1-42}$ were used to assess the likelihood of underlying AD versus non-AD pathologies; cases deemed to have probable underlying AD pathology had tau >307pg/ml and Aß$_{1-42}$< 325pg/ml (cut points derived from local data with 85% sensitivity for AD).

All participants underwent a standardized battery of neuropsychological testing. General intellect (IQ) was assessed using the Wechsler Abbreviated Scale of intelligence (Wechsler, 1999). Recognition memory was tested using The Recognition Memory Test for faces (Warrington, 1984), which presents 50 faces with an orienting question. The participant is then presented with the target paired with an unfamiliar face and asked to judge that they have seen before. The same procedure is used for the Recognition Memory Test for words. Single-word comprehension was assessed using The British Picture Vocabulary Scale (Dunn, Dunn & Whetton, 1982) whereby participants must match one of four pictures to a target word of increasing difficulty. Formal naming was assessed using The Graded Naming Test (McKenna & Warrington, 1983). This requires participants to name line drawings that become increasingly less common. Mathematical ability was assessed using The Graded Difficulty Arithmetic Test (Jackson & Warrington, 1986), which allows participants 10 seconds to perform increasingly difficult mental arithmetic sums. Perceptual skills were assessed using the Object Decision subtest of the Visual Object and Space Perception battery (Warrington & James, 1991). This requires participants to identify the silhouette of a 75 degree rotated real object from three nonsense silhouettes of similar complexity. Finally executive function was assessed using The Delis-Kaplan Executive function system (Delis et al., 2001). The colour-word Interference test assesses executive function using a progressively challenging set of tests, first requiring subjects to name consecutive coloured rectangles, then read aloud printed colour names and finally identify the ink colour where colour words are presented in a conflicting colour. Additional neurolingustic tests were performed in those with suspected PPA. This included repetition of 30 single words, with progressively

more syllables, repetition of 10 phrases of 3-10 words in length and an assessment of receptive grammar, which involved a description of a scenario and forced choice selection of this scenario from four pictures (Kay, 1992). When participants were unable to attempt a test after prompting or were unable to complete a trial they were assigned either the chance or floor score for that particular test. Each patient's clinical history, examination and neuropsychological profile along with standard clinical MRI sequences were reviewed at a consensus diagnosis meeting, which included several experienced cognitive neurologists, were a diagnosis was reached in accordance with the consensus criteria listed.

2.1.3 Genetic Analysis

Given the high prevalence of genetic associated bvFTD (and less so PPA) all subjects were requested to provide a blood sample for DNA analysis for commonly associated genetic mutations. In rare instances participants declined to provide a sample, although this was not an exclusion criterion for the study, and 93% of those with bvFTD were screened. Following obtainment of consent genetic analysis was carried out to determine if mutations in *MAPT, PGRN or C9ORF72* were present using either direct Sanger sequencing or with next generation sequencing technology using Life Technology's Ion Torrent Personal Genome Machine sequencing; which additionally screened for mutations within fused-in-sarcoma, valosin-containing protein, charged multivesicular body protein 2B, prion protein, TAR DNA-binding protein 43, presenilin 1 and 2, amyloid precursor protein and colony stimulating factor 1 receptor genes, was performed (Beck et al., 2014).

2.2 Imaging Techniques

2.2.1 Image Acquisition

All MRI scans were acquired on the same Siemens Trio Tim 3-Tesla scanner (Siemens, Erlangen) using a 32-channel head-coil. The image protocol consisted of a 3-D volumetric MRI, two back-to-back DTI acquisitions - the two acquisitions were then averaged to improve signal-to-noise (den Dekker and Sijbers, 2014), and a fluid-attenuated inversion recovery (to screen for white matter pathology).

2.2.2 Volumetric Acquisition

A sagittal 3-D magnetization-prepared rapid gradient echo T1-weighted volumetric MRI was acquired (echo time/repetition time/inversion time = 2.9/2200/900 Ms, dimensions of 256 × 256 × 208, voxel size of 1.1 × 1.1 × 1.1 mm).

2.2.3 Diffusion Tensor Imaging acquisition

Two 64-direction DTI sequences were acquired with a single shot, spin-echo echo planar imaging sequence (55 contiguous axial 2.5mm slices with 240 mm field of view and 96 x 96 matrix, yielding 2.5mm isotropic voxels; repetition time: 6800 Ms; echo time: 91 Ms; b value: 1000 s/mm^2), augmented with parallel imaging acceleration to reduce susceptibility artefacts. Nine images without diffusion weighting were also acquired (b = 0 s/mm^2).

2.2.4 Volumetric image analysis

Whole brain measurement was carried out using a semi-automated process of brain segmentation with initial threseholding of the MRI brain and a subsequent process of multiple erosions and dilations, using MIDAS software (Freeborough et al., 1997), to result in a brain region separated from dura and skull, and yielding a whole brain volume. Longitudinal whole brain volume changes were derived as follows: baseline and follow-up scans were spatially aligned to standard space and then underwent an affine registration (12 degrees of freedom) to align the follow-up scan to the baseline scan. Change in brain volume was calculated using the boundary shift integral (Freeborough and Fox, 1997), which determines the total volume at the boundaries of a structure, in this case the cerebrum, which have moved (which in neurodegenerative disease can be viewed as brain atrophy). This yields a volume in millilitres. The interval between scans and baseline whole brain volume can then be used to calculate the percentage per year change in brain volume.

2.2.5 Voxel-based morphometry

Group level comparisons of differences in grey matter volume (density) were carried out using voxel-based morphometry (VBM), which assesses differences in voxel density across a series of structurally aligned volumetric MRI scans. For all VBM analyses Statistical Parametric Mapping (SPM) version 8 (http://www.fil.ion.ucl.ac.uk/spm) was used running the DARTEL toolbox (Ashburner, 2007). DARTEL improves inter-subject alignment by generating forward and backward deformations. From the initial segmentations each tissue class undergoes rigid transformation to approximate

alignments. Both grey and white matter is then simultaneously registered producing an initial group-wise template, which is then iteratively refined, and individual subject data then warped to match this final group-wise template. Following a visual inspection of each volumetric MRI scan to ensure no significant motion artefact volumetric MRI scans undergo the following pre-processing steps:

1. An initial realignment of each volumetric image is carried out using the *Check Reg* function to align the anterior commissure at x=0, y=0, z=0.
2. Each tissue class (grey matter, white matter and CSF) is then identified using the *New Segment* module using default parameters. Segmentations are outputted in both native space and "DARTEL imported" space. Segmentations are visually inspected to ensure tissue classes are not contaminated or degraded.
3. DARTEL grey and white matter output images are Jacobian scaled and spatially normalized to Montreal neuroimaging template (MNI) space using the '*Normalise to MNI space*' module in SPM 8 using default parameters. To provide normally distributed data for statistical analysis images undergo smoothing using a 6mm kernel size.
4. Total intracranial volume (TIV), reported in millilitres, were calculated by summing the native space segmentation for grey matter, white matter and CSF for each subject.
5. Statistical analyses were performed using linear regression models which included disease group membership as the covariate of interest and age, gender, TIV and disease duration (as a marker of disease severity) included as nuisance co-

variants. In line with DTI analysis regional differences in grey matter volume were assessed using voxel-wise non-parametric permutation testing (n=10,000 permutations). Results underwent correction for multiple comparisons using family-wise error ($p<0.05$) and threshold free cluster enhancement.

6. A study specific average brain in MNI space was generated using the *imcalc* module of SPM8 and statistical maps of difference in grey matter volume overlaid.

2.2.6 DTI Image pre-processing

Following acquisition each diffusion-weighted sequence is visually inspected to ensure adequate brain coverage and to identify any artefacts (e.g. excessive movement resulting in checker-boarding, field distortions). If an abnormality is detected, were possible, the participant is recalled for repeat scanning as soon as possible. The presence of persistent image artefacts is considered an exclusion criterion from the study and is indicated in the subsequent studies. All images were motion and eddy current corrected by registering each diffusion-weighted imaged to the first b = 0 image using 12 degrees of freedom FLIRT (Jenkinson and Smith, 2001). Tensor fitting was performed using the Camino Diffusion MRI toolkit (Cook et al., 2006) and the following DTI metrics were calculated: Fractional Anisotropy (FA), Axial Diffusivity (AX), Trace Diffusivity (TR), Mean Diffusivity (MD) and Radial Diffusivity (RD).

2.2.7. Cross-sectional DTI analysis: Tract based spatial statistics

An overview of the imaging pipeline described below is found in Figure 2.1. Following tensor fitting cross-sectional DTI data were analysed at group level using tract-based

spatial statistics (TBSS) using the standard TBSS pipeline unless otherwise stated (Smith et al., 2006). TBSS was chosen, as it is a relatively unbiased technique allowing voxel-wise whole brain analysis of white matter tract changes between control and disease groups. It attempts to address the issue of mis-alignment of white matter structures by generating a white matter tract skeleton which is common to each subject and then projecting each individual subject's FA data onto a mean FA tract skeleton before carrying out voxel-wise statistics to assess for differences between groups. Each step is outlined below:

1. Each subject's FA image is slightly eroded to remove outlier data from the raw diffusion tensor image.
2. All FA images undergo an initial affine registration and then nonlinear alignment to a standard study specific space. To minimise the effect of excessive warping, the FA image that is most representative of the group is selected as the *target* image. The *target* image is identified by registering each subject's FA to each other, and then identifying the FA image with the minimum mean distance from the other images. The *target* image is then affine transformed to MNI 152 space.
3. All subject's FA images are then transformed to MNI 152 space by combining the nonlinear transformation to the *target* image with the affine transformation from the *target* image to MNI 152.
4. All study subject's FA images are then averaged to create a mean FA image combined into a single 4-D image file. The white matter tracts undergo a process of skeletisation. This aims to identify white matter tracts, which are common to all study subjects. These are represented as a contiguous line, which runs along an

approximate centre line of each tract. The voxels that comprise the skeleton are chosen after a search of each voxel to determine the voxel with the highest FA value, and this voxel is then labelled as being at the centre of the tract. To determine the orientation of the tract the vectors perpendicular to the centre of the tract are calculated by finding the centre-of-gravity of a 3 x 3 x 3 region of voxels. A voxel that is closer to the centre of the tract will have a higher FA value and a voxel away from the centre of the tract will have a lower FA. This process is repeated until a voxel is identified as being on the centre of the tract resulting in a final skeleton on which statistical analysis can be performed.

5. To minimise contamination from grey matter voxels the mean FA skeleton is then thresholded at 0.2 prior to analysis.
6. Each subject's FA image is then 'projected' onto the mean FA skeleton to improve alignment in the tract perpendicular. At each point in the skeleton each subject's FA image is "searched" to find the maximum FA value this is then assigned to the corresponding skeleton voxel.
7. The aligned data are now ready to be feed into a voxelwise statistical analysis pipeline. Carrying out statistical analysis on *only* the skeletonised data has an advantage of reducing the total number of statistical tests by limiting analysis to only the voxels within the skeleton. This reduces the likelihood of false positive results.
8. First a design matrix is generated including disease group membership as the covariate of interest and age, gender, disease duration (as a measure of disease severity) as nuisance covariates.

9. Non-parametric permutation based statistics (Nichols and Holmes, 2002) are used to compare t-statistics at each voxel using 10,000 permutations to build the null distribution using FSL's *randomise* module (Winkler et al., 2014), and controlling for multiple comparison using family-wise error rate $p<0.05$.
10. The test statistic is generated using Threshold-free cluster enhancement (TFCE) (Smith and Nichols, 2009). This method finds clusters (i.e. voxels with some spatial contiguity) and then enhances them, rather than performing single voxel-wise threseholding. Normal cluster based threseholding requires an arbitrary initial cluster to be defined. TFCE finds clusters based on the presence of cluster-like features using the voxel-wise values from the initial voxel-wise statistical image.
11. Family-wise error and TFCE corrected statistical maps are then overlaid on a study specific mean FA image in standard (e.g. MNI 152) space to assess the anatomical profile of alterations in DTI metrics between groups.
12. Region-of-interest analysis is performed to characterise the anatomical extent and statistical significance of the differences between groups. A series of tract-specific masks were applied to the corrected whole brain results. White matter structures were selected from a probabilistic atlas (Mori et al., 2004), and to adjust for anatomical variability of the tract thresholded at a likelihood of over-lap across individuals of 20%, this moderately stringent threshold is also likely to reduce contamination within regions-of-interest by reducing partial volume effects and erroneous inclusion of grey matter. This figure was chosen following a review of varying thresholds. This threshold was deemed to be appropriate as it

consistently included core parts of the tract (i.e. provided high anatomical specificity), whilst excluding neighbouring tracts, CSF or grey matter.

13. Information on statistical differences within the mask were explored using the *fslstats* module of FSL which provides information on the number of significant voxels above a certain threshold (FWE-corrected $p<0.05$) and level of significance.
14. The proportion of significantly affected voxels within each tract was calculated by dividing the number of significant voxels identified by the total number of voxels within each tract limited to within the skeleton. The decision to express tract involvement predominantly using this threshold-dependent, extent based measure rather than (for example) a mean diffusivity value across the whole tract was chosen for two reasons: firstly, averaging diffusivity values over tract masks would be strongly influenced by partial volume effects (e.g. inclusion of CSF in the mask) and/or crossing fibres; and secondly, the extent of tract involvement gives an indication of the anatomical distribution of change that is not captured using a mean diffusivity value. Thus by focussing on thresholded extent maps, it is hoped to focus more precisely on disease effects.
15. To assess the anatomical reliability of the results obtained at group level analysis, the results maps were de-projected and overlaid on each individual participant's FA image to confirm good anatomical alignment.
16. Non-FA images (RD, AX, MD and TR) are also analysed using the same steps. All subjects images are transformed to the same MNI 152 space as the FA images using the original nonlinear registration. Steps 3-14 above are then repeated for each diffusion metric.

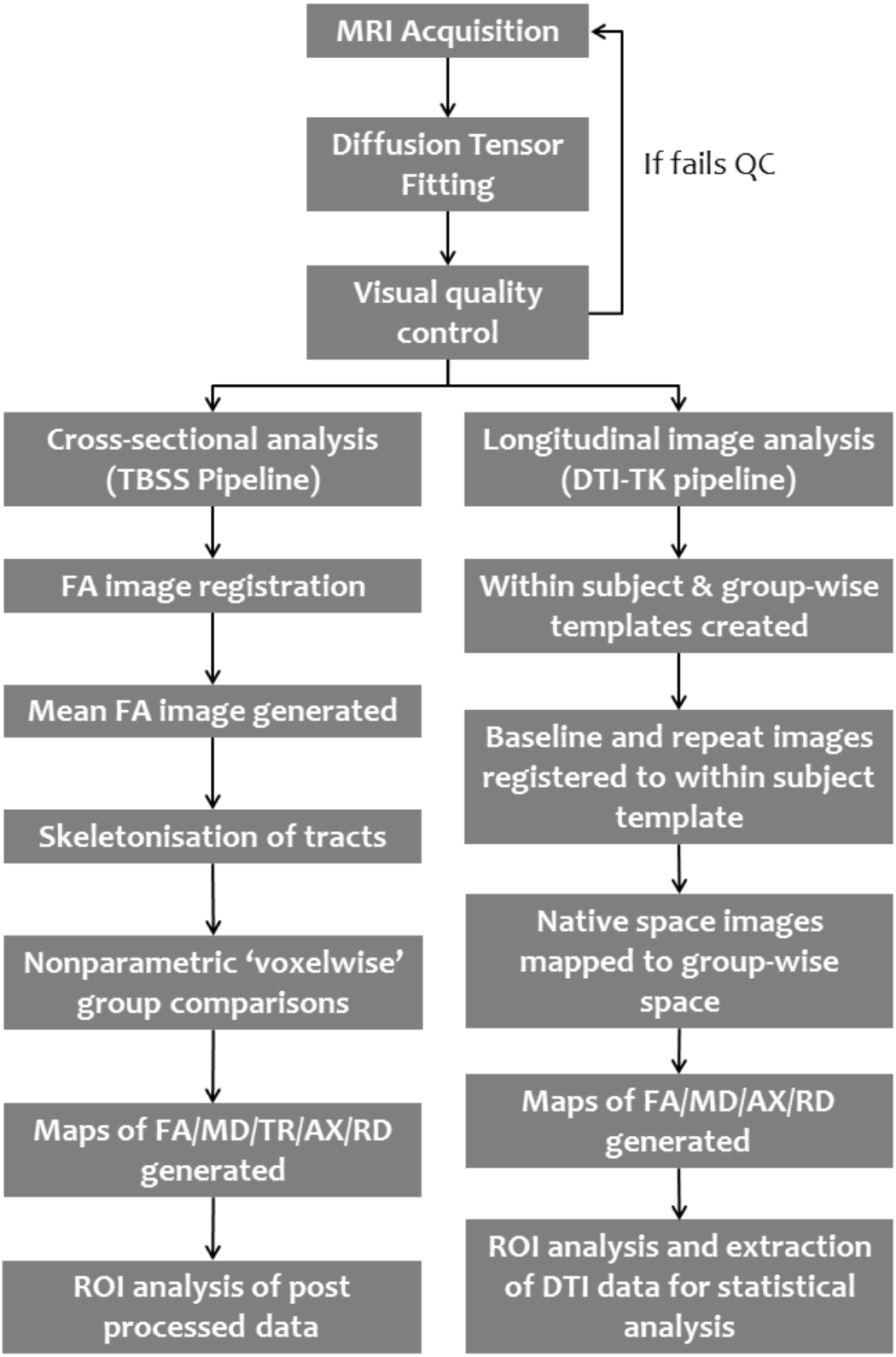

Figure 2.1. Overview of DTI imaging methods used.

2.2.8 Longitudinal DTI image analysis

Chapters 4 and 6 will deal with longitudinal analysis of DTI data, little is known about longitudinal TBSS analysis, and in particular issues surrounding registration of longitudinal data. For this reason an in-house pipeline was developed to deal with longitudinal DTI data. This pipeline primarily uses DTI-TK version 2.2 software package (Zhang et al., 2006), which was specifically developed to deal with DTI registration and has been shown to have the best performance in terms of registration compared to other methods (Wang et al., 2011). Another major factor in choosing this software was that it has good reproducibility between subjects scanned back-to-back as evidence by low variability (Keihaninejad et al., 2013). Unlike registration of volumetric MRI, which is driven by simple scalar measurements, DTI is multidimensional (i.e. multiple tensor orientations), making registration of images more complex. However DTI-TK offers a robust spatial normalisation module ensuring this high dimensionality is maintained during registration of images. DTI-TK allows use of whole tensor information by incorporating tensor orientation and tract similarity measures (rather than using a simple scalar value such as FA) to drive the registration process. An overview of the imaging pipeline can be seen in Figure 2.1 and further step-by-step information on the process is provided below:

1. Images undergo pre-processing as per the description in section 2.5.
2. A within-subject template is generated from baseline and follow-up scanning to avoid interpolation asymmetries from registering follow-up images to baseline, thus avoiding bias towards a particular time point.

3. Baseline and follow-up images are then registered to this average within subject template.
4. A group-wise template is then created from each subject's average image using iterative linear and non-linear registration.
5. Each subject's native space scan is then mapped to the group-wise space by applying a deformation field created by combining the mapping parameters used when creating the within-subject average image and the group-wise image.
6. Maps of each DTI metric for each subject and time-point are created in the group-wise space.
7. To allow a region-of-interest analysis the FA map (in group-wise space) is segmented using locally adaptive tool (LoAd), part of the NiftySeg software package (Cardoso, 2011). A binary mask of white matter tracks was created and matter mater structures were identified using the ICBM-DTI-81 atlas (Mori, 2005).
8. The ICBM-DTI-81 atlas is then linearly and non-linearly registered to the final template FA image.
9. Binary masks of each region-of-interest were generated using a threshold of 50% on the white matter probability map with a further 1mm erosion around the boundary of each mask to provide high anatomical specificity (unless otherwise specified).
10. DTI metric data including mean value and standard deviation are then selected from each region-of-interest.
11. Extracted DTI metric data undergoes statistical analysis comparing rates of change in each group over time.

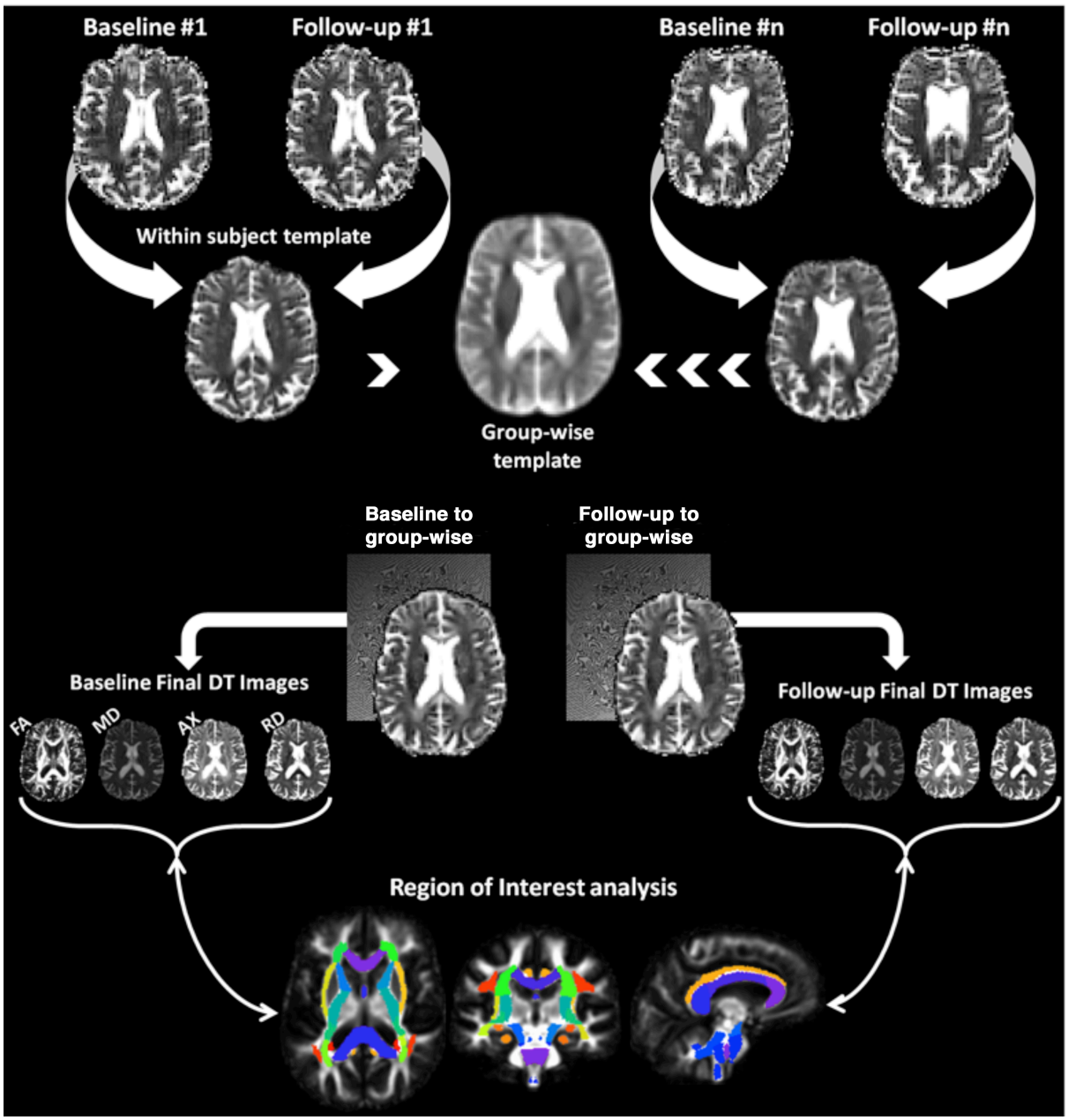

Figure 2.2. Overview of processing pipeline for longitudinal DTI analysis.

3. Cross-sectional profiles of white matter pathology in behavioural variant frontotemporal dementia

3.1 Introduction

Network disintegration in bvFTD has been demonstrated using functional MRI and distributed grey matter changes compatible with network breakdown have been established (Rohrer et al., 2011; Seeley et al., 2009; Whitwell et al., 2005). As mentioned in the introduction the anteriorly directed 'salience' processing network appears to be a key network which shows selective vulnerability in bvFTD (Seeley et al., 2009). Despite a vast literature on functional and volumetric imaging in the area of bvFTD, there remains a paucity of information on the changes occurring within white matter tracts. This is significant as these structures provide the structural connectivity underpinning large-scale brain networks by binding together cortical and subcortical regions. Furthermore, besides common syndromic profiles of network damage there may be distinct neuroanatomical subgroups within the bvFTD spectrum with relative specificity for particular molecular pathologies (Warren et al., 2012). Identifying profiles of white matter tract pathology along molecular lines in bvFTD would both validate the concept of network-led degeneration and potentially allow additional (or more robust) stratification of neuroanatomical subgroups within the bvFTD spectrum that might map more closely onto pathological and genetic substrates.

DTI may allow such white matter tract profiles to be delineated in bvFTD. A particular potential strength of DTI is the generation of multiple quantitative metrics of white

matter alteration (diffusivity) during a single acquisition. The neurobiological significance of these metrics remains relatively little explored, particular in bvFTD, and whilst fractional anisotropy (FA) is the most widely cited metric, more recent studies have suggested that use of the individual parameters of diffusion may be more appropriate in neurodegeneration (Acosta-Cabronero et al., 2010). The primary aim of this chapter is to apply DTI as a means of characterising profiles of white matter tract pathology cross-sectionally, in a clinically and molecularly characterised cohort of patients with bvFTD. Secondly this study aims to explore and compare multiple DTI metrics to establish if particular metrics are more suited than others in the detection of white matter tract pathology in this clinical cohort.

3.2 Previous studies using DTI in bvFTD

Whilst the number of studies using DTI to study bvFTD remains comparatively small in comparison to other imaging methods, there have been a number of previous studies (see Table 3.1), and there is increasing evidence pointing to several tracts, which appear to be selectively vulnerable in those with bvFTD.

To our knowledge Borroni and colleagues carried out the first study of white matter alterations in bvFTD in 2007. Compared with cognitively normal individuals they identified reduced FA in the superior longitudinal fasciculus in '*frontal variant*' bvFTD and reduced FA in the inferior longitudinal fasciculus in '*temporal variant*' bvFTD (Borroni et al., 2007). Although this was a well-powered study it did not attempt robust DTI registration, it is also unclear how the sub-groups were defined, as if defined on imaging grounds this

could lead to some circularity in the findings. A number of other studies followed, which identified further pathological changes within corpus callosum, as well as the uncinate fasciculus and inferior longitudinal fasciculus. (Matsuo et al., 2008). Two further studies shortly after this began to report changes in other DTI metrics, including AX, RD and MD, highlighting their sensitivity in detecting pathological changes in bvFTD (Whitwell et al., 2010; Zhang et al., 2009). These studies identified pathological changes in uncinate fasciculus and anterior cingulum across a number of different DTI metrics. Furthermore these studies also suggested that some DTI metrics such as RD might be more sensitive than others, identifying a wider anatomical profile of pathology compared to more traditional metrics such as FA. Zhang and colleagues also reported the first profiles of white matter pathology comparing bvFTD with Alzheimer's patients, with those in the bvFTD having significantly reduced FA values in frontal white matter (Zhang et al., 2009). Until the advent of TBSS there had been a number of issues with the registration of white matter tracts to one-another, potentially creating a bias in reporting of results. TBSS has increasingly become established as a key methodology for group-level DTI studies, and at the time of writing this has been citied in over 300 publications as a methodology of choice, across a range of disorders from neurodegenerative conditions to neuro-inflammatory, psychiatric disorders and neonatal brain disorders. This robustness was a major factor in the decision to use this pipeline for this cross-sectional study. The first study of white matter in bvFTD using TBSS was published in 2011 and like the previous studies showed the most striking changes in white matter tracts occurred within the uncinate fasciculus, corpus callosum and cingulum as well as the parahippocampus (Agosta et al., 2011). This study additionally revealed that white matter changes were

very extensive, occurring in posterior regions, often thought more consistent with Alzheimer's disease (Acosta-Cabronero et al., 2010), and extending beyond the limit of maximal grey matter atrophy. More recent studies have attempted to study a broader clinical phenotype including patients within the motor-neuron disease spectrum, which overlaps with bvFTD (Lillo et al., 2012), as well as attempting to improve the methodologies to make better comparisons between white matter and grey matter changes (Zhang et al., 2013).

Table 3.1 highlights publications in this area, but it is important to point out limitations in these previous studies. Firstly, the study participants, many of the inclusion criteria used to select patients use earlier classification criteria which do not state that there must be biomarker evidence of neurodegeneration, meaning that patients with the so-called phenocopy syndrome (Kipps et al., 2010) or psychiatric diagnosis may have been included. Furthermore each study fails to include individuals with molecularly defined syndromes, i.e. those with genetic or pathological confirmation of diagnosis. Imaging methods are also sub-optimal; many early studies use only region-of-interest based approaches to study white matter, which leads to a bias in reporting. Large differences in the degree and area of brain atrophy in bvFTD may result in misalignment between structures during registration, making it difficult to ensure accurate comparisons between structures. Previous TBSS studies may also suffer with excessive warping between subjects given this wide variability in brain morphology.

The aim of this study is to establish if clinically and molecular defined profiles of white matter pathology occur. To establish this hypothesis the current study will also address many of these limitations of previous studies by improving on selection criteria, having higher quality DTI acquisitions (in this case using 64 directions and back-to-back acquisitions to improve signal-to-noise), using a state-of-the art image registration pipeline to minimise issues surrounding the neuroimaging heterogenitiy of bvFTD and to apply a more robust approach to statistical analysis.

Study	Participants	MRI acquisition	Software	Tract selection	Statistical method	Tracts
Borroni et al., 2007	36 FTD	1.5 Tesla 6 Directions	BrainVisa, SPM2	White matter mask	Linear regression	SLF, ILF
Matsuo et al., 2008	12 FTD 17 Controls	1.5 Tesla 15 directions	PRIDE	ROI	Mann-Whitney U	AF, UF, ILF, CC
Zhang et al., 2009	18 FTD 18 AD 19 Controls	4 Tesla 6 directions	Volume-one/dTV	Whole brain, ROI	MANOVA/ Multiple regression	Anterior CC, UF, anterior/ descending / left posterior CB
Whitwell et al., 2010	16 FTD 19 Controls	3 Tesla 21 directions	DTI Studio	ROI	ANCOVA	Anterior CB, UF, SLF, right anterior ILF, right CST
Agosta et al., 2011	13 FTD 25 Controls	3 Tesla 32 directions	FDT/ TBSS	Whole brain, ROI	Permutation test (n=5000)	CB, Fornix, CC, SLF, UF, ILF, Parahippocampus
Lillo et al., 2012	15 FTD 18 Controls	3 Tesla 32 directions	FDT/ TBSS	Whole brain	Permutation test (n=5000)	Anterior CC, anterior ILF, CST
Zhang et al., 2013	13 FTD 19 Controls	4 Tesla 6 directions	SPM8	Whole brain, ROI	Two-sample t-test	UF, anterior CC
Present study	27 FTD 25 AD 20 Controls	3 Tesla 64 directions	Camino/ TBSS	Whole brain, ROI	Permutation test (n=10000)	UF, CB, CC, SLF, ILF, ATR, CST

Table 3.1 Comparison of fractional anisotropy changes in studies of frontotemporal dementia using diffusion tensor imaging. Tracts listed are bilateral unless otherwise stated. A statistical threshold of p <0.05 was used for citing tracts with significant change from individual papers.

3.3 Methods

Twenty-seven consecutive patients who fulfilled a diagnosis of probable or definite bvFTD based on current consensus criteria were recruited from the Specialist Cognitive Disorders Clinic at the National Hospital for Neurology and Neurosurgery. The bvFTD cohort included 14 patients with either neuropathologic confirmation or pathogenic mutations in the *MAPT* or *C9ORF72* genes. Twenty healthy controls and 25 patients with a diagnosis of probable AD (Dubois et al., 2007) also participated. Participants underwent a structured clinical and neuropsychological assessment (see section 2.1.2. for details) and MRI to exclude significant vascular disease or other focal cerebral lesions. Demographic and neuropsychological data were analysed in STATA12® (Statacorp) using Student's *t* test and Wilcoxon rank-sum tests of statistical significance.

All 27 patients were asked to contribute a DNA sample for genetic analysis; one patient declined and one patient later withdrew consent for testing; neither of these patients had a family history and were therefore considered to have sporadic disease. The remaining 25 patients underwent genetic sequencing of *MAPT, PGRN or C9ORF72* and other genes as previously specified (see section 2.1.3. for details)

All subjects underwent MRI acquisition with both volumetric and diffusion weighted imaging acquired and underwent pre-processing as specified previously (see section chapter 2, section 2.2.1 for details on image acquisition). As there is significant heterogeneity in the imaging phenotype of bvFTD (i.e. some have right temporal lobe atrophy, some have frontal lobe, some have only minimal atrophy) an additional

processing step was applied to the DTI data acquired for this study. The aim of this step was to improve the quality of the registration and reduce the effects of atrophy-related distortion in registering and projecting to a common white matter skeleton. The creation of this group-wise skeleton followed a previously published pipeline which can be incorporated as part of the existing TBSS pipeline (Keihaninejad et al., 2012). This methodology aims to improve the quality of image registration in neurodegenerative conditions by minimising the effects of stretch and distortion seen when attempting to warp a brain affected by significant neurodegeneration onto the standard FMRIB58 image (which is based on 58 scans of healthy individuals aged 20-50 years). It also reduces image distortion in regions affected by severe atrophy and provides greater detail on more distal sections of white matter tracts compared with the standard TBSS pipeline (compare images generated using this customised method versus standard TBSS in Figure 3.1). The volumetric images were analysed within SPM using the DARTEL module, which also uses a group-wise template to minimise the image distortions as outlined above.

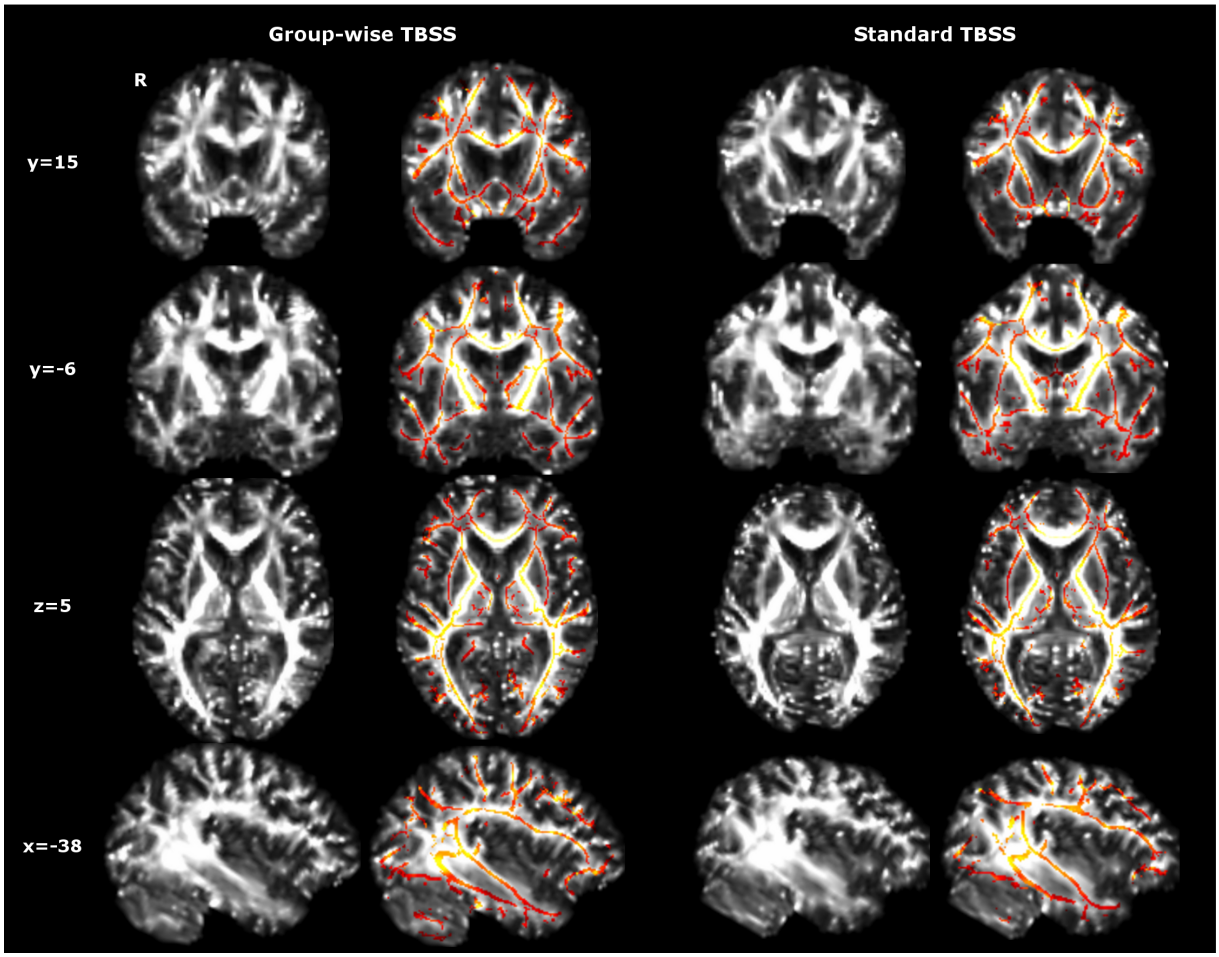

Figure 3.1 Comparison of customised 'group-wise' TBSS image pipeline (left) with standard TBSS pipeline (right) performed on the same single participant. Images reflect single participant fractional anisotropy volume registered to the group-wise template on left and FMRIB58 template on right. The participant's white matter skeleton is overlaid (red-yellow) on right of each panel. Spatial coordinates of the plane of each section are indicated on the left of the figure.

To assess disease effects on white matter structures a general linear model was created with disease group membership as the factor of interest and age, gender, and disease duration included as nuisance covariates. Each metric (AX/RD/TR/FA) was analysed with the above model, and additionally with a model that included the overall mean of the metric under study as an additional covariate. The latter model reveals areas that are specifically affected after adjusting for widespread global differences, analogous to controlling for total grey matter volume in voxel-based morphometry (Mechelli et al.,

2005). Models were contrasted with both healthy and disease control groups. A genetic subgroup analysis was performed comparing *MAPT* and *C9ORF72* mutation groups with healthy individuals, the AD disease group and with each other using the same model design. Statistical analyses were carried out as specified previously (see section 2.6. for details). Significant results were projected onto a study-specific average brain registered to standard (MNI) space. To provide accurate anatomic localisation a series of tract-specific masks were applied to the significant whole brain results using a probabilistic atlas (Mori et al., 2004), and chosen based on *apriori* hypothesis of involvement or previously published imaging data. A total of 14 binary masks were created, covering major white matter pathways including right and left inferior longitudinal fasciculus (ILF), superior longitudinal fasciculus (SLF), uncinate fasciculus (UF), anterior thalamic radiation (ATR), cingulum bundle (CB), corticospinal tract (CST), corpus callosum (CC), and fornix. To adjust for the anatomical variability additional masking of tracts was carried out as previously specified and data from each masked tract extracted for analysis (see section 2.6).

To determine the sensitivity and specificity of different DTI metrics in classifying individual participants into separate groups (bvFTD/healthy individual/AD) receiver operating characteristic (ROC) curves were constructed and areas-under-curve (AUC) were calculated. Two approaches were used for the classification, assessing respectively the mean of each individual metric (FA, AX, RD, MD) across the whole white matter skeleton and the mean values within individual tracts identified as prominently involved in the initial DTI analysis. Mean values were extracted using the '*fslmeants*' command.

ROC curves and AUC values were calculated for both global and individual tract diffusivity data.

3.4 Results

3.4.1 Participant clinical characteristics

Subjects' demographics, clinical and neuropsychological characteristics are detailed in table 3.2. 27 patients with bvFTD were identified (mean age 62.5 ± 9.0 years; male=20); 14 met criteria for a diagnosis of definite bvFTD, and 13 met criteria for a diagnosis of probable bvFTD (Rascovsky et al., 2011). Of those with definite bvFTD nine had mutations in the *MAPT* gene (five harboured the intron 10 +16 mutation, two harboured the exon 13 R406W mutation, one harboured the exon 10 P301S mutation and one harboured a novel mutation in exon 12 resulting in a single amino acid substitution at codon 351 (Q351R)), four had mutations in *C9ORF72* and one patient who subsequently died was found to have Pick's disease pathology at post-mortem. In addition to meeting diagnostic criteria for bvFTD, 2 patients had symptoms compatible with Progressive Supranuclear Palsy (both having sporadic bvFTD), 2 had symptoms compatible with motor neuron disease (one having a *C9ORF72* mutation, one being sporadic) and 1 had symptoms compatible with corticobasal syndrome (being sporadic).

Characteristic	BvFTD n=27 (M20:F7)		AD n=25 (M17:F=8)		Controls n=20 (M13: F7)		Group comparisons: p-value		
	Mean	*SD*	Mean	*SD*	Mean	*SD*	bvFTD v Control	bvFTD v AD	AD v Control
Clinical									
Age all subjects (years) *Sporadic* *MAPT* *C9ORF72*	62.5 64.9 58.2 64.1	9.0 8.6 9.0 8.7	63.1	5.2	64.5	4.5	ns	ns	ns
MMSE (/30)	24.2	5.9	20.0	5.1	29.6	0.6	**<0.001**	**<0.01**	**<0.001**
Duration all subjects (years) *Sporadic* *MAPT* *C9ORF72*	6.5 6.0 6.0 9.4	4.9 4.4 5.4 5.9	5.7	3.4	-	-	-	ns	-
CSF (bvFTD n=13, AD n=11) Total Tau (pg/ml) Abeta1-42 (pg/ml)	 287 676	 141 281	 833 240	 229 73					
Neuropsychological*									
VIQ	81.2	23.4	90.6	19.4	123.3	9.6	**<0.001**	ns	**<0.001**
PIQ	88.6	19.1	83.3	18.7	118.1	10.9	**<0.001**	ns	**<0.001**
Recognition Memory: Words (/50)	33.3	10.1	29.4	7.8	48.1	2.3	**<0.001**	0.08	**<0.001**
Recognition Memory : Faces (/50)	32.8	6.8	33.7	6.3	41.9	4.7	**<0.001**	ns	**<0.001**
Digit Span: Forward(/12)	7.1	2.2	6.3	2.2	9.1	1.4	**0.002**	ns	**<0.001**
Digit Span: Reverse(/12)	5.5	2.7	4.3	3.0	6.8	1.8	ns	0.09	**0.002**
BPVS (/150)	116.5	38.0	132.5	24.3	147.9	1.5	**<0.001**	**0.02**	**<0.001**
Graded Naming Test (/30)	10.8	9.1	13.9	8.4	26.0	2.1	**<0.001**	ns	**<0.001**
Graded Arithmetic Test (/24)	12.1	6.9	5.3	4.0	14.1	5.4	0.4	**<0.001**	**<0.001**
VOSP (/20)	15.7	3.2	15.0	3.3	18.8	1.1	**<0.001**	ns	**<0.001**
DKEFS : Colour Naming (max 90 secs)	45.6	22.9	55.0	18.7	31.2	4.7	**0.03**	**0.03**	**<0.001**
DKEFS: Word Naming (max 90 secs)	35.1	23.6	36.6	15.3	21.5	3.4	**0.02**	**0.1**	**<0.001**
DKEFS: Ink Naming (max 180 secs)	100.4	48.4	141.0	44.0	56.8	11.5	**<0.001**	**0.003**	**<0.001**

Table 3.2 Summary of demographic, clinical and neuropsychological data for all groups. Group comparisons significant at p<0.05 are shown in bold. *neuropsychological data not collected for one patient with bvFTD and two patients with AD.

All AD patients had a typical memory-led presentation. The healthy control and AD groups were comparable in age and gender characteristics (healthy control group mean age 64.5 ± 4.5 years, male=13/20; AD group mean age 63.1 ±5.2 years; male=17/25). CSF data was available on 13/27 bvFTD patients; all had profiles compatible with non-Alzheimer's pathology (normal Abeta1-42 and normal or elevated total tau), although one subject had low Abeta1-42 and low/normal tau, which was felt to be consistent with a handling error. CSF data was available on 11/25 AD patients; all had profiles compatible with AD pathology (low Abeta1-42, elevated total tau). A detailed general neuropsychological assessment was completed in 69/72 participants (one patient with bvFTD and two with AD were unable to comply with testing). Profiles of performance in the patient groups were in keeping with clinical syndromes: both disease groups showed widespread deficits compared with the healthy control group, however the AD group performed inferiorly to the bvFTD group on tests of arithmetic and general executive capacity while the bvFTD group performed inferiorly to the AD group on tests of semantic processing.

3.4.2 Signatures of white matter pathology in bvFTD

Widespread white matter tract pathology was identified in the bvFTD group compared with both the healthy control group and the AD group (Figures 3.2 and 3.3).

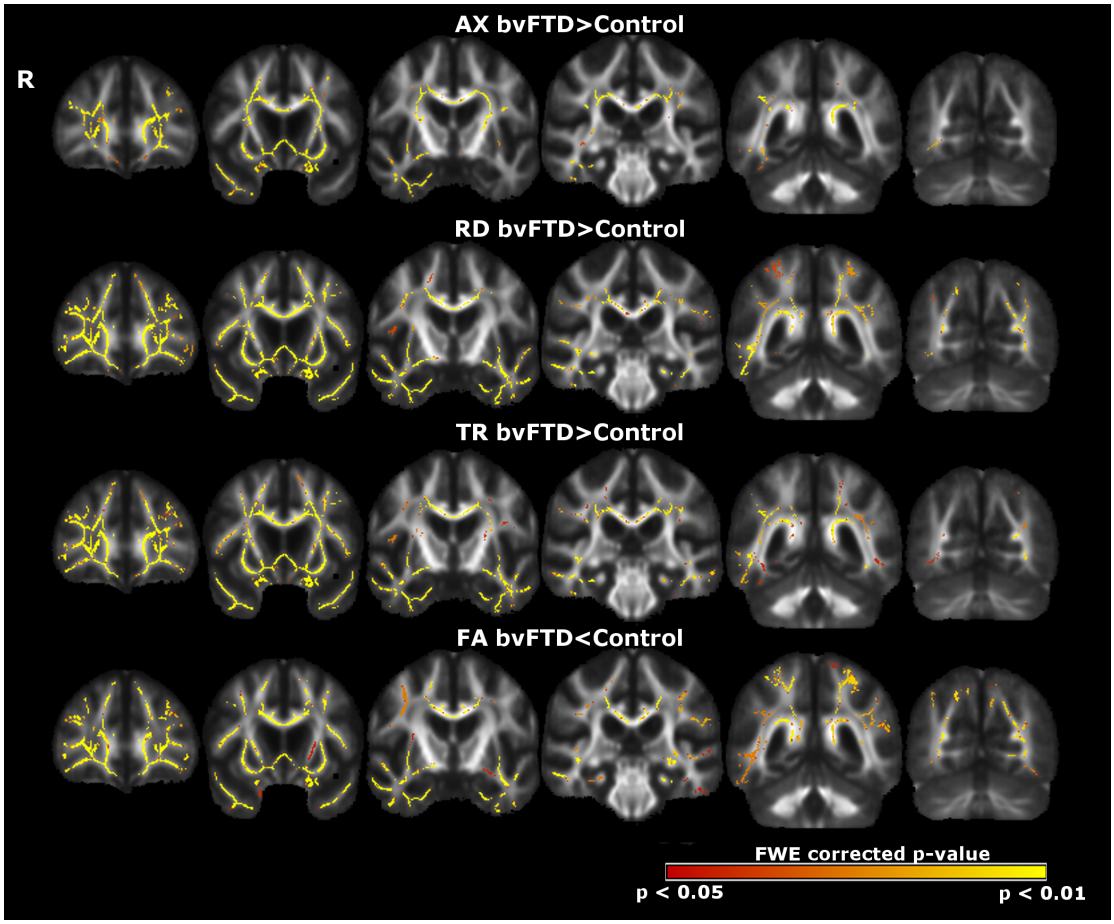

Figure 3.2 Unadjusted white matter tract data: Patterns of white matter alteration in the bvFTD group compared with healthy participants. Right (R) hemisphere is shown on the left. The colour scale indexes p-values after family-wise error correction for multiple comparisons over the whole brain.

Data without correction for global DTI metric effects are first reported, in order to present a complete picture of white matter tract alterations. Data after global DTI metric correction is then reported, identifying white matter pathology with greater anatomical specificity. Uncorrected data quantifying the extent and significance of

differences within white matter tracts compared with healthy controls and AD are listed in tables 3.3 and 3.4 (ordered by % of tract involved) and in figures 3.2 and 3.3 respectively.

RD bvFTD>Controls				TR bvFTD>Controls			
Tract	p-value	Voxels	% Voxels	Tract	p-value	Voxels	% Voxels
R UF	0.001	390	99.5	R UF	0.002	389	99.2
L UF	0.002	623	95.3	L UF	0.002	605	92.5
R CB	0.003	151	82.5	R CB	0.01	121	66.1
L CB	0.004	634	74.8	CC	0.005	9818	66
CC	0.004	9700	65.2	L CB	0.007	525	61.9
L ILF	0.01	1069	40.6	L ILF	0.01	1093	41.5
R SLF	0.02	899	37.8	R ILF	0.02	750	40.3
R ILF	0.007	542	29.1	R SLF	0.01	845	35.5
L SLF	0.02	751	27.6	L SLF	0.03	882	32.4
R ATR	0.004	316	25.5	L ATR	0.003	395	25.3
L ATR	0.003	389	24.9	R ATR	0.003	313	25.2
Fornix	0.001	112	20	Fornix	0.001	112	20
R CST	0.01	213	3.2	R CST	0.02	269	4
L CST	0.006	94	1.3	L CST	0.008	197	2.7
AX bvFTD>Controls				**FA bvFTD<Controls**			
Tract	p-value	Voxels	% Voxels	Tract	p-value	Voxels	% Voxels
R UF	0.004	269	68.6	R UF	0.003	349	89
L UF	0.002	407	62.2	R CB	0.007	152	83.1
CC	0.006	6717	45.1	L CB	0.004	669	78.9
R ILF	0.01	580	31.1	L UF	0.003	500	76.5
R SLF	0.008	598	25.1	CC	0.005	9470	63.6
R CB	0.01	45	24.6	R SLF	0.03	893	37.5
R ATR	0.007	271	21.9	L ILF	0.01	875	33.2
L ATR	0.004	331	21.2	L SLF	0.02	784	28.8
Fornix	0.002	112	20	R ILF	0.01	490	26.3
L CB	0.009	141	16.6	L ATR	0.01	306	19.6
L SLF	0.01	262	9.6	R ATR	0.008	219	17.7
R CST	0.005	316	4.7	R CST	0.008	343	5.1
L CST	0.006	293	4	L CST	0.009	171	2.3

Table 3.3 Summary of unadjusted diffusivity data by diffusivity metric and region of interest comparing bvFTD with healthy controls. Results are ordered by % of tract involvement.

Corrected data comparing bvFTD with controls and AD are reported in tables 3.5 and 3.6 and figures 3.4 and 3.5 respectively.

Compared with the healthy control group (see figure 3.2 and table 3.3), the bvFTD group showed most significant and consistent white matter pathology across DTI metrics (increased AX/RD/TR, decreased FA in bvFTD) in bilateral uncinate fasciculus, cingulum bundle, corpus callosum, and somewhat less prominently in SLF, ILF, ATR and fornix. Comparing DTI metrics, the most extensive white matter damage (% of significant voxels within a white matter tract) was detected in right uncinate fasciculus using TR and RD.

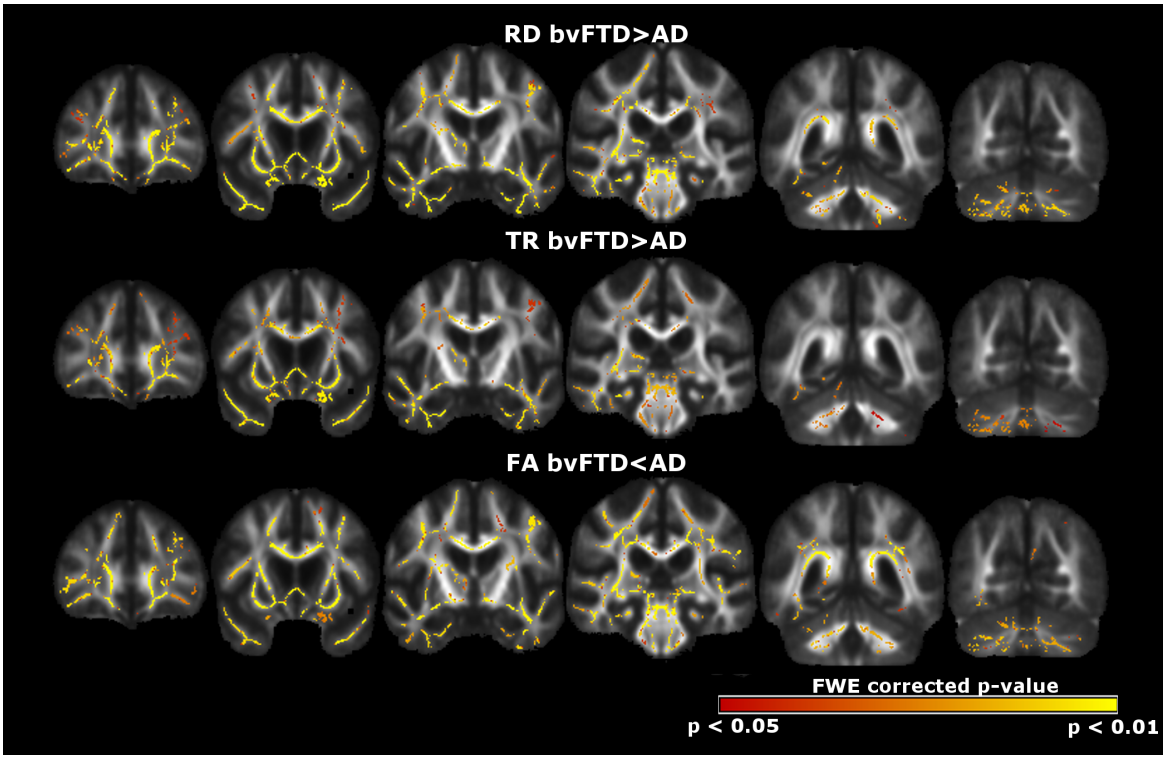

Figure 3.3 Unadjusted white matter tract data: Patterns of white matter alteration in the bvFTD group compared with the AD group. Right hemisphere is shown on the left. The colour scale indexes p-values after family-wise error correction for multiple comparisons over the whole brain.

Compared with the AD group (see figure 3.3 and table 3.4), the bvFTD group again showed most significant and consistent white matter pathology across metrics (increased RD/TR, decreased FA in bvFTD) in bilateral uncinate fasciculus, cingulum bundle and corpus callosum, and somewhat less prominently in superior longitudinal fasciculus, inferior longitudinal fasciculus, anterior thalamic radiation and fornix; comparing DTI metrics, comparably extensive white matter pathology was detected in right uncinate fasciculus using RD, FA or TR.

The reverse contrasts (increased AX/TR/RD, decreased FA in the healthy control and AD groups) did not identify any areas of significant white matter alteration.

RD bvFTD>AD				TR bvFTD>AD			
Tract	p-value	Voxels	% Voxels	Tract	p-value	Voxels	% Voxels
R UF	0.002	370	94.4	R UF	0.006	338	86.2
L UF	0.003	588	89.9	L UF	0.006	550	84.1
L CB	0.003	524	61.8	R CB	0.008	417	49.2
CC	0.007	7588	51	CC	0.008	74	40.4
R CB	0.003	81	44.3	L ATR	0.02	465	37.5
R ATR	0.01	441	35.6	L CB	0.01	4959	33.3
R ILF	0.008	615	33	R SLF	0.01	593	31.8
R SLF	0.01	647	27.2	R ILF	0.01	454	17.2
Fornix	0.008	124	22.2	R CST	0.04	89	15.9
L ATR	0.01	333	21.3	L SLF	0.01	230	14.7
L ILF	0.007	470	17.8	L ILF	0.02	691	10.3
L SLF	0.03	376	13.8	R ATR	0.03	187	7.9
R CST	0.01	904	13.5	Fornix	0.03	479	6.5
L CST	0.01	604	8.2	L CST	0.04	98	3.6
FA bvFTD<AD				AX bvFTD<AD			
Tract	p-value	Voxels	% Voxels	Tract	p-value	Voxels	% Voxels
R UF	0.004	350	89.3	No significant results			
L UF	0.004	563	86.1				
R CB	0.004	585	69				
L CB	0.006	8908	59.8				
CC	0.004	89	48.6				
R ATR	0.009	1054	44.3				
R SLF	0.01	777	41.7				
L CST	0.01	1023	37.6				
L ATR	0.01	412	33.2				
R ILF	0.01	661	25.1				
L SLF	0.01	345	22.1				
L ILF	0.007	1070	15.9				
Fornix	0.01	911	12.4				

Table 3.4 Summary of unadjusted diffusivity data by diffusivity metric and region of interest comparing bvFTD with Alzheimer's disease. Results are ordered by % of tract involvement.

3.4.3 Results following adjustment for global diffusivity

After correction for the effects of global mean diffusivity values, more focal profiles of white matter alteration emerged.

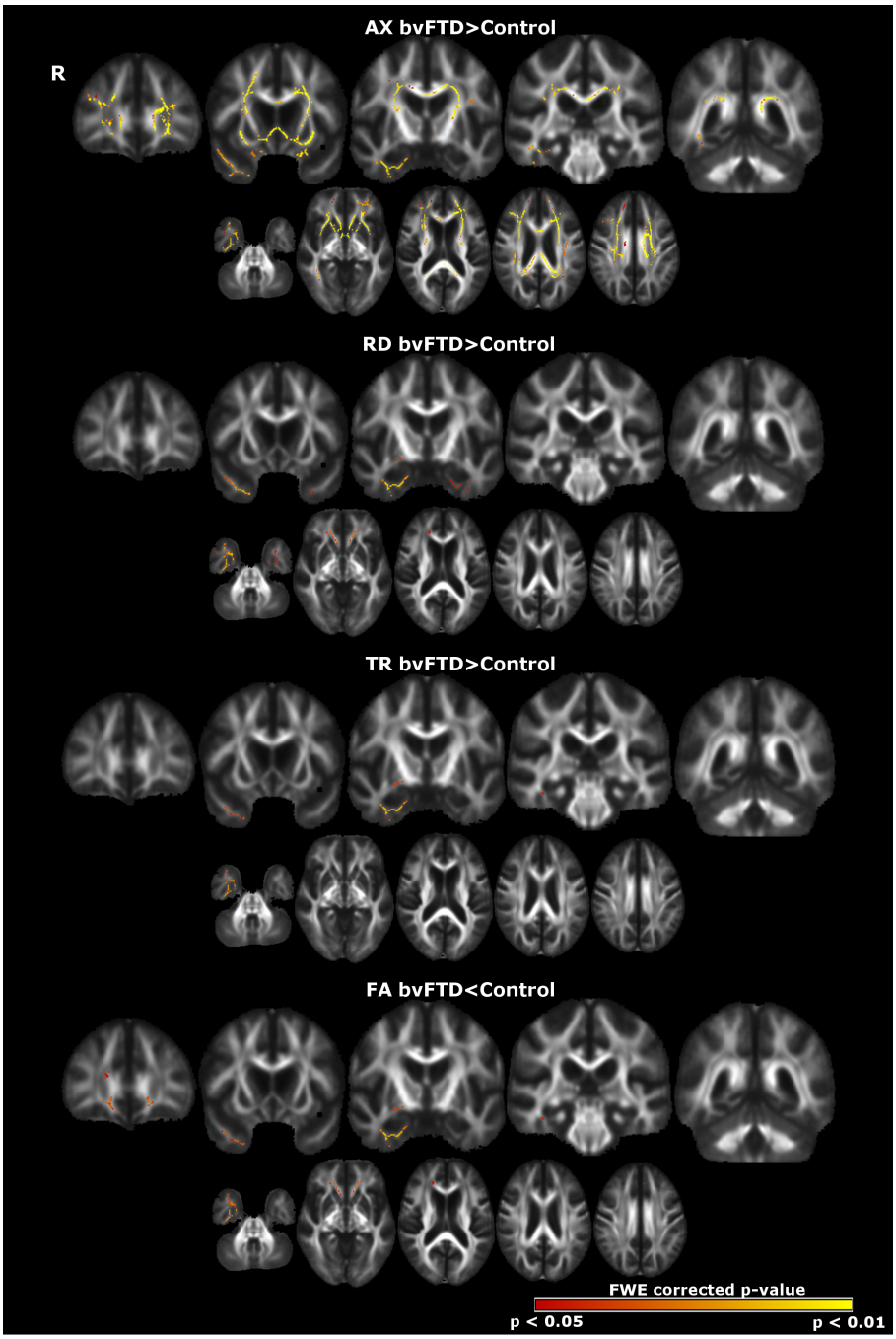

Figure 3.4 Adjusted white matter tract data: Patterns of white matter alteration in the bvFTD group compared with the healthy control group after correction for mean global diffusivity value. Results for particular DTI metrics (AX, FA, RD, TR) are shown separately. The colour scale indexes *P* values after family-wise error correction for multiple comparisons over the whole brain

Compared with the healthy control group (see figure, 3.4 and table 3.5), the bvFTD group showed the most significant and consistent (i.e. change in all DTI metrics) white matter tract pathology in right uncinate fasciculus; comparing DTI metrics, the most extensive white matter damage was detected in right uncinate fasciculus using AX.

RD bvFTD>Controls				**TR bvFTD>Controls**			
Tract	p-value	Voxels	% Voxels	Tract	p-value	Voxels	% Voxels
R UF	0.03	17	4.3	R UF	0.03	9	2.3
R ILF	0.03	8	0.4	R ILF	0.04	3	0.2
L UF	0.05	1	0.2				
AX bvFTD>Controls				**FA bvFTD<Controls**			
Tract	p-value	Voxels	% Voxels	Tract	p-value	Voxels	% Voxels
L UF	0.003	379	58	CC	0.04	875	5.9
R UF	0.008	198	50.5	R UF	0.04	17	4.3
CC	0.01	4843	32.5	L UF	0.04	11	1.7
R ILF	0.02	526	28.2	L ATR	0.05	1	0.1
Fornix	0.005	111	19.9				
L ATR	0.007	276	17.7				
R SLF	0.01	385	16.2				
R ATR	0.03	138	11.1				
L CB	0.01	72	8.5				
L SLF	0.02	151	5.6				
R CST	0.01	156	2.3				
L CST	0.01	143	1.9				
R CB	0.05	1	0.5				

Table 3.5 Summary of adjusted diffusivity data by diffusivity metric and region of interest comparing bvFTD with healthy controls after adjustment for global diffusivity. Results are ordered by % of tract involvement.

Compared with the AD group (see figure 3.5 and table 3.6), the bvFTD group showed the most significant and consistent white matter pathology in bilateral uncinate fasciculus; comparing DTI metrics, the most extensive white matter

damage was detected in right uncinate fasciculus using RD followed by TR. Conversely, compared with the bvFTD group, the AD group showed greater white matter damage (increased TR/RD in AD) in posterior left hemispheric white matter tracts (SLF and ILF) (see figure 3.5 and table 3.6); comparing DTI metrics, the most extensive white matter alterations in the AD group compared with bvFTD group were detected in left inferior longitudinal fasciculus using TR.

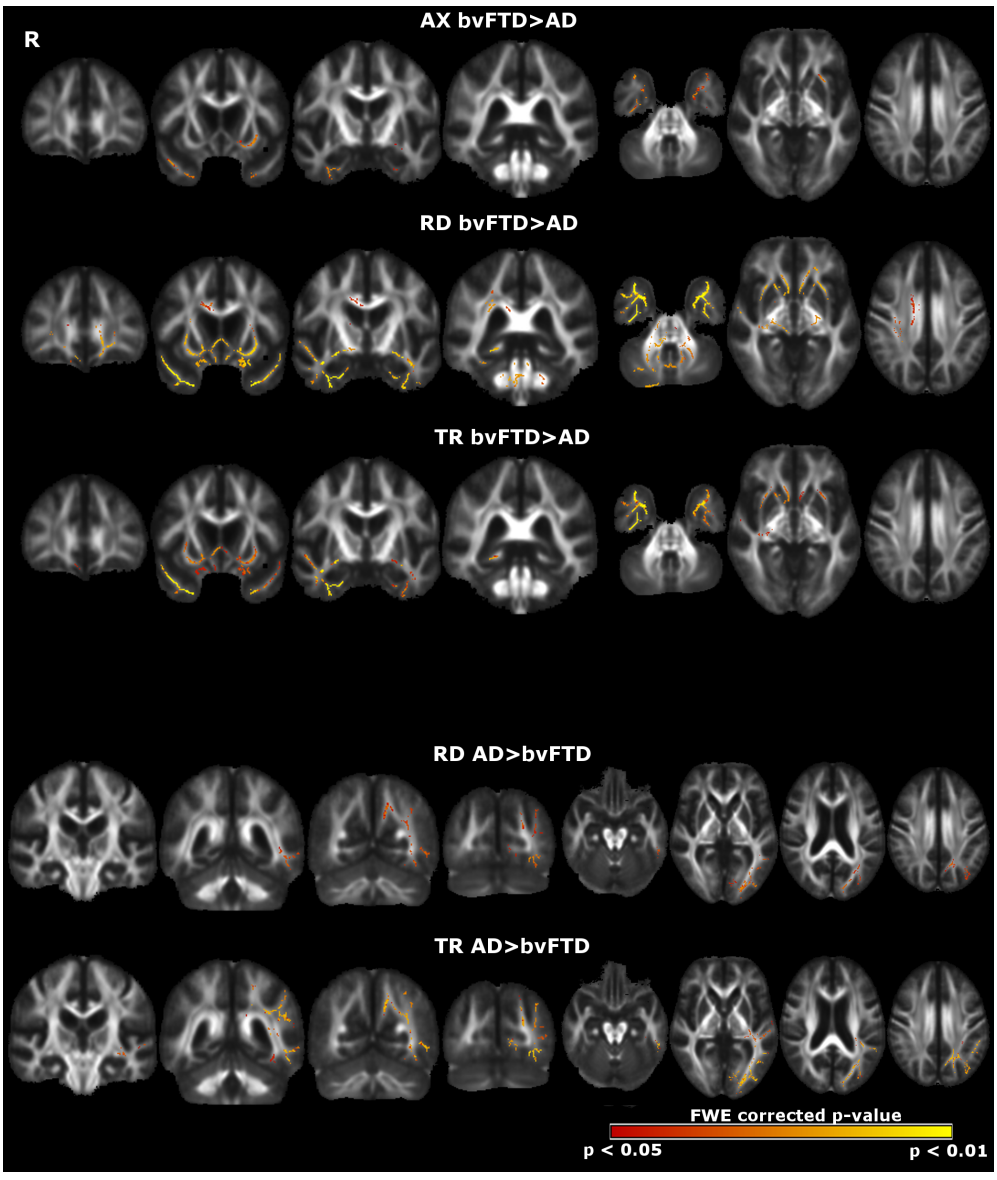

Figure 3.5 Adjusted white matter tract data: Patterns of white matter alteration in the bvFTD group compared with the healthy control group after correction for mean global diffusivity value. Results for particular DTI metrics (AX, FA, RD, TR) are shown separately. The colour scale indexes *P* values after family-wise error correction for multiple comparisons over the whole brain.

RD bvFTD>AD				TR bvFTD>AD			
Tract	p-value	Voxels	% Voxels	Tract	p-value	Voxels	% Voxels
R UF	0.02	263	67.1	R UF	0.02	215	54.8
L UF	0.01	390	59.6	L UF	0.03	237	36.2
R CB	0.04	52	28.4	R ILF	0.02	306	16.4
CC	0.03	1919	12.9	L ILF	0.03	123	4.7
R ATR	0.03	146	11.8	CC	0.03	246	1.7
R ILF	0.01	181	9.7	R CST	0.04	88	1.3
L ILF	0.02	210	8	AX bvFTD>AD			
R CST	0.02	378	5.6	Tract	p-value	Voxels	% Voxels
R SLF	0.03	124	5.2	L UF	0.04	107	16.4
L ATR	0.02	80	5.1	R UF	0.03	13	3.3
L CST	0.02	232	3.2	R ILF	0.02	3	0.2
L CB	0.02	10	1.2	CC	0.05	2	0.01

Table 3.6 Summary of diffusivity data indicating regions of interest with greater white matter pathology in those with bvFTD when compared with Alzheimer's disease), after adjustment for global mean diffusivity. Each DTI metric was contrasted in both directions only results surviving FWE correction p<0.05 are displayed above. Results are ordered by % of tract involvement.

RD AD>bvFTD				TR AD>bvFTD			
Tract	p-value	Voxels	% Voxels	Tract	p-value	Voxels	% Voxels
L ILF	0.03	289	11	L ILF	0.03	736	27.9
L SLF	0.04	87	3.2	L SLF	0.02	524	19.3
CC	0.03	162	1.1	CC	0.02	303	2
				L CB	0.02	10	1.2

Table 3.7 Summary of diffusivity data indicating regions of interest with greater white matter pathology in those with Alzheimer's disease (AD) when compared with bvFTD, after adjustment for global mean diffusivity. Each DTI metric was contrasted in both directions only results surviving FWE correction p<0.05 are displayed above. Results are ordered by % of tract involvement.

3.4.4 White matter tract alterations in bvFTD subgroups

Analyses based on small numbers of cases revealed white matter tract signatures associated with particular genetic subgroups of bvFTD (mutations in *MAPT* versus *C9ORF72*), after global mean value correction (Figure 3.6 and Table 3.7). Compared to the healthy control group, the *MAPT* mutation subgroup showed consistent alterations in left uncinate fasciculus across DTI metrics, albeit highly variable in extent within the tract; the most extensive alterations were detected with AX, which revealed additional involvement of right uncinate fasciculus, corpus callosum, fornix and bilateral inferior longitudinal fasciculus and superior longitudional fasciculus. Compared to the AD group, the *MAPT* mutation subgroup showed altered RD and TR in corticospinal tract, anterior thalamic radiation, inferior longitudinal fasciculus and TR, ILF and uncinate; again, these alterations varied widely in extent between DTI metrics.

Alterations detected in the smaller *C9ORF72* mutation subgroup were less extensive: compared to the healthy control group, the *C9ORF72* mutation cases showed increased AX in corpus callosum and cingulum bundle. On direct comparison of *MAPT* with *C9ORF72* those with *MAPT* showed alterations in white matter within the anterior temporal pole, as measured by reduced FA. Contrasts of *MAPT* and *C9ORF72* mutations subgroups with sporadic bvFTD were examined but did not reach statistical significance.

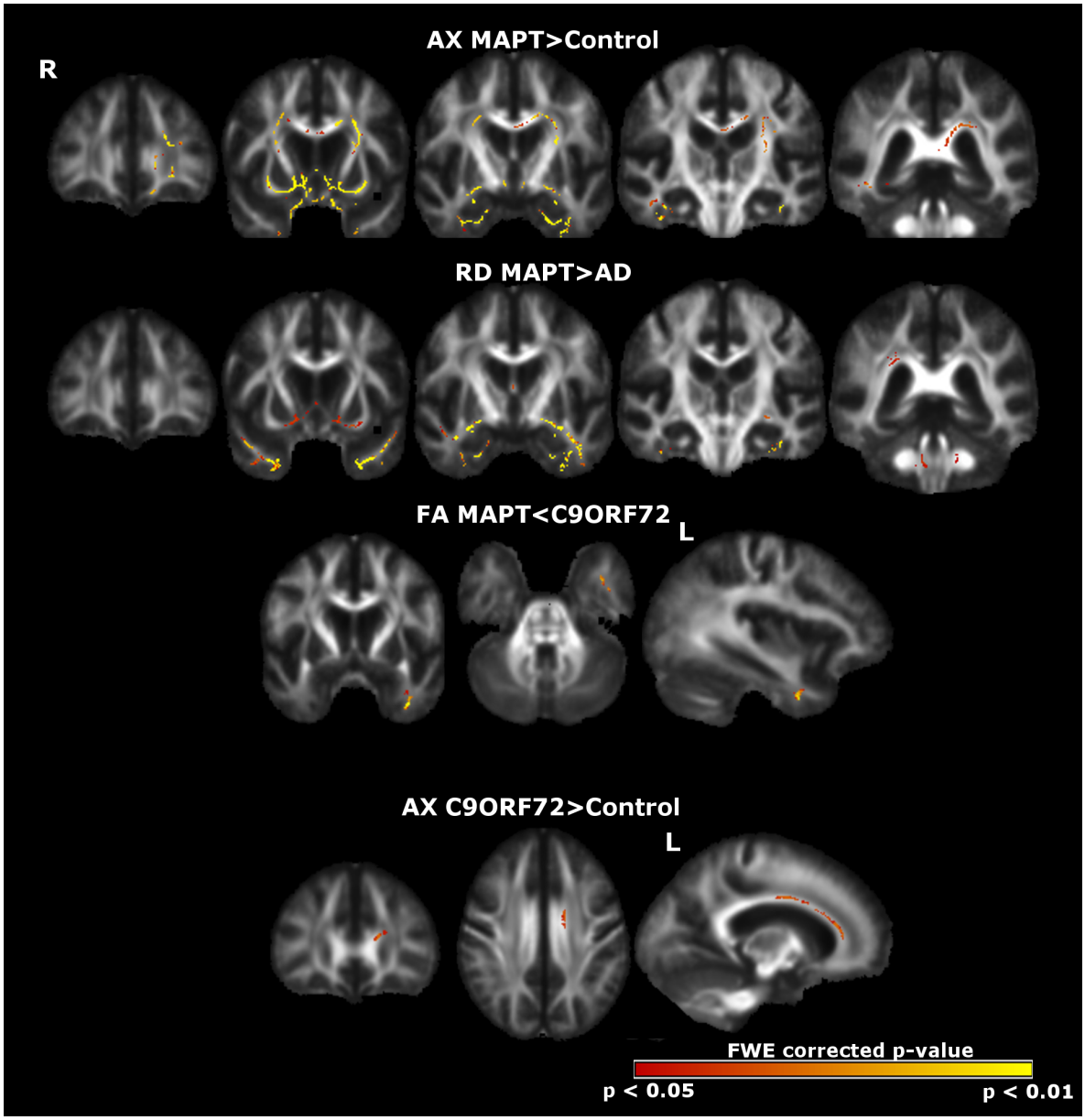

Figure 3.6 Patterns of white matter alteration in the MAPT and C9ORF72 mutation groups compared with the healthy control group and the AD group, after correction for mean global diffusivity value. The colour scale indexes P values after family-wise error correction for multiple comparisons over the whole brain.

MAPT>CONT RD				MAPT>CONT TR			
Tract	p-value	Voxels	%Voxels	Tract	p-value	Voxels	%Voxels
L UF	0.008	53	8.1	L UF	0.009	37	5.7
L ILF	0.01	82	1.6	L ILF	0.01	59	2.2
Fornix	0.05	9	1.6	Fornix	0.04	49	8.8
				CC	0.04	21	0.1
MAPT>CONT AX				**MAPT<CONT FA**			
Tract	p-value	Voxels	%Voxels	Tract	p-value	Voxels	%Voxels
Fornix	0.004	123	22	L UF	0.01	62	9.5
L UF	0.006	275	42	Fornix	0.02	169	30.2
R UF	0.008	180	45.9	L ILF	0.02	130	4.9
L ATR	0.009	140	9	R ATR	0.02	21	1.7
R ATR	0.02	13	1	L ATR	0.02	12	0.8
L CB	0.02	90	10.6				
CC	0.03	2477	16.6				
L CST	0.03	106	1.4				
L SLF	0.03	52	1.9				
L ILF	0.03	13	0.5				
R ILF	0.03	184	9.9				
R CB	0.05	7	3.8				
C9>CONT AX							
Tract		p-value		Voxels		%Voxels	
CC		0.04		278		1.9	
L CB		0.03		32		3.8	
MAPT>AD RD				**MAPT>AD TR**			
Tract	p-value	Voxels	%Voxels	Tract	p-value	Voxels	%Voxels
L ILF	0.02	209	7.9	L ILF	0.02	188	7.1
L UF	0.02	136	20.8	R UF	0.03	105	26.8
R UF	0.03	44	11.2	L UF	0.03	277	42.4
R ILF	0.03	84	4.5	R ILF	0.03	200	10.7
Fornix	0.04	145	25.9	CC	0.04	172	1.2
R ATR	0.04	35	2.8	L ATR	0.05	25	1.6
CC	0.05	92	0.6				
R CST	0.05	11	0.2				
MAPT>AD AX							
Tract		p-value		Voxels		%Voxels	
L ILF		0.04		24		0.9	

Table 3.8 Summary of DTI metrics comparing genetic subgroups with healthy controls and Alzheimer's disease. Data displayed are adjusted for the global mean value of the metric. DTI metric was contrasted in both directions only results surviving FWE correction p<0.05 are displayed above. Results are ordered by % of tract involvement.

3.4.5 Comparison of DTI metrics

Comparing AUC data between DTI metrics (Figure 3.7), whole brain mean RD had the greatest sensitivity (82%) and specificity (80%) for distinguishing the bvFTD group from the healthy control group; TR performed comparably, and AX and FA somewhat less favourably.

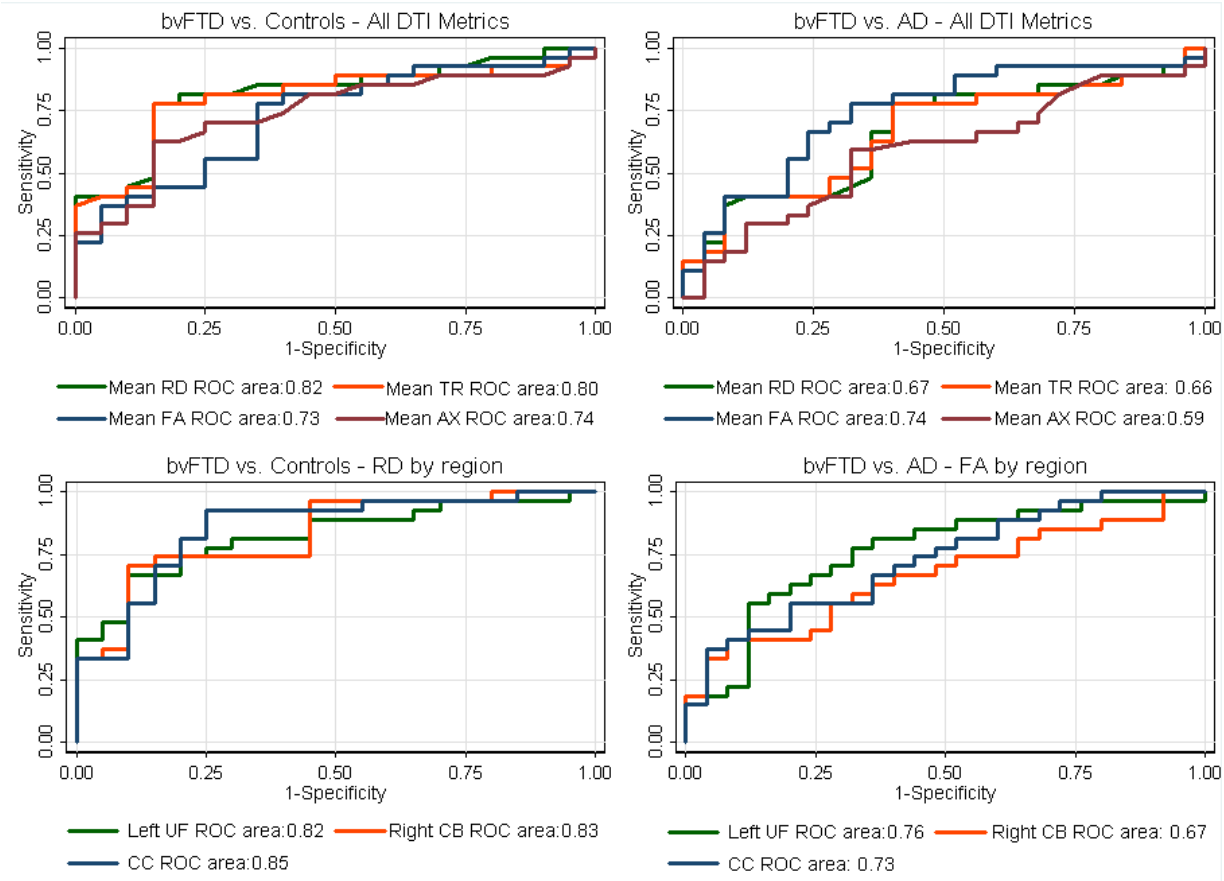

Figure 3.7 ROC curves for classification of individuals to the bvFTD group and healthy control group (left) or AD group (right), based on each participant's global mean diffusivity data (above) and each participant's unadjusted mean diffusivity data within a tract region of interest (below). ROC curves for particular DTI metrics (AX, FA, RD, TR) and white matter tracts of interest (CB, CC, UF) are shown separately; area-under-curve is displayed for each curve (area-under-curve = 1 corresponds to ideal separation of groups).

Comparing specific white matter tracts of interest using mean RD (see Figure 3.7), corpus callosum, left uncinate fasciculus, and left cingulum bundle showed greatest sensitivity (93%, 82% and 74% respectively) and specificity (75%, 75% and 70%

respectively) for distinguishing the bvFTD group from the healthy control group. Whole brain mean FA had the greatest sensitivity (78%) and specificity (68%) for distinguishing the bvFTD group from the AD group (see Figure 3.7); RD, TR and AX performed somewhat less favourably. Comparing specific white matter tracts of interest using mean FA (see Figure 3.7), left uncinate fasciculus showed the greatest sensitivity (77%) and specificity (68%); left cingulum bundle and corpus callosum showed slightly lower sensitivity (63% and 56% respectively) but greater specificity (80% for both).

3.4.6 White matter tract alterations compared with grey matter atrophy

In the VBM analysis, compared with the healthy control group the bvFTD group showed, as anticipated, areas of significantly ($p<0.05$ after whole-brain FWE correction for multiple voxel-wise comparisons with TFCE) reduced grey matter predominantly distributed in frontal and temporal cortices in both cerebral hemispheres (Figure 3.8). Regions of grey matter atrophy included bilateral orbitofrontal cortex, superior and inferior frontal gyri, insular cortex, left cingulate gyrus, bilateral amygdala, right middle and inferior temporal gyri.

The intersection map of DTI metrics with grey matter atrophy in the bvFTD group (Figure 3.8) showed that white matter damage generally occurred in close anatomical proximity to areas of grey matter atrophy, particularly noting the proximity right anterior temporal lobe atropy and white matter tract pathology of the right uncinate fasciculus. However, compared with the distribution of grey matter atrophy overall, white matter tract pathology across DTI metrics was

spatially more extensive, with anatomical involvement of more dorsal and posterior parts of both cerebral hemispheres.

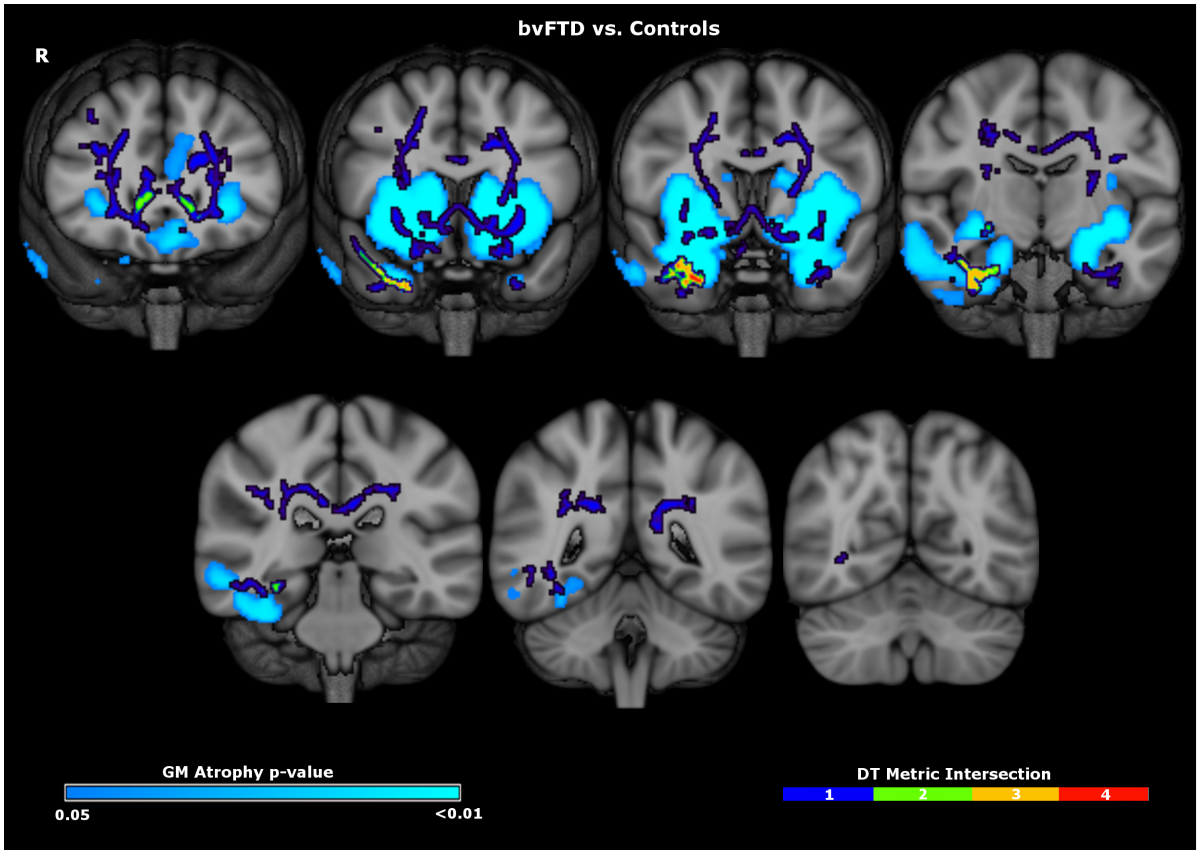

Figure 3.8 Maps of grey matter (GM) atrophy (light blue) and regions of intersection of all four white matter DTI metrics (adjusted for mean global diffusivity value) in the bvFTD group compared with the healthy control group. Maps are overlaid on representative coronal sections of the MNI152 template brain; the right hemisphere (R) is shown on the left. The diffusivity tensor (DT) metric data intersection colour scale indexes the extent of overlap between metrics, i.e. dark blue indicates change in only one metric whereas red indicates change in all four metrics; the GM colour scale indexes *P* values after family-wise error correction for multiple comparisons over the whole brain.

3.5 Discussion

3.5.1 Overview of results

The work presented in this chapter has employed quantitative, state-of-the-art image registration-based DTI methods to demonstrate profiles of white matter tract pathology in a large cohort of patients with bvFTD, representing both major genetic and sporadic disease subtypes. Considering the bvFTD cohort firstly as a whole, white matter changes in comparison to healthy controls were extensive, distributed in both cerebral hemispheres with particularly prominent involvement of the uncinate fasciculus, cingulum bundle and corpus callosum. This white matter profile was identified after taking disease severity into account; moreover, a similar emphasis of white matter tract alterations was identified when the bvFTD group was compared with the AD group, suggesting that involvement of these tracts may be a relatively specific index of pathologies in the bvFTD spectrum. Adjusting for the effects of global mean diffusivity further consolidated the findings: after global adjustment, involvement of uncinate fasciculus was a prominent and consistent indicator of bvFTD pathology compared both with healthy individuals and patients with AD.

These findings further build upon those studies listed in table 3.1 and further extend our knowledge of the role of white matter pathology in bvFTD. Comparing tract profiles in the present study with those performed previously it is of note that the uncinate fasciculus, corpus callosum, inferior longitudinal fasciculus and cingulum bundle appeared consistently involved. However, the extent of reported white matter pathway involvement has varied considerably between studies. The

extensive profile of white matter alterations demonstrated here may be in part attributable to the use of a customised white matter template as well as the comparatively large cohort, which is likely to have sampled a range of underlying pathologies within the bvFTD spectrum.

3.5.2 Neurobiological relevance of profiles of white matter pathology

The white matter pathways delineated here are plausible candidates to mediate brain network dysfunction and the most prominently involved tracts have previously been correlated with a range of cognitive deficits in the bvFTD syndrome (Tartaglia et al., 2012). The uncinate fasciculus has been associated with a range of cognitive functions and recently has been particularly implicated in the evaluation of affective and other inter-personal signals (Von Der Heide et al., 2013), and in the pathogenesis of neuropsychiatric symptoms (Phan et al., 2009) and risk-taking behaviours (Linke et al., 2013): such processes are likely to be relevant to various canonical features of bvFTD (Rascovsky et al., 2011). The uncinate fasciculus has also been directly implicated in the modulation of inhibition in patients with bvFTD (Hornberger et al., 2011). The cingulum bundle is intimately associated with cingulate cortex, previously identified as a key component of the 'salience network', breakdown of which has been implicated in the pathogenesis of the bvFTD syndrome (Kim et al., 2012; Seeley et al., 2009; Zhou et al., 2012). The cingulum bundle has also been implicated in the pathogenesis of obsessive–compulsive symptoms and executive dysfunction (Bora et al., 2011; Linke et al., 2013). The corpus callosum is the major commissure integrating right and left

hemispheric cognitive processes. Damage to the corpus callosum has been linked to a range of abnormal social behaviours (van der Knaap and van der Ham, 2011) and may lead to disconnection between brain regions which integrate semantic knowledge with emotional meaning impacting on the ability to interpret paralinguistic information and situational context, a common feature in bvFTD (Rankin et al., 2009). The ATR has been linked to aspects of attention and executive function (Andreasen et al., 1996; Schmahmann and Pandya, 2008; Van der Werf et al., 2003) as well as the pathogenesis of autism (Cheon et al., 2011); while the fornix has recently been identified as a key locus of damage in bvFTD (Hornberger et al., 2012). The disease specificity of other white matter tracts identified here, in particular, involvement of the long intra-hemispheric tracts SLF and ILF, is less clear: portions of these tracts were found to be involved more prominently in either bvFTD or AD. This apparent paradox may reflect evolution of pathology across white matter pathways common to the distributed brain networks that are targeted in these different neurodegenerative diseases. Howevr, longitudinal data comparing syndromes and diseases will be required to resolve this.

3.5.3 Molecular considerations

This study further suggests that DTI can delineate molecularly defined profiles of white matter pathology within the broader bvFTD spectrum. Most striking were alterations within the uncinate fasciculus in those with *MAPT* mutations, which persisted when compared with AD and *C9ORF72* groups. These more localised changes suggest that *MAPT* mutations may direct pathological changes to target

this ventro-medial network. Furthermore, breakdown of these tracts may account for deficits in cognitive processes such as episodic memory, semantic knowledge and emotion processing seen in *MAPT* mutation carriers (Janssen et al., 2005; Von Der Heide et al., 2013). In contrast those with *C9ORF72* mutations tended to have more dorsal white matter tract pathology, which targeted the cingulum bundle and corpus callosum. These findings are in line with evidence from previous neuroanatomical studies of genetic subtypes of bvFTD (Mahoney et al., 2012a, 2012b; Rohrer et al., 2011). Notably a significant difference was not generated when *MAPT* was contrasted with the sporadic bvFTD group. Whilst the absence of a group difference is certainly not a conclusive finding it could be speculated that this finding could result from overlapping profiles of white matter pathology in these two groups, at least in part.. This subgroup analysis does not fully resolve neuroanatomical subtyping of molecularly defined bvFTD: case numbers across subgroups were small (precluding, for example, differentiation of individual mutations within each subgroup) while certain key bvFTD phenotypes (in particular, bvFTD due to progranulin gene mutations and sporadic forms of bvFTD associated syndromes of atypical parkinsonism or motor neurone disease) were either underrepresented or not represented at all. The likely variability of pathologies within the sporadic bvFTD group may also have limited the ability to detect white matter changes specific to this group. Taking these caveats into account, the above findings provide further evidence that the profile of regional brain network disintegration in bvFTD may be modulated by underlying molecular pathologies (Warren et al., 2012) and that DTI can assist in differentiating these pathologies in vivo.

3.5.4 Comparison of DTI metrics in bvFTD

The compatibility of different DTI metrics is an issue of considerable clinical and neurobiological relevance to the application of DTI in neurodegenerative disease. The current study suggests partial convergence of metrics for particular white matter tracts, although it is also noteworthy that there was also substantial divergence in the white matter profiles generated using different DTI metrics across both sporadic and genetic forms of bvFTD (compare Figures 3.2 and 3.3 to Figures 3.4 and 3.5). In principle, there is likely to be a trade-off between higher sensitivity and higher specificity for any candidate DTI metric, presenting a practical problem of optimisation if particular metrics are in future to be used as disease biomarkers. It may be that some DTI metrics have higher inter-subject variability, in both healthy and affected individuals, and after discounting for these affects (as has been done here by adjusting for global mean diffusivity); the overall extent of change may be less emphatic. After adjusting for global mean diffusivity values to enhance regional anatomical specificity, disproportionate involvement of uncinate fasciculus was identified, suggesting it may be a candidate tract for monitoring white matter pathology in bvFTD across DTI metrics. In addition it is notable that alterations in AX were more apparent, both across the group as a whole and within the genetically defined group. This may suggest that this particular DTI metric is less likely to result in a 'false positive' result, and this greater specificity may be due to certain DTI metrics being better suited to detect particular underlying neuropathology. Data from the current study suggest that the absolute values of diffusion (AX/RD/TR) performed better than FA in detecting

pathology when comparing *MAPT* patients with both controls and AD patients, whilst also noting that FA performed well when comparing the overall bvFTD group with controls and AD patients. One caveat to the above is that AD and *MAPT* associated bvFTD are both tauopathies so one might expect similar findings; however at least two possible explanations for these findings exist, first AD is a process involving two pathological proteins and secondly the degree of white matter pathology in the *MAPT* group may simply be greater in this particular cohort.

A comparison of DTI metrics was further expanded on by a formal ROC analysis assessing the seperability of bvFTD from healthy individuals and patients with AD (see Figure 3.7). Comparing global brain diffusivity values, RD and TR appeared most sensitive in distinguishing bvFTD from healthy controls, in keeping with previous work (Acosta-Cabronero et al., 2010; F Agosta et al., 2012; Mahoney et al., 2013), and suggesting these metrics might potentially assist in early bvFTD diagnosis. On the other hand, FA appeared to be have a greater specificity in distinguishing bvFTD from AD, suggesting that this metric might be preferred as a future disease biomarker (for example, in treatment trials targeting particular pathologies). However, data in the genetic subgroups (see Table 3.8) suggest that the 'optimal' diffusivity metric may be further stratified within the bvFTD spectrum.

In line with some of the variability in metric performance above, the current literature on the performance of DTI metrics is also not clear-cut. For example previous studies suggest that AX or RD may have greater sensitivity to FA in

detecting white matter pathology in AD (Acosta-Cabronero et al., 2010), although unlike the current study this study lacks comparisons between different disease groups. Whilst a number of other studies within other degenerative conditions have demonstrated that FA has some specificity in distinguishing different disease subtypes (Menke et al., 2012; Prakash et al., 2009). This underlines the need to take the specific application into account, such as the likely underlying pathology and whether the study is cross-sectional or longitudinal, when evaluating candidate DTI metrics (Acosta-Cabronero et al., 2010). Variation among DTI metrics may in addition potentially hold neurobiological insights: for example, the apparent discrepancy between RD and FA in signifying bvFTD (whether referenced to healthy controls or to AD) might be driven by changes in either RD or AX as change in either metric could affect FA. It is likely that some discrepancies in DTI metric performance will remain until such time as better specific prior hypothesis about DTI metrics are available, likely requiring detailed white matter histopathological and imaging data correlation.

3.5.5 Relationship of grey matter atrophy and white matter pathology

A related key issue concerns the relationship of grey matter atrophy to white matter pathology in bvFTD. Here, changes in white matter tracts occurred in close anatomical proximity to regions of grey matter loss but were more spatially distributed (see Figure 3.8). In line with this another recent study has also found somewhat more widespread white matter changes in bvFTD when compared with AD (Zhang et al., 2011). White matter and grey matter alterations were most

robustly co-localised in the right anterior temporal lobe including the most consistently involved white matter tract, the uncinate fasciculus. There is a need for caution when comparing different neuroimaging modalities, such as DTI and VBM, as they use very different methodologies to assess anatomy and the outcome metrics of DTI and VBM are not directly comparable units of measurement. However, the greater spatial extent of white matter damage might reflect distal propagation of pathology from primarily involved regions adjacent to regions of grey matter damage (due for example to pathogenic protein diffusion or withdrawal of trophic support) (Hardy and Revesz, 2012; Warren et al., 2012); alternatively, however, white matter pathology might drive grey matter loss, such that over time grey matter atrophy spreads to become more contiguous with white matter damage. Substantial emerging histopathological evidence suggests that white matter pathology may be significant in bvFTD (Ahmed et al., 2011; Hiji et al., 2008; Neumann et al., 2007), may develop early in the disease process (Broe et al., 2004; Martin et al., 2001) and may promote subsequent upstream cortical degeneration (Drzezga et al., 2011; Villain et al., 2008). An early pathophysiological role for white matter pathology has already been suggested by previous neuroimaging evidence in asymptomatic mutation carriers with neurodegeneration disorders (Borroni et al., 2008; Ringman et al., 2007).

3.5 Chapter summary

This cross-sectional study has identified profiles of white matter tract pathology in a large, representative cohort of patients with bvFTD, using a group-wise image registration technique. This study identified a distributed signature of white matter alterations likely to be core to the pathophysiology of this syndrome and suggesting that this signature is further modulated by specific underlying molecular pathologies. These findings are supported by the neurobiological relevance of the affected tracts, in particular the uncinate fasciculus. This data also suggests that the choice of DTI metric, and indeed choice of region of interest, is of importance with variations in each DTI metrics sensitivity and specificity. There are of course a number of limitations, which include relatively small numbers of molecularly defined individuals and lack of confirmatory histopathology, as well as methodological constraints in comparing differing imaging modalities. Notwithstanding these issues the current data suggest that DTI may be a useful candidate clinical biomarker and neurobiological probe in bvFTD. Addressing the trajectory of change within white matter tracts is also important in understanding the underlying pathophysiology as well as having practical implications for disease monitoring, which will be further explored in the next chapter of this thesis.

4. Longitudinal profiles of white matter pathology in behavioural variant frontotemporal dementia

4.1 Introduction

4.1.1 Background

Given that bvFTD is a common cause of early onset dementia the development of disease modifying therapies is of high priority. Potential disease modifying therapies for neurodegenerative disease are now emerging, creating an urgent need to develop biomarkers with improved accuracy to detect and monitor disease progression in bvFTD, not least because a high proportion of cases have a genetic basis, making pre-symptomatic intervention a real prospect (Dopper et al., 2013). To date, longitudinal MRI has been shown to be a useful biomarker in neurodegenerative diseases given its wide availability, ease of interpretation and its sensitivity in detecting change (most typically in brain volume) over time. Furthermore longitudinal imaging allows us to better understand the natural history of bvFTD, establishing where the disease starts and which brain networks are particularly vulnerable, as it allows us to use each subject as his/her own control minimising bias (see Figure 1.4 as a demonstration of the usefulness of longitudinal MRI).

4.1.2 Previous longitudinal imaging studies in bvFTD

Previous longitudinal imaging studies of bvFTD have used structural MRI to measure rates of whole brain and ventricular change (Gordon et al., 2010; Knopman et al., 2009; Mahoney et al., 2012b; Whitwell et al., 2006) and are

discussed in section 1.4. However with the current study in mind, it is worth pointing out their limitations; the tendency to measure rates of whole brain atrophy, which may be insensitive to the focal losses often seen in bvFTD; volumetric MRI may miss microstructural damage and may not provide sufficient sensitivity to detect meaningful change in individuals with slowly progressive forms of bvFTD, or in pre-symptomatic individuals with little macroscopic brain atrophy (Brodtmann et al., 2013; Dopper et al., 2013).

A further problem in tracking progression in bvFTD is its broad pathological and clinical heterogeneity. Predicting underlying pathology on clinical or radiological grounds remains challenging. As such, the use of current clinical or neuroimaging measures to evaluate treatments, which will likely target specific molecular pathologies, is problematic. As already alluded to monitoring molecularly vulnerable brain networks such as the Salience Network may offer greater specificity in tracking disease trajectory in bvFTD. Longitudinal DTI may offer the methodology to monitor large-scale structural network degeneration over time. At the time of writing only one prior study has applied this methodology. Lam and colleagues studied 12 patients with bvFTD and found widespread longitudinal declines in FA and increased RD, AX and MD in both right and left uncinate fasciculus and corpus callosum. They noted that FA and RD seemed to be more sensitive at tracking longitudinal change, compared with AX and MD (Lam et al., 2014). However this study did not quantify the extent of change within individual white matter tracts, nor did it use robust imaging methodologies to register images longitudinally to minimise issues such as time-point bias.

The current study aimed to improve upon this previous study by investigating longitudinal white matter change in key white matter structures in a group of patients with bvFTD with serial scanning approximately 1.2 years from baseline, using quantifiable methods as well as a robust image registration pipeline. Furthermore this study used quantitative data to assess the utility of DTI as a potential biomarker for clinical trials by comparing DTI measures of change with established MRI and neuropsychological measures, to estimate sample size requirements for potential future clinical trials.

4.2 Methods

4.2.1 Study Participants

Patients were recruited from 2009-2014 as part of a prospective study tracking disease progression in patients suspected to have Frontotemporal Lobar Degeneration at the Specialist Cognitive Disorders Clinic, National Hospital for Neurology and Neurosurgery, London, United Kingdom. All patients met current consensus criteria (Rascovsky et al., 2011) for a diagnosis of either probable or definite bvFTD and had two clinical and neuropsychological assessments and MRI scans (to include both T1-volumetric and DTI sequences) a minimum of six months apart were considered for study inclusion. All patients in the current study also participated in the study contained in Chapter 3 of this thesis and as such underwent the same clinical, neuropsychological and genetic assessments as described previously. 23 participants were identified as fulfilling inclusion criteria. 4 participants were not included in the DTI analysis for the following reasons: two had significant artefact on follow-up DTI scans, one had an incomplete sequence

due to scanner intolerance, and another had a sphenoid wing meningioma. 18 age and gender-matched controls were also included and underwent the same test batteries as those with bvFTD. Each study participant underwent the same battery of neuropsychological and clinical tests at baseline and follow-up. Patients and controls underwent volumetric MRI and DTI acquisition on the same scanner at baseline and follow-up as per the image acquisition protocols discussed previously (see chapter 2 for details).

4.2.2 Image processing

All subjects' baseline and follow-up DTI scans underwent processing as specified in the longitudinal DTI image-processing pipeline (see chapter 2, section 2.2.8.). As specified an initial within subject template was created followed by a group-wise template to which each baseline and follow-up scan was registered. FA, MD, AX and RD were then computed from these final images. As per the pipeline in section 2.7 a ROI based analysis was performed, with tracts chosen either based on *apriori* prediction of disease involvement or based on the previous chapters cross-sectional results. Regions-of-interest included genu, body and splenium of the corpus callosum, bilateral uncinate fasciculus, parahippocampal (ventral) cingulum bundle, paracallosal (dorsal) cingulum bundle, corticospinal tract, superior cerebellar peduncle and fornix. The uncinate fasciculus did not undergo any additional erosion, as on inspecting this tract after erosion, too few voxels remained resulting in high variance in mean values between subjects, thus reducing sensitivity to detect change in this tract.

Analysis of baseline and follow-up (on average 1.2 year later) volumetric MRI scans were performed as per section 2.3 of this thesis with the brain boundary shift integral calculated and expressed as annualised volume change as a percentage of the baseline brain volume.

4.2.3 Statistical analysis and sample size estimates

Statistical analyses of clinical and behavioural data were carried out using STATA 12© (Statacorp, College Station, TX). Cross-sectional DTI metric data were compared between disease and cognitively normal groups using a linear regression model adjusting for age, gender and disease duration. Mixed-effects linear regression models with random intercept were used to compare longitudinal change between groups for each DTI metric and region of interest, adjusting for age, gender and disease duration. For longitudinal models the log of each DTI metric was the dependent variable, with disease group, time from baseline scan in years and interaction between disease group and time included in order to provide estimates of differences in the rate of change as a percentage per year. This methodology was also used to compare cross-sectional and longitudinal neuropsychological data between groups.

To determine the accuracy, sensitivity and specificity of each DTI metric in classifying individual participants into separate groups (bvFTD or control) ROC curves were constructed using either raw DTI metric data (for baseline measurement) or the estimated mean difference in the rate of change for each diffusivity metric (for longitudinal measurement). Areas-under-curve were

calculated for regions of interest which were significantly different when compared with controls.

Estimation of sample sizes for future trials were calculated (using STATA) with 80% power and 5% two-tailed significance using the mean difference in the rate of change between groups for each DTI metric and neuropsychological score, and whole-brain atrophy, using the brain boundary shift integral, to detect a 20, 30, 40 and 50% reduction in yearly change.

4.3 Results

4.3.1 Demographics, neuropsychological performance and changes in whole brain volume

Demographic and volumetric imaging characteristics of study participants are shown in table 4.1. Out of a total of 23 bvFTD patients included: eleven had apparently sporadic bvFTD, having no family history of bvFTD and a negative test for relevant genetic mutations; eight patients had mutations in *MAPT* (five exon 10 +16 mutation, two R407W mutation and one P301L mutation); four patients had a *C9ORF72* mutation. Patients and controls were matched for age, gender and total intracranial volume. Compared with controls, those with bvFTD had significantly lower mini-mental state examination (MMSE) scores ($p<0.01$) and whole brain volumes ($p\leq0.001$) at baseline and follow-up. Rates of atrophy were greatest ($p=0.002$) in the bvFTD group, with the highest rate of volume loss occurring in those with *MAPT* mutations ($p=0.001$).

	Controls (n=18)		MAPT (n=8)		C9ORF72 (n=4)		Sporadic (n=11)		All bvFTD (n=23)		p-value*
	Mean	SD	Mean	SD	Mean	SD	Mean	SD	Mean	SD	
Age at baseline (years)	61.3	9.5	56.7	8.9	64.1	8.7	68.8	8.4	63.8	10.0	0.4
Disease duration at baseline (years)			5.2	5.4	9.3	5.9	6.8	4.7	6.7	5.1	N/A
Sex, male/female	12/6		5/3		4/0		10/1		18/5		0.7§
Interscan Interval (years)	1.4	0.5	1.3	0.5	1.0	0.1	1.2	0.5	1.2	0.4	0.2
Education (years)	16.55	1.42	14.6	3.9	15.5	4.1	16.6	3.0	15.5	3.5	0.3
MMSE baseline	29.7	0.6	25.5	4.2	2.5	6.9	25.8	3.4	25.3	4.2	<0.001^
MMSE follow-up	29.7	0.5	26.3	5.4	25.3	4.3	25.1	3.5	25.6	4.2	0.002^
TIV (ml)	1572	134	1503	135	1649	135	1565	123	1556	137	0.6
Whole brain volume, baseline (ml)	1193	91	1047	88	1192	93	1026	48	1070	95	0.001
Whole brain volume, follow-up (ml)	1184	95	1028	95	1167	93	1001	37	1047	95	<0.001
BBSI ml/year	5.2	6.7	15.7	6.7	14.4	17.8	14.8	10.6	15.2	10.4	0.002

Table 4.1. Study participant's clinical and imaging characteristics. * Linear regression comparing controls with all bvFTD subjects (n=23), § Fisher's exact test, ^ Wilcoxon rank-sum test.

Neuropsychological performance at baseline and longitudinally is shown in table 4.2 for the entire bvFTD group and controls. Neuropsychological performance for each bvFTD subgroup is shown in table 4.3. Compared with controls, at baseline, those with bvFTD had significantly poorer performance on tests of general intellect, recognition memory, naming, object perception, executive function, emotion recognition and social inference. Longitudinally the greatest change observed in the bvFTD group was a 30.4% decline in score on the graded naming test.

	Control (n=18)				BvFTD (n=23)			
	Baseline	Change over time from baseline			Baseline	Change over time from baseline		
	Raw Score (SD)	%/year	95% CI		Raw score (SD)	%/year	95% CI	
WASI								
VIQ	122.1 (9.4)	-2.6	-6.2	1.0	87.3** (22.1)	0.1	-5.0	5.3
PIQ	120.1 (9.2)	-1.4	-4.6	1.9	89.9** (19.3)	4.0	-0.7	8.7
RMT Words (/50)	47.9 (2.6)	0.7	-4.1	5.5	33.3** (6.6)	0.0	-7.0	7.0
RMT Faces (/50)	43.4 (4.6)	2.3	-2.7	7.3	36.0** (8.3)	-5.5	-12.7	1.8
Graded Naming Test (/30)	26.4 (2.2)	2.0	-9.2	13.2	11.6** (8.5)	-30.4**	-47.2	-13.6
Graded Difficulty Arithmetic (/24)	14.7 (4.5)	-3.1	-11.6	5.4	13.0 (6.4)	-8.9	-21.0	3.1
VOSP (/20)	19.1 (1.0)	-2.3	-11.0	6.3	16.0** (3.8)	6.0	-6.6	18.5
Executive Function								
DKEFS Colour Naming (max 90 secs)	30.2 (3.2)	0.9	-7.0	8.8	42.3* (20.3)	5.4	-6.0	16.8
DKEFS Ink Colour Naming (max 180 secs)	55.7 (11.6)	0.1	-6.3	6.5	88.8** (37.6)	8.1	-1.1	17.3
TASIT^								
Emotion Recognition (/14)	11.4 (1.2)	-1.2	-10.7	8.4	8.0** (1.9)	-3.7	-17.3	9.9
Social Inference Task (/36)	32.1 (2.9)	2.0	-3.9	7.9	22.5** (4.8)	-5.1	-13.4	3.3

Table 4.2 Study participants neuropsychological performance at baseline and follow up. Scores shown are raw scores for each test with maximum scores shown in parentheses. * and ** denotes p-values of <0.05 and <0.001 respectively comparing behavioural scores (raw score at baseline and change from baseline over time) of all bvFTD (n=23) participants with control participants after adjustment for age, gender and disease duration. ^ Total scores on the TASIT are scaled scores.

	Sporadic (n=11)				MAPT (n=8)				C9ORF72 (n=4)			
	Baseline	Change over time from baseline			Baseline	Change over time from baseline			Baseline	Change over time from baseline		
	Raw score (SD)	%/year	95% CI		Raw score (SD)	%/year	95% CI		Raw score (SD)	%/year	95% CI	
WASI												
VIQ	95.3** (17.2)	-3.8	-9.5	2	80.6** (25.7)	2.1	-2.3	6.5	78.8** (24.8)	17.0**	9.1	25
PIQ	91.2** (17.8)	0.1	-4.6	4.9	91.1** (18.3)	6.4*	2.1	10.8	83.8** (28.9)	16.5**	8.8	24.3
Recognition Memory Test												
Words (/50)	33.1** (6.8)	-9.1**	-14.2	-4.1	33.9** (6.8)	-6	-15.9	3.9	35.5** (7.4)	19.0**	7.6	30.5
Faces (/50)	37.6** (8.4)	-2.3	-10.8	6.1	34.0** (9.1)	3.7	-1.8	9.2	32.8** (7.6)	1.9	-4.9	8.7
GNT (/30)	12.6** (7.8)	-45.3**	-62.2	-28.5	6.6** (7.8)	-18.5*	-36.4	-0.7	18.8** (6.7)	0.6	-12.8	13.9
GDA (/24)	14.4 (6.3)	-10.9	-22.2	0.4	13.1 (4.5)	-12.4	-29.5	4.7	8.8 (9.4)	16.4	-10.2	43
VOSP (/20)	16.4* (4.3)	3.7	-11.1	18.6	16.1** (2)	2	-4.8	8.8	15.0** (5.7)	27.5*	5.4	49.7
Executive Function												
DKEFS-IC (Max 90 sec)	46.3* (22.5)	11.5*	2.8	20.2	31.5 (7)	9.9	-0.1	20	53.0** (26.4)	-35.7*	-61.1	-10.3
DKEFS-CN (Max 180 sec)	91.9** (38.4)	10.8*	2.2	19.3	71.6** (20.9)	9.1	-1.7	20	114.5** (52.3)	-5.8	-23.9	12.2
TASIT												
Emotion Recog. (/14)	7.3** (1.8)	-3.6	-20.9	13.7	8.7** (2.3)	-6.5	-17.6	4.6	8.7** (1.2)	9.6	-9.8	29
Social Inf. (/36)	21.4** (4.7)	-10.7*	-18.8	-2.5	23.3** (5.9)	4	-6.2	14.2	24.0** (3.6)	0.7	-7.8	9.1

Table 4.3 bvFTD subgroup neuropsychological performances at baseline and follow up. * and ** denotes p-values of <0.05 and <0.001 respectively comparing behavioural scores (raw score at baseline and change from baseline over time) of all bvFTD (n=23) participants with control participants after adjustment for age, gender and disease duration.. ^ Total scores on the TASIT are scaled scores.

4.3.2 Cross-sectional DTI results

Cross-sectional DTI metric data for FA, MD, RD and AX are shown in tables 4.4 to 4.7 respectively and should be compared with data from the previous chapter (although noting different methodologies), broadly results presented in the current chapter show similar anatomical profiles of cross-sectional pathology, as well as showing similar profiles of DTI metric alterations comparing bvFTD with controls, the largest differences detected using RD and MD. For example in the bvFTD group as a whole the largest difference within the right uncinate fasciculus

was detected by RD (14.7%; 95% CI 6.1% to 23.2%; p=0.001), followed by MD (13.5%; 95% CI 4.8% to 22.2%; p=0.003, AX (11%; 95% CI 1.3% to 20.7%; p 0.03) and FA (-4.7%; 95% CI -8.6% to -0.7%; p=0.02).

	Controls (n=18)		**BvFTD (n=19)**		% Difference	95% Confidence Interval		p-value*
Regions of interest (FA)	Mean	SD	Mean	SD				
Genu Corpus Callosum	0.74	0.03	0.73	0.04	0.3	-2.6	3.3	0.8
Body Corpus Callosum	0.7	0.04	0.66	0.04	-4.9	-8.9	-1.1	0.01
Splenium Corpus Callosum	0.79	0.02	0.78	0.02	-1.3	-3.2	0.6	0.2
Cingulum (paracallosal) R	0.63	0.05	0.58	0.06	-4.3	-9.3	0.7	0.09
Cingulum (paracallosal) L	0.6	0.04	0.55	0.07	-2.3	-7.1	2.6	0.4
Cingulum (parahippocampal) R	0.43	0.04	0.38	0.04	-5.8	-9.6	-2.0	0.004
Cingulum (parahippocampal) L	0.45	0.04	0.4	0.04	-5.3	-9.2	-1.3	0.01
Fornix	0.59	0.03	0.57	0.04	-1.9	-4.2	0.4	0.1
Uncinate Fasciculus R	0.48	0.05	0.43	0.04	-4.7	-8.6	-0.7	0.02
Uncinate Fasciculus L	0.48	0.04	0.43	0.07	-6.2	-11.3	-1.2	0.02
Corticospinal tract R	0.62	0.05	0.62	0.07	-1.5	-7.2	4.3	0.6
Corticospinal tract L	0.65	0.04	0.64	0.05	-2.2	-6.1	1.8	0.3
SCP R	0.79	0.05	0.78	0.06	-2.2	-7.2	2.7	0.4
SCP L	0.79	0.04	0.77	0.05	-2.9	-7.2	1.4	0.2

Table 4.4 Baseline FA for individual white matter regions of interest for control participants and patients. *Linear regression comparing bvFTD (n=19) with controls after adjusting for age, gender and disease duration. Data is uncorrected for multiple comparisons.

	Controls (n=18)		BvFTD (n=19)		% Difference	95% Confidence Interval		p-value*
Regions of interest (MD 10-3mm 2/s)	Mean	SD	Mean	SD				
Genu Corpus Callosum	0.76	0.04	0.8	0.08	0.3	-4.8	5.4	0.9
Body Corpus Callosum	0.8	0.06	0.88	0.08	8.7	2.6	14.8	0.01
Splenium Corpus Callosum	0.74	0.03	0.77	0.05	3.8	-0.1	7.7	0.06
Cingulum (paracallosal) R	0.72	0.04	0.72	0.05	1.6	-2.5	5.8	0.4
Cingulum (paracallosal) L	0.71	0.04	0.73	0.05	0.5	-3.5	4.4	0.8
Cingulum (parahippocampal) R	0.74	0.03	0.85	0.12	9.3	1.5	17.2	0.02
Cingulum (parahippocampal) L	0.73	0.04	0.83	0.11	10.6	3.1	18.2	0.007
Fornix	0.84	0.06	0.91	0.1	5.4	-0.1	11.0	0.05
Uncinate Fasciculus R	0.7	0.04	0.83	0.13	13.5	4.8	22.2	0.003
Uncinate Fasciculus L	0.71	0.03	0.85	0.18	14.9	2.7	27.1	0.02
Corticospinal tract R	0.66	0.06	0.67	0.09	1.8	-5.3	9.0	0.6
Corticospinal track L	0.62	0.05	0.62	0.09	2.5	-4.3	9.2	0.5
SCP R	0.85	0.07	0.87	0.09	5.4	-2.0	12.8	0.1
SCP L	0.78	0.07	0.8	0.07	4.2	-2.3	10.7	0.2

Table 4.5 Baseline MD for individual white matter regions of interest for control participants and patients. *Linear regression comparing bvFTD (n=19) with controls after adjusting for age, gender and disease duration. Data is uncorrected for multiple comparisons.

	Controls (n=18)		BvFTD (n=19)		% Difference	95% Confidence Interval		p-value*
Regions of interest ($RD\ 10^{-3}mm^2/s$)	Mean	SD	Mean	SD				
Genu Corpus Callosum	0.34	0.05	0.38	0.09	-0.3	-5.7	5.2	0.92
Body Corpus Callosum	0.39	0.06	0.48	0.09	9.3	2.5	16.1	0.01
Splenium Corpus Callosum	0.3	0.03	0.33	0.05	3.1	-0.5	6.7	0.09
Cingulum (paracallosal) R	0.41	0.05	0.45	0.06	3.9	-1.9	9.3	0.15
Cingulum (paracallosal) L	0.43	0.05	0.48	0.07	1.9	-3.2	7.1	0.45
Cingulum (parahippocampal) R	0.55	0.04	0.68	0.12	10.6	2.3	19.0	0.01
Cingulum (parahippocampal) L	0.54	0.05	0.65	0.11	11.2	3.2	19.1	0.01
Fornix	0.51	0.06	0.59	0.1	5.4	-0.4	11.1	0.07
Uncinate Fasciculus R	0.5	0.05	0.64	0.12	14.7	6.1	23.2	0.001
Uncinate Fasciculus L	0.51	0.04	0.66	0.18	16.6	4.4	28.9	0.01
Corticospinal tract R	0.4	0.07	0.41	0.09	2.05	-5.6	9.7	0.59
Corticospinal track L	0.36	0.05	0.37	0.08	3.11	-2.9	9.1	0.3
SCP R	0.36	0.08	0.38	0.11	5.58	-3.0	14.1	0.19
SCP L	0.32	0.07	0.35	0.08	5.16	-1.9	12.2	0.14

Table 4.6 Baseline RD for individual white matter regions of interest for control participants and patients. *Linear regression comparing bvFTD (n=19) with controls after adjusting for age, gender and disease duration. Data is uncorrected for multiple comparisons.

	Controls (n=18)		BvFTD (n=19)		% Difference	95% Confidence Interval		p-value*
Regions of interest (AX $10^{-3}mm^2/s$)	Mean	SD	Mean	SD				
Genu Corpus Callosum	1.59	0.04	1.62	0.08	1.4	-3.4	6.3	0.55
Body Corpus Callosum	1.62	0.05	1.68	0.08	7.4	2.2	12.6	0.01
Splenium Corpus Callosum	1.63	0.05	1.67	0.07	5.3	-0.1	10.7	0.06
Cingulum (paracallosal) R	1.32	0.06	1.27	0.05	-2.9	-7.8	2.1	0.24
Cingulum (paracallosal) L	1.28	0.06	1.23	0.06	-2.5	-8.2	3.3	0.39
Cingulum (parahippocampal) R	1.11	0.03	1.2	0.11	6.7	-0.7	14.1	0.07
Cingulum (parahippocampal) L	1.1	0.04	1.19	0.11	9.6	2.4	16.8	0.01
Fornix	1.49	0.05	1.56	0.1	5.6	0.3	10.9	0.04
Uncinate Fasciculus R	1.11	0.05	1.22	0.14	11.0	1.3	20.7	0.03
Uncinate Fasciculus L	1.12	0.04	1.24	0.19	11.4	-1.4	24.1	0.08
Corticospinal tract R	1.17	0.06	1.18	0.11	1.4	-6.8	9.6	0.73
Corticospinal tract L	1.14	0.06	1.12	0.14	1.1	-9.0	11.3	0.82
SCP R	1.85	0.1	1.85	0.11	5.1	-4.3	14.4	0.28
SCP L	1.69	0.1	0.8	0.07	2.3	-7.0	11.6	0.61

Table 4.7 Baseline AX for individual white matter regions of interest for control participants and patients. *Linear regression comparing bvFTD (n=19) with controls after adjusting for age, gender and disease duration. Data is uncorrected for multiple comparisons.

4.3.3 Longitudinal DTI changes in bvFTD

Rates of change for each region of interest as measured by FA, MD, RD and AX are shown in tables 4.8 to 4.11 respectively. Individual subject's trajectories of change in FA over time are displayed for key affected tracts in figures 4.1 to 4.3. Longitudinally, compared with controls, bvFTD patients as a group had the largest reductions in FA within bilateral paracallosal cingulum (right, -6.8%/year, 95% CI, -8.0% to -2.7% p<0.001; left, -5.5%/year, 95% CI -6.9% to -2.2%, p<0.001), and bilateral uncinate fasciculus (right, -4.2%/year, 95% CI -8.7% to -2.7%, p<0.001; left, -3.1%/year, 95% CI-8.6% to -1.5% p=0.005).

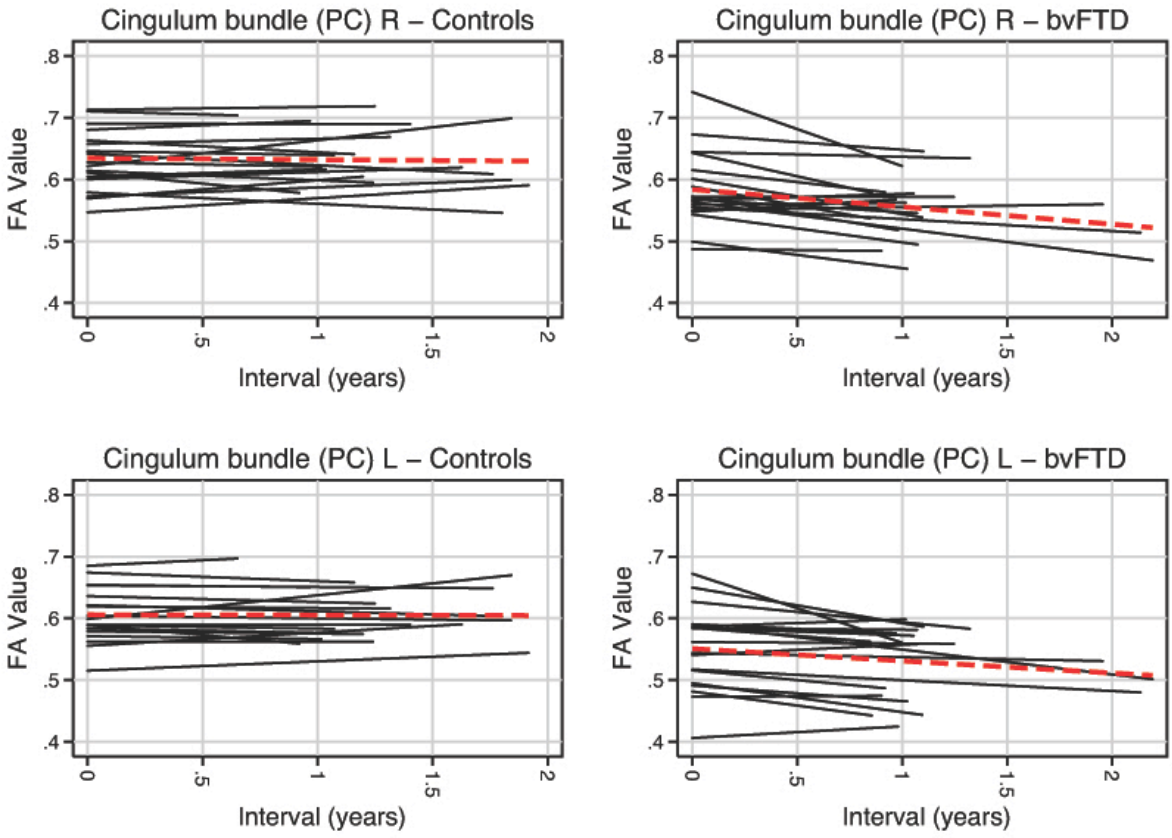

Figure 4.1 Individual trajectories of change in FA over time within right and left paracallosal cingulum bundles. The red dashed line indicates mean trajectory.

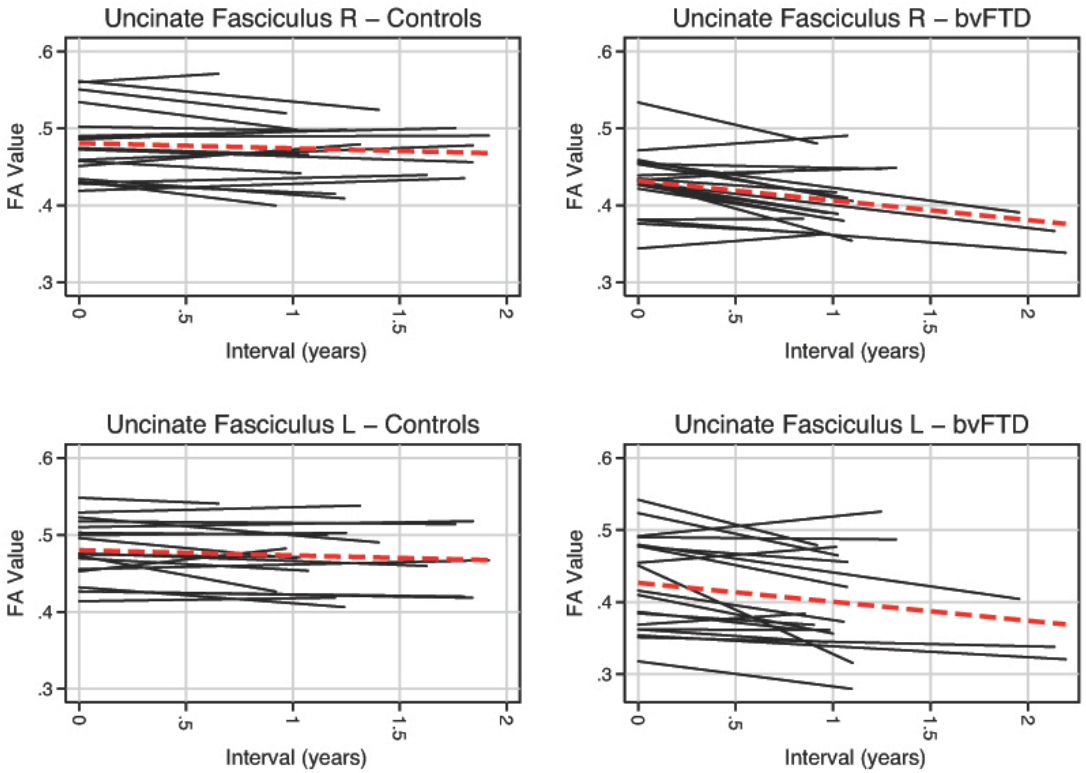

Figure 4.2 Individual trajectories of change in FA over time within right and left uncinate. fasciculus. The red dashed line indicates mean trajectory.

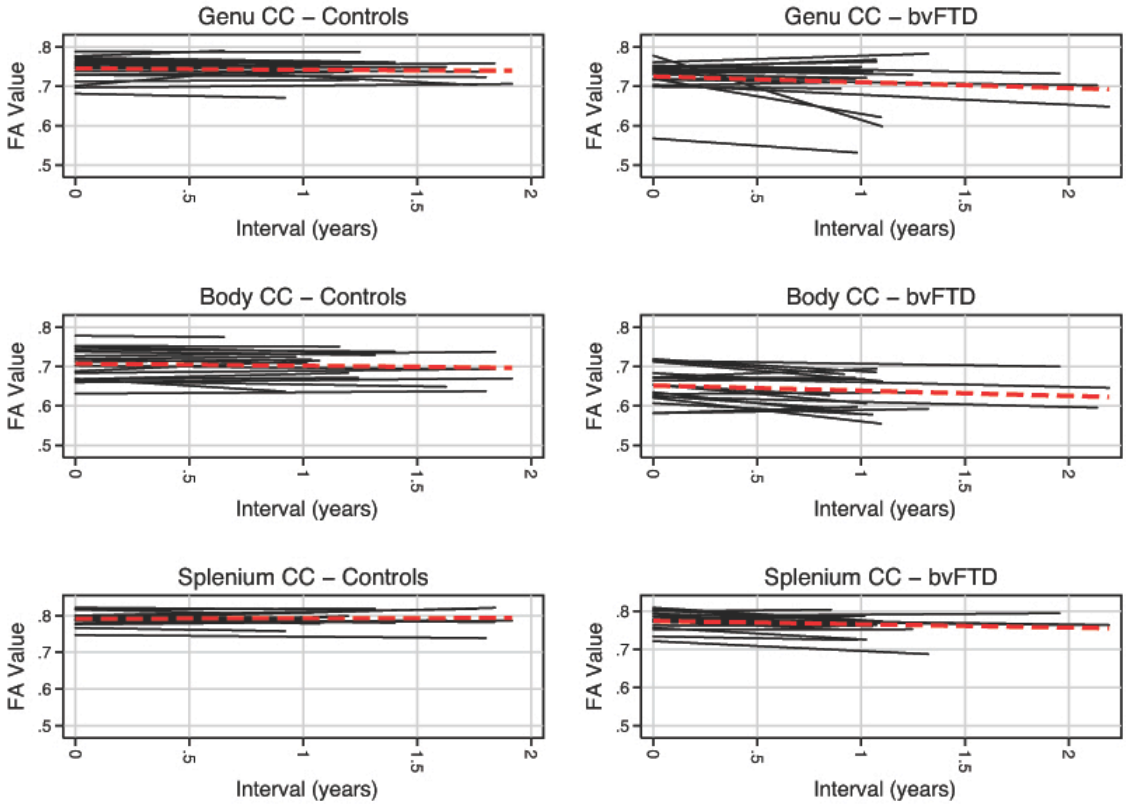

Figure 4.3 Individual trajectories of change in FA over time within the body of the corpus callosum fasciculus. The red dashed line indicates mean trajecto

	BvFTD (n=19)		BvFTD – MAPT (n=8)		BvFTD – C9ORF72 (n=4)		BvFTD – Sporadic (n=7)	
Regions of interest (FA)	**%/year change (95% CI)**	**p value**	**%/year change (95% CI)**	**p value**	**%/year change (95% CI)**	**p value**	**%/year change (95% CI)**	**p value**
Genu CC	-2 (-4.7 to 0.3)	0.09	-2 (-5.2 to 1.2)	0.22	0.5 (-1.9 to 2.9)	0.68	-3.1 (-5.5 to -0.8)	0.01
Body CC	-2.4 (-4 to -0.8)	0.003	-3.3 (-4.8 to -1.8)	<0.001	-2.1 (-4.7 to 0.6)	0.13	-1.5 (-3.4 to 0.4)	0.12
Splenium CC	-2.1 (-2.4 to -0.7)	0.001	-1.4 (-2.4 to -0.4)	0.004	-2.1 (-3.8 to -0.3)	0.02	-1.4 (-2.4 to -0.4)	0.005
Cingulum PC R	-6.8 (-8 to -2.7)	<0.001	-4 (-7.2 to -0.8)	0.01	-6.8 (-11.3 to -2.2)	0.004	-6.7 (-10 to -3.4)	<0.001
Cingulum PC L	-5.5 (-6.9 to -2.2)	<0.001	-4.6 (-7.4 to -1.8)	0.001	-1.7 (-5.6 to 2.1)	0.38	-5.6 (-8.3 to -2.8)	<0.001
Cingulum PH R	3.5 (-3.4 to 2.7)	0.82	-1.5 (-5.2 to 2.2)	0.42	-2.7 (-8.9 to 3.5)	0.39	1.9 (-1.9 to 5.7)	0.98
Cingulum PH L	-1.8 (-7.7 to 0.9)	0.12	-6.5 (-11.2 to -1.8)	0.007	-2.4 (-11.4 to 6.6)	0.6	0.1 (-5.4 to 5.6)	0.01
Fornix	-1.2 (-4.1 to 0.3)	0.09	-1.8 (-4.6 to 0.9)	0.19	0.8 (-1.2 to 2.8)	0.45	-2.7 (-5 to -0.5)	0.02
UF R	-4.2 (-8.1 to -2.7)	<0.001	-7.2 (-9.7 to -4.7)	<0.001	-4.3 (-9.1 to 0.5)	0.08	-3.5 (-7.2 to 0.2)	0.07
UF L	-3.1 (-8.6 to -1.5)	0.005	-7.9 (-12 to -3.7)	<0.001	-4.8 (-9.6 to -0.1)	0.05	-1.5 (-4.6 to 1.6)	0.34
CST R	-2.9 (-8.6 to 0.3)	0.07	-3.4 (-8.5 to 1.7)	0.19	0.5 (-7.5 to 8.4)	0.91	-6.6 (-12.5 to -0.7)	0.03
CST L	-1.8 (-8.2 to 0.1)	0.06	-4 (-9.1 to 1)	0.12	-7.8 (-16.9 to 1.2)	0.09	-3.2 (-8.6 to 2.3)	0.25
SCP R	0.4 (-5 to 1.3)	0.25	-1.2 (-4.5 to 2.1)	0.48	-6.8 (-13.8 to 0.3)	0.06	-1.2 (-4.5 to 2.1)	0.48
SCP L	-0.5 (-5.1 to 0.9)	0.18	-2.6 (-5.6 to 0.4)	0.09	-1.3 (-8.9 to 6.3)	0.74	-1.8 (-5 to 1.4)	0.09

Table 4.8 Estimated percentages per year difference in the rate of change of FA for bvFTD patients and bvFTD subgroups, by region, compared with controls. Data is uncorrected for multiple comparisons.

The largest increases in MD were within bilateral uncinate fasciculus (right, 5.1%/year, 95% CI 2.3% to 8.0%, p<0.001; left, 6.2%/year, 95% CI 1.6% to 10.8%, p=0.01;) and bilateral parahippocampal cingulum (right, 4.3%/year, 95% CI 1.6% to 7.1%, p=0.002; left, 5.0%/year, 95% CI 1.1% to 9.0%, p=0.01).

	BvFTD (n=19)		BvFTD – MAPT (n=8)		BvFTD – C9ORF72 (n=4)		BvFTD – Sporadic (n=7)	
Regions of interest (MD)	**%/year change (95% CI)**	**p value**	**%/year change (95% CI)**	**p value**	**%/year change (95% CI)**	**p value**	**%/year change (95% CI)**	**p value**
Genu CC	2.7 (-1.1 to 6.6)	0.16	2.5 (-2.8 to 7.8)	0.36	-0.7 (-4.8 to 3.4)	0.73	3.6 (0.4 to 6.8)	0.03
Body CC	2.5 (0.8 to 4.3)	0.003	3.1 (1.3 to 4.9)	0.001	3.6 (0.7 to 6.6)	0.01	1.4 (-0.9 to 3.8)	0.23
Splenium CC	2.7 (0.9 to 4.5)	0.003	2.8 (0.5 to 5.1)	0.02	3.2 (-0.4 to 6.7)	0.08	2.4 (0.4 to 4.4)	0.02
Cingulum PC R	2.9 (0.8 to 4.9)	0.01	2.3 (-0.4 to 5)	0.09	2.0 (-1.8 to 5.7)	0.30	3.8 (1.5 to 6)	0.001
Cingulum PC L	2.7 (0.6 to 4.8)	0.01	2.3 (-0.3 to 4.9)	0.08	1.9 (-1.7 to 5.5)	0.29	3.4 (0.8 to 6.1)	0.01
Cingulum PH R	4.3 (1.6 to 7.1)	0.002	5.6 (2.7 to 8.6)	<0.001	4.5 (-1.8 to 10.7)	0.16	3.3 (-0.2 to 6.8)	0.06
Cingulum PH L	5.0 (1.1 to 9)	0.01	8.3 (4.3 to 12.2)	<0.001	2.8 (-4.4 to 10.1)	0.44	1.8 (-2.8 to 6.3)	0.45
Fornix	1.8 (-1.1 to 4.8)	0.22	1.8 (-2.1 to 5.7)	0.38	-0.9 (-4.2 to 2.4)	0.59	2.4 (-0.5 to 5.2)	0.11
UF R	5.1 (2.3 to 8)	<0.001	6.7 (3.7 to 9.6)	<0.001	3.0 (-2.6 to 8.6)	0.30	4.0 (0.7 to 7.4)	0.02
UF L	6.2 (1.6 to 10.8)	0.01	10.9 (5.2 to 16.5)	<0.001	6.0 (0.8 to 11.2)	0.02	0.8 (-1.7 to 3.3)	0.52
CST R	2.2 (-3.2 to 7.6)	0.43	3.2 (-3.9 to 10.2)	0.38	-1.1 (-12.1 to 9.9)	0.84	2.8 (-3.9 to 9.6)	0.41
CST L	3.9 (-1.5 to 9.4)	0.16	4.3 (-2.9 to 11.5)	0.24	9.3 (-2.4 to 21)	0.12	2.0 (-4.7 to 8.6)	0.56
SCP R	2.2 (-3.2 to 7.6)	0.43	3.2 (-3.9 to 10.2)	0.38	-1.1 (-12.1 to 9.9)	0.84	2.8 (-3.9 to 9.6)	0.41
SCP L	5.1 (0.7 to 9.5)	0.02	5.6 (0.7 to 10.5)	0.02	7.4 (-2.5 to 17.2)	0.14	4.0 (-1.0 to 9.0)	0.12

Table 4.9 Estimated percentages per year difference in the rate of change of MD for bvFTD patients and bvFTD subgroups, by region, compared with controls. Data is uncorrected for multiple comparisons.

The largest increases in RD were within bilateral paracallosal cingulum (right, 8.6%/year, 95% CI 2.8% to 11.6%, p<0.001; left 6.9%/year, 95% CI 2.5% to 10.0%, p<0.001.), bilateral uncinate fasciculus (right, 5.6%/year, 95% CI 3.0% to 10.7%,

p<0.001; left, 7.4%/year, 95% CI 2.0% to 13.8%, p=0.01) and splenium of the corpus callosum (7.3%/year, 95% CI 2.5% to 10.1%, p<0.001).

	BvFTD (n=19)		BvFTD – MAPT (n=8)		BvFTD – C9ORF72 (n=4)		BvFTD – Sporadic (n=7)	
Regions of interest (RD)	**%/year change (95% CI)**	**p value**	**%/year change (95% CI)**	**p value**	**%/year change (95% CI)**	**p value**	**%/year change (95% CI)**	**p value**
Genu CC	4.8 (-2.2 to 13.5)	0.2	4.8 (-4.5 to 16.8)	0.3	-2.5 (-10.6 to 6.9)	0.7	6.4 (-0.3 to 14.5)	0.1
Body CC	5.8 (1.9 to 9.0)	0.002	7.4 (3.4 to 10.6)	<0.001	6.2 (-0.6 to 12.3)	0.1	3.4 (-1.5 to 7.8)	0.2
Splenium CC	7.3 (2.5 to 10.1)	0.001	7.3 (1.5 to 11.1)	0.01	8.7 (-0.1 to 15.3)	0.1	6.8 (1.3 to 10.2)	0.01
Cingulum PC R	8.6 (2.8 to 11.6)	0.001	7.7 (0.3 to 12.2)	0.04	7.8 (-1.2 to 13.9)	0.1	9.5 (3.0 to 13.0)	0.002
Cingulum PC L	6.9 (2.5 to 10.0)	0.001	6.9 (1.4 to 11.2)	0.01	3.4 (-3.6 to 9.1)	0.4	8.0 (2.9 to 11.7)	0.001
Cingulum PH R	2.5 (0.9 to 8.3)	0.01	3.7 (1.8 to 9.7)	0.01	3.6 (-2.5 to 14.3)	0.2	0.9 (-1.9 to 7.9)	0.2
Cingulum PH L	4.8 (0.8 to 11.4)	0.03	8.7 (4.7 to 15.6)	<0.001	2.1 (-7.5 to 15.1)	0.5	-0.2 (-5.3 to 7.5)	0.7
Fornix	1.6 (-1.8 to 7.8)	0.2	1.7 (-2.9 to 9.7)	0.3	-2.9 (-6.9 to 3.6)	0.5	2.2 (-1.4 to 8.3)	0.2
UF R	5.6 (3.0 to 10.7)	<0.001	7.4 (4.7 to 12.6)	<0.001	3.3 (-3.2 to 12.4)	0.2	4.3 (0.5 to 10.6)	0.03
UF L	7.4 (2.0 to 13.8)	0.01	12.7 (6.3 to 20.6)	<0.001	8.2 (1.4 to 16.1)	0.02	0.5 (-2.8 to 4.6)	0.6
CST R	3.0 (-5.1 to 14.3)	0.4	4.5 (-6.7 to 19.0)	0.3	-7.0 (-24.0 to 13.1)	0.6	4.9 (-5.9 to 18.6)	0.3
CST L	4.9 (-1.7 to 15.9)	0.1	5.7 (-3.7 to 19.6)	0.2	11.4 (-5.3 to 32.3)	0.2	2.3 (-7.1 to 15.7)	0.5
SCP R	3.0 (-5.1 to 14.3)	0.4	4.5 (-6.7 to 19.0)	0.3	-7.0 (-24.0 to 13.1)	0.6	4.9 (-5.9 to 18.6)	0.3
SCP L	6.3 (-0.8 to 19.8)	0.1	8.1 (-0.5 to 23.2)	0.1	2.2 (-18.1 to 30.3)	0.6	4.6 (-5.0 to 20.8)	0.2

Table 4.10 Estimated percentages per year difference in the rate of change of RD for bvFTD patients and bvFTD subgroups, by region, compared with controls. Data is uncorrected for multiple comparisons.

The largest increases in AX were within bilateral parahippocampal cingulum (right, 3.3%/year, 95% CI 2.0% to 5.9%, p<0.001; left, 3.2%/year, 95% CI 1.2% to 6.5%, p=0.005) and bilateral uncinate fasciculus (right, 2.6%/year, 95% CI 1.3% to 5.1%, p<0.001; left, 4.7%/year, 95% CI 1.1% to 7.7%, p=0.009).

	BvFTD (n=19)		**BvFTD – MAPT (n=8)**		**BvFTD – C9ORF72 (n=4)**		**BvFTD – Sporadic (n=7)**	
Regions of interest (AX)	**%/year change (95% CI)**	**p value**	**%/year change (95% CI)**	**p value**	**%/year change (95% CI)**	**p value**	**%/year change (95% CI)**	**p value**
Genu CC	0.9 (-0.8 to 3.0)	0.2	0.3 (-2.0 to 3.4)	0.6	-0.4 (-2.3 to 1.8)	0.8	1.4 (0.1 to 3.0)	0.03
Body CC	1.2 (-0.2 to 1.8)	0.1	1.2 (-0.3 to 1.9)	0.1	2.8 (0.8 to 3.9)	0.003	0.6 (-1.2 to 1.7)	0.8
Splenium CC	1.2 (0.2 to 2.5)	0.02	1.4 (0.1 to 3.0)	0.04	1.2 (-0.8 to 3.6)	0.2	0.8 (-0.4 to 2.3)	0.2
Cingulum PC R	0.1 (-1.4 to 1.0)	0.8	0.1 (-1.8 to 1.5)	0.9	-1.1 (-3.9 to 1.1)	0.3	0.4 (-1.3 to 1.7)	0.8
Cingulum PC L	-0.1 (-1.3 to 1.4)	0.9	-0.6 (-2.2 to 1.2)	0.6	1.0 (-1.4 to 3.6)	0.4	0.0 (-1.9 to 2.1)	0.9
Cingulum PH R	3.3 (2.0 to 5.9)	<0.001	4.7 (3.2 to 7.4)	<0.001	2.8 (-1.2 to 7.7)	0.1	2.8 (0.8 to 6.0)	0.01
Cingulum PH L	3.2 (1.2 to 6.5)	0.005	5.4 (3.5 to 8.6)	<0.001	1.4 (-2.6 to 6.7)	0.4	1.0 (-1.6 to 4.7)	0.3
Fornix	0.4 (-0.8 to 2.4)	0.3	-0.1 (-1.7 to 2.7)	0.6	-0.8 (-2.3 to 1.5)	0.7	0.8 (-0.4 to 2.7)	0.1
UF R	2.6 (1.3 to 5.1)	0.001	3.8 (2.2 to 6.6)	<0.001	0.8 (-2.4 to 5.3)	0.5	1.9 (0.3 to 4.7)	0.03
UF L	4.7 (1.1 to 7.7)	0.009	8.0 (3.7 to 12.0)	<0.001	4.1 (0.4 to 7.3)	0.03	0.8 (-1.2 to 2.2)	0.6
CST R	-0.1 (-2.7 to 3.4)	0.8	0.6 (-3.0 to 5.0)	0.6	1.0 (-5.1 to 8.1)	0.7	-0.7 (-4.4 to 3.8)	0.9
CST L	0.8 (-1.7 to 5.2)	0.3	1.0 (-2.4 to 6.5)	0.4	4.5 (-1.7 to 12.4)	0.1	-0.7 (-4.1 to 4.4)	0.9
SCP R	-0.1 (-2.7 to 3.4)	0.8	0.6 (-3.0 to 5.0)	0.6	1.0 (-5.1 to 8.1)	0.7	-0.7 (-4.4 to 3.8)	0.9
SCP L	2.9 (0.8 to 5.6)	0.008	2.8 (0.4 to 5.8)	0.03	6.8 (2.4 to 11.8)	0.003	2.2 (-0.4 to 5.4)	0.1

Table 4.11 Estimated percentage per year difference in the rate of change of AX for bvFTD patients and bvFTD subgroups, by region, compared with controls. Data is uncorrected for multiple comparisons.

4.3.4 Longitudinal DTI changes in bvFTD subgroups

Rates of change for each region of interest and as measured by FA, MD, RD and AX, by bvFTD subgroup, are shown in Table 4.8 to 4.11 respectively. Compared with controls the largest reduction in FA were within bilateral uncinate fasciculus (right, -7.2%/year, 95% CI -9.7% to -4.7%, p<0.001; left, -7.9%/year, 95% CI -12.0% to -3.7%, p<0.001) in *MAPT* mutation carriers; bilateral paracallosal cingulum bundle (right, -6.7%/year, 95% CI -10.0% to -3.4%, p<0.001; left, -5.6%/year, 95% CI -8.3% to -2.8%, p<0.001) in those with sporadic bvFTD; and in right paracallosal cingulum bundle (6.8%/year, 95% CI -11.3% to 2.2%, p=0.004) in *C9ORF72* mutation carriers. Compared with controls the largest increased in MD were in bilateral uncinate fasciculus (right, 6.7%/year, 95% CI 3.7% to 9.6%, p<0.001; left, 10.9%/year, 95% CI 5.2% to 16.5%, p<0.001) in *MAPT* mutation carriers; bilateral paracallosal cingulum bundle (right, 3.8%/year, 95% CI 1.5% to 6.0%, p=0.001; left, 3.4%/year, 95% CI 0.8% to 6.1%, p=0.01) in sporadic bvFTD; and in left uncinate fasciculus (6.0%/year, 95% CI 0.8% to 11.2%, p=0.02) in *C9ORF72* mutation carriers. Compared with controls the largest increase in RD were within bilateral uncinate fasciculus (right, 7.4%/year, 95% CI 4.7% to 12.6%, p<0.001; left 12.7%/year, 95% CI 6.3% to 20.6%, p<0.001) in *MAPT* mutation carriers; bilateral paracallosal cingulum (right, 9.5%/year, 95% CI 3.0% to 13.0%, p=0.002; left, 8.0%/year, 95% CI 2.9% to 11.7%, p=0.001) in sporadic bvFTD; and within left uncinate fasciculus (8.2%/year, 95% CI 1.4% to 16.1%, p=0.02) in *C9ORF72* mutation carriers. Compared with controls the largest increase in AX were within bilateral uncinate fasciculus (right, 3.8%/year, 95% CI 2.2% to 6.6%, p<0.001; left, 8.0%/year, 95% CI 3.7% to 12%, p<0.001) in *MAPT* mutation carriers; right parahippocampal cingulum (2.8%/year, 95% CI 0.8% to 6.0%, p=0.01), in sporadic bvFTD; and in left superior

cerebellar peduncle (6.8%/year, 95% CI 2.4% to 11.8%, p=0.003), in *C9ORF72* mutation carriers.

4.3.5 Cross-sectional and longitudinal DTI metric sensitivity and specificity

To determine optimal DTI metrics AUC data were calculated and indicated that classification of control and bvFTD groups cross-sectionally were best achieved using RD, measured within the right uncinate fasciculus (AUC=0.86, specificity 94%, sensitivity 68%); followed by MD (AUC=0.83, specificity 89%, sensitivity 74%), FA (AUC=0.79, specificity 67%, sensitivity 84%) and AX (AUC=0.75, specificity 83%, sensitivity 74%). This is similar to the findings from the study in Chapter 3 (see Figure 3.7), despite the current study having a different methodology in determining DTI metric values. Classification of control and bvFTD groups longitudinally were best achieved using FA change, measured within the right cingulum bundle (AUC=0.79, specificity 94%, sensitivity 63%); followed by MD (AUC=0.77, specificity 89%, sensitivity 68%) and RD (AUC=0.76, specificity 100%, sensitivity 58%), with AX performing less favorably (AUC=0.53, specificity 67%, sensitivity 47%).

4.3.6 Sample size estimations

Sample sizes required for future clinical trials were calculated using annualised change score in three potential outcome measures; whole brain atrophy (using BBSI), change in graded naming test, chosen as this was the only longitudinal neuropsychological measure to show statistical difference from cognitively normal participant over time, and DTI change for each metric within either right

paracallosal cingulum or right uncinate fasciculus (chosen on the basis of statistical significance). Sample size estimates corrected for control rates of change are displayed in table 4.12. Sample size estimates based on changes in FA were smaller than sample size estimates based on other outcome measures.

	DTI change (%/year)				BBSI (ml/year)	Change in Graded Naming Test
	Right Cingulum Bundle			R UF		
% Change	*FA*	*MD*	*RD*	*AX*		
20	276	1031	531	1229	507	1524
30	123	459	236	546	226	685
40	69	258	133	308	127	381
50	45	165	85	197	82	246

Table 4.12. Sample Size Estimates per treatment arm of a putative clinical trial comparing 3 different outcome measures to detect a 20 to 50% reduction in rates of change. β = 80%, α = 0.05.

4.4 Discussion

4.4.1 Overview of results

This study is one of the first to demonstrate the feasibility of carrying out longitudinal DTI in patients with bvFTD as well as reporting on rates of change in DTI metrics in key white matter structures. Compared with the only previous study known at the time of writing, the current study has adopted an improved approach for DTI spatial normalization, which enforces longitudinally and cross-sectionally consistent and accurate ROI segmentations, thus reducing potential time-point biases and reducing issues such excessive warping due to atrophy and partial volume effects during the registration process. Using these improved DTI methods, this study reports (1) both core and mutation specific patterns of white matter change in bvFTD; and (2) demonstrates that longitudinal DTI is a feasible

outcome measure for clinical trials, requiring smaller sample sizes than other more conventional outcome measures, as has also been shown in AD when comparing FA change within the fornix and hippocampal atrophy (Fellgiebel et al., 2006; Nowrangi et al., 2013).

The current study found that decreasing FA and increasing MD, RD and AX were a consistent finding within both right and left uncinate fasciculus. The cingulum bundle was also preferentially involved across metrics with decreasing FA and increasing MD and RD within the paracallosal portions, and increasing MD, TR and AX within the parahippocampal portions. The corpus callosum was also consistently involved across all DTI metrics, with the splenium showing the most robust change, followed by the body of the corpus callosum. These findings are in line with a number of cross-sectional DTI studies in bvFTD as well as the cross-sectional findings in the preceding chapter (Agosta et al., 2012; Lillo et al., 2012; Whitwell et al., 2010; Zhang et al., 2009).

Once again these findings are supported by the biological role of these tracts, as previously discussed in Chapter 3, with the cingulum bundle being a key tract linking anterior cingulate and prefrontal cortices and likely underpinning many executive and social cognitive processes. It is of interest that the greatest cross-sectional differences in the cingulum were within the parahippocampal subdivision. This suggests this ventral subdivision of the cingulum, linking structures within the limbic system such as hippocampus and posterior cingulate cortex, is involved early in the disease process, and indeed may account for some

of the more subtle changes in general intellectual function seen in early bvFTD (Janssen et al., 2005). However, over time the paracallosal cingulum, linking cingulate and prefrontal cortices and overlapping with the functionally relevant 'Salience Network' (Seeley et al., 2009), showed greater disease progression, with the exception of AX, which showed greatest disease progression within the parahippocampal formation. One possible explanation for this could be that AX is more suitable at detecting white matter pathology occurring due to specific toxic proteins, which localizes to this region, for example tau pathology. Of course this assumption would need confirmation through histopathology, something the current study lacks. However it is noteworthy that in the *MAPT* mutation group (which is a tauopathy), highly significant change in this white matter tract was detected using AX, offering some limited support for this notion.

4.4.2 Relevance to previous longitudinal studies

These longitudinal imaging changes may be associated with the clinical evolution of bvFTD with progressive disintegration of social cognition and executive skills such as response inhibition and set shifting (Linke et al., 2013; Metzler-Baddeley et al., 2012). These findings build on the cross-sectional data already presented in chapter 3 and detailed discussions of the neurobiological relevance of these tracts can be found there. Longitudinal DTI studies are limited, however many of the relevant studies, examining conditions which result in abnormal social cognition and executive dysfunction, show concordance with the findings here. For example previous longitudinal studies in mild cognitive impairment and AD have also implicated the cingulum bundle, corpus callosum and uncinate fasciculus (Kitamura

et al., 2013; Teipel et al., 2010). A recent study in Huntington's disease has also implicated the corpus callosum in disease progression (Poudel et al., 2014), whilst a study in Motor Neuron Disease, a condition which overlaps with bvFTD, has demonstrated changes in white matter beyond just the corticospinal tracts, with frontal white matter tract involvement also (Keil et al., 2012). Longitudinal studies in psychiatric disorders are few however one study did show the corpus callosum having progressive reduction in FA in patients with chronic schizophrenia (Mitelman et al., 2009).

4.4.3 Molecular considerations

Different patterns of white matter change were associated with different bvFTD subtypes: in *MAPT* mutation carriers the most robust changes were within bilateral uncinate fasciculus, bilateral paracallosal and parahippocampal cingulum and the body of the corpus callosum; in the *C9ORF72* mutation carriers within corpus callosum and right paracallosal cingulum bundle; and in sporadic bvFTD within the bilateral paracallosal cingulum bundle. *MAPT* mutation carriers were the only group to have significant change over time within both right and left uncinate fasciculus, with a high burden of white matter change occurring in medial temporal lobe regions. Breakdown of these tracts is biologically plausible given that these tracts link grey matter structures which show preferentially more longitudinal atrophy in affected *MAPT* mutation carriers (Rohrer et al., 2010c). Compelling evidence for involvement of the uncinate fasciculus in *MAPT* related bvFTD comes from a recent study of presymptomatic *MAPT* mutation carriers (Dopper et al., 2013). Although interpretation of change within the *C9ORF72* group must be viewed in terms of the

small sample size it is of interest that only this group showed significant difference in bilateral superior cerebellar peduncles cross-sectionally and neared significance (p=0.06) longitudinally. This might be surprising for a "frontotemporal" dementia, however this finding is consistent with other data suggesting that changes within the cerebellum and associated structures may be a particular hallmark of *C9ORF72* mutation carriers (Downey et al., 2012; Mahoney et al., 2012a, 2012b). In addition another recent longitudinal DTI study of motor neuron disease, which *C9ORF72* is the most frequent genetic cause, identified reduced FA in the cerebellar vermis (Keil et al., 2012). These converging lines of evidence appear to offer support for the idea that the cerebellar involvement may be a specific signature of bvFTD due to *C9ORF72*. In the sporadic bvFTD group bilateral paracallosal cingulum bundle was the primary region-of-interest affected, which is in keeping with the broader group level finding. The heterogeneity of the group could provide a possible explanation for the emergence of a more limited profile of white matter change in this group. However, it is noteworthy that the paracallosal cingulum displayed significant differences from controls across subgroups both cross-sectionally and longitudinally. This suggests that damage to these fibres is common across the spectrum of bvFTD, making it a potentially appealing tract to study longitudinally.

4.4.4. DTI metrics

An important issue that remains poorly understood is the choice of DTI metric to detect and track white matter change. To date most longitudinal DTI studies have reported only changes in FA (Mielke et al., 2009; Teipel et al., 2010), although more recently studies have also reported on changes in mean diffusivity (Keihaninejad et

al., 2013; Nowrangi et al., 2013). The current study compared the performance of a range of DTI metrics and suggest that the optimal region-of-interest and DTI metric may differ cross-sectionally and longitudinally. Data from the current study as well as the cross-sectional study contained in chapter 3 suggests that RD is to the most sensitive cross-sectional DTI metric, particularly when sampled within the right uncinate fasciculus. FA change within the right paracallosal cingulum bundle performed best longitudinally, with largest area under the curve and yielding the lowest sample size estimation. These differences may in part be explained by variations in disease neurobiology and tract anatomy. Changes in RD and AX are thought to reflect local changes in myelination and axonal damage respectively whilst FA, a composite of these measures, reflects changes in the overall direction of diffusion reflecting more general white matter integrity. RD and AX may have superior ability to detect focal white matter pathology, thus making them sensitive cross-sectional metrics. The longitudinal changes detected may reflect Wallerian degeneration, rather than focal white matter demyelination, a process commonly seen in a range of neurodegenerative disorders (Raff et al., 2002), which may be better detected by FA (Brennan et al., 2013). However, it could not be validly argued that FA is the only metric to capture change; particularly as FA values are determined to some degree by changes in RD. The performance of particular DTI metrics is also likely affected by individual patient variability, particularly relevant to bvFTD given its pathological heterogeneity, which may result in variable trajectories of disease progression (see figures 4.1 to 4.3). It is also possible that certain white matter structures are more suited to longitudinal measurements than others, perhaps due to their orientation or size thus allowing better

registration. For example change within the genu and body of the corpus callosum appeared more stable in control participants whilst in other structures the trajectory of change was more variable (see figure 4.3).

Understanding how disease neurobiology results in specific changes to DTI metrics will require further studies with larger pathologically confirmed cohorts, including the progranulin genetic subtype, which the current study lacks. Notwithstanding these limitations the current study has demonstrated that a within-subject measure of DTI change is a potentially useful disease biomarker with the ability to detect greater differences across white matter regions compared with cross-sectional measures. The current study also identified that FA, as an outcome measure, requires fewer subjects compared to more traditional outcome metrics. These findings suggests that longitudinal DTI may be an important biomarker for disease monitoring with particular implications for future clinical trials.

4.5 Chapter summary

This study represents one of the first studies to explore within-subject trajectories of white matter change over time, offering new insights into the disease progression of bvFTD. As a group bvFTD shows progressive alteration of white matter within the paracallosal cingulum bundle, an area that overlaps the functionally important salience network. This study provides new data confirming these white matter structures as a key site of pathology in bvFTD. Furthermore this study shows the utility of longitudinal DTI in monitoring these large-scale structural networks over time. The uncinate fasciculus and body and splenium of the corpus callosum showed the most consistent involvement and rate of change across DTI metrics. Molecularly defined profiles of disease progression also emerged with the uncinate fasciculus being the sight of maximal change in the *MAPT* group, and some weaker evidence suggesting change within the superior cerebellar peduncle may be a signature of *C9ORF72* disease. Other longitudinal DTI studies examining conditions with similar clinical phenotypes have found similar evidence for involvement of these white matter structures. Comparison of DTI metrics revealed that FA had the best performance at separating bvFTD from healthy participants longitudinally, and identified the discrepancies between cross-sectional and longitudinal sensitivities of specific DTI metrics. Finally change in FA was found to be a superior outcome measure than neuropsychological or volumetric brain measurement in a sample size calculation.

5. Cross-sectional profiles of white matter pathology in the primary progressive aphasias.

5.1 Introduction

5.1.1 Overview

The primary progressive aphasias (PPA) or 'language-led dementias' are important on both clinical and neurobiological grounds (Gorno-Tempini et al., 2011; Grossman, 2010; Rohrer et al., 2010d). Clinically, PPA is associated with the selective but relentless erosion of language functions, while neurobiologically PPA illustrates regional vulnerability of brain language systems to neurodegenerative pathologies that are collectively characterised by abnormal protein accumulation. The spectrum of PPA is clinically, anatomically and pathologically heterogeneous (Grossman, 2010). The clinical, radiological and pathological hallmarks of the PPA's are outlined in detail in the introductory chapter.

Despite the recent formulation of new consensus diagnostic criteria for PPA (Gorno-Tempini et al., 2011), substantial nosological difficulties remain (Knibb et al., 2006). These include the frequent occurrence of overlap syndromes, clinico-anatomical convergence between syndromic subtypes and pathological heterogeneity (Rogalski et al., 2011; Rohrer et al., 2011; Rohrer et al., 2008). A recent wealth of genetic and neuropathological data has enabled certain clinical PPA phenotypes to be correlated with particular pathological substrates. However, despite these advances, predicting tissue pathology or indeed making an accurate clinical diagnosis remains challenging for the diseases in the PPA spectrum. This is

compounded by a paucity of robust in-vivo biomarkers to detect disease onset and track disease progression.

5.1.2 Overview of previous neuroimaging studies in PPA

As already speculated studying changes within large-scale connectivity networks, in this case those that underpin language, may offer a potentially powerful framework for understanding the regionally specific but distributed effects of PPA. However, whereas substantial evidence has been amassed concerning regional cortical profiles of PPA (Mummery et al., 2000; Gorno-Tempini et al., 2004; Josephs et al., 2006; Pereira et al., 2009; Rohrer et al., 2009b; Rohrer et al., 2010c), relatively little information is available concerning changes in white matter tracts within brain language networks produced by neurodegenerative disease (Agosta et al., 2010; Whitwell et al., 2010; Zhang et al., 2009). Previous white matter tract studies in PPA (Acosta-Cabronero et al., 2011; Agosta et al., 2012; Agosta et al., 2010; Galantucci et al., 2011; Iaccarino et al., 2015; Mandelli et al., 2014; Schwindt et al., 2011) have shown considerable anatomical and methodological variability (see table 5.1). There remain few detailed comparisons between PPA subtypes and other neurodegenerative diseases, and between grey matter (GM) and white matter changes in these diseases. Besides facilitating diagnosis and tracking of PPA (Larsson et al., 2004; Schmierer et al., 2007) identification of white matter tract signatures of PPA syndromes might improve our understanding of the pathophysiology of network disintegration in these diseases and could yield important insights into the molecular organisation of vulnerable language networks (Raj et al., 2012; Warren et al., 2012; Zhou et al., 2012).

The aim of this chapter is to assess white matter tract pathology in each of the canonical PPA syndromes using multiple DTI metrics with a relatively anatomically unbiased whole brain analysis technique. The primary hypothesis for the current study is that distinct profiles of white matter pathology will emerge for each of the PPA syndromes, reflecting the role of specific white matter tracts within the distributed language network.

Paper	Subjects	Tract selection	Dir	Statistical method	Software	UF			ILF			SLF			Other		
						NV	LV	SV	NV	LV	SV	NV	LV	SV	NV	LV	SV
Agosta 2010	SV=5 Control=8	ROI (L ILF/L SLF/ L UF/CC)	55	Linear mixed effects model	In-house	nt	nt	L	nt	nt	-	nt	nt	L[1]	nt	nt	CC[2]
Whitwell 2010	NV=7, SV=4 Control=19	ROI n=16	21	ANCOVA	DTI Studio	-	nt	-	-	nt	L[3]	R[4]	nt	-	nt	nt	nt
Galantucci 2011	NV=9, LV=9, SV=9, Control=21	ROI (ILF/UF/SLF)	64	ANCOVA	PROBTRACKX	-	-	B	-	-	B[5]	L	L[6]	L[7]	nt	nt	nt
Acosta-Cabrenaro 2011	SV=10, Control=21	Whole brain	63	Non-parametric permutation test	FMRIB/TBSS/ Tractography	nt	nt	-	nt	nt	L^	nt	nt	-	nt	nt	nt
Agosta 2011	NV=9, LV=4 SV=7, Control=27	Whole brain	32	Non-parametric permutation test	FDT/TBSS	L	-	B	L[8]	-	L[8]	L	-	-	B CB, CC, FO	FO	CC, L CB, FO
Schwindt 2013	SV=9, NV=9 Control=16	Whole brain	23	Non-parametric permutation test	FDT/TBSS	L	nt	B	L	nt	B	-	nt	B	nt	nt	L ATR, B FM, CC
Madelli 2014	NV=9, SV=8, LV=8, Control=21	ROI (left-sided only)	64	ANCOVA	Q-BALL Imaging (HARDI)	-	-	L	-	L	L	L	-	-	AF, IFOF		AF
Iaccarino 2014	SV=3, Control=20	ROI	32	Confidence intervals	PROBTRACKX	nt	nt	B	nt	nt	B	nt	nt	-			
Present study	NV=13, LV=10 SV=10,AD=20 Control=20	Whole brain	64	Non-parametric permutation test	CAMINO/TBSS	L	L	B	-	L	L	-	-	-	L CST	L CB, FO	L ATR, R CB

Table 5.1 Comparison of FA changes in DTI studies of PPA. Results reported reflect most statistically robust findings (for present study, only significance values p<0.01 are included here; see also Table 5.2 to 5.5). *=only left hemispheric tracts reported. ^=Results reported based on authors figures. nt = data not reported/tested, - indicates no significant result found. [1]=Arcuate and fronto-parietal SLF, [2]=Genu, [3]=Posterior ILF, [4]=Anterior SLF, [5]= Bilateral anterior ILF and left medial ILF, [6]=SLF temporo-parietal fibres, [7]=Arcuate and SLF temporo-parietal, [8]=Inferior fronto-occipital fasciculus.

5.2 Methods

5.2.1 Subjects

Consecutive patients fulfilling current consensus criteria (see table 1.2) for a diagnosis of PPA were recruited from the Specialist Cognitive Disorders Clinic at the National Hospital for Neurology and Neurosurgery. Subjects underwent a structured clinical and neurolinguistic assessment and structural MRI to exclude significant white matter disease or other focal cerebral lesions. For purposes of syndrome definition, a general neuropsychological assessment using standardised tests was performed (see methods, section 2.1.2. for details). Demographic and neuropsychological data were analysed statistically in STATA 10 (Statacorp, Texas, USA) using Student's t-test and Wilcoxon Rank-sum tests of significance. In addition, CSF data (if available) were analysed to assess the extent to which particular syndromes were likely to have underlying AD (versus non-AD) pathology (see Methods for details of local CSF ranges indicative of AD pathology).

5.2.2 Image processing

Volumetric and DTI MRI scans were acquired for all subjects, using the same acquisition parameters as described previously. Raw diffusion weighted images were processed as per the cross-sectional DTI pipeline outlined within the general methods chapter (see Methods, section 2.6 for details). Statistical analysis of post-processed DTI data were also carried out as outlined previously, with models fitted separately to FA, RD, AX and TR. Each PPA subgroup was contrasted with both the healthy and disease control groups and with each of the other PPA subgroups. In addition as lvPPA is associated with AD pathology, an additional contrast

comparing patients with typical AD and controls was generated for each DTI metric. Post statistical analysis involved projecting significant results onto a study specific mean brain registered to standard (MNI) space and performing a ROI analysis. To provide accurate anatomical localisation a series of tract specific masks were applied: 14 masks were generated, including right and left inferior longitudinal fasciculus, superior longitudinal fasciculus, uncinate fasciculus, anterior thalamic radiation, cingulum bundle and corticospinal tract, as well as corpus callosum (CC) and fornix. The extent of tract involvement within each disease group and for each DTI metric (FA, AX, RD and TR) was calculated and expressed as a proportion of the entire white matter region of interest.

Grey matter analyses were carried out on each subject's volumetric MRI scans using VBM following the steps outlined in the Methods chapter (see methods, section 2.4. for details). Grey and white matter analyses were carried out using the same statistical methodology (i.e. a non-parametric permutation test). Maps of grey matter atrophy were overlaid onto a standard (MNI152) brain following FWE correction ($p<0.05$) with TFCE.

5.3 Results

5.3.1 Subject characteristics, demographic and neuropsychological details

Thirty-three consecutive patients with PPA (mean age 65.2 ± 7.9 years; 24 females) were identified as meeting current consensus criteria (Gorno-Tempini et al., 2011). Patients were characterised as follows, thirteen having nvPPA, ten having lvPPA

and 10 having svPPA. Twenty age and gender comparable cognitively normal individuals also participated (mean age 64.7 ± 5.5 years; 12 females). Twenty age and gender comparable patients with a diagnosis of AD were also included (mean age 62.8 ±5.0 years; 11 females) to act as disease controls. 30 of 33 subjects completed a detailed neuropsychological assessment; the remaining three patients were unable to comply with behavioural testing, or declined and their syndromes were defined based on bedside clinical assessment alone. In addition a further two patients presented with a cognitive syndrome compatible with Granulin associated aphasia (GAA) (mean age 61 ± 14.1 years; 1 female; disease duration 2.8 ± 1.8 years) (Rohrer et al., 2010a) and were subsequently confirmed to have a GRN mutation (both exon 2 c31fs). Whilst this group is of high interest it was decided not to study these subjects due to the group size being so small. In addition given the molecular basis and unique clinical features of this group it is quite probable that it may have a unique signature of white matter pathology, precluding their inclusion within another syndromic group.

Demographic and neuropsychological data for all subjects are summarised in table 5.2. There were no significant differences in age or gender between disease and control groups. Neuropsychological profiles were in keeping with the clinical syndromic diagnosis.

	nvPPA		lvPPA		svPPA		AD		Controls	
No (female)	13 (10)		10 (5)		10 (7)		20 (11)		20 (12)	
	Mean	**S.D**	**Mean**	**S.D**	**Mean**	**S.D**	**Mean**	**S.D**	**Mean**	**S.D**
Age	65.7	9.4	67.0	6.1	63.4	6.7	62.8	5.0	64.7	5.5
Disease Duration	3.3	1.2	4.0	1.4	5.0	2.0	5.6	3.8		
MMSE (/30)	18.0	10.9	16.9	8.5	20.6	8.5	21.0	4.6	29.6*	0.5
RMT - Words (/50) †	40.5	8.9	29.9	9.1	32.0	8.0	30.1	6.1	47.1*	2.3
RMT - Faces (/50) ††	36.7	5.8	29.8	7.4	31.7	7.8	33.7	6.0	41.8*	5.0
BPVS (/150)^	120.6	41.0	87.4	46.4	65.6	49.2	135.5	22.8	147.8*	1.5
GNT (/30)^^	10.8	10.6	4.4	4.3	1.6	4.3	13.4	8.7	26.8*	1.7
GDA (/24)#	4.2	2.6	0.1	0.3	8.3	8.8	5.1	4.3	12.9**	4.4
VOSP (/20)	16.5	3.1	14.6	6.2	14.6	4.3	15.7	2.5	18.0*	3.5
Stroop Colour Naming (secs)##	74.5	21.4	68.0	20.6	56.8	23.0	55.2	18.6	30.2*	3.8
Word Repetition (/45) §	21.8	16.0	40.3	5.1	43.9	1.4			44.3**	1.0
Sentence Repetition (/10) §§	3.7	3.9	6.2	3.1	9.6	0.7			9.8**	0.6
Receptive Grammar -PALPA55 (/24)	16.1	7.4	11.6	6.0	21.1	3.0			23.5*	0.7
Baxter Spelling Test (/30)	11.2	9.7	6.7	5.9	14.0	10.4			26.9**	1.3
	CSF N=7		CSF N=9		CSF N=5		CSF N=10			
CSF Total Tau (pg/ml)	540	370	888	318	350	131	770	355		
CSF ABeta$_{1-42}$	384	148	256	122	669	156	240	64		

***** p<0.05 control vs. all disease groups
****** p<0.05 control vs. nvPPA/lvPPA
† p<0.05 nvPPA vs. AD
†† p<0.05 nvPPA vs. lvPPA/svPPA; p <0.05 lvPPA vs. svPPA
^ p<0.05 svPPA vs. all groups; p <0.05 lvPPA vs. nvPPA/AD
^^ p<0.05 svPPA vs. all groups; p<0.05 lvPPA vs. AD
# p<0.05 lvPPA vs. all groups
p<0.05 nvPPA vs. AD
§ p<0.05 nvPPA vs. lvPPA/svPPA
§§ p<0.05 svPPA vs. nvPPA/lvPPA
~ p<0.05 lvPPA vs. svPPA

Table 5.2 Summary of demographics, neuropsychological and CSF data for PPA groups, AD patients and healthy controls. Statistical significance of between group comparisons is displayed in the legend at the bottom of the table.

CSF data were available on 31 (56%) of all 53 affected individuals (comprising seven nvPPA, nine lvPPA, five svPPA, 10 AD). Two of seven nvPPA cases (29%) had CSF consistent with underlying non-AD pathology and eight of nine lv-PPA cases (89%) had CSF consistent with AD pathology. All svPPA cases had CSF consistent with non-AD pathology. All clinically diagnosed AD cases had CSF consistent with AD pathology.

5.3.2 PPA groups versus healthy controls and AD disease-controls

White matter tract alterations were identified for each PPA syndromic group compared with healthy controls (Figures 5.1 to 5.3) and AD disease-controls (Figure 5.4) groups. Maps of altered diffusivity for AD disease-controls compared with healthy controls are presented Figure 5.5.

Individual tracts are listed and their involvement in each PPA syndrome relative to healthy controls is quantified in tables 5.3 to 5.6; quantitative data relative to the AD group are presented in table 5.7; quantitative date comparing PPA syndromic groups with each other are presented in table 5.8. The overall profile of white matter tract pathology in each syndrome, taking all DTI metrics into account, is discussed in the following section with differences in the pattern of involvement considered subsequently.

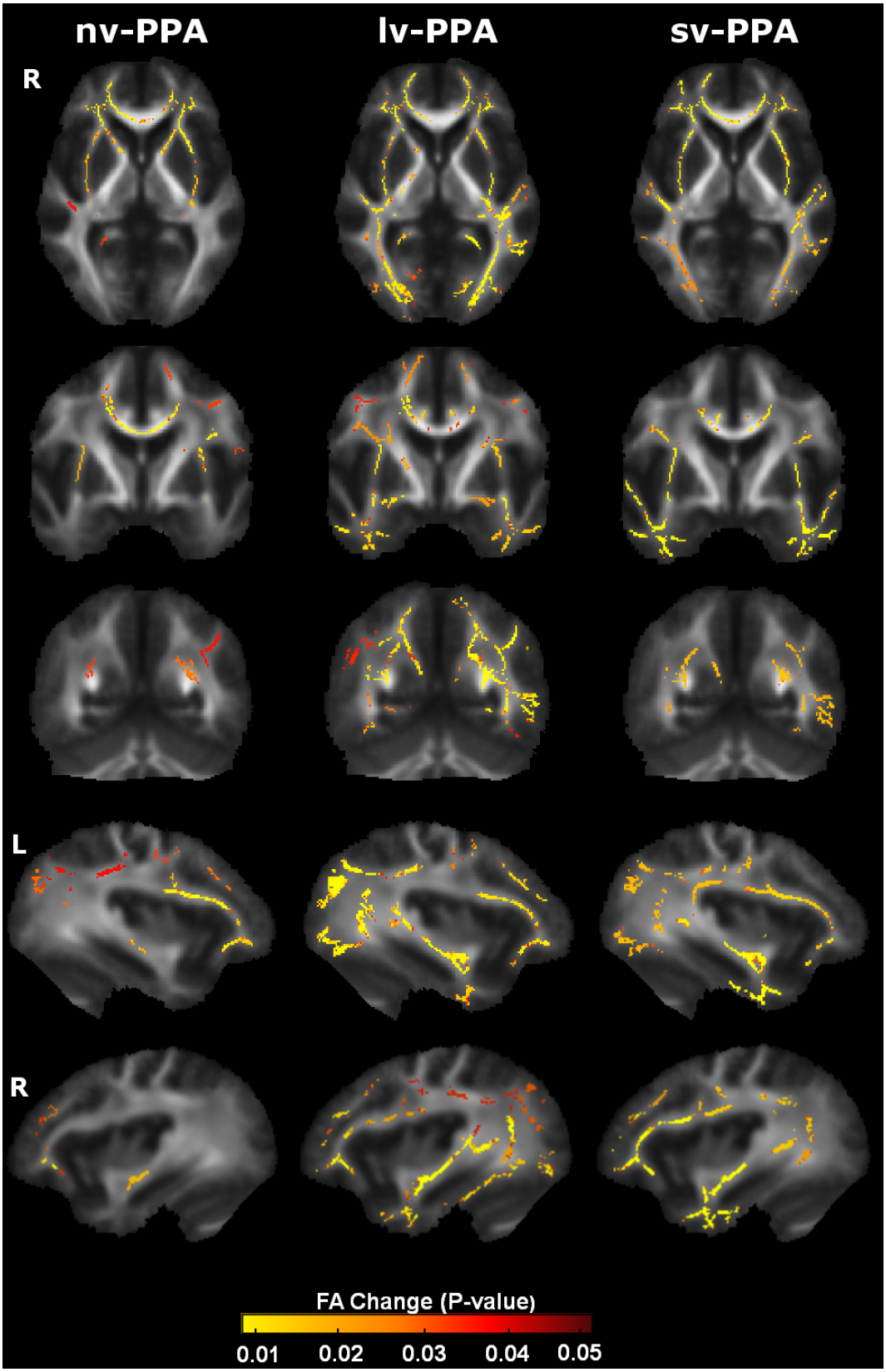

Figure 5.1. Patterns of decreased FA in PPA groups compared with controls. Results are overlaid on representative sections derived from the FA skeleton. For coronal and axial sections, the right hemisphere is shown on the left. The colour scale indexes P values after family-wise error correction for multiple comparisons over the whole brain.

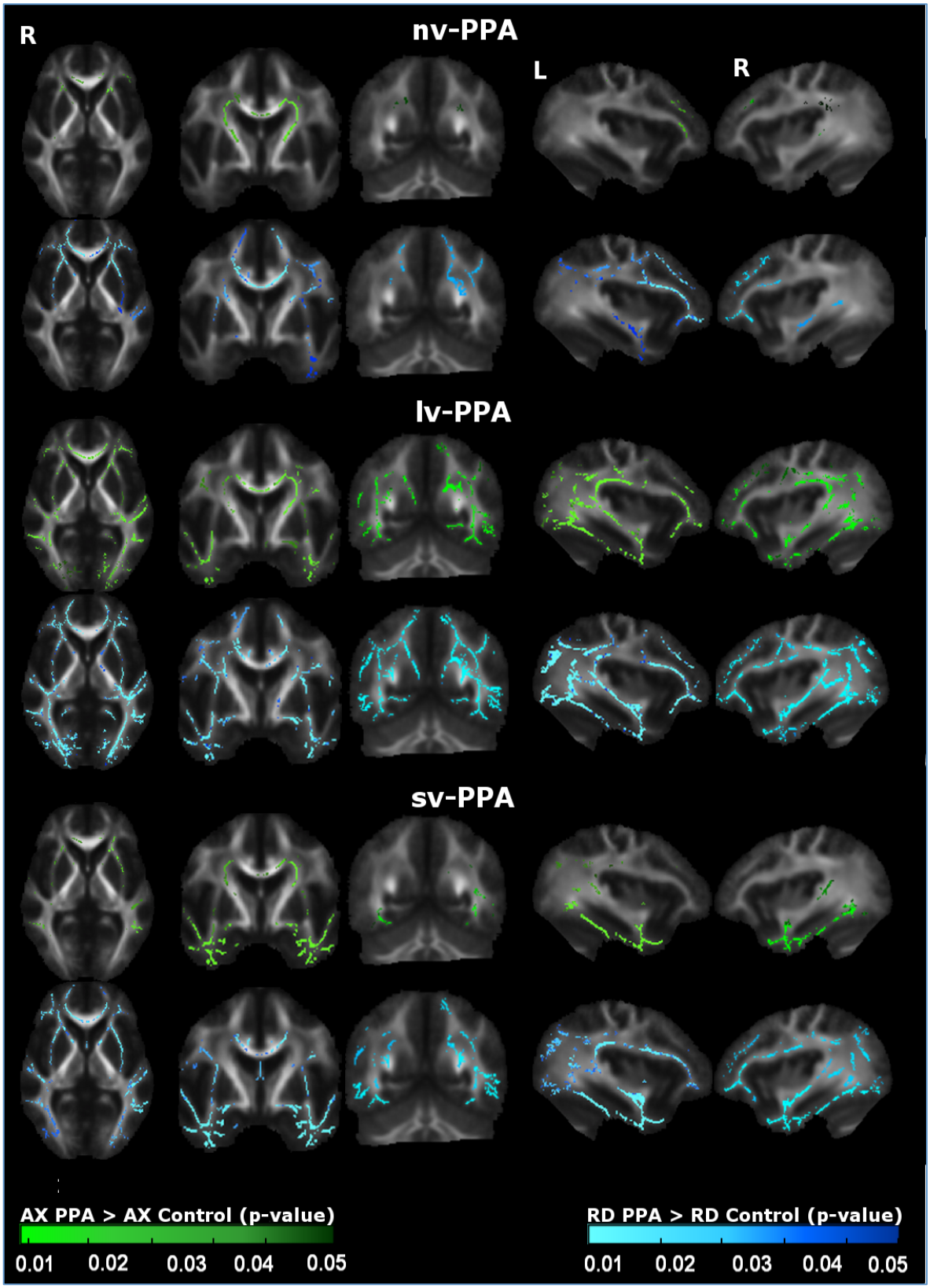

Figure 5.2. Patterns of increased AX and RD in PPA groups compared with controls. For each panel, the AX map (green) is displayed on the top and the RD map (blue) on the bottom. Results are overlaid on representative sections derived from the average FA skeleton. For coronal and axial sections, the right hemisphere is shown on the left. The colour scale indexes P values after family-wise error correction for multiple comparisons over the whole brain.

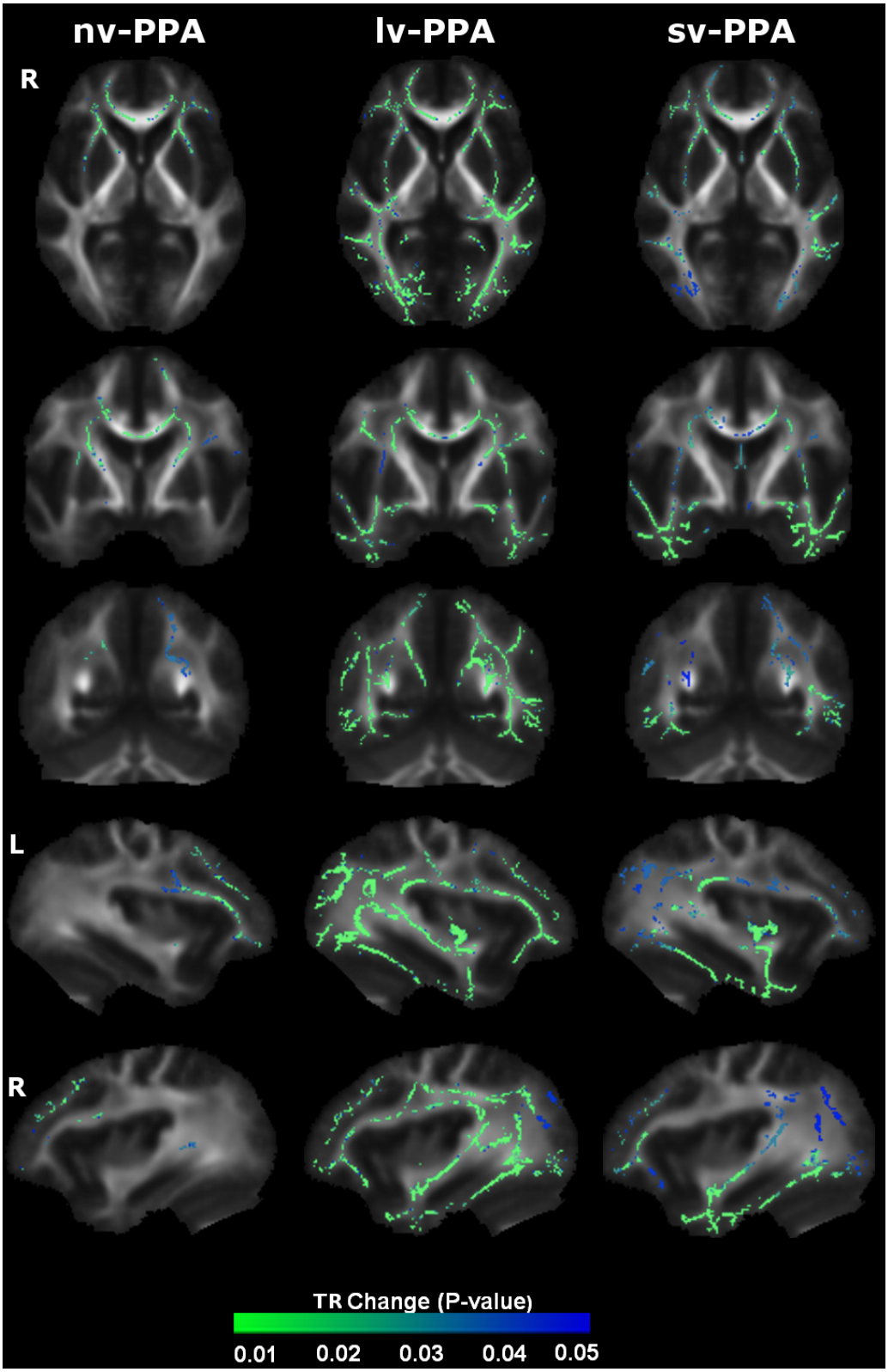

Figure 5.3. Patterns of increased TR in PPA groups compared with controls. Results are overlaid on representative sections derived from the FA skeleton. For coronal and axial sections, the right hemisphere is shown on the left. The colour scale indexes P values after family-wise error correction for multiple comparisons over the whole brain.

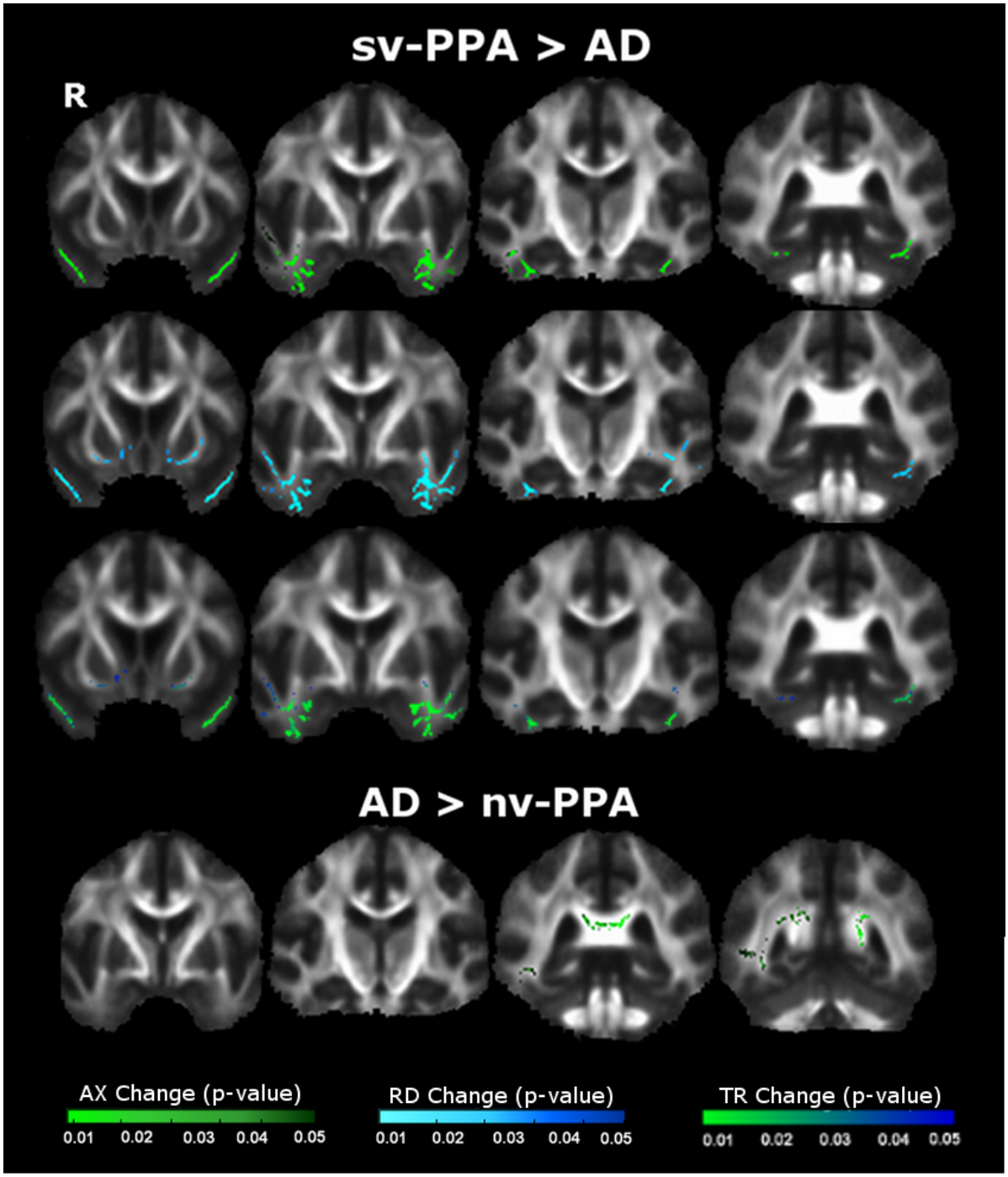

Figure 5.4. Top panel shows areas of altered white matter in svPPA compared with AD patients; indicating profiles of increased AX (top), RD (middle) and TR bottom. Results are overlaid on representative sections (MNI co-ordinates shown on left) derived from the average FA skeleton. For coronal and axial sections, the right hemisphere is shown on the left. The colour bar (bottom) codes significance (FWE corrected p-value).

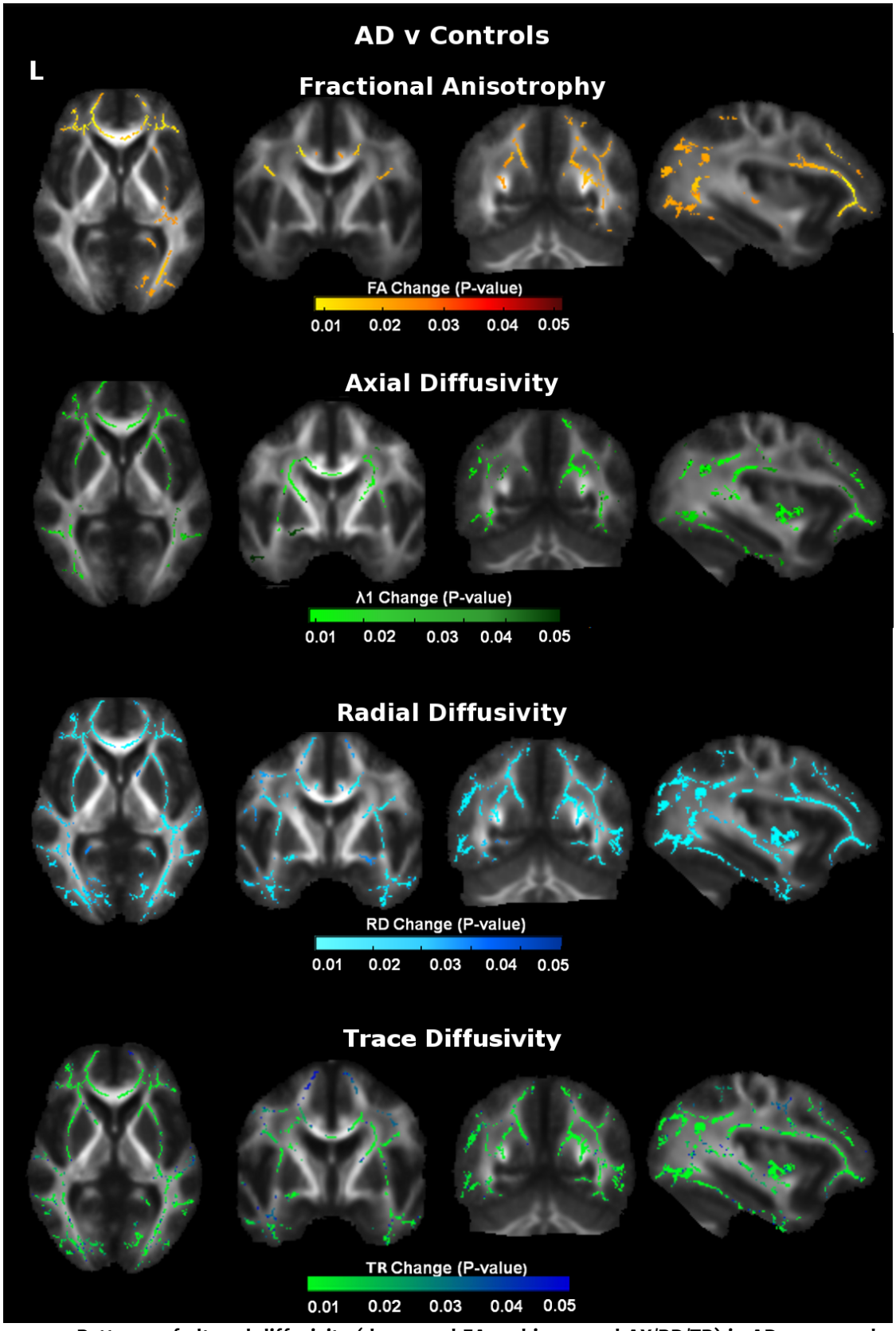

Figure 5.5. Patterns of altered diffusivity (decreased FA and increased AX/RD/TR) in AD compared with healthy controls. Results are overlaid on representative sections derived from the average FA skeleton. For coronal and axial sections, the right hemisphere is shown on the left. The colour bar (bottom) codes significance (FWE corrected p-value).

Compared with both healthy subjects and AD patients, the svPPA group had evidence of white matter tract pathology involving both hemispheres with an emphasis on fronto-temporal tracts, in particular within anterior-ventral fibres of bilateral uncinate fasciculus and bilateral inferior longitudinal fasciculus, with less significant involvement of dorsal and posterior white matter tracts. Comparing DTI metrics, the most extensive changes (% of significant voxels within a white matter tract) were detected by RD, followed by TR, FA and AX. Compared with healthy subjects, the nvPPA group had white matter tract pathology within both cerebral hemispheres predominantly involving the left anterior frontal lobe (uncinate fasciculus) and subcortical (anterior thalamic radiations and corticospinal tracts) projections; comparing nvPPA with AD, the AD group showed more extensive posterior hemisphere white matter tract pathology (splenium corpus callosum, fornix, right inferior longitudinal fasciculus, right superior longitudinal fasciculus). Comparing DTI metrics, the most extensive change in white matter was detected by RD, followed by TR, FA and AX.

Fractional Anisotropy

svPPA				nvPPA				lvPPA			
Tract	**p-value**	**voxels**	**%**	**Tract**	**p-value**	**voxels**	**%**	**Tract**	**p-value**	**voxels**	**%**
L UF	0.003	526	80.4	L UF	0.005	334	51.1	L UF	0.009	459	70.2
R UF	0.002	309	78.8	CC	0.01	7334	49.3	CC	0.01	9711	65.2
CC	0.01	8694	58.4	L ATR	0.01	618	39.5	L ILF	0.009	1628	61.8
L ILF	0.008	1265	48	R ATR	0.01	288	23.2	R ILF	0.015	1085	58.3
L SLF	0.01	1229	45.2	R UF	0.02	90	23	L CB	0.009	392	46.2
R ILF	0.01	767	41.2	L SLF	0.03	595	21.9	R CB	0.013	245	40.8
R CB	0.004	243	40.5	Fornix	0.01	33	5.9	R UF	0.014	145	37
R SLF	0.02	853	35.8	L ILF	0.03	78	3	L ATR	0.012	526	33.7
L CB	0.01	244	28.8	R CB	0.04	15	2.5	R SLF	0.032	719	30.2
L ATR	0.008	133	8.5	R ILF	0.02	15	0.8	L SLF	0.012	788	29
Fornix	0.02	45	8.1	R SLF	0.02	17	0.7	R ATR	0.019	300	24.2
R ATR	0.03	36	2.9	L CST	0.009	47	0.6	Fornix	0.006	41	7.3
L CST	0.02	17	0.2	L CB	0.01	3	0.4	R CST	0.02	284	4.2
R CST			0	R CST	0.01	19	0.3	L CST	0.019	223	3

Table 5.3. Profiles of changes in FA in each PPA groups compared with healthy controls. Results are FWE corrected p <0.05. Results are ordered by % of tract involvement.

Axial Diffusivity											
svPPA				nvPPA				lvPPA			
Tract	p-value	voxels	%	Tract	p-value	voxels	%	Tract	p-value	voxels	%
R UF	0.02	257	65.6	L ATR	0.007	672	43	CC	0.005	9711	65.2
L UF	0.004	405	61.9	CC	0.02	4164	28	R UF	0.007	233	59.4
L ILF	0.004	1113	42.2	R UF	0.03	66	16.8	R ILF	0.006	994	53.4
R ILF	0.01	685	36.8	L UF	0.02	71	10.9	L ILF	0.004	1381	52.4
CC	0.02	3268	22	R ATR	0.03	111	9	L SLF	0.004	1303	47.9
L SLF	0.02	542	19.9	R SLF	0.05	210	8.8	L ATR	0.004	724	46.3
L ATR	0.01	308	19.7	L CST	0.01	312	4.3	L UF	0.009	262	40.1
R ATR	0.02	108	8.7	R CST	0.02	267	4	R SLF	0.006	913	38.3
R SLF	0.02	67	2.8	Fornix	0.04	10	1.8	R ATR	0.011	281	22.7
L CST	0.03	196	2.7	L CB	0.04	7	0.8	L CB	0.005	172	20.3
R CST	0.04	147	2.2	L SLF	0.02	15	0.6	L CST	0.006	276	3.8
Fornix	0.04	12	2.1	L ILF			0	R CST	0.007	190	2.8
L CB			0	R CB			0	R CB	0.022	17	2.8
R CB			0	R ILF			0	Fornix	0.019	9	1.6

Table 5.4. Profiles of changes in AX in each PPA groups compared with healthy controls. Results are FWE corrected p <0.05. Results are ordered by % of tract involvement.

Radial Diffusivity											
svPPA				nvPPA				lvPPA			
Tract	p-value	voxels	%	Tract	p-value	voxels	%	Tract	p-value	voxels	%
R UF	0.001	371	94.6	L UF	0.01	395	60.4	CC	0.004	11278	75.8
L UF	0.002	566	86.5	CC	0.01	7853	52.8	R ILF	0.004	1403	75.3
L ILF	0.01	1621	61.5	L ATR	0.01	672	43	L ILF	0.003	1888	71.6
Fornix	0.01	330	59	R UF	0.01	134	34.2	L UF	0.005	394	60.2
R ILF	0.01	1077	57.8	R ATR	0.01	406	32.7	L SLF	0.01	1470	54
CC	0.01	8139	54.7	L SLF	0.02	752	27.6	L ATR	0.01	711	45.5
L SLF	0.01	1286	47.3	R CB	0.02	99	16.5	L CB	0.005	374	44.1
L CB	0.02	338	39.9	Fornix	0.02	33	5.9	R SLF	0.01	979	41.1
L ATR	0.01	584	37.4	L ILF	0.04	98	3.7	R CB	0.01	237	39.5
R SLF	0.01	831	34.9	L CB	0.03	21	2.5	R ATR	0.01	351	28.3
R CB	0.01	205	34.2	R ILF	0.04	27	1.5	R UF	0.01	237	9
R ATR	0.01	378	30.5	L CST	0.01	49	0.7	Fornix	0.005	45	8.1
L CST	0.01	221	3	R SLF	0.01	16	0.7	R CST	0.02	233	3.5
R CST			0	R CST	0.02	16	0.2	L CST	0.01	253	3.4

Table 5.5. Profiles of changes in RD in each PPA group compared with healthy controls. Results are FWE corrected p <0.05. Results are ordered by % of tract involvement.

Trace Diffusivity											
svPPA				nvPPA				lvPPA			
Tract	p-value	voxels	%	Tract	p-value	voxels	%	Tract	p-value	voxels	%
R UF	0.003	364	92.9	L UF	0.01	323	49.4	CC	0.004	12320	82.8
L UF	0.004	573	87.6	CC	0.01	7184	48.3	R ILF	0.004	1349	72.4
Fornix	0.02	349	62.4	L ATR	0.01	644	41.2	L ILF	0.002	1848	70.1
L ILF	0.008	1508	57.2	R UF	0.02	111	28.3	R UF	0.005	241	61.5
R ILF	0.01	1025	55	R ATR	0.01	300	24.2	L SLF	0.005	1577	58
CC	0.02	7578	50.9	Fornix	0.02	20	3.6	L UF	0.005	366	56
L SLF	0.01	1200	44.1	L SLF	0.03	77	2.8	L ATR	0.005	728	46.6
L ATR	0.01	537	34.4	L CB	0.02	18	2.1	R SLF	0.01	1012	42.5
R SLF	0.03	608	25.5	R CST	0.02	106	1.6	R ATR	0.01	364	29.4
R ATR	0.02	312	25.2	R SLF	0.03	28	1.2	L CB	0.002	230	27.1
L CB	0.04	202	23.8	L CST	0.03	40	0.5	Fornix	0.01	50	8.9
R CB	0.03	83	13.8	R CB	0.03	1	0.2	R CB	0.01	41	6.8
L CST	0.03	206	2.8	L ILF			0	R CST	0.01	209	3.1
R CST			0	R ILF			0	L CST	0.01	192	2.6

Table 5.6. Profiles of changes in TR in each PPA group compared with healthy controls. Results are FWE corrected p <0.05. Results are ordered by % of tract involvement.

Compared with healthy subjects, the lvPPA group had extensive white matter tract pathology within bilateral fronto-temporo-parietal regions, more marked posteriorly and within the left hemisphere with involvement of both dorsal and ventral white matter tracts (ILF, UF, SLF, CB, ATR, fornix) and also corpus callosum; when compared with the AD group, no significant white matter tract differences were observed. Comparing maps of altered diffusivity in lvPPA versus healthy control (e.g. figure 5.2) and AD disease-controls versus healthy controls (figure 5.5) similar profiles are white matter tract pathology are observerd. Comparing DTI metrics, the most extensive change in white matter was detected by RD, followed by TR, FA and AX.

White Matter changes in svPPA vs. AD											
Axial Diffusivity (svPPA>AD)				Radial Diffusivity (svPPA>AD)				Trace Diffusivity (svPPA>AD)			
Tract	**p**	**voxels**	**%**	**Tract**	**p**	**voxels**	**%**	**Tract**	**p**	**voxels**	**%**
R UF	0.01	90	5.2	L UF	0.01	385	13.8	L UF	0.02	298	10.7
L UF	0.003	132	4.7	R UF	0.02	207	12	R UF	0.02	162	9.4
L ILF	0.01	393	4.1	L ILF	0.01	512	5.4	L ILF	0.01	463	4.9
R ILF	0.02	213	3.2	R ILF	0.02	236	3.5	R ILF	0.02	214	3.2
CC	0.02	18	0.1	CC	0.04	12	0.2	CC	0.02	7	0.1

White Matter changes in AD vs. nvPPA			
Axial Diffusivity (AD>nvPPA)			
Tract	**p**	**voxels**	**%**
R ILF	0.05	216	3.2
CC	0.04	1244	1.4
R SLF	0.05	36	0.3
Fornix	0.04	2	0.1

Table 5.7. Profiles of DTI metric change in PPA groups compared with AD patients. Results are FWE corrected p <0.05. Results are ordered by % of tract involvement.

5.3.3 Comparisons between PPA groups

Differences in profiles of white matter tract pathology between PPA syndromic groups were also identified (for details see figure 5.5 and table 5.8).

SvPPA was associated with greater alterations in bilateral inferior longitudinal fasciculus and uncinate fasciculus (left > right) relative to nvPPA; and in bilateral inferior longitudinal fasciculus (left > right) and left uncinate fasciculus relative to lvPPA. LvPPA was associated with more posterior bilateral white matter tract pathology in most tracts, with the most striking difference in bilateral inferior longitudinal fasciculus, superior longitudinal fasciculus and the splenium of the corpus callosum, relative to nvPPA; and the splenium of CC alone, relative to svPPA.

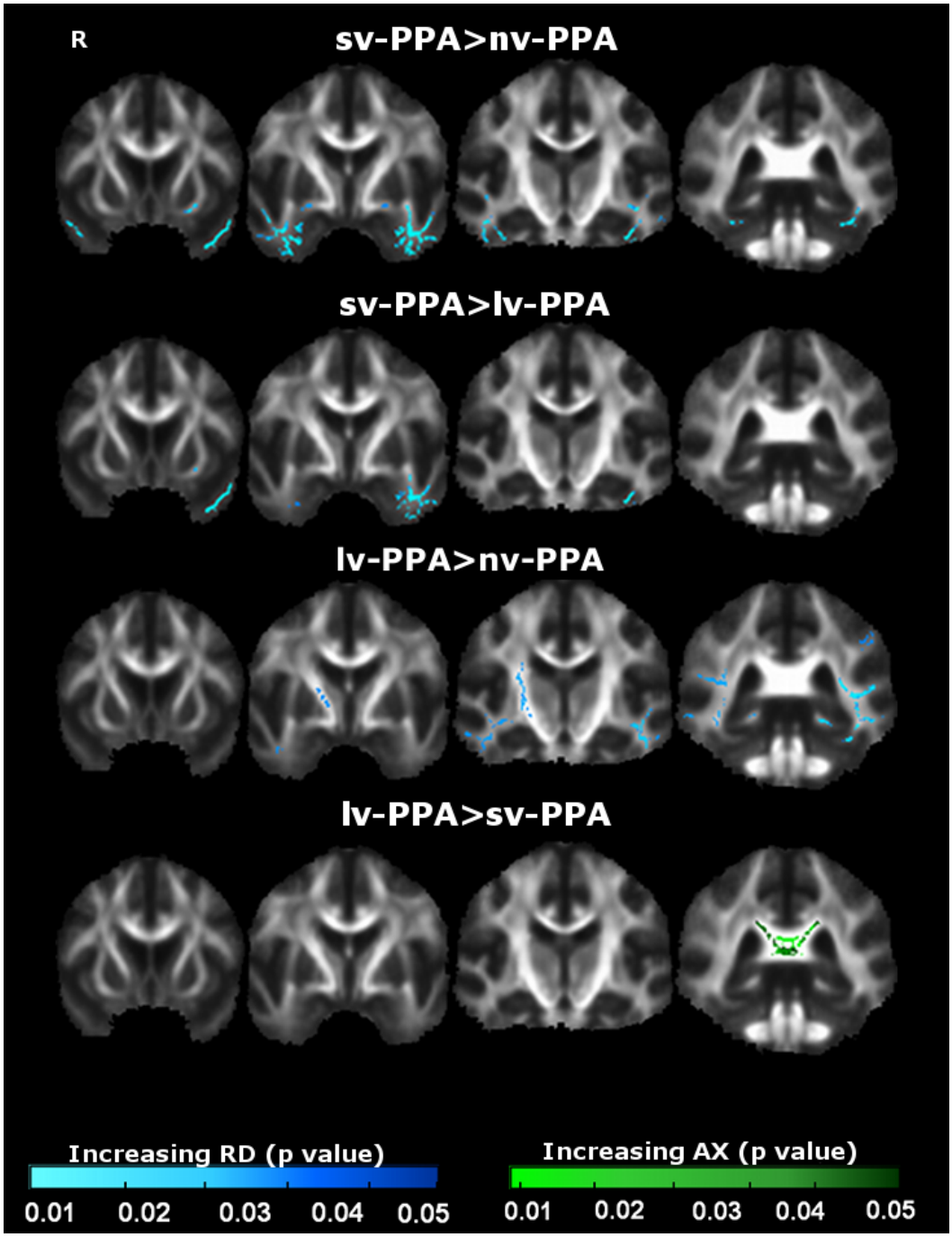

Figure 5.6. Comparison of WM tract degeneration between PPA syndromic groups. Each tile shows significant WM tract (FWE corrected p <0.05) differences between groups as measured by increased AX (green) and RD (blue). The colour bar (bottom) codes significance (FWE corrected p-value).

	svPPA>nvPPA				svPPA>lvPPA				lvPPA>svPPA				lvPPA>nvPPA			
	Tract	**p-**	**voxels**	**%**	**Tract**	**p-**	**voxels**	**%**	**Tract**	**p-**	**voxels**	**%**	**Tract**	**p-**	**voxels**	**%**
Axial Diffusivity	L ILF	0.01	622	6.6	L UF	0.009	125	4.5	CC	0.03	1496	1.6	L ILF	0.01	1565	16.5
	L UF	0.004	129	4.6	L ILF	0.01	190	2.0	L CST	0.05	25	0.3	R ILF	0.01	998	14.9
	R ILF	0.02	303	4.5									R SLF	0.02	848	7.6
	R UF	0.02	67	3.9									R CST	0.02	437	6.5
	CC	0.03	102	0.1									L SLF	0.02	817	5.9
													CC	0.02	4427	4.9
													L CST	0.02	271	3.7
													R UF	0.04	42	2.4
													L CB	0.02	66	2.2
													R ATR	0.02	63	0.6
													L ATR	0.02	31	0.3
Radial Diffusivity	L UF	0.01	314	11.3	L UF	0.02	271	9.7					L ILF	0.02	1262	13.3
	R UF	0.02	109	6.3	L ILF	0.02	278	2.9					R ILF	0.04	794	11.9
	L ILF	0.02	516	5.4									R CST	0.04	245	3.7
	R ILF	0.02	309	4.6									CC	0.03	2601	2.9
	CC	0.03	6	0									L SLF	0.03	381	2.8
													R SLF	0.05	93	0.8
													R ATR	0.04	30	0.3
Trace Diffusivity	L UF	0.01	232	8.3	L UF	0.01	144	5.2					L ILF	0.01	1636	17.2
	L ILF	0.02	556	5.9	L ILF	0.02	259	2.7					R ILF	0.01	1150	17.2
	R ILF	0.02	280	4.2									R CST	0.03	490	7.3
	R UF	0.02	88	5.1									L SLF	0.01	813	5.9
	CC	0.02	13	0.1									L CB	0.01	170	5.6
													CC	0.01	4452	4.9
													L CST	0.03	262	3.6
													R SLF	0.02	372	3.4
													R UF	0.02	29	1.7
													R ATR	0.04	126	1.2
													L UF	0.03	30	1.1
													L ATR	0.04	45	0.4
													Fornix	0.02	5	0.1
FA													R CST	0.05	68	1
													L ILF	0.04	85	0.9
													CC	0.05	170	0.2

Table 5.8 White matter tract comparisons between PPA groups. All results are FWE corrected p <0.05 and ordered by p-value. %, percentage of altered voxels within each tract.

5.3.4 Grey matter analysis

In the VBM analysis, each PPA syndromic group showed the anticipated profile of regional grey matter atrophy compared with the healthy control group (Figure 5.6).

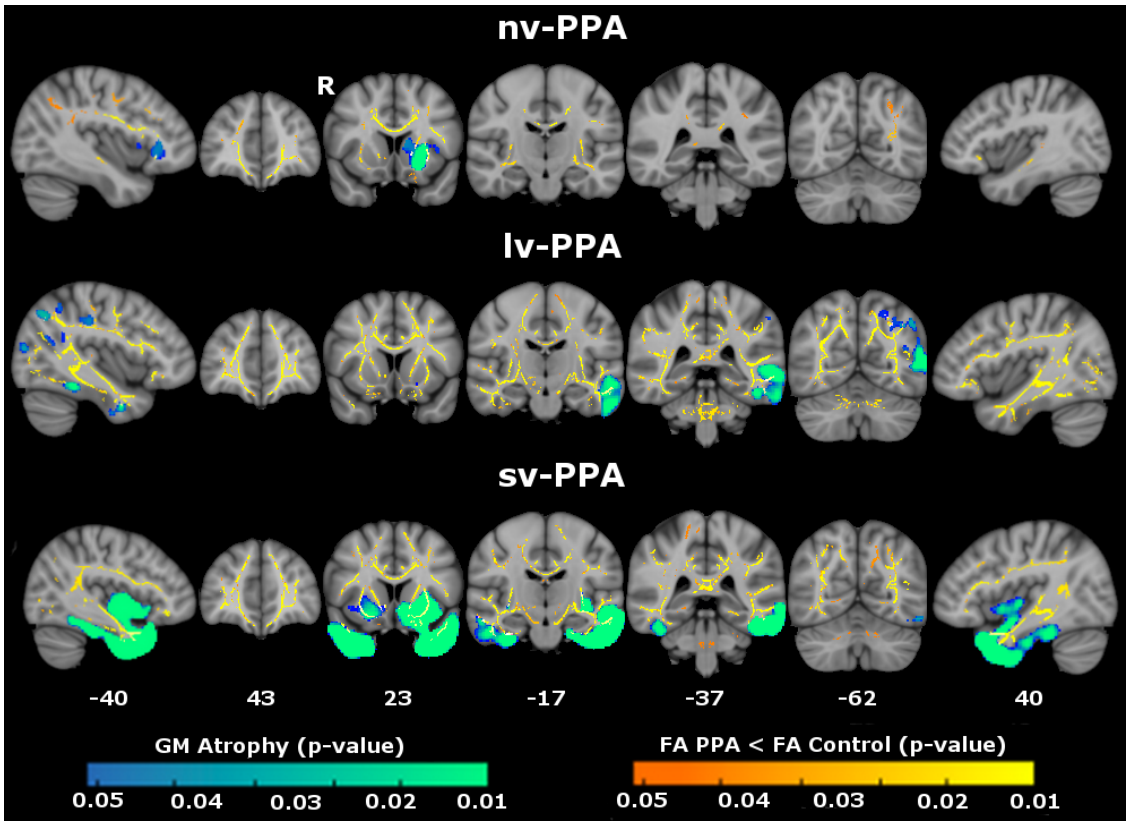

Figure 5.7. Maps of grey matter (GM) atrophy (blue-green) and reduced white matter fractional anisotropy (FA) (orange-yellow) in PPA syndromic groups compared to healthy controls overlaid on a MNI152 template brain. GM and FA maps are thresholded at p <0.05 after family-wise error correction with threshold-free cluster enhancement. MNI co-ordinates are displayed. R=right. Colour bars (bottom) code FWE corrected p-values (blue-green) for GM atrophy and FA change (red-yellow).

svPPA was associated with bilateral but predominantly left-sided atrophy of antero-inferior temporal and orbitofrontal cortices. nvPPA was associated with atrophy of left inferior frontal and opercular cortex. lvPPA was associated with more extensive left hemispheric atrophy involving inferior and posterior-superior temporal lobe, temporo-

parietal and temporo-occipital junctions. Regions of white matter tract pathology closely neighboured atrophic cortical regions within each syndrome (i.e. left uncinate fasciculus and left insular cortex in nvPPA, left inferior longitudinal fasciculus and left temporo-parietal cortex in lvPPA, anterior inferior longitudinal fasciculus and anterior temporal cortices in svPPA.). However the tract alterations were spatially more distributed, extending beyond the zones of grey matter loss. This anatomical disparity was most evident for lvPPA, and less evident for nvPPA and svPPA. The extent of white matter tract pathology varied with regards to the diffusivity metric used across all disease groups, with RD being associated with more extensive changes than AX or FA.

5.4 Discussion

5.4.1 Overview of results

This study has identified signatures of white matter tract pathology across the PPA spectrum both in relation to healthy controls and patients with a diagnosis of AD. Differences in the profile of white matter tract pathology also emerged on direct group-wise comparisons of PPA syndromes, suggesting relative specificity of white matter pathology for particular syndromes and pathologies. Broad anatomical profiles of white matter tract pathology were identified for each of the disease groups. These profiles of tract pathology demonstrated show some convergence with previous studies (Acosta-Cabronero et al., 2011; Agosta et al., 2012; Agosta et al., 2010; Galantucci et al., 2011; Schwindt et al., 2011; Whitwell et al., 2010) (see Table 5.1); however, a number of additional white matter tracts were also identified for each of the syndromic groups, and there was substantial overlap between PPA syndromes. On visual inspection, white

matter pathology appeared more widespread compared to areas of grey matter atrophy. These findings provide further evidence that what matter tract metrics constitute markers of structural neural network disintegration across the PPA spectrum and help to define network-level substrates for individual PPA syndromes that may be helpful in diagnosis and tracking of PPA. These profiles align with patterns of network breakdown previously identified in svPPA, nvPPA and lvPPA (Seeley et al., 2009; Rohrer et al., 2010c) and with language pathways proposed in the healthy brain (Saur et al., 2008). Whilst syndromic profiles did emerge there were also white matter tract pathology which overlapped across all syndromes. This may be in keeping with the fact that over time clinical syndromes converge with one another (Kertesz et al., 2005) and may account for the high proportion of patients with 'mixed PPA' who are not classifiable under the current PPA criteria, often owing to the presence clinical features compatible with more than one syndrome (Sajjadi et al., 2012).

5.4.2 Neurobiological relevance of the current findings

Here, nvPPA was associated in particular with more marked involvement of more dorsal anterior and subcortical tracts and relative sparing of more inferior temporal lobe tracts: this would be consistent with previous evidence concerning the neuroanatomical substrates of articulatory, phonemic and grammar processing (Katanoda et al., 2001; Skosnik et al., 2002; Papagno, 2011; Wilson et al., 2011). Previous studies have demonstrated prominent involvement of left superior longitudinal fasciculus in nvPPA (F Agosta et al., 2012; Galantucci et al., 2011; Schwindt et al., 2011); whilst involvement of left superior longitudinal fasciculus was also demonstrated here (see figures 5.1 to 5.3), with prominent involvement of left-sided anterior/frontal fibres, there was substantial

variability in significance levels for each DTI metrics (see Table 5.3 to 5.6), and this, along with the boundary limits of the ROI masks used, may explain why more prominent involvement of this particular tract was not seen. Indeed n the next chapter (which contains many of the some subjects), where a different methodology tracking longitudinal change, involvement of the SLF becomes more apparent in this group, confirming its role in the pathogenesis of nvPPA. The profiles delineated above also provide a substrate for the non-language cognitive difficulties reported in nvPPA, in particular executive dysfunction (Rohrer et al., 2010b). svPPA here was associated in particular with involvement of inferior longitudinal fasciculus and uncinate fasciculus: these tracts could support the putative anterior temporal – inferior frontal network mediating semantic and evaluative processing of words and nonverbal objects (Awad et al., 2007; Parker et al., 2005; Scott et al., 2000). lvPPA was associated with involvement of both dorsally-directed (superior longitudinal fasciculus and cingulum bundle) and ventrally-directed (inferior longitudinal fasciculus) tracts, prominently including more posterior temporo-parietal projections and similar to the pattern seen in typical AD (Acosta-Cabronero et al., 2011): these widely distributed tracts are likely to support a distributed network that in the dominant hemisphere mediates phonological working memory as well as praxis and other parietal functions (Awad et al., 2007; Simon et al., 2002), and which has been previously implicated in the lvPPA syndrome (Rohrer, et al., 2010d; Gorno-Tempini et al., 2011). Whilst inferior longitudinal fasciculus pathology has been inconsistently reported in lvPPA, identification of this tract in the lvPPA group in the current study is consistent with the known engagement of the ventral language network in lexical retrieval (Wong et al., 2011) and with previous studies of lvPPA linking lexical retrieval deficits with more ventral grey matter atrophy (Wilson et al., 2010). Despite

their distinct clinical phenotypes there was no significant difference in white matter tract involvement when the lvPPA and AD groups were directly compared: this suggests at least partial overlap of white matter tract degeneration in these syndromes, in keeping with a common underlying disease pathology. Reviewing the maps of alterations in DTI metrics compared with healthy controls for both lvPPA and AD we also note that there is strong anatomical convergence between these two syndromes, particularly for RD and TR (see figures 5.2 and 5.5).

5.4.2 Relationship to grey matter changes

It is noteworthy that, for each of the PPA syndromes, white matter tract pathology occurred in proximity to regions of grey matter atrophy but also extended more widely within each cerebral hemisphere (see Figure 5.6). While caution is needed in comparing different neuroimaging modalities and in calibrating for the effects of local atrophy on DTI metrics, it is unlikely that this disparity is attributable simply to technical factors: the white matter profiles delineated here were based on robust methodologies, for example the use of permutation testing which does not assume normality (Nichols and Holmes, 2002) and TFCE correction which is robust to non-stationarity (Smith and Nichols, 2009). In addition, changes more extensive than grey matter atrophy have been documented in previous white matter tract studies of PPA syndromes, albeit inconsistently between studies (Acosta-Cabronero et al., 2011; Agosta et al., 2012; Agosta et al., 2010; Galantucci et al., 2011; Schwindt et al., 2011), and indeed for bvFTD seen in chapter 3 of this thesis; this inconsistency may be at least partly attributable to methodological differences and small patient cohorts. Moreover, in the present study, the apparent disparity in the distribution of grey and white matter changes varied between PPA syndromes. Possible

reasons for this anatomical disparity between neuroimaging metrics have been discussed previously, and may be due to either purely technical differences in assessing structural change, the possibility that white matter pathology occurs in advance of grey matter pathology, or a combination of both. To evaluate this issue further pre-symptomatic studies measuring both white matter and grey matter are required; however longitudinal studies in affected individuals may also give us insights into the temporal order of the brain changes in PPA, and as such the next chapter will provide data on the longitudinal trajectory of white matter changes in PPA.

5.4.3 Role of individual DTI metrics in PPA

Whilst the role of particular DTI metrics in defining neurodegenerative pathologies remains controversial the current study has replicated findings from a number of other studies (Acosta-Cabronero et al., 2010; Agosta et al., 2012); (see table 5.1). Together this evidence suggests that DTI metrics may vary in their potential to identify white matter pathology across the spectrum of PPA. For example in this study, across all groups, RD seemed to identify the greatest extent of white matter pathology, while AX showed the least. These findings are also in keeping with previous evidence in PPA (Schwindt et al., 2011; Galantucci et al., 2011). Tracts with the most marked involvement on voxel-wise analysis (e.g., uncinate fasciculus in svPPA; see table 5.3 to 5.5) tended to show broadly similar patterns of involvement across DTI metrics. This suggests that the sensitivity of metrics for detecting white matter pathology may relate to the extent of tract damage, at least cross-sectionally, or that particular metrics (e.g., RD; see Table 5.5) may detect change earlier or may be intrinsically more sensitive to particular tissue pathologies (such as, potentially, AX for AD pathology, since AX revealed more extensive damage in the

lvPPA group. relative to other metrics and compared with nvPPA or svPPA subtypes in this study, although the lack of confirmatory histopathology means that this is purely speculative.

5.4.4 Conclusions

The signatures of white matter tract pathology identified were at the level of large-scale networks; no single tract showed specificity for a particular syndrome (nor by inference, for a particular pathology), suggesting that much of the clinical phenotype of PPA results from large-scale network breakdown. However, comparing tract signatures across disease groups (Figures 5.1 to 5.3), certain tracts seem to have a greater burden of pathology: svPPA was associated with predominant ventral tract involvement, nvPPA with more anterior-dorsal tract involvement and lvPPA with more widespread tract changes.

This study corroborates previous work suggesting that the overall profile of tract involvement may signal particular pathologies. For example, the fornix and cingulum bundle were most markedly involved in lvPPA: these structures have been identified as potentially useful anatomical biomarkers in the detection of AD pathology, which underpins a high proportion of lvPPA cases (Huang et al., 2011; Keihaninejad et al., 2012; Oishi et al., 2011). Other tracts (for example, uncinate fasciculus and corpus callosum) were involved across syndromes: such tracts could potentially play a critical role in the diffusive spread of pathogenic proteins, which may constitute a common mechanism of network disintegration in neurodegenerative diseases (Raj et al., 2012; Warren et al., 2012; Zhou et al., 2012). The present findings support the concept of differentially

vulnerable neuronal networks in particular PPA syndromes and proteinopathies with the tractographic delineation of PPA contributing new information about the pathophysiology of language network breakdown and underlying molecular architecture.

5.5 Chapter summary

This chapter provides further new data on the profiles of white matter tract pathology across the spectrum of PPA. In particular it focuses on identifying changes within tracts of a clinically and molecularly (through use of CSF analysis) well-defined cohort with the core clinical hallmark of impaired language. These relatively circumscribed cognitive problems should lend themselves particularly well to the evaluation of changes across large-scale cognitive networks, which underpin language. A broad profile of white matter tract pathology emerged, with svPPA having evidence of bilateral anterior-ventral white matter pathology, nvPPA having evidence of more left-sided frontal-dorsal white matter pathology, and lvPPA having diffuse, both ventral and dorsal profiles of white matter pathology. These differing profiles may account for the clinical variability seen across the PPA spectrum. Tracts such as the uncinate fasciculus and corpus callosum were commonly involved across the PPA spectrum, indicating a degree of overlap across distributed language-networks, which may account for some of the observed convergence of each clinical phenotype with one another over time. Whilst much of the pathology neighboured grey matter atrophy, the profiles had a wider anatomical distribution suggesting that white matter pathology either leads grey matter atrophy or that it simply yields a more sensitive imaging metric.

6. Longitudinal profiles of white matter pathology in the primary progressive aphasias

6.1. Introduction

6.1.1 Background

The previous chapter set about establishing cross-sectional profiles of white matter pathology in PPA. Whilst syndromic signatures emerged there was still overlapping profiles of pathology across syndromes. Further information on syndromic profiles of white matter pathology may be generated by studying change in the same individual over time, improving the quality of potential future syndrome specific imaging biomarkers. This is of current interest, as whilst there has been much progress in the clinicopathological correlations within PPAs, there remains an absence of measures, which have the robustness and sensitivity to tract PPA over time. These issues in turn present challenges for planning future clinical trials of disease-modifying therapies in PPA: such trials are likely to target specific pathologies and to seek to initiate treatments early in the disease course to minimise cognitive decline. Having sensitive biomarkers is of particular importance as language decline is often insidious and it is plausible that changes within language networks are occurring in advance of clinical symptoms.

6.1.2 Previous longitudinal imaging studies in PPA

Unlike other neurodegenerative conditions longitudinal imaging studies in PPA are few, most likely due to a combination of under recognition of these syndromes, as well as relative rarity in comparison to other neurodegenerative conditions. A number of longitudinal studies examining whole brain and grey matter atrophy have been reported.

Gordon and colleagues reported an annual rate of whole brain atrophy of 2.5% above controls in svPPA and 2.8% in nvPPA (Gordon et al., 2010). Some contradictory data exists regarding which brain regions atrophy greater in PPA with some studies suggesting that atrophy of the right hemisphere accelerates over time compared to the left (Rohrer et al., 2008), whilst others argue that progression of atrophy remains largely asymmetric within the language dominant (left hemisphere) over time (Rogalski et al., 2014). At the time of writing one longitudinal DTI study has been performed although it did not include lvPPA or report tract specific data. Within the nvPPA group changes in bilateral inferior longitudinal fasciculus and superior longitudinal fasciculus were reported, with greater change seen on the left; within the svPPA group change over time was only observed within left sided tracts including cingulum bundle, inferior longitudinal fasciculus, superior longitudinal fasciculus and uncinate fasciculus (Lam et al., 2014). Overall the trajectory of disease across PPA remains somewhat unclear, and there is a need for further neuroimaging studies, using more sophisticated techniques, to clarify these discrepancies.

The current study will aim to build and expand on previous studies of longitudinal imaging changes in PPA. The primary aim here is to assess the potential role of longitudinal DTI as a clinical biomarker in tracking progression of white matter pathology in PPA and comparing with other traditional biomarkers. In addition, longitudinal DTI may hold important insights into more basic aspects of the neurobiology of PPA and secondary aims include establishing if common or syndrome specific trajectories of white matter change emerge over time and if there is an optimal DTI metric for assessing longitudinal white matter change in PPA.

6.2 Methods

6.2.1 Study Participants

Patients were recruited from 2009-2014 as part of a prospective study tracking disease progression in patients suspected to have frontotemporal lobar degeneration at the specialist cognitive disorders clinic, National Hospital for Neurology and Neurosurgery, London, United Kingdom. All patients met current consensus criteria (Gorno-Tempini et al., 2011) for a diagnosis of probable or define PPA and were also included in the Chapter 5 of this Thesis. Participants who had two clinical and neuropsychological assessments and MRI scans (to include both T1-volumetric and DTI sequences), a minimum of six months apart, were considered for study inclusion. 32 participants were identified as fulfilling the criteria for study inclusion, with 11 participants further meeting the diagnosis of svPPA, 13 meeting the diagnostic criteria for nvPPA and 6 meeting the diagnostic criteria for lvPPA. 4 participants had unclassifiable PPA and were not considered in this study to maintain clinical homogeneity. 20 age and gender-matched controls were also included and underwent the same test batteries as those with PPA. Clinical and imaging tests were the same at baseline and follow-up visits, although in some circumstances, due to clinical progression, some affected participants were unable to fully complete all neuropsychological tests. Volumetric MRI and DTI acquisition were the same at both time points (see chapter 2, section 2.2.1. for details).

6.2.2 Image processing

All participants' baseline and follow-up DTI scans underwent processing as previously specified in the section describing longitudinal DTI image processing (see chapter 2, section 2.2.8.) ROI based analysis was performed, with tracts chosen either based on

apriori prediction of disease involvement, given their likely roles in linking a distributed language network, or based on the cross-sectional whole brain analysis results from chapter 5. Regions-of-interest included genu, body and splenium of the corpus callosum, bilateral inferior and superior longitudinal fasciculus and bilateral uncinate fasciculus. The uncinate fasciculus did not undergo any additional erosion, as this would have limited the mask size, reducing sensitivity to detect change in this tract.

Analysis of baseline and follow-up volumetric MRI scans were performed as per chapter 2, section 2.2.2 of this thesis with the brain boundary shift integral calculated and expressed as annualised volume change as a percentage of the baseline brain volume.

6.2.3 Statistical analysis and sample size estimates

Statistical analyses were carried out using STATA 12© (Statacorp, College Station, TX). Statistical analysis for cross-sectional and longitudinal data mirrored the analysis used in chapter 4, applying a mixed-effects linear regression model, with confounds of age, gender and disease duration included within the model design (see chapter 5, section 2.3 for details). Accuracy, sensitivity and specificity of each DTI metric in classifying individual participants into separate groups (PPA subtype or control) and estimation of sample sizes for clinical trials were also calculated using the same methodology as described previously in chapter 4.

6.3 Results

6.3.1 Demographics, neuropsychological performance and changes in whole brain volume

Data on demographics and whole brain volumes for controls and PPA groups are shown in table 6.1. Average follow-up from baseline was 1 year. Data on baseline and longitudinal neuropsychological performance for controls and PPA groups are shown in table 6.2.

At baseline, compared with controls, those with PPA performed significantly worse ($p<0.05$) on tests of general intellect and most other neuropsychological measures. nvPPA performed significantly worse on all measures except single word comprehension and spatial perception. svPPA performed significantly worse on all measures except spatial perception. Those with lvPPA were significantly impaired on all neuropsychological measures.

Longitudinal change in neuropsychological performance for PPA sub-groups is also shown in table 6.2 and is reported as the estimated percentage per year change in performance from baseline. Over time those with nvPPA displayed the most significant ($p<0.05$) reductions in neuropsychological performance on tests of naming (55.9%/year) and executive function (18%/year); those with svPPA showed the most significant reductions on tests of naming (50.3%/year), arithmetic (27.9%/year) and executive function (16.5%/year); and those with lvPPA showed the most significant reductions on tests of naming (84.5%/year), sentence repetition (83.8%/year), single-word comprehension (31.2%/year) and spatial perception (11.1%/year).

	Controls (n=20)		Non-fluent/agrammatic variant PPA (n=13)			Semantic variant PPA (n=11)			Logopenic variant PPA (n=6)		
	Mean	SD	Mean	SD	p-value	Mean	SD	p-value	Mean	SD	p-value
Age at baseline (years)	61.6	8.6	67.1	5.5	0.1	65.1	6.1	0.3	67.0	7.5	0.2
Disease duration at baseline (years)	N/A		4.0	2.5	0.7	5.0	1.5	0.1	3.8	1.0	0.6
Sex, male/female	11/9		2/11		0.07§	6/5		0.4§	4/2		0.1§
Interscan Interval (years)	1.3	0.4	1.0	0.2	0.02	1.1	0.6	0.3	1.0	0.3	0.1
MMSE baseline	29.7	0.6	23.4	6.2	<0.001	20.1	9.4	<0.001	19.8	9.0	<0.001
Whole brain volume, baseline (ml)	1179	87	1021*	90	<0.001	1034	112	<0.001	1003	98	<0.001
Whole brain volume, follow-up (ml)	1172	90	1003*	61	<0.001	1010	113	<0.001	999	95	<0.001
BBSI ml/year	6.8	7.1	28*	14	<0.001	22	14	<0.001	15	7	0.02

Table 6.1. Study participants' clinical and imaging characteristics. Linear regression comparing controls with each PPA sub-group, § Fisher's exact test. * BBSI is only available for 8 patients with nvPPA due to significant motion artefact in either baseline or follow-up scan.

	Controls (n=20)		Non-fluent variant PPA (n=13)					Semantic variant PPA (n=11)					Logopenic variant PPA (n=6)				
	Baseline		Baseline		Change over time			Baseline		Change over time			Baseline		Change over time		
	Mean	SD	Mean	SD	%/year	95% CI		Mean	SD	%/year	95% CI		Mean	SD	%/year	95% CI	
VIQ	122.2	8.3	72.3*	16.6	-6.1	-12.7	0.6	66.9*	19.9	**-5.8**	**-11.4**	**-0.3**	63.5*	9.4	6.3	-1.1	13.8
PIQ	119.1	8.2	91.3*	20.4	0.7	-4.9	6.2	105.1*	19.7	-2.6	-6.3	1	74.8*	17.3	-1.6	-9.3	6.1
RMT Faces (/50)	47.2	3.5	36.7*	7.5	**-9**	**-15.9**	**-2.1**	30.4*	6.7	-1.1	-6.5	4.2	33.8*	11.1	2.3	-5.5	10.2
RMT Words (/50)	45.7	3.2	37.6*	10.2	**-13.8**	**-24.3**	**-3.3**	30.8*	7.8	-3.2	-9.8	3.5	33.4*	10.4	-9.5	-20.2	1.2
GNT (/30)	26	2.3	10.3*	8.8	**-55.9**	**-104.2**	**-7.7**	1.3*	3.3	**-50.3**	**-64.9**	**-35.6**	7.8*	7.8	**-84.5**	**-110.7**	**-58.2**
BPVS (/150)	147.8	1.7	122.1	47.1	-3.7	-21.5	14.1	68.9*	47.2	-6.6	-19.2	6	108.3*	35.1	**-31.2**	**-46.2**	**-16.2**
Word Rep (/45)	44.2	1.5	19.3*	14.4	-33.9	-68	19.2	42.1*	3.8	1.8	-0.6	4.3	39.4*	4.6	**-11.2**	**-16.9**	**-5.4**
Sent Rep (/10)	9.9	0.4	3.6*	4	-17.5	-49.3	14.3	9.4*	0.7	-2.9	-7	1.1	3.9*	3.1	**-83.8**	**-128.7**	**-38.8**
GDA (/24)	13.2	6	4.8*	6.4	-0.6	-46.9	45.6	7.7*	7.9	**-27.9**	**-54.8**	**-1.1**	0.7*	1.2	-0.4	-59.3	58.5
VOSP (/20)	18.8	1.1	15.4	4.6	**14.2**	**2**	**26.4**	16.5	5.9	-6.3	-16.3	3.7	16.3*	4.4	**-11.1**	**-20.3**	**-1.9**
Colour Naming (<90sec)	29.8	3.8	64.9*	23.3	**-18**	**-7.3**	**-28.7**	64.5*	22.6	**-10.8**	**-1.8**	**-19.7**	72.2*	19.4	-11.2	0.4	-22.8
Ink Naming (<180 sec)	30.1	5.1	77.4*	24.7	**-15.5**	**-1.6**	**-29.4**	71.9*	23.1	**-16.5**	**-5.5**	**-27.5**	85.2*	25	-7.1	1.1	-15.4

Table 6.2. Neuropsychological performance at baseline and longitudinally displayed as estimated mean difference from controls with change expressed as a percentage per year. *Indicates baseline values signifantly (p<0.05) different from controls. Bold values indicate significant (p<0.05) change over time.

6.3.2 Cross-sectional DTI results in PPA subtypes

Cross-sectional DTI metric data for FA, MD, RD and AX are shown in tables 6.4 to 6.7 respectively and should be compared with data from the previous chapter (noting different methodologies used to determine metric values). Broadly results presented in the current chapter show similar anatomical profiles of cross-sectional white matter pathology. Absolute values representing white matter pathology were greater using TBSS, particularly in the case of the nvPPA group were baseline differences were relavtively few in the current study. Individual DTI metrics showed a similar ordering in terms of their sensitivity in detecting differences in white matter pathology, the the largest differences detected using RD and MD (the average of TR).

	Controls (n=18)	**NvPPA**			**SvPPA**			**LvPPA**		
ROI FA	Mean (SD)	Mean (SD)	% Difference (95% CI)	P*	Mean (SD)	% Difference (95% CI)	p	Mean (SD)	% Difference (95% CI)	p
Genu CC	0.74 (0.04)	0.73 (0.02)	-1.0 (-4.6 to 2.6)	0.60	0.71 (0.03)	-4.1 (-7.6 to -0.7)	0.02	0.70 (0.03)	-5.1 (-9.2 to -1.1)	0.01
Body CC	0.72 (0.04)	0.66 (0.06)	-6.1 (-13.7 to 1.6)	0.12	0.68 (0.03)	-6.4 (-10.6 to -2.2)	0.003	0.68 (0.04)	-5.5 (-11 to -0.3)	0.04
Spl CC	0.78 (0.03)	0.78 (0.03)	1.3 (-1.3 to 4.0)	0.33	0.76 (0.02)	-2.2 (-4.7 to 0.2)	0.07	0.76 (0.01)	-2.7 (-5.6 to 0.3)	0.08
ILF R	0.6 (0.05)	0.62 (0.06)	-3.7 (-1.7 to 9.1)	0.18	0.53 (0.07)	-11.1 (-18.5 to -3.7)	0.003	0.59 (0.04)	-0.7 (-6.3 to 4.9)	0.80
ILF L	0.56 (0.03)	0.57 (0.06)	3.8 (-2.8 to 10.4)	0.26	0.51 (0.07)	-10.9 (-18.4 to -3.5)	0.004	0.56 (0.04)	1.5 (-4.0 to 7.1)	0.59
SLF R	0.54 (0.04)	0.51 (0.05)	-2.8 (-9.2 to 3.6)	0.40	0.49 (0.03)	-8.5 (-13.4 to -3.7)	0.001	0.50 (0.04)	-7.0 (-13.0 to -0.9)	0.02
SLF L	0.53 (0.04)	0.51 (0.03)	-1.6 (-7.4 to 4.1)	0.58	0.51 (0.04)	-3.2 (-7.9 to 1.5)	0.18	0.50 (0.03)	-5.0 (-10.9 to 0.9)	0.09
UF R	0.53 (0.08)	0.50 (0.04)	-3.6 (-13.9 to 6.7)	0.50	0.38 (0.09)	-35.3 (-47 to -23.3)	<0.001	0.45 (0.02)	-14.7 (-26.0 to -3.4)	0.01
UF L	0.52 (0.06)	0.52 (0.07)	-0.2 (-9.5 to 9.1)	0.97	0.43 (0.12)	-23.6 (-35.2 to -12)	<0.001	0.51 (0.04)	-2.6 (-11.8 to 6.7)	0.59

Table 6.4 Baseline FA values and estimated mean differences within white matter regions of interest comparing control participants and PPA syndromic groups. * p-value following linear regression comparing PPA syndromic group with controls adjusting for age, gender and disease duration. Data is uncorrected for multiple comparisons.

	Controls (n=18)	NvPPA			SvPPA			LvPPA		
ROI MD	Mean (SD)	Mean (SD)	% Difference (95% CI)	p	Mean (SD)	% Difference (95% CI)	p	Mean (SD)	% Difference (95% CI)	p
Genu CC	0.80 (0.06)	0.82 (0.05)	-0.1 (-5.5 to 5.4)	0.98	0.85 (0.06)	5.6 (0.6 to 10.7)	0.03	0.88 (0.06)	8.8 (2.9 to 14.7)	0.003
Body CC	0.81 (0.06)	0.91 (0.1)	8.1 (-0.2 to 16.4)	0.06	0.89 (0.05)	9.6 (4.7 to 14.5)	<0.001	0.89 (0.07)	8.1 (1.9 to 14.2)	0.01
Spl CC	0.78 (0.07)	0.77 (0.04)	-2.4 (-7.4 to 2.5)	0.34	0.82 (0.04)	4.5 (-0.2 to 9.2)	0.06	0.84 (0.02)	7.4 (1.8 to 13.0)	0.01
ILF R	0.82 (0.06)	0.82 (0.08)	-1.7 (-7.0 to 3.6)	0.53	1.03 (0.17)	19.9 (12.2 to 27.6)	<0.001	0.88 (0.03)	6.0 (1.3 to 10.7)	0.01
ILF L	0.88 (0.1)	0.9 (0.09)	1.6 (-7.0 to 10.1)	0.72	1.12 (0.37)	21.3 (9.3 to 33.3)	0.001	0.92 (0.06)	3.5 (-4.9 to 11.8)	0.41
SLF R	0.73 (0.05)	0.74 (0.04)	1.1 (-3.1 to 5.3)	0.61	0.77 (0.05)	5.1 (0.9 to 9.2)	0.02	0.76 (0.03)	4.0 (-0.4 to 8.5)	0.07
SLF L	0.73 (0.05)	0.73 (0.04)	0.1 (-4.2 to 4.4)	0.97	0.74 (0.04)	1.1 (-2.7 to 4.8)	0.58	0.76 (0.02)	4.5 (0.0 to 9.0)	0.05
UF R	0.75 (0.07)	0.77 (0.06)	0.2 (-5.9 to 6.4)	0.94	0.97 (0.23)	24.7 (14.5 to 35.0)	<0.001	0.78 (0.08)	3.1 (-4.0 to 10.2)	0.39
UF L	0.74 (0.04)	0.72 (0.09)	-4.8 (-11.4 to 1.8)	0.15	0.91 (0.28)	18.5 (7.3 to 29.7)	0.001	0.76 (0.08)	1.7 (-3.7 to 7.0)	0.54

Table 6.5 Baseline MD values and estimated mean differences within white matter regions of interest comparing control participants and PPA syndromic groups. * p-value following linear regression comparing PPA syndromic groups with controls adjusting for age, gender and disease duration. Data is uncorrected for multiple comparisons.

	Controls (n=18)	NvPPA			SvPPA			LvPPA		
ROI RD	Mean (SD)	Mean (SD)	% Difference (95% CI)	p	Mean (SD)	% Difference (95% CI)	p	Mean (SD)	% Difference (95% CI)	p
Genu CC	0.37 (0.06)	0.39 (0.05)	2.6 (-9.4 to 14.5)	0.67	0.42 (0.05)	13.9 (2.9 to 24.9)	0.01	0.44 (0.07)	17.5 (4.2 to 30.8)	0.01
Body CC	0.38 (0.07)	0.50 (0.13)	18.9 (1.6 to 36.2)	0.03	0.46 (0.06)	20.7 (8.9 to 32.5)	0.001	0.46 (0.08)	16.6 (1.4 to 31.9)	0.03
Spl CC	0.32 (0.07)	0.32 (0.04)	-5.4 (-16.6 to 5.8)	0.34	0.36 (0.04)	10.5 (0.5 to 20.6)	0.04	0.37 (0.02)	13.8 (1.6 to 25.9)	0.03
ILF R	0.5 (0.06)	0.50 (0.09)	-5.6 (-15.0 to 3.8)	0.24	0.70 (0.18)	27.8 (15.9 to 39.8)	<0.001	0.55 (0.05)	6.1 (-2.1 to 14.4)	0.14
ILF L	0.58 (0.09)	0.58 (0.1)	-1.4 (-14.3 to 12)	0.83	0.81 (0.39)	28.8 (12.8 to 44.9)	<0.001	0.60 (0.06)	2.5 (-9.0 to 13.9)	0.67
SLF R	0.49 (0.05)	0.52 (0.06)	2.8 (-4.8 to 10.5)	0.47	0.54 (0.05)	9.9 (3.4 to 16.4)	0.003	0.54 (0.04)	8.6 (0.9 to 16.3)	0.03
SLF L	0.49 (0.05)	0.51 (0.05)	1.6 (-5.7 to 9.0)	0.66	0.51 (0.04)	3.1 (-2.9 to 9.2)	0.31	0.53 (0.04)	7.7 (0.0 to 15.4)	0.05
UF R	0.51 (0.09)	0.54 (0.05)	3.3 (-8.0 to 14.5)	0.57	0.78 (0.24)	41.5 (26.7 to 56)	<0.001	0.57 (0.06)	12.8 (0.1 to 25.5)	0.05
UF L	0.50 (0.06)	0.49 (0.1)	-5.1 (-16.5 to 6.4)	0.39	0.70 (0.28)	28.8 (13.1 to 44.6)	<0.001	0.52 (0.07)	4.5 (-5.7 to 14.6)	0.39

Table 6.6 Table 6.5 Baseline RD values and estimated mean differences within white matter regions of interest comparing control participants and PPA syndromic groups. * p-value following linear regression comparing PPA syndromic groups with controls adjusting for age, gender and disease duration. Data is uncorrected for multiple comparisons.

	Controls (n=18)	NvPPA			SvPPA			LvPPA		
ROI AX	Mean (SD)	Mean (SD)	% Difference (95% CI)	p	Mean (SD)	% Difference (95% CI)	p	Mean (SD)	% Difference (95% CI)	p
Genu CC	1.67 (0.06)	1.67 (0.06)	-1.1 (-3.8 to 1.6)	0.44	1.70 (0.07)	1.9 (-0.7 to 4.4)	0.15	1.76 (0.04)	4.7 (2.0 to 7.5)	0.001
Body CC	1.66 (0.05)	1.73 (0.09)	3.0 (-0.7 to 6.6)	0.11	1.74 (0.05)	4.4 (2.5 to 6.3)	<0.001	1.74 (0.06)	4.0 (1.8 to 6.2)	<0.001
Spl CC	1.69 (0.08)	1.68 (0.04)	-1.1 (-4.0 to 1.7)	0.44	1.73 (0.06)	2.3 (-0.5 to 5.0)	0.11	1.79 (0.03)	5.1 (1.8 to 8.4)	0.002
ILF R	1.45 (0.08)	1.48 (0.07)	0.8 (-3.4 to 4.9)	0.71	1.69 (0.16)	13.8 (8.6 to 18.9)	<0.001	1.55 (0.03)	6.0 (1.5 to 10.4)	0.009
ILF L	1.49 (0.13)	1.54 (0.09)	3.5 (-2.7 to 9.6)	0.27	1.75 (0.34)	14.5 (6.2 to 22.8)	0.001	1.57 (0.07)	4.2 (-2.5 to 10.9)	0.22
SLF R	1.20 (0.05)	1.19 (0.03)	-0.4 (-2.9 to 2.0)	0.73	1.22 (0.06)	1.1 (-1.8 to 4.0)	0.45	1.21 (0.02)	0.2 (-2.7 to 3.1)	0.89
SLF L	1.19 (0.06)	1.17 (0.05)	-1.2 (-4.4 to 2.0)	0.46	1.19 (0.06)	-0.6 (-3.7 to 2.5)	0.71	1.22 (0.02)	1.9 (-1.5 to 5.2)	0.28
UF R	1.24 (0.09)	1.23 (0.10)	-2.1 (-7.7 to 3.5)	0.47	1.35 (0.24)	8.8 (1.1 to 16.4)	0.03	1.20 (0.13)	-4.6 (-11.2 to 2.0)	0.17
UF L	1.21 (0.05)	1.17 (0.09)	-5.1 (-9.2 to -1.1)	0.01	1.34 (0.27)	8.5 (0.6 to 16.4)	0.04	1.22 (0.09)	-0.4 (-4.0 to 3.3)	0.85

Table 6.7 Baseline AX values and estimated mean differences within white matter regions of interest comparing control participants and PPA syndromic groups. * p-value following linear regression comparing PPA syndromic group with controls adjusting for age, gender and disease duration. Data is uncorrected for multiple comparisons.

6.3.3 Longitudinal DTI results in PPA subtypes

Rates of change over time for each PPA subtype are shown in tables 6.8 to 6.10. Individual subjects trajectories of change in FA over time are displayed for key affected tracts in Figures 6.1 to 6.3. Longitudinally, compared with controls, nvPPA patients showed widespread changes in white matter tract pathology, the largest changes (reported after adjusting for controls rates of change) in FA were within the body and genu of the corpus callosum (body, -10.6%/year, 95% CI -15.1% to -4.9%, p<0.001; genu, -5.2%/year, 95% CI -6.0% to -2.3%, p<0.001), right and left superior longitudinal fasciculus (right SLF, -5.7%/year, 95% CI-7.6% to -2.2%, p<0.001; left SLF, – 4.3%/year, 95% CI -5.9% to -1.1%, p=0.004) and right uncinate fasciculus (-6.2%/year, 95% CI -10.4% to -0.3%, p=0.04).

Similar profiles of increasing MD were observed comparing nvPPA with controls. The largest magnitudes of change were observed using RD, with the greatest increases within the body and genu of the corpus callosum (body, 19.4%/year, 95% CI 9.0% to 29.7%, p<0.001; genu, 13.5%/year 95% CI 7.6% to 19.5%, p<0.001), with all other tracts, with the exception of the left uncinate fasciculus, showing significant increases in RD. Significant increases, but of lower magnitude, were also observed using AX with the most significant increases occurring in the left inferior longitudinal fasciculus (4.4%/year, 95% CI 1.6% to 7.3%, p=0.002) and right superior longitudinal fasciculus (3.4%/year, 95% CI 2.0% to 4.8%, p<0.001).

Compared with controls those with svPPA showed the largest changes in FA within the right uncinate fasciculus (14.7%/year, 95% CI -19.6% to -8.1%, p<0.001), the right and left inferior longitudinal fasciculus (right ILF, 9.8%/year, 95% CI -11.7% to -6.0%, p<0.001; left ILF, 6.5%/year, 95% CI -8.3% to -1.4%, p=0.006) and the right and left superior longitudinal fasciculus (right SLF, 3.6%/year, 95% CI -4.7% to -0.9%, p=0.004; left SLF -4.1%/year, 95% CI -5.1% to -1.6%, p<0.001). Similar anatomical profiles of increasing MD and RD were also observed, with broadly similar magnitudes of change. No significant longitudinal differences in AX were detected comparing those with svPPA with controls. Longitudinal changes in those with lvPPA, compared with cognitively healthy participants were relatively limited. The largest change in FA occurred within the body of the corpus callosum (3.4%/year 95% CI -5.3% to 0.0%, p=0.05). Increasing RD and AX was observed within the right inferior longitudinal fasciculus (RD, 5.8%/year 95% CI 0.3% to 11.4%, p=0.04; AX, 0.8%/year, 95% CI 0.3% to 11.4%, p=0.04). No significant differences in MD were detected when lvPPA patients were compared with controls.

	NvPPA - FA		NvPPA - MD		NvPPA - RD		NvPPA - AX	
ROI	**%/year change (95% CI)**	**p value**	**%/year change (95% CI)**	**p value**	**%/year change (95% CI)**	**p value**	**%/year change (95% CI)**	**p value**
Genu CC	-5.2 (-6.0 to -2.3)	<0.001	6.7 (3.8 to 9.5)	<0.001	13.5 (7.6 to 19.5)	<0.001	3.2 (1.8 to 4.6)	<0.001
Body CC	-10.6 (-15.1 to -4.9)	<0.001	9.8 (3.9 to 15.8)	0.001	19.4 (9.0 to 29.7)	<0.001	3.6 (0.3 to 6.8)	0.03
Spl CC	-3.0 (-4.5 to -0.2)	0.04	4.4 (0.6 to 8.1)	0.02	10.0 (2.0 to 18.0)	0.01	2.1 (0.1 to 4.2)	0.04
ILF R	-3.8 (-5.9 to 0.3)	0.07	3.6 (0.6 to 6.6)	0.02	6.5 (1.0 to 11.9)	0.02	1.8 (0.2 to 3.4)	0.02
ILF L	-6.2 (-9.4 to 0.3)	0.07	6.8 (1.8 to 11.8)	0.01	9.9 (2.1 to 17.7)	0.01	4.4 (1.6 to 7.3)	0.002
SLF R	-5.7 (-7.6 to -2.2)	<0.001	5.3 (2.9 to 7.7)	<0.001	7.4 (3.8 to 11.1)	<0.001	3.4 (2.0 to 4.8)	<0.001
SLF L	-4.3 (-5.9 to -1.1)	0.004	3.5 (1.1 to 5.9)	0.005	5.0 (1.4 to 8.5)	0.01	2.1 (0.6 to 3.6)	0.01
UF R	-6.2 (-10 to -0.3)	0.04	5.2 (0.5 to 9.9)	0.03	7.6 (0.8 to 14.3)	0.03	2.9 (-0.3 to 6.2)	0.08
UF L	-1.8 (-10.2 to 2.7)	0.26	6.8 (0.1 to 13.6)	0.05	9.2 (-0.7 to 19.1)	0.07	5.4 (0.7 to 10.2)	0.02

Table 6.8 Estimated percentage per year difference in the rate of change for each DTI metric for non-fluent/agrammatic PPA patients (nvPPA), by region, compared with controls. Data is uncorrected for multiple comparisons.

	SvPPA - FA		SvPPA - MD		SvPPA - RD		SvPPA - AX	
ROI	**%/year change (95% CI)**	**p value**	**%/year change (95% CI)**	**p value**	**%/year change (95% CI)**	**p value**	**%/year change (95% CI)**	**p value**
Genu CC	-3.3 (-4.0 to -0.6)	0.007	3.6 (1.5 to 5.8)	0.001	7.1 (2.4 to 1..8)	0.003	1.9 (-0.6 to 2.4)	0.24
Body CC	-3.8 (-5.5 to -0.8)	0.008	2.8 (0.1 to 5.5)	0.04	6.9 (0.6 to 13.3)	0.03	0.5 (-1.4 to 1.8)	0.79
Spl CC	-2.0 (-3.1 to -0.4)	0.12	2.5 (-0.4 to 5.4)	0.09	5.3 (-0.9 to 11.4)	0.09	1.3 (-2.9 to 1.8)	0.64
ILF R	-9.8 (-11.7 to 6.0)	<0.001	8.0 (5.2 to 10.7)	<0.001	12.2 (8.1 to 16.4)	<0.001	4.0 (-0.9 to 2.6)	0.35
ILF L	-6.5 (-8.3 to -1.4)	0.006	5.2 (1.3 to 9.1)	0.009	7.7 (1.8 to 13.6)	0.01	3.2 (-1.9 to 4.4)	0.43
SLF R	-3.6 (-4.7 to -0.9)	0.004	2.4 (0.5 to 4.2)	0.01	3.6 (0.8 to 6.4)	0.01	1.2 (-1.3 to 2.3)	0.60
SLF L	-4.1 (-5.1 to -1.6)	<0.001	2.5 (0.5 to 4.5)	0.02	4.4 (1.5 to 7.2)	0.003	0.8 (-1.9 to 1.8)	0.95
UF R	-14.7 (-19.6 to -8.1)	<0.001	9.9 (4.5 to 15.2)	<0.001	13.7 (6.1 to 21.3)	<0.001	5.5 (-4.8 to 3.6)	0.77
UF L	3.0 (-4.5 to 6.6)	0.70	1.3 (-3.1 to 5.6)	0.58	0.6 (-6.1 to 7.2)	0.86	1.6 (-4.9 to 0.7)	0.15

Table 6.9 Estimated percentage per year difference in the rate of change for each DTI metric for semantic PPA patients (svPPA), by region, compared with controls. Data is uncorrected for multiple comparisons.

	LvPPA - FA		LvPPA - MD		LvPPA - RD		LvPPA - AX	
ROI	**%/year change (95% CI)**	**p value**	**%/year change (95% CI)**	**p value**	**%/year change (95% CI)**	**p value**	**%/year change (95% CI)**	**p value**
Genu CC	-2.1 (-2.9 to 0.8)	0.26	1.8 (-1.0 to 4.6)	0.22	3.7 (-2.1 to 9.5)	0.22	0.9 (-2.1 to 9.5)	0.22
Body CC	-3.4 (-5.3 to 0)	0.05	2.4 (-1.1 to 6.0)	0.18	7.1 (-1.1 to 15.4)	0.09	0.2 (-1.1 to 15.4)	0.09
Spl CC	-0.2 (-2.4 to 3.3)	0.77	-0.9 (-5.5 to 3.7)	0.70	-1.9 (-12.0 to 8.2)	0.71	-0.6 (-12.0 to 8.2)	0.71
ILF R	-4.5 (-2.4 to 3.1)	0.81	2.9 (-0.3 to 6.1)	0.08	5.8 (0.3 to 11.4)	0.04	0.8 (0.3 to 11.4)	0.04
ILF L	-2.5 (-2.3 to 3.0)	0.79	1.9 (-3.2 to 7.0)	0.47	2.9 (-5.0 to 10.7)	0.47	1.3 (-5.0 to 10.7)	0.47
SLF R	-0.5 (-6.7 to 7.9)	0.87	0.3 (-2.5 to 3.1)	0.83	0.2 (-4.1 to 4.4)	0.94	0.5 (-4.1 to 4.4)	0.94
SLF L	-0.5 (-4.4 to 9.0)	0.50	-0.2 (-3.0 to 2.7)	0.91	-0.2 (-4.4 to 3.9)	0.91	-0.1 (-4.4 to 3.9)	0.91
UF R	-0.2 (-6.8 to -0.4)	0.03	-1.1 (-7.5 to 5.4)	0.74	-2.2 (-11.8 to 7.3)	0.65	-0.6 (-11.8 to 7.3)	0.65
UF L	4.2 (-5.4 to 3.6)	0.70	-3.4 (-8.1 to 1.2)	0.15	-5.3 (-13.0 to 2.4)	0.18	-2.1 (-13.0 to 2.4)	0.18

Table 6.10 Estimated percentage per year difference in the rate of change for each DTI metric for logopenic PPA patients (lvPPA), by region, compared with controls. Data is uncorrected for multiple comparisons.

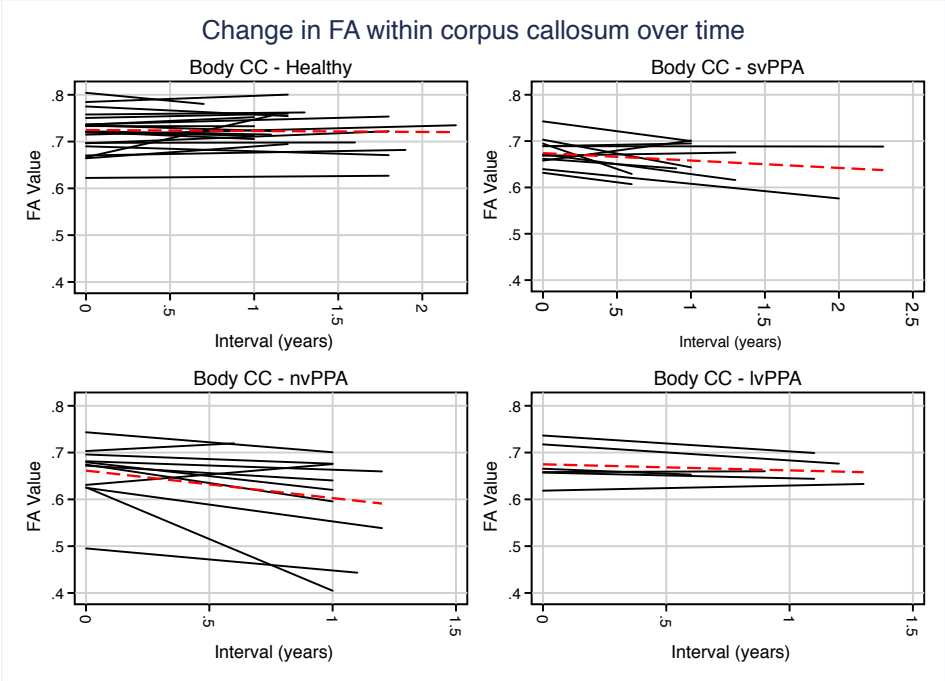

Figure 6.1 Individual trajectories of change in FA (y-axis) over time (x-axis in years) within body of the corpus callosum in each PPA syndrome. The red dashed line indicates mean trajectory.

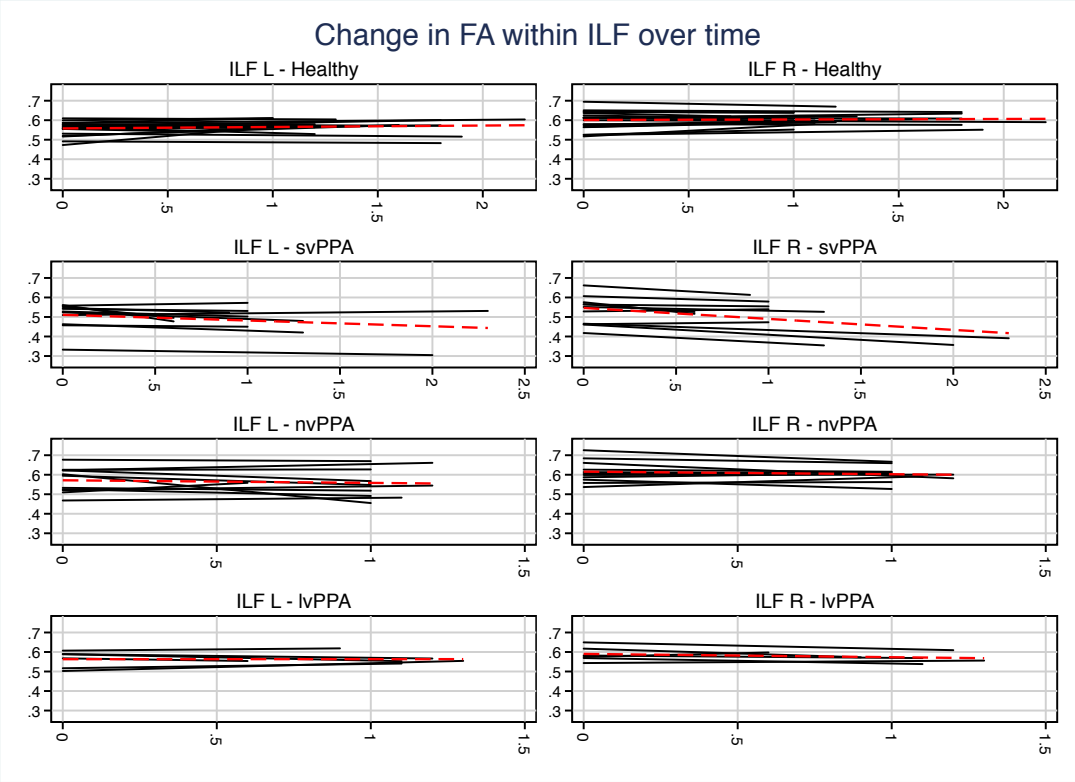

Figure 6.2 Individual trajectories of change in FA (y-axis) over time (x-axis in years) within the ILF in each PPA syndrome. The red dashed line indicates mean trajectory.

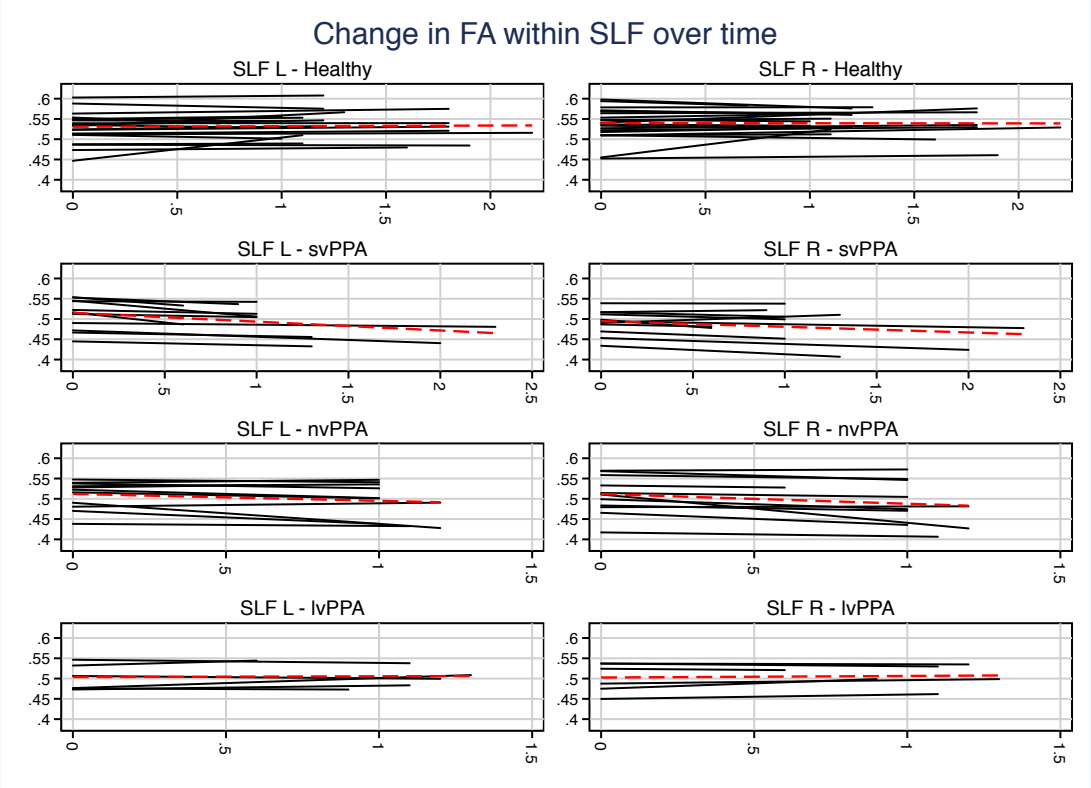

Figure 6.3 Individual trajectories of change in FA (y-axis) over time (x-axis in years) within the SLF in each PPA syndrome. The red dashed line indicates mean trajectory.

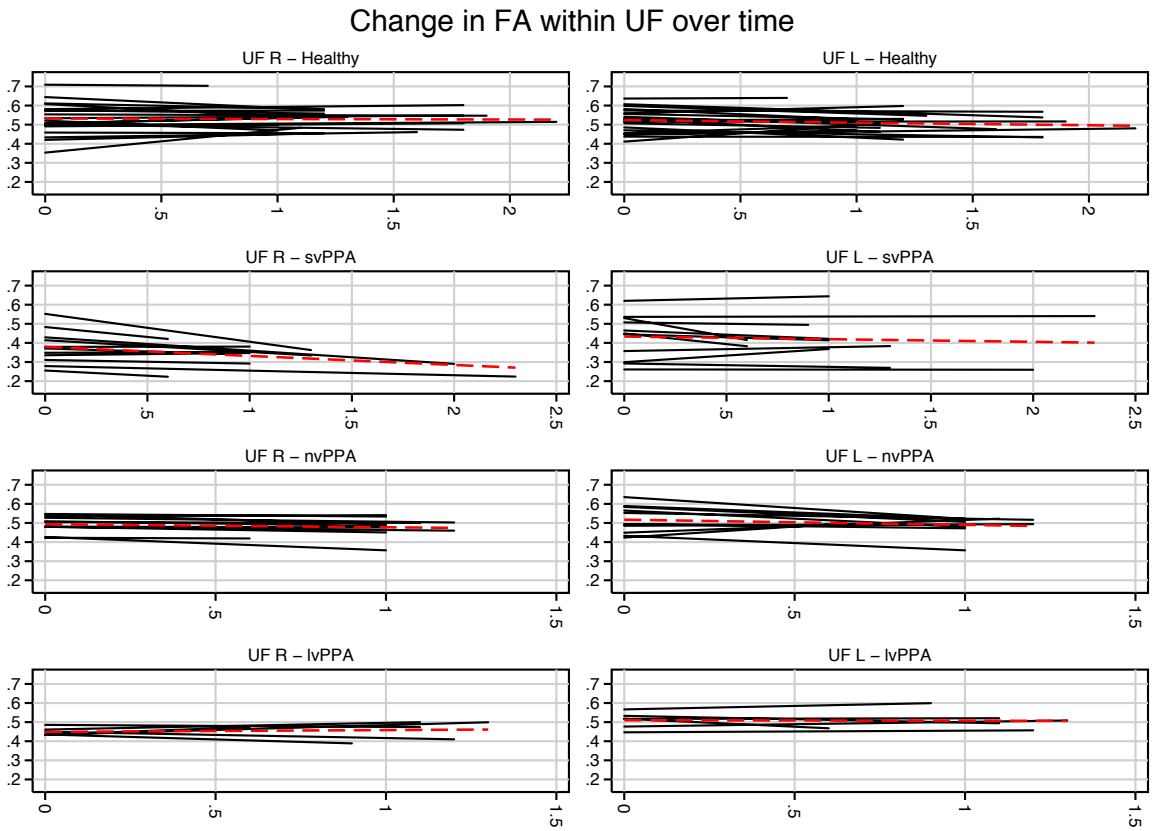

Figure 6.4 Individual trajectories of change in FA (y-axis) over time (x-axis in years) within the uncinate fasciculus in each PPA syndrome. The red dashed line indicates mean trajectory.

6.3.4 Sensitivity and specificity of cross-sectional and longitudinal DTI metrics

To determine optimal DTI metrics AUC data were calculated to determine the specificity and sensitivity in classifying PPA syndromic groups from controls. Calculations were made for both cross-sectional values and longitudinal rates of change. Examining cross-sectional data first, in those with svPPA, measurements within the right inferior longitudinal fasciculus achieved the best classification, with MD performing best (AUC 0.93, sensitivity 100%, specificity 80%, correctly classified 87%), followed by AX (AUC 0.91, sensitivity 91%, specificity 85%, correctly classified 87%), RD (AUC 0.88, sensitivity 82%, specificity 85%, correctly classified 84%), and FA (AUC 0.78, sensitivity 64%, specificity 85%, correctly classified 77%). In those with nvPPA, measurements within the body of the

corpus callosum achieved the best classification, with MD best (AUC 0.82, sensitivity 73%, specificity 85%, correctly classified 81%), followed by RD (AUC 0.82, sensitivity 64%, specificity 90%, correctly classified 81%), FA (AUC 0.79, sensitivity 73%, specificity 80%, correctly classified 77%) and AX (AUC 0.79, sensitivity 45%, specificity 95%, correctly classified 77%). In those with lvPPA, measurements within the splenium of the corpus callosum, achieved the best classification, with AX performing best (AUC 0.88, sensitivity 100%, specificity 85%, correctly classified 88%), followed jointly by RD and MD (AUC 0.86, sensitivity 83%, specificity 85%, correctly classified 84%) and FA (AUC 0.86, sensitivity 83%, specificity 80%, correctly classified 81%). Examining longitudinal rates of change, in svPPA change within right inferior longitudinal fasciculus achieved the best classification overall, with FA performing best (AUC 0.86, sensitivity 73%, specificity 95%, correctly classified 87%), followed by RD (AUC 0.85, sensitivity 82%, specificity 90%, correctly classified 87%), MD (AUC 0.83, sensitivity 64%, specificity 100%, correctly classified 87%) and AX (AUC 0.76, sensitivity 64%, specificity 100%, correctly classified 87%). In nvPPA change within the right superior longitudinal fasciculus achieved the best classification overall, with AX performing best (AUC 0.95, sensitivity 100%, specificity 80%, correctly classified 87%), followed by MD (AUC 0.93, sensitivity 91%, specificity 85%, correctly classified 87%), RD (AUC 0.89, sensitivity 73%, specificity 95%, correctly classified 87%), and FA (AUC 0.85, sensitivity 82%, specificity 85%, correctly classified 84%). In lvPPA change within the genu of the corpus callosum achieved the best classification overall, with RD performing best (AUC 0.77, sensitivity 50%, specificity 95%, correctly classified 85%), followed by MD (AUC 0.77, sensitivity 50%, specificity 90%, correctly classified 81%), AX (AUC 0.73, sensitivity 33%, specificity 90%, correctly classified 77%), and FA (AUC 0.7, sensitivity 67%, specificity 95%, correctly classified 88%).

6.3.5 Sample size estimates

To assess the utility of DTI as an outcome measure sample size calculations were obtained to detect a reduction in the rate of change ranging from 20-40% per year. Change within three regions-of-interest were used for these calculations (chosen based on their significance in terms of longitudinal change); two DTI metrics were chosen, FA based on it being the most commonly reported metric and RD as it exhibited the largest magnitude of change. To compare against more traditional measures, calculations were also made based on rates of whole brain atrophy. Neuropsychological measures were not included as on inspection of raw data many individuals scored at or near floor and as such had low variability in terms of change (i.e. a change of 50%/year could results from a score of 4/30 on the GNT falling to 2/30, for example, as such the variance as a proportion of the total score is low, thus limiting the utility of this metric in longitudinal assessment). The lowest sample size estimates were identified using DTI, although estimates varied by syndrome, ROI and metric. The choice of a specific ROI was determined by it having the largest AUC on the classification analysis; the choice of FA was based on its overall longitudinal performance across syndromes, again based on values from the classification analysis. In svPPA the lowest sample size estimates were obtained assing FA change within the right inferior longitudinal, in nvPPA the lowest sample size estimates were obtained when assessing FA change within the right superior longitudinal fasciculus, and in lvPPA had the lowest sample size estimates were obtained when assessing change within the right inferior longitudinal fasciculus.

	Right ILF					
Sample Size	**FA**			**RD**		
	SvPPA	**NvPPA**	**LvPPA**	**SvPPA**	**NvPPA**	**LvPPA**
20%	59	464	238	86	481	63
30%	26	207	106	38	216	28
40%	15	116	60	21	122	16
	Body CC					
	FA			**RD**		
	SvPPA	**NvPPA**	**LvPPA**	**SvPPA**	**NvPPA**	**LvPPA**
20%	268	162	255	613	196	642
30%	120	72	117	269	88	283
40%	68	41	67	149	50	159
	Right SLF					
	FA			**RD**		
	SvPPA	**NvPPA**	**LvPPA**	**SvPPA**	**NvPPA**	**LvPPA**
20%	194	159	9681	427	174	67201
30%	87	70	4824	188	77	51451
40%	49	39	2881	106	43	32929
	BBSI					
	SvPPA		**NvPPA**		**LvPPA**	
20%	342		175		301	
30%	152		78		134	
40%	86		44		76	

Table 6.11 Sample size estimates per treatment arm of a clinical trial comparing 2 DTI metrics (FA and RD) and whole brain atrophy (BBSI) to detect a 20%, 30% and 40% reduction in rates of change. β = 80%, α = 0.05.

6.4 Conclusions

6.4.1 Overview of results

The current study is one of the first to track longitudinal changes in white matter across the spectrum of PPA, including all three major phenotypes: svPPA, nvPPA and lvPPA. This study has demonstrated the feasibility of longitudinally DTI in PPA. It builds on the data presented in the previous chapter by providing novel data, giving further insights into the evoloution of PPA. This study also suggests that longitudinal DTI may be a potentially useful disease biomarker. Across syndromic groups, both cross-sectionally and

longitudinally, decreasing FA and increasing MD, RD and AX was observed, with specific trajectories of white matter change emerging. In those with svPPA the most notable change over time occurred within the right inferior longitudinal fasciculus and uncinate fasciculus, with up to a 12%/year change from controls; in nvPPA the most notable change over time occurred within bilateral superior longitudinal fasciculus, with up to a 7%/year change from controls; in lvPPA the most notable change over time occurred within the body of the corpus callosum and right inferior longitudinal fasciculus, with up to a 7%/year change from controls.

6.4.2 Relationship to previous longitudinal studies of PPA

Relatively few studies of longitudinal imaging in PPA have been carried out. One study has examined longitudinal change in white matter tracts in patients with PPA, although did not include patients with lvPPA (Lam et al., 2014). Similar to the current study, this study found bilateral (left>right) changes in superior longitudinal fasciculus, inferior longitudinal fasciculus and corpus callosum at baseline, and overtime changes became more apparent within the right hemisphere, which is similar to the current studies findings. The authors also commented that changes were most pronounced when measured using MD and RD with AX not being particularly sensitive. In those with svPPA at baseline white matter pathology was restricted to the left hemisphere however over time white matter changes became more apparent within the right hemisphere, frontal tracts and the corpus callous. Whilst there are few longitudinal DTI studies there is a greater body of information concerning longitudinal profiles of grey matter or whole brain atrophy in PPA. The majority of these studies suggest that whilst atrophy continues within core components of the left-sided language network, there is evidence of disease

progression beyond these regions, most often mirroring the same regions within the contralateral hemisphere (Brambati et al., 2009; Czarnecki et al., 2008; Faria et al., 2014; Rogalski et al., 2011; Rohrer et al., 2008; Rohrer et al., 2013). In one recent study progressive atrophy in the right temporal lobe was also shown to be correlated with further declines in word comprehension (Faria et al., 2014) providing evidence that this atrophy may have a clinical correlate. A number of longitudinal functional imaging studies have suggested that within these 'mirror regions' there is an initial increase in activation activity on specific language tasks (Heim et al., 2014; Maguire et al., 2010). This is thought to be a compensatory mechanism to help maintain cognition, but over time this activity reduces and eventually specific cognitive abilities collapse. These areas of increased activity may cause heightened nodal stress in an already diseased brain, resulting in acceleration of neurodegeneration within these regions, eventually resulting in the brain atrophy, but possibly, as the current study suggests, led by changes in white matter integrity.

6.4.3 Neurobiological relevance of longitudinal DTI in PPA

As seen in the previous cross-sectional study much of the white matter tract pathology identified occurred remote to the sites of maximal grey matter atrophy. The current study adds further support for this finding as much of the largest pathological change within white matter tracts occurred in the hemisphere contralateral (in this case right) to maximal grey matter atrophy. The current study does indicate that there is progression of left sided white matter tract pathology over-time, and indeed cross-sectional data indicate significant left hemispheric tract pathology at baseline, however the rate of change within the right hemisphere appears to accelerate more rapidly. PPA could

therefore be viewed as a bihemispheric disease process, which initially targets specific brain networks, in this case left-sided language networks, but over time encroaches on other brain regions. The pattern of progression observed may results from the fact that one hemisphere has relatively more 'healthy' white matter and as such the density of white matter tracts is greater so change is more likely to be detected. The topography of progression is also of interest, as in svPPA the pathological change over time mirrors the tracts involved cross-sectionally i.e. the same tracts are involved, but within the opposite hemisphere. Whilst traditionally the left hemisphere has been viewed as the primary language hemisphere, increasing evidence indicates that the right hemisphere is important in paralinguistic processing, such as sarcasm perception and contextualising other external stimuli (Rankin et al., 2009), as well as being associated with problems in accent processing and voice recognition (Hailstone et al., 2010). The right hemisphere also plays a key role in giving objects meaning, and has been linked with visual agnosia for both objects and faces (Chan et al., 2009; Garrido et al., 2009). These non-verbal deficits often become more apparent with time in svPPA and in some cases may be the presenting feature, as in a right-side predominant svPPA. Data from the current study would suggest that prior concepts of svPPA being a predominantly unilateral disease are incorrect and that overtime it evolves to involve the contra-lateral hemisphere, possibly being facilitated by connections via commissural pathways, which were also display significant pathological change over time (Fletcher and Warren, 2011; Warren et al., 2012). In those with nvPPA cross-sectional differences from controls were relatively few, with the body of the corpus callosum being most consistently involved. However longitudinal changes were much more evident with significant rates of change in FA, RD, MD and AX observed in most white matter tracts. In particular large changes were observed within

the body of the corpus callosum and within bilateral superior longitudinal fasciculus. The finding of superior longitudinal fasciculus involvement is of particular interest as this tract has been identified as a key structure involved in both articulation of speech and phoneme encoding for speech (Davtian et al., 2008; Han et al., 2014). The superior longitudinal fasciculus is a long intra-hemispheric tract and is likely to support a distributed speech production network connecting brain regions traditionally associated with speech production (i.e. Broca's area), with regions such as the parietal lobe and cerebellum, which are increasing recognised as areas that modulate speech production (Simonyan and Fuertinger, 2015; van Geemen et al., 2014). The discrepancy between cross-sectional and longitudinal differences was most notable within the nvPPA group. This may suggest that the trajectory of nvPPA may be somewhat multiphasic with acceleration of disease pathology over time. The current study data also suggests that longitudinal DTI offers both greater sensitivity and specificity at detecting and tracking nvPPA, compared to cross-sectional metrics, as evidenced by the larger AUC calculated. In those with lvPPA the most consistent pathological changes were observed within the corpus callosum and SLF. Of note all three subsections of the corpus callosum showed a significant difference from controls cross-sectionally. Longitudinal changes in those with lvPPA were somewhat more variable depending on the DTI metric as well as being less conspicuous when compared with changes seen in those with svPPA and nvPPA. Some of these differences may be explained in part by the smaller size of this group, and of course given this small group size these results should be viewed with some caution. Overall change within the body of the corpus callosum and right inferior longitudinal fasciculus appeared the most consistent feature across DTI metrics in those with lvPPA.

6.4.4 DTI metrics – syndromic and molecular consideration in PPA

As outlined previously it is unclear if one particular DTI metric offers better specificity/sensitivity than another, and it has been a major aim of the current work to improve our understanding of this. In the case of PPA syndromes a somewhat variable pattern emerged, reviewing each syndrome's cross-sectional and longitudinal performances. Some insights on DTI metric performance are provided by the ROC-curve data, which aimed to classify the highest proportion of patients with PPA from healthy controls. Taking each syndrome in turn, in svPPA change in the right inferior longitudinal fasciculus as measured with MD achieved the best classification (sensitivity of 91%, specificity 85%). A notable finding was that in svPPA, FA was the worst cross-sectional metric, but the best longitudinal metric, suggesting that FA is a better longitudinal index of overall white matter integrity, at least in svPPA. In nvPPA each DTI marker performed relatively poorly cross-sectionally, this is in line with the relatively sparse cross-sectional profiles of white matter pathology seen in whole brain analysis of nvPPA in the previous chapter (see Figures 5.1 to 5.3). However sensitivities and specificities were enhanced when longitudinal rates of change were used to classify groups, with MD and AX performing best, and enhanced further by targeting change in the superior longitudinal fasciculus (right SLF sensitivity 91%, specificity 85%). Finally in those with lvPPA, AX appeared to perform best cross-sectionally, achieving up to 100% sensitivity and 85% specificity within the corpus callosum, although there was poor performance across all metrics in this group longitudinally. As pointed out in the previous chapter svPPA is known to be associated with TDP pathology and lvPPA with AD pathology, and the current finding of relatively better performance of AX in lvPPA may suggest this metric

has a particular sensitivity for AD pathology. One notable omission from this longitudinal study is the absence of the fornix as a region of interest. In the previous chapter it was noted that pathology within this white matter structure seemed more evident in those with lvPPA compared to other PPA groups, suggesting that pathology within this structure may be a relatively specific feature of lvPPA. This region was not considered longitudinally as following review of raw data obtained from this region, an unacceptably high level of variation between subjects was seen, which may reflect limitations in the registration of this small and complex anatomical structure. The pathological heterogeneity of nvPPA may also explain why there was relatively little change captured cross-sectionally, but when intra-subject comparisons (rather than inter-subject comparisons) are made there is a greater ability to detect change. Again it is important to point out that the choice between having a highly sensitive metric, i.e. a test that screens a population for disease, or a highly specific metric, i.e. a test that can distinguish pathological subtypes, depends on the question being asked. If the purpose of the biomarker is to simply track the same disease longitudinally than a highly sensitive DTI metric may be required; however if we wish to compare disease biology, or the effect of a particular treatment across multiple pathologies, a more specific marker may be required. The current data suggest that overall, cross-sectional DTI metrics may offer greater sensitivity while longitudinal DTI metrics may offer greater specificity.

6.5 Chapter summary

The current study is one of the first studies to monitor white matter tract changes across all subtypes of PPA. Particular trajectories of pathological change have been identified for individual PPA subtypes, suggesting longitudinal DTI may have a role as an outcome measure for clinical trials in future. This potential role is supported by the sample size estimates calculated, particularly when compared to more traditional outcome measures such as whole brain atrophy. The cross-sectional data presented here, calculated using a different methodology, are broadly concordant with that seen in chapter 5. The longitudinal data suggest that there is acceleration of white matter tract pathology, particularly in contra-hemispheric tracts remote to areas of maximal cross-sectional grey and white matter pathology. In svPPA this was most apparent in the right inferior longitudinal fasciculus and uncinate fasciculus; in nvPPA this was apparent within the right superior longitudinal fasciculus; and in lvPPA within the corpus callosum and right inferior longitudinal fasciculus. In those with svPPA and lvPPA both cross-sectional and longitudinal DTI performed well in separating PPA from healthy controls, this was not the case in those with nvPPA where longitudinal analysis was more sensitive and specific. The current study also adds further support to the concept that DTI metrics may signal specific molecular vulnerability, demonstrated by the performance of AX in those with lvPPA, which is likely underpinned by AD pathology.

7. Conclusions

7.1 Overview of research presented

Over the past number of decades our understanding of the collection of clinical and pathological syndromes that make up FTLD has evolved rapidly. New proteins and molecular mechanisms have been identified, new genetic mutations uncovered thanks to next generation sequencing, novel frameworks for understanding how these diseases start and evolve, thanks to complex mathematical techniques such as graph theory. The next major challenge to the scientific community is to apply many of these clinical and basic science discoveries to develop biomarkers, which can accurately, diagnose and track these complex neurobiological conditions allowing disease-modifying treatments to be tested. This was a major motivation for performing these studies.

As outlined in the opening chapter this Thesis had four major aims:

1. Establish the profiles of white matter tract pathology in bvFTD and PPA by examining clinically, and where possible genetically, defined phenotypes using both cross-sectional and longitudinal DTI.
2. Establish the relationship of white matter and grey matter pathology to one another.
3. Establish the usefulness of DTI as a potential disease biomarker, with which FTLD can be monitored.
4. Establish the sensitivity and specificity of individual DTI metrics in the monitoring of FTLD.

Regarding aim 1 this study has demonstrated that DTI can be applied to study white matter pathology in patients with bvFTD and PPA, with potential practical advantages

including availability and tolerability by patients, and its biological application in identifying syndrome specific profiles of white matter pathology cross-sectionally and trajectories of white matter change longitudinally. These studies further refine the neuroimaging phenotype of bvFTD and PPA by providing detailed profiles of white matter tract pathology, which may aid in the diagnosis and monitoring of these conditions. Tables 7.1 and 7.2 provide an overview of the profiles of white matter tract pathology identified longitudinally and cross-sectionally. Across the bvFTD group we note bilateral antero-ventral white matter tract pathology. A key finding was the involvement of the cingulum bundle across subtypes of bvFTD, indicating it likely has a key role in modulating the clinical phenotype. The absence of strongly asymmetric profiles of white matter tract pathology is perhaps somewhat surprising, given that FTLD is commonly associated with an asymmetric neuroimaging phenotype, this may in part relate to either the absence of the *GRN* mutations which are the most asymmetric of the FTLDs, or more generally it may relate to the sensitivity of DTI in detecting pathological change. In those with PPA, syndrome specific profiles of white tract pathology were identified, although no clear tract signalled a syndrome by itself; relative involvement of particular white matter tracts appears to signal individual phenotypes: for example the inferior longitudinal fasciculus and uncinate fasciculus in svPPA, the superior longitudinal fasciculus in nvPPA and all three of the above tracts and the fornix in lvPPA. Again perhaps an unexpected finding is the degree of pathological white matter tract change within the right (non-language) hemisphere. Again this signifies that DTI may offer greater sensitivity in detecting pathology, but also that strucutural changes in PPA syndromes progress to regions not traditionally associated with language, which is perhaps why many paralingustic functions decline in PPA (Hailstone et al., 2010; Rankin et

al., 2009). More broadly these microstructural findings in both bvFTD and PPA support a concept of quite spatially distributed neurodegenerative processes, perhaps more so than other structural imaging would suggest. Whilst these findings do not provide direct evidence for the mechanism underpining disease propogation it provides further indirect evidence that these clinical syndromes are associated with initially local patterns of white matter pathology followed by disruption of more wide-spread white matter tracts, likely contributing to the disruption of multiple, both linguistic and non-lingusitic, cognitive networks (Schroeter et al., 2008; Seeley et al., 2007).

Regarding aim 2, chapters 3 and 5 compared the profiles of grey and matter pathology in bvFTD and PPA respectively. Methodological limitations notwithstanding, the anatomical extent of white matter tract pathology was greater than that of grey matter atrophy, although the most significant areas of white matter pathology were co-localised to sites of maximal grey matter atrophy, supporting the notion that there is a common degenerative process resulting in pathological change to both grey and white matter. Overall, there is compelling evidence across for anatomically distributed patterns of white matter tract pathology, which is in line with the notion that FTLD (and other neurodegenerative syndromes), target large-scale brain networks, which in the current study is signalled by disintegration of distributed structural networks, occurring in advance of grey matter atrophy. The concept of white matter involvement being a key feature in the FTLDs is also based on the numerous imaging studies reporting wide spread white matter tract pathology (Agosta et al., 2011; Galantucci et al., 2011; Lam et al., 2014; Whitwell et al., 2010), as well as histopathological data which provide evidence of pathogenic proteins localised to white matter (Hiji et al., 2008; Neumann et al., 2007).

Indeed emerging pathological evidence suggests that in some circumstances white matter pathology may be more florid than grey matter pathology across the spectrum of FTLD assocatied clinical syndromes (Ahmed et al., 2013; Caroppo et al., 2014; Irwin et al., 2014).

Aim 3 was to establish the usefulness of DTI as a disease biomarker, both in terms of it's a abilty to detect a disease, as well as its potential role as a surrogate-outcome measaure for clinical trials. Data from each experiment show that DTI can be both a sensitive (i.e. identifying an abnormality in the first instance) and specific (i.e. correctly classifying those with FTLD from controls) measure of pathology. It should be noted that in some instances specific DTI metrics did not necessarily fulfil criterion to be a suitable biomarker, for example in those with lvPPA the FA change in the copus callosum only reached an AUC of 0.7. However it is only through these assessments that we will begin to form an understanding of how each metric relates to particular syndromes and pathologies, and by doing so we will have a better understanding of the relationship between changes occurring within axons and changes seen on DTI. On the other hand a specific merit of DTI, over other imaging methods, is that it results in a quantitative measure, meaning it may have a role as a personalised biomarker, rather than say fMRI or VBM, which require group studies to identify pathological changes as well as being more labour intensive. In addition data from both longitudinal studies show that DTI may perform more favourably as an outcome measure when compared with more traditional biomarkers, emphasised by the sample size estimations, which in most cases were lower than other outcome measures such as rates of global brain atrophy.

Aim 4 asked the question was one particular DTI metric better than another in assessing white matter tract pathology in bvFTD and PPA? This was perhaps the most difficult

question asked by this study, particularly as specific hypotheses on the role of individual DTI metrics are lacking. Table 7.3 compares the overall performance of individual DTI metrics in this study. DTI metrics were assessed in all disease groups, both longitudinally and cross-sectionally. RD seemed to offer the best overall sensitivity in terms of both extent and magnitude of pathological change. Some differences did appear on subgroup analysis; for example FA appeared to have better qualities in monitoring longitudinal changes in svPPA, whilst MD performed better in monitoring longitudinal changes in nvPPA. At first glance AX appeared to be the least sensitive, however when results were adjusted for global DTI metrics in the cross-sectional bvFTD study, AX performed better than other metrics. This may represent a technical signpost and may signal that AX has greater specificity than other metrics. In addition, AX performed relatively better as a measure of white matter pathology in those with lvPPA indicating it may have a greater specificity for particular histopathologies such as AD, or perhaps tauopathies, as on bvFTD subgroup analysis of *MAPT* mutation carriers, both cross-sectionally and longitudinally, AX identified the greatest degree of white matter tract pathology in this group, which is known to be associated with tau pathology.

Whilst it must be acknowledged that much of the above suggestions are hypothetical, given the lack of histopathological correlation, it is at least worth pointing out that technical modifications (such as correcting for global DTI mean) can provide substantially different results, and as such warrant further evaluation, particularly when deciding on which DTI metric is 'best'. Of course given that these metrics are all collected simultaneously during the same scan acquisition, along with other metrics not discussed here, such as the mode of anisotropy, which has been suggested as a superior metric for

assessing change in anisotropy in areas of crossing fibres (Douaud et al., 2011), it seems worthwhile, for now at least, to collect this data to allow further studies in establishing the utility of individual DTI metrics in FTLD. Of course the downside of this is large volumes of data to analyse and from large volumes of data comes to risk of increased false positivity. Overtime it may well be necessary to apply a biologically customised suite of DTI metrics rather than a 'one size fits all' approach.

	BvFTD					
	Cross-Sectional			Longitudinal		
Tract	**All bvFTD**	**MAPT**	**C9ORF72**	**All bvFTD**	**MAPT**	**C9ORF72**
R UF	++++	+++		++	+++	
L UF	++++	+++		++	++	++
R CB	++++	++		+	++	
L CB	++++	++	+	+	++	
R ILF	+++	+				
L ILF	++	+				
CC	+++	++	+	+	++	+
R CST	+			+		
L CST						
Fornix	++	++				

Table 7.1 Overview of WM tract involvement in bvFTD cross-sectionally and longitudinally based on FA data. Cross-sectional data: ++++ >50% tract involved, +++25-50%, ++ 10-25%, + 5-10%, blank minimal/no involvement. Longitudinal data: +++ >10%/year change, ++5-10%/year change +, 2.5-5%/year change, blank <2.5%/year change.

	PPA					
	Cross-Sectional			Longitudinal		
Tract	**SvPPA**	**NvPPA**	**LvPPA**	**SvPPA**	**NvPPA**	**LvPPA**
CC	++++	+++	++++	++	+++	
ILF R	++++	+++	++++	++	++	++
ILF L	++++	++	++++	+	++	
SLF R	++++	++	+++	+	++	
SLF L	+++	+	+++			
UF R	++	+	+++			
UF L	+++	++	++++	+	++	+
Fornix			++	ns	ns	ns

Table 7.2 Overview of WM tract involvement in PPA cross-sectionally and longitudinally based on FA data. Cross-sectional data: ++++ >50% tract involved, +++25-50%, ++ 10-25%, + 5-10%, blank minimal/no involvement. Longitudinal data: +++ >10%/year change, ++5-10%/year change +, 2.5-5%/year change, blank <2.5%/year change. Key: ns, not studied longitudinally.

	All bvFTD	**SvPPA**	**NvPPA**	**LvPPA**
Cross-sectional				
FA	++	++	+	+
MD/TR	++	++	+	++
RD	++	++	+	+
AX	+	++	+	++
Longitudinal				
FA	++	+++	++	-
MD/TR	++	++	+++	+
RD	++	++	++	+
AX	+	+	++	+

Table 7.3 Overview of individual DTI metrics performance reflecting potential as a disease biomarker. Table constructed using data obtained from ROC curve analysis to determine sensitivity and specificty. Increasing number of + signs denotes increasing performance as a biomarker and is based on quantative AUC values. Key: +++ AUC>0.9, ++ AUC=0.8-0.9, + AUC=0.7-0.8, - AUC<0.7.

7.2 Relevance of the current studies network-led degeneration

At a basic neuroscience level this study provides evidence that a breakdown of structural brain networks is a key factor in the neurobiology of bvFTD and PPA. Examining the change across structural brain networks may offer a more useful way of tying together proteinopathies, clinical symptoms and macroscopic brain atrophy, or indeed multiple discrete regions of atrophy or reduce functionality (Warren et al., 2013; Zhou et al., 2012). Figure 7.1 provides an overview of pathological changes to normal brain networks identified in the current study, and highlights the extent of white matter tract pathology across each syndrome, and provides a framework for explaining how cognitive dysfunction may occur in areas remote to maximal grey matter atrophy. Historically it has long been held that damage to structural connections within the brain can lead to specific clinical syndromes, with Geschwind, the most prominent 'connectionist' of the twentieth century, describing multiple disconnection syndromes. One aspect of Geschwinds' research seems relevant to the current study: the concept that lesions within white matter association tracts would also result in a 'lesion' within the cortex it connects, particularly emphasising higher cortical functions such as behaviour and language, and further that lesions within association cortex, which are region that show high interconnection, may also lead to widespread widespread cognitive demise (Geschwind, 1965). More recently Geschwinds theories on disconnection between brain regions have been updated to reflect new evidence on brain connectivity based on a multidiude of functional and structural imaging studies as well as high quality animal tracing studies (Schmahmann et al., 2007). These new theories reflect the fact the connections can work in a feed-forward and feed-back fashion (Geshwinds view was that 'information' flowed from temporoparietal regions *exclusively* anterogradely towards

limbic regions), as well as excerting both inhibitory and excitatory functions (Catani, 2007; Catani and ffytche, 2005; Warren et al., 2013). In addition our understanding of the role of association cortex has also been updated, to reflect the fact that many of these regions anatomically overlap with network hubs, which have a central position in integratrion and disementaion of 'information' throughout brain networks, and when damaged or disconnected can result in widespread cognitive failure (van den Heuvel and Sporns, 2013). Whereas Geschwind tended to focus on disconnection between long-range association tracts newer models also emphasise the fact that cognitive dysfunction can also result from failure of short-range connections within intraterritorial regions. Additionally these models also allow an explanation for cognitive dysfunction based hyperconnectivity between brain regions – either through loss of inhibitory connections, damage to regions involved in gating certain modalities or through on overall imbalance in connectivity. This may explain some of the more *positive* clinical feautres seen in FTLD such as hyperorality, echolalia and hallucinosis.

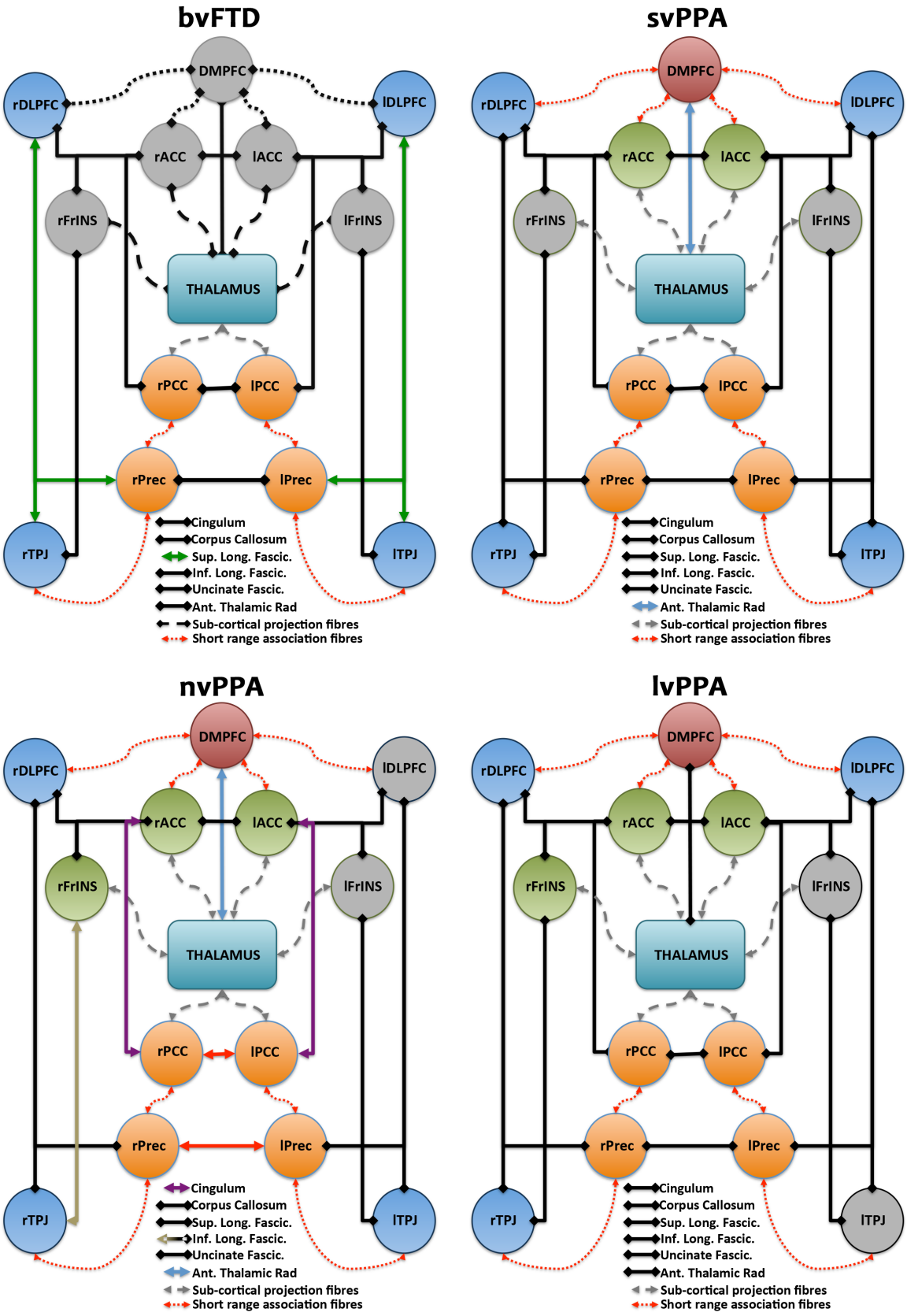

Figure 7.1. Overview of pathology across distributed brain networks in each syndromic group based on findings from the current study. Black lines with diamond caps indicate tracts with prominent white matter pathology (based on FA). Grey circles indicate regions with grey matter atrophy. Compare these patterns of structural and functional network change with patterns of normal connectivity in figure 1.3.

These concepts of network disconnection have some face validity in terms of the current study, evidenced by the increasing extent of white matter pathology within regions less affected at baseline. DTI can only assess what is happening at a given point in time and a relative weakness is that it can not continusouly monitor changes in diffusion *in vivo,* neither does it tell us what are the mechanisms which result in both baseline and longitudinal white matter pathology. A number of mechanisms may support a gradual spatial evolution of disease, possibly facilitated by cognitive networks, and may include transynaptic spread of toxic proteins, wallerian degeneration, or loss of trophic support from downstream network components, which have undergone degeneration (Clavaguera et al., 2013; Pievani et al., 2011). This tracjectory of change shares some commonality with longitudinal grey matter changes, and whilst not assessed in this study, previous studies have shown that acceleration in grey matter atrophy also occurs in regions contralateral to baseline regions of atrophy (Faria et al., 2014; Rohrer et al., 2008; Rohrer et al., 2013), supporting the idea that initial focal damage (or disconnection) can lead to remote cortical damage and progressive cognitive dysfunction. The mechanisms for this are unclear but it is plausible that white matter pathology may facilitate downstream grey matter damage, leading to further deterioration in higher cognitive abilities. As mentioned in previous chapters it is unlikely that white matter is the sole driver of pathology in FTLD, however it is increasingly clear that it plays an important role, likely in concert with grey matter, to result in particular clinical phenotypes. This 'disconnection' between brain regions, is evidenced in the current study by the extent of white matter tract pathology compared with grey matter atrophy, and may explain why there is deterioration in parietal skills such as space perception, in the absence of significant grey matter pathology. This theory may also explain why in

groups such as *C9ORF72* mutation carriers, there can be in some cases only minimal grey matter atrophy but florid global cognitive impairment (Mahoney et al., 2012b).

A major theme, which runs through the current studies, relates to the role to which brain networks, which includes both grey and white matter, facilitate neurodegeneration; the idea of network-led degeneration. This concept should not be so surprising, given that over the last two decades a wealth of data from healthy individuals have confirmed that most complex cognitive tasks result from synchronous brain activity across multiple brain regions (Cabeza and Nyberg, 2000). Therefore the concept of cognitive demise due to loss of connectivity between these brain regions is plausible (Greicius et al., 2004; Hornberger et al., 2012; Seeley et al., 2009). Somewhat more hypothetical is the notion that the initial phase of neurodegeneration involves toxic proteins targeting specific brain networks, and that these networks have certain characteristics that make them tractable to certain proteinopathies (possible reasons for this are discussed in the opening chapter). Following this initial insult abnormal proteins may then either impair normal cellular process such as axonal transport, leading to local axonal degeneration, and then either spread to, and ultimately damage, other brain regions via direct (white matter tracts) or indirect (i.e. loss of input from other functional networks) connections (Raj et al., 2012; Warren et al., 2012). This concept of abnormal proteins spreading between structures and regions in neurodegeneration has long been understood, perhaps best exemplified through the studies of tau staging in AD, which follows a fairly set pattern of anatomical spread (Braak and Braak, 1996). Recently pathological tau has been shown to be highly transmissible between brain regions, with evidence to suggest tau has a templating effect (i.e. one abnormal isoform of tau can induce changes in

healthy tau) and the ability to spread along axons and cross synapses (Goedert et al., 2014; Liu et al., 2012). Yet despite this acquired pathogenicity of tau in certain tauopathies, such as AD or *MAPT* mutations, tau propagation seems to follow a fairly ordered anatomical pattern (see Figure 1.2), rather than say uniformly diffusing throughout the brain. It may be that physical barriers and compartments within the brain constrict the spread of disease; or it may be that spread is, at least initially, confined to particular brain networks. The role of networks in neurodegeneration is underpinned by the fact that patients with bvFTD who have significant frontal atrophy, have normal activations within their default mode network, which involves prefrontal cortex (Zhou et al., 2010); whilst patients with AD, who have a significant burden of amyloid and tau pathology within their frontal lobes (Klunk et al., 2004) overlapping areas of the salience network, show normal or increased activations in this region (Agosta et al., 2012). This suggests that a mechanism beyond either focal grey matter atrophy or the presence or absence of a particular protein is required to facilitate neurodegeneration, both clinically and histopathological. The current studies provide some support for this given that syndrome specific signatures of white matter pathology, which signal structural network degeneration between functional brain regions, were identified. Over time syndrome specific trajectories of white matter pathology, linking dysfunctional brain regions to relatively more functional brain regions also emerged. Providing evidence that certain clinical syndromes show specific trajectories of white matter pathology, rather than arbitrarily disseminating throughout the brain, perhaps owing to specific tracts linking functionally connected brain regions (Warren et al., 2012).

As potential new disease modifying treatments are a real possibility over the next decade the development of robust outcome measures will be of high importance. For patients the most important measure will be halting the degenerative process or indeed an improvement in symptoms; however from previous experience with disease modifying treatments, such as Bapinizumab in AD (Salloway et al., 2014), we know that neuropsychological and clinical measures may not actually improve; whilst it is still possible that a particular treatment has a disease modifying effect, at least at a pathological level, and it is therefore important to have other biomarkers available to capture these changes, as this data may be important in further drug discovery. Traditionally brain atrophy measures have a strong role to play in the clinical diagnosis of many neurodegenerative conditions and this is exemplified by their inclusion in many of the international diagnostic criteria used. In addition whole brain imaging has been used as an outcome measure for a number of neurological conditions, in particular in Alzheimer's disease, firstly as a safety endpoint, with the ability to detect treatment related problems such as amyloid related imaging abnormalities related to monocloncal antiobodies, but also as secondary endpoints to determine clinical efficacy of a particular treatment (Cash et al., 2014). However based on larger population studies structural imaging still requires 100-200 subjects per treatment arm to detect large changes (approximately 25% reduction) in brain atrophy, providing challenges in terms of recruitment and cost (Weiner et al., 2012). Furthermore whilst the FDA are open to using surrogate-endpoints such as imaging to accelerate treatments in neurodegenerative disorders, there remains an ongoing lack of robust data to confirm a strong correlation between imaging and clinically meaningful endpoints, and as no current clinical trial is using an imaging biomarker as a primary outcome measure. With regards to bvFTD and

PPA studies reviewing lobar and whole brain atrophy, cortical thickness and voxel-based morphometry have been discussed in chapter 4 and 6, and it is likely that rates of whole brain atropy, as well as more specific measures of regional atrophy will continue to have an important role as outcome measures, and may complement novel imaging metrics such as DTI. The data from the current study identifies DTI as a useful metric cross-sectionally and longitudinally, offering levels of sensitivity and specificity comparable with other accepted biomarkers in other neurodegenerative conditions (Shaw et al., 2007). This is of importance as it has been difficult to identify robust biomarkers in FTLD previously, most likely owing to the degree of heterogeneity across syndromes. Of course the degree of sensitivity and specificity depends on which DTI metric is measured as well as the region-of-interest used. It is likely the use of DTI can be further refined by better alignment of the molecular and clinical syndrome through the use of multi-modal data including structural imaging, novel neuropsychological paradigms and wet biomarkers including CSF and blood; indeed it is noteworthy that large differences in sample sizes between bvFTD and PPA were observed, possibly due to the greater pathological heterogeneity of bvFTD, emphasising the need for better phenotyping of syndromes.

7.3 Limitations and future directions

Data from the studies contained within this thesis offer new insights into the neurobiology of bvFTD and PPA, however there are a number of limitations, which will need to be addressed in future studies. The clinical cohorts used in these studies present a number of limitations. Firstly this study required motivated participants and carers and is unlikely to have sampled the full range of patients with FTLD syndromes, as such a

degree of assertainment bias is likely to have occurred. Equally patients within the severe spectrum could not be sampled owing to inability to consent and perform even basic elements of the assessment. Indeed several subjects included had elements of their imaging excluded due to excessive motion artefact, again meaning that those with more behavioural phenotypes are perhaps under represented within the study population. Whilst the current study hypothesises that the signatures of white matter pathology may relate to specific underlying molecular pathologies, there is a paucity of confirmed histopathological data within the current disease cohort. Larger studies encompassing the broad range of genetic and pathological subtypes will be required to confirm these putative molecularly defined white matter profiles of pathology. In particular the lack of patients with *PGRN* mutations is noteworthy, as this is one of the three major genes associated with FTLD pathology. More broadly there is a poor understanding of the relationships between the cellular histopathology, including the presumed underlying axonal degeneration and demyelination and the changes observed *in vivo* imaged using DTI. Whilst the current study posits that certain changes may reflect axonal degeneration or demyelination we do not as yet have precise enough data to confirm these assumptions. This will be a difficult challenge given that post-mortem brains are likely to take on different characteristics to those imaged in living subjects however an important study in the longer-term will be one involving pre-mortem and post-mortem imaging comparisons in the same individuals, comparing changes seen in vivo with higher resolution post-mortem imaging and then further comparing these changes with cellular histopathology using stereotactic approaches to maximise co-localisation of imaging regions with anatomical dissection. Additional techniques such as combining imaging with post-mortem tract imaging techniques such as autoradiography may also improve

the improve anatoimical robustness of current findings and may allow for better mapping of imaging to histopathology.

A further limitation of this study relates to the imaging methods used. Whilst the current study attempted to capture whole brain changes, as well as assessing individual ROIs, it is likely that these studies do not capture the entirety of white matter pathology. The current study focused on providing greater anatomical specificity by choosing certain ROIs to study, in particular long-range association tracts and commissural fibres. It is plausible, however that shorter range, intra-nodal, white matter tracts play a role in disease pathology, perhaps playing an early role in disruption of local networks, an event which may precede failure of long-range association fibres. Improvements in imaging acquisition and analysis, such as the recently proposed neurite orientation dispersion and density imaging (NODDI) (Zhang et al., 2012), may yield improved data and allow us to better resolve juxta-cortical white matter tracts. Other technical limitations of DTI also exist, including the issue of crossing or kissing fibres. This poses a particular problem in assessing tracts that lie in close proximity to one another, such as the anterior sections of the inferior longitudinal fasciculus and uncinate fasciculus. Techniques such as tractography and directionally dependent measurement may improve the reliability of assessments in these regions (Jbabdi et al., 2010).

A further major question posed by this current study is whether white matter or grey matter pathology occurs first, or indeed simultaneously. Whilst the current data suggests that DTI can detect more widespread white matter tract pathology, different methodologies were used to assess white and grey matter changes, so direct

comparisons are difficult to make, despite the current study using similar statistical models to minimise methodological bias. Direct comparisons between measures that reflect a simple scaler within a grey matter voxel, as in VBM, is not directly comparible to DTI metrics which represent composites of highly dimensional data. Multi-model imaging studies that can simultaneously assess white and grey matter structures will increase the robustness of these comparisons. Beyond offering greater spatial resolution, NODDI is a multi-shell imaging technique offering a unified model for white and grey matter, making it suitable for these combined assessments, and has already been applied to longitudinal imaging (Eaton-Rosen et al., 2015).

A further limitation relates to the use of models that are based on the healthy brain. The diffusion tensor model is relatively simplistic and makes a number of assumptions that may not be accurate in the diseased brain. Given issues such as highly non-normally distributed data (reflected by high SD values in some of the previous experiments), perhaps not surprising in syndromes as heterogenous as FTLD, imaging methods which better take account of non-Gaussian distributions may be better suited to studying diseased brains. One emerging imaging method is diffusion kurtosis imaging (DKI) (Jensen et al., 2005), which aims to characterise the degree of diffusion that deviates from a normal distribution. Additionaly DKI seems to provide better a better assessment of what is occurring in white matter, and is less affected by contamination from grey matter and CSF containing voxels. By combining data acquired from DTI and DKI a better model of diffusion in complex tissue structures may be acquired. Limited data is available but one encouraging study in an APP mouse model of Alzheimer's disease has shown

that reductions in DKI occur in areas of high amyloid deposition in the absence of DTI changes (Vanhoutte et al., 2013).

Whilst lower sample size estimates were obtained compared to volumetric imaging or neuropsychology numbers overall numbers for clinical trials remain quite high creating practical implications for any disease modifying trials. Approachs to reduce sample sizes will be required through improved phenotyping of syndromes by applying multimodal clinical and imaging data. Importantly in order for DTI to be a potentially useful biomarker with a possible role as a surrogate outcome measure, it must be able to capture clinically relevant changes, which allow it to accurately predict clinical outcomes. For example if a 20% reduction in the rate of change of FA in a white matter tract was shown to result in a decline or stabilisation in a measure reflecting cognitive change, whilst requiring fewer subjects to achieve statistical significance, then this may be an appropriate surrogate end point for a clinical trial. This study does not correlate clinical measures with changes in white matter and this is clearly an important issue going forward. One reason this is lacking from the current study relates to the fact that robust clinical outcome measures are relatively few in FTLD. Clincal heterogeneity as well as highly variable measures such as disease duration have created difficulty in establishing reliable clinically outcome measures. Recently measures such as the Frontotemporal dementia rating scale have been introduced to provide better accuaracy regarding disease stage (Mioshi et al., 2010). However in the current study correlations of these disease stages with white matter pathology is lacking, and this is a clear priority, particular with the need to verify if DTI may be a suitable biomarker. The flexibility of techniques such as TBSS analysis also allow us to directly correlate clinical measures with

white matter on a voxel-wise basis. This allows us to test interactions between cognition and white matter and may in turn provide for better development of clinical measures which track the progression of FTLD, although of course there is a need to avoid circularity with such techniques. Whilst the role of grey matter and lobar atrophy has not been discussed at length in this study it is important to recognise these imaging techniques along with other techniques such as fMRI and radioligands could be used in conjunction with DTI to provide more optimal sensitivity and specificity values, thereby further reducing sample sizes for clinical trials. For example resting-state fMRI could be used to identify areas of reduced functional activity and these co-ordinates could then be used to seed a tractography model to allow a better understanding of the inter-relationship between functional and structural network degeneration. A possible problem with DTI is that is may be *too* sensitive, and therefore in presymptomatic clinical trials it may result in over inclusion of subjects, perhaps exposing them to hazardous compounds. However if measures of whole brain volume or cortical thickness were also included this may enrich the presymptomatic cohort with those who are at close proximity to disease onset.

This in turn leads to the next future challenge which is to use multiple modes of data and multivariate statistics to provide better sensitivity and specificity. A significant limitation of this study was the use of rather basic statistical analysis, for example the use of linear regression models with basic nussaince co-variates. Whilst regions of interests were choosen based on strong hypotheses, there is the potential of type II errors from sampling a multidude of regions without appropriate levels of statistical correction. And whilst much of the data presented here is exploratory, this is an important requirement

for future studies. One reason for this approach was that clear guidance on the most appropriate statistical models for large volume datasets, such as those produced from DTI analysis are lacking, leading to a variety of statistical approaches (Jones et al., 2013). Validation and agreement of common statistical approaches (and indeed other methodologies) across research centres is a clear goal for neuroimaging community. Beyond the need for the introduction in common standards there is also the need to evolve statistical techniques that can better take account of the complexity of changes occurring within cells, and more broadly within white and grey matter. With the evolution of increasingly sophisticated computing power large amounts of data can be analysed and compared allowing for complex multivariate analysis. To improve disease detection and syndromic classification pattern recognition, combining multiple modes of data, may be of particular value in syndromes like FTD with its diverse range of pathological and clinical subtypes. Use of classification algorithims such as support vector machines holds much promise, and its potential has already been highlighted in other neurodegenerative conditions (Orrù et al., 2012) As mentioned in the introduction understanding network dynamics in neurodegenerative conditions is also an increasingly recognised research priority. The increasing use of methods such as graph theory allow us to conseptualise these network interactions in a simple manner. A benefit is that multiple metrics can be used as inputs to the graph, combining DTI, volumetric MRI, fMRI and even data from cell cultures such as electrode spike timing recordings. These data can then be used to create a map of there inter-relations, using an adjacency matrix, and from this construct a brain graph from which information on the strength of brain connectivity can be derived. Combining multiple metrics within one statisitical model will

provide for greater multidimensionality of data and may provide a better reflection of the complex changes that are occurring within the white matter microstructure.

Further determination of specific molecular pathologies in vivo may become possible with the emergence of radio-ligands with affinity for specific proteins (Maruyama et al., 2013). Furthermore as we gather increasing information on how genetics influence brain network activity it will become increasingly important to incorporate genetic information within multi-model analysis pipelines (Vergara et al., 2014). New emerging imaging technologies utilising optogenetics and nanoparticles may also provide opportunities to study molecular changes owing to alterations in gene expression (Mehta et al., 2014), providing a comprehensive way of linking together genotype-phenotype. Whilst new methods emerge to establish underlying molecular pathologies it will also be important to continue to establish metrics to allow for assessment of disease proximity, particular when there may be a long latency between pathological protein deposition and clinical syndrome.

In conclusion shorter-term aims should be:

1. To verifty that changes seen in this study map onto clinical measures such as the Frontotemporal Dementia rating scale and correlate other cognitive measures with white matter pathology.
2. Confirm the profiles of white matter pathology by using other DTI methods such as tractography, using methods which better account for crossing fibres.
3. Identify the profiles of white matter pathology in *GRN* mutations

In the medium term aims should include:

1. Improving statistical models, using techniques such as *support vector machines* and graph theory, with inclusion of other modes of data (e.g. whole brain atrophy, cortical thickness etc.), in a multivariate analysis pipeline.
2. Expand studies to include presymptomatic mutation carriers.
3. Develop new acquisition parameters, such as NODDI and DKI, and acquire imaging on clinically and genetically defined cohorts, comparing these findings with existing DTI findings.

In the long-term

1. Create large data sets across multiple sites to confirm initial findings and assess the stability of diffusion based imaging as a disease biomarker.
2. Correlation of *in vivo* imaging with histopathology to improve our understanding of the pathological changes measured by diffusion imaging (both DTI and newer techniques such as DKI).
3. Establish if diffusion imaging has a role as an outcome measure in clinical trials and use along with more conventional imaging measures as therapeutic interventions emerge.

This thesis provides a comprehensive account of white matter tract changes in bvFTD and PPA utilising sophisticated imaging techniques to ensure robust data are presented. It is hoped this data will support the development of DTI as useful imaging modality, both at a clinical and systems neuroscience level and will be of use to other researchers as well as acting as an impetus to continue to refine our understanding of the role of white matter in FTLD and more broadly the concept of network-led degeneration.

References

Acosta-Cabronero, J., Alley, S., Williams, G.B., Pengas, G., Nestor, P.J., 2012. Diffusion Tensor Metrics as Biomarkers in Alzheimer's Disease. PLoS ONE 7, e49072. doi:10.1371/journal.pone.0049072

Acosta-Cabronero, J., Patterson, K., Fryer, T.D., Hodges, J.R., Pengas, G., Williams, G.B., Nestor, P.J., 2011. Atrophy, hypometabolism and white matter abnormalities in semantic dementia tell a coherent story. Brain 134, 2025–2035. doi:10.1093/brain/awr119

Acosta-Cabronero, J., Williams, G.B., Pengas, G., Nestor, P.J., 2010. Absolute diffusivities define the landscape of white matter degeneration in Alzheimer's disease. Brain 133, 529–539. doi:10.1093/brain/awp257

Agosta, F., Henry, R.G., Migliaccio, R., Neuhaus, J., Miller, B.L., Dronkers, N.F., Brambati, S.M., Filippi, M., Ogar, J.M., Wilson, S.M., Gorno-Tempini, M.L., 2010. Language networks in semantic dementia. Brain 133, 286–299. doi:10.1093/brain/awp233

Agosta, F., Pievani, M., Geroldi, C., Copetti, M., Frisoni, G.B., Filippi, M., 2012. Resting state fMRI in Alzheimer's disease: beyond the default mode network. Neurobiology of Aging 33, 1564–1578. doi:10.1016/j.neurobiolaging.2011.06.007

Agosta, F., Pievani, M., Sala, S., Geroldi, C., Galluzzi, S., Frisoni, G.B., Filippi, M., 2011. White matter damage in Alzheimer disease and its relationship to gray matter atrophy. Radiology 258, 853–863. doi:10.1148/radiol.10101284

Agosta, F., Scola, E., Canu, E., Marcone, A., Magnani, G., Sarro, L., Copetti, M., Caso, F., Cerami, C., Comi, G., Cappa, S.F., Falini, A., Filippi, M., 2012. White Matter Damage

in Frontotemporal Lobar Degeneration Spectrum. Cereb. Cortex 22, 2705–14. doi:10.1093/cercor/bhr288

Agustus, J.L., Mahoney, C.J., Downey, L.E., Omar, R., Cohen, M., White, M.J., Scott, S.K., Mancini, L., Warren, J.D., 2015. Functional MRI of music emotion processing in frontotemporal dementia: fMRI of music emotion in FTD. Annals of the New York Academy of Sciences 1337, 232–240. doi:10.1111/nyas.12620

Ahmed, R.M., Paterson, R.W., Warren, J.D., Zetterberg, H., O'Brien, J.T., Fox, N.C., Halliday, G.M., Schott, J.M., 2014. Biomarkers in dementia: clinical utility and new directions. Journal of Neurology, Neurosurgery & Psychiatry 85, 1426–1434. doi:10.1136/jnnp-2014-307662

Ahmed, Z., Bigio, E.H., Budka, H., Dickson, D.W., Ferrer, I., Ghetti, B., Giaccone, G., Hatanpaa, K.J., Holton, J.L., Josephs, K.A., Powers, J., Spina, S., Takahashi, H., White, C.L., Revesz, T., Kovacs, G.G., 2013. Globular glial tauopathies (GGT): consensus recommendations. Acta Neuropathologica 126, 537–544. doi:10.1007/s00401-013-1171-0

Ahmed, Z., Doherty, K.M., Silveira-Moriyama, L., Bandopadhyay, R., Lashley, T., Mamais, A., Hondhamuni, G., Wray, S., Newcombe, J., O'Sullivan, S.S., Wroe, S., Silva, R., Holton, J.L., Lees, A.J., Revesz, T., 2011. Globular glial tauopathies (GGT) presenting with motor neuron disease or frontotemporal dementia: an emerging group of 4-repeat tauopathies. Acta Neuropathologica 122, 415–428. doi:10.1007/s00401-011-0857-4

Alami, N.H., Smith, R.B., Carrasco, M.A., Williams, L.A., Winborn, C.S., Han, S.S.W., Kiskinis, E., Winborn, B., Freibaum, B.D., Kanagaraj, A., Clare, A.J., Badders, N.M., Bilican, B., Chaum, E., Chandran, S., Shaw, C.E., Eggan, K.C., Maniatis, T., Taylor,

J.P., 2014. Axonal Transport of TDP-43 mRNA Granules Is Impaired by ALS-Causing Mutations. Neuron 81, 536–543. doi:10.1016/j.neuron.2013.12.018

Al-Sarraj, S., King, A., Troakes, C., Smith, B., Maekawa, S., Bodi, I., Rogelj, B., Al-Chalabi, A., Hortobágyi, T., Shaw, C.E., 2011. p62 positive, TDP-43 negative, neuronal cytoplasmic and intranuclear inclusions in the cerebellum and hippocampus define the pathology of C9orf72-linked FTLD and MND/ALS. Acta Neuropathologica. doi:10.1007/s00401-011-0911-2

Andreasen, N.C., O'Leary, D.S., Cizadlo, T., Arndt, S., Rezai, K., Ponto, L.L., Watkins, G.L., Hichwa, R.D., 1996. Schizophrenia and cognitive dysmetria: a positron-emission tomography study of dysfunctional prefrontal-thalamic-cerebellar circuitry. Proc. Natl. Acad. Sci. U.S.A. 93, 9985–9990.

Armstrong, R.A., Cairns, N.J., 2013. Spatial patterns of the tau pathology in progressive supranuclear palsy. Neurol. Sci. 34, 337–344. doi:10.1007/s10072-012-1006-0

Ashburner, J., 2007. A fast diffeomorphic image registration algorithm. Neuroimage 38, 95–113. doi:10.1016/j.neuroimage.2007.07.007

Awad, M., Warren, J.E., Scott, S.K., Turkheimer, F.E., Wise, R.J.S., 2007. A common system for the comprehension and production of narrative speech. J. Neurosci 27, 11455–11464. doi:10.1523/JNEUROSCI.5257-06.2007

Bachevalier, J., Parkinson, J.K., Mishkin, M., 1985. Visual recognition in monkeys: effects of separate vs. combined transection of fornix and amygdalofugal pathways. Experimental Brain Research 57. doi:10.1007/BF00237842

Baker, M., Mackenzie, I.R., Pickering-Brown, S.M., Gass, J., Rademakers, R., Lindholm, C., Snowden, J., Adamson, J., Sadovnick, A.D., Rollinson, S., Cannon, A., Dwosh, E., Neary, D., Melquist, S., Richardson, A., Dickson, D., Berger, Z., Eriksen, J.,

Robinson, T., Zehr, C., Dickey, C.A., Crook, R., McGowan, E., Mann, D., Boeve, B., Feldman, H., Hutton, M., 2006. Mutations in progranulin cause tau-negative frontotemporal dementia linked to chromosome 17. Nature 442, 916–919. doi:10.1038/nature05016

Barbas, H., 2000. Connections underlying the synthesis of cognition, memory, and emotion in primate prefrontal cortices. Brain Res. Bull 52, 319–330.

Barkhof, F., Haller, S., Rombouts, S.A.R.B., 2014. Resting-State Functional MR Imaging: A New Window to the Brain. Radiology 272, 29–49. doi:10.1148/radiol.14132388

Basser, P.J., Mattiello, J., LeBihan, D., 1994. MR diffusion tensor spectroscopy and imaging. Biophysical Journal 66, 259–267. doi:10.1016/S0006-3495(94)80775-1

Beck, J., King, A., Scahill, R., Warren, J.D., Fox, N.C., Rossor, M.N., Collinge, J., Mead, S., 2008. A distinct clinical, neuropsychological and radiological phenotype is associated with progranulin gene mutations in a large UK series. Brain 131, 706–720. doi:10.1093/brain/awm320

Beck, J., Pittman, A., Adamson, G., Campbell, T., Kenny, J., Houlden, H., Rohrer, J.D., de Silva, R., Shoai, M., Uphill, J., Poulter, M., Hardy, J., Mummery, C.J., Warren, J.D., Schott, J.M., Fox, N.C., Rossor, M.N., Collinge, J., Mead, S., 2014. Validation of next-generation sequencing technologies in genetic diagnosis of dementia. Neurobiol. Aging 35, 261–265. doi:10.1016/j.neurobiolaging.2013.07.017

Beirowski, B., Morreale, G., Conforti, L., Mazzola, F., Di Stefano, M., Wilbrey, A., Babetto, E., Janeckova, L., Magni, G., Coleman, M.P., 2010. WldS can delay Wallerian degeneration in mice when interaction with valosin-containing protein is weakened. Neuroscience 166, 201–211. doi:10.1016/j.neuroscience.2009.12.024

Benson, D.F., Sheremata, W.A., Bouchard, R., Segarra, J.M., Price, D., Geschwind, N., 1973. Conduction aphasia: a clinicopathological study. Archives of Neurology 28, 339–346.

Binney, R.J., Embleton, K.V., Jefferies, E., Parker, G.J.M., Lambon Ralph, M.A., 2010. The Ventral and Inferolateral Aspects of the Anterior Temporal Lobe Are Crucial in Semantic Memory: Evidence from a Novel Direct Comparison of Distortion-Corrected fMRI, rTMS, and Semantic Dementia. Cerebral Cortex 20, 2728–2738. doi:10.1093/cercor/bhq019

Biomarkers and surrogate endpoints: Preferred definitions and conceptual framework, 2001. . Clinical Pharmacology & Therapeutics 69, 89–95. doi:10.1067/mcp.2001.113989

Bock, D.D., Lee, W.-C.A., Kerlin, A.M., Andermann, M.L., Hood, G., Wetzel, A.W., Yurgenson, S., Soucy, E.R., Kim, H.S., Reid, R.C., 2011. Network anatomy and in vivo physiology of visual cortical neurons. Nature 471, 177–182. doi:10.1038/nature09802

Bora, E., Harrison, B.J., Fornito, A., Cocchi, L., Pujol, J., Fontenelle, L.F., Velakoulis, D., Pantelis, C., Yücel, M., 2011. White matter microstructure in patients with obsessive-compulsive disorder. J Psychiatry Neurosci 36, 42–46. doi:10.1503/jpn.100082

Borroni, B., Alberici, A., Premi, E., Archetti, S., Garibotto, V., Agosti, C., Gasparotti, R., Di Luca, M., Perani, D., Padovani, A., 2008. Brain magnetic resonance imaging structural changes in a pedigree of asymptomatic progranulin mutation carriers. Rejuvenation Res 11, 585–595. doi:10.1089/rej.2007.0623

Borroni, B., Brambati, S.M., Agosti, C., Gipponi, S., Bellelli, G., Gasparotti, R., Garibotto, V., Di Luca, M., Scifo, P., Perani, D., Padovani, A., 2007. Evidence of white matter changes on diffusion tensor imaging in frontotemporal dementia. Arch. Neurol. 64, 246–251. doi:10.1001/archneur.64.2.246

Boxer, A.L., Mackenzie, I.R., Boeve, B.F., Baker, M., Seeley, W.W., Crook, R., Feldman, H., Hsiung, G.-Y.R., Rutherford, N., Laluz, V., Whitwell, J., Foti, D., McDade, E., Molano, J., Karydas, A., Wojtas, A., Goldman, J., Mirsky, J., Sengdy, P., Dearmond, S., Miller, B.L., Rademakers, R., 2011. Clinical, neuroimaging and neuropathological features of a new chromosome 9p-linked FTD-ALS family. J. Neurol. Neurosurg. Psychiatr. 82, 196–203. doi:10.1136/jnnp.2009.204081

Braak, H., Braak, E., 1996. Evolution of the neuropathology of Alzheimer's disease. Acta Neurol. Scand., Suppl.c 165, 3–12.

Brambati, S.M., Rankin, K.P., Narvid, J., Seeley, W.W., Dean, D., Rosen, H.J., Miller, B.L., Ashburner, J., Gorno-Tempini, M.L., 2009. Atrophy progression in semantic dementia with asymmetric temporal involvement: a tensor-based morphometry study. Neurobiol. Aging 30, 103–111. doi:10.1016/j.neurobiolaging.2007.05.014

Brandmeir, N.J., Geser, F., Kwong, L.K., Zimmerman, E., Qian, J., Lee, V.M.-Y., Trojanowski, J.Q., 2008. Severe subcortical TDP-43 pathology in sporadic frontotemporal lobar degeneration with motor neuron disease. Acta Neuropathol. 115, 123–131. doi:10.1007/s00401-007-0315-5

Brennan, F.H., Cowin, G.J., Kurniawan, N.D., Ruitenberg, M.J., 2013. Longitudinal assessment of white matter pathology in the injured mouse spinal cord through ultra-high field (16.4T) in vivo diffusion tensor imaging. NeuroImage 82, 574–585. doi:10.1016/j.neuroimage.2013.06.019

Brodtmann, A., Cowie, T., McLean, C., Darby, D., 2013. Phenocopy or variant: a longitudinal study of very slowly progressive frontotemporal dementia. BMJ Case Rep Published Online. doi:10.1136/bcr-2012-008077

Broe, M., Kril, J., Halliday, G.M., 2004. Astrocytic degeneration relates to the severity of disease in frontotemporal dementia. Brain 127, 2214–2220. doi:10.1093/brain/awh250

Buckner, R.L., Andrews-Hanna, J.R., Schacter, D.L., 2008. The brain's default network: anatomy, function, and relevance to disease. Ann. N. Y. Acad. Sci. 1124, 1–38. doi:10.1196/annals.1440.011

Cabeza, R., Nyberg, L., 2000. Imaging Cognition II: An Empirical Review of 275 PET and fMRI Studies. Journal of Cognitive Neuroscience 12, 1–47. doi:10.1162/08989290051137585

Cairns, N.J., Bigio, E.H., Mackenzie, I.R.A., Neumann, M., Lee, V.M.-Y., Hatanpaa, K.J., White, C.L., 3rd, Schneider, J.A., Grinberg, L.T., Halliday, G., Duyckaerts, C., Lowe, J.S., Holm, I.E., Tolnay, M., Okamoto, K., Yokoo, H., Murayama, S., Woulfe, J., Munoz, D.G., Dickson, D.W., Ince, P.G., Trojanowski, J.Q., Mann, D.M.A., Consortium for Frontotemporal Lobar Degeneration, 2007. Neuropathologic diagnostic and nosologic criteria for frontotemporal lobar degeneration: consensus of the Consortium for Frontotemporal Lobar Degeneration. Acta Neuropathol. 114, 5–22. doi:10.1007/s00401-007-0237-2

Caroppo, P., Le Ber, I., Camuzat, A., Clot, F., Naccache, L., Lamari, F., De Septenville, A., Bertrand, A., Belliard, S., Hannequin, D., Colliot, O., Brice, A., 2014. Extensive White Matter Involvement in Patients With Frontotemporal Lobar Degeneration: Think Progranulin. JAMA Neurology 71, 1562. doi:10.1001/jamaneurol.2014.1316

Carrington, S.J., Bailey, A.J., 2009. Are there theory of mind regions in the brain? A review of the neuroimaging literature. Hum Brain Mapp 30, 2313–2335. doi:10.1002/hbm.20671

Cash, D.M., Rohrer, J.D., Ryan, N.S., Ourselin, S., Fox, N.C., 2014. Imaging endpoints for clinical trials in Alzheimer's disease. Alzheimer's Research & Therapy 6. doi:10.1186/s13195-014-0087-9

Catani, M., 2007. From hodology to function. Brain 130, 602–605. doi:10.1093/brain/awm008

Catani, M., ffytche, D.H., 2005. The rises and falls of disconnection syndromes. Brain 128, 2224–2239. doi:10.1093/brain/awh622

Cees De Groot, J., De Leeuw, F.-E., Oudkerk, M., Van Gijn, J., Hofman, A., Jolles, J., Breteler, M.M.B., 2000. Cerebral white matter lesions and cognitive function: The Rotterdam scan study. Annals of Neurology 47, 145–151. doi:10.1002/1531-8249(200002)47:2<145::AID-ANA3>3.0.CO;2-P

Chan, D., Anderson, V., Pijnenburg, Y., Whitwell, J., Barnes, J., Scahill, R., Stevens, J.M., Barkhof, F., Scheltens, P., Rossor, M.N., Fox, N.C., 2009. The clinical profile of right temporal lobe atrophy. Brain 132, 1287–1298. doi:10.1093/brain/awp037

Cheon, K.-A., Kim, Y.-S., Oh, S.-H., Park, S.-Y., Yoon, H.-W., Herrington, J., Nair, A., Koh, Y.-J., Jang, D.-P., Kim, Y.-B., Leventhal, B.L., Cho, Z.-H., Castellanos, F.X., Schultz, R.T., 2011. Involvement of the anterior thalamic radiation in boys with high functioning autism spectrum disorders: a Diffusion Tensor Imaging study. Brain Res. 1417, 77–86. doi:10.1016/j.brainres.2011.08.020

Chevalier-Larsen, E., Holzbaur, E.L.F., 2006. Axonal transport and neurodegenerative disease. Biochimica et Biophysica Acta (BBA) - Molecular Basis of Disease 1762, 1094–1108. doi:10.1016/j.bbadis.2006.04.002

Chhatwal, J.P., Schultz, A.P., Johnson, K., Benzinger, T.L.S., Jack, C., Ances, B.M., Sullivan, C.A., Salloway, S.P., Ringman, J.M., Koeppe, R.A., Marcus, D.S., Thompson, P., Saykin, A.J., Correia, S., Schofield, P.R., Rowe, C.C., Fox, N.C., Brickman, A.M., Mayeux, R., McDade, E., Bateman, R., Fagan, A.M., Goate, A.M., Xiong, C., Buckles, V.D., Morris, J.C., Sperling, R.A., 2013. Impaired default network functional connectivity in autosomal dominant Alzheimer disease. Neurology 81, 736–744. doi:10.1212/WNL.0b013e3182a1aafe

Ciccarelli, O., Catani, M., Johansen-Berg, H., Clark, C., Thompson, A., 2008. Diffusion-based tractography in neurological disorders: concepts, applications, and future developments. Lancet Neurol 7, 715–727. doi:10.1016/S1474-4422(08)70163-7

Clavaguera, F., Akatsu, H., Fraser, G., Crowther, R.A., Frank, S., Hench, J., Probst, A., Winkler, D.T., Reichwald, J., Staufenbiel, M., Ghetti, B., Goedert, M., Tolnay, M., 2013. Brain homogenates from human tauopathies induce tau inclusions in mouse brain. Proc. Natl. Acad. Sci. U.S.A. 110, 9535–9540. doi:10.1073/pnas.1301175110

Clement, A.M., 2003. Wild-Type Nonneuronal Cells Extend Survival of SOD1 Mutant Motor Neurons in ALS Mice. Science 302, 113–117. doi:10.1126/science.1086071

Cook, P., Bai, Y., Nedjati-Gilani, S., Seunarine, K., Hall, M., Parker, G., Alexander, D., 2006. Camino: Open-Source Diffusion-MRI Reconstruction and Processing. Presented at the 14th Scientific Meeting of the International Society for Magnetic Resonance in Medicine, Seattle, WA, USA, p. p2759.

Czarnecki, K., Duffy, J.R., Nehl, C.R., Cross, S.A., Molano, J.R., Jack, C.R., Shiung, M.M., Josephs, K.A., Boeve, B.F., 2008. Very early semantic dementia with progressive temporal lobe atrophy: an 8-year longitudinal study. Arch. Neurol. 65, 1659–1663. doi:10.1001/archneurol.2008.507

Davtian, M., Ulmer, J.L., Mueller, W.M., Gaggl, W., Mulane, M.P., Krouwer, H.G., 2008. The superior longitudinal fasciculus and speech arrest. J Comput Assist Tomogr 32, 410–414. doi:10.1097/RCT.0b013e318157c5ff

Dejesus-Hernandez, M., Mackenzie, I.R., Boeve, B.F., Boxer, A.L., Baker, M., Rutherford, N.J., Nicholson, A.M., Finch, N.A., Flynn, H., Adamson, J., Kouri, N., Wojtas, A., Sengdy, P., Hsiung, G.-Y.R., Karydas, A., Seeley, W.W., Josephs, K.A., Coppola, G., Geschwind, D.H., Wszolek, Z.K., Feldman, H., Knopman, D.S., Petersen, R.C., Miller, B.L., Dickson, D.W., Boylan, K.B., Graff-Radford, N.R., Rademakers, R., 2011. Expanded GGGGCC Hexanucleotide Repeat in Noncoding Region of C9ORF72 Causes Chromosome 9p-Linked FTD and ALS. Neuron. doi:10.1016/j.neuron.2011.09.011

Delis, D., Kaplan, E., Kramer, J., 2001. Delis-Kaplan executive function system, in: Psychological Corporation. Psychological Corporation, San Antonio, Texas.

Den Dekker, A.J., Sijbers, J., 2014. Data distributions in magnetic resonance images: A review. Physica Medica 30, 725–741. doi:10.1016/j.ejmp.2014.05.002

Devenney, E., Hornberger, M., Irish, M., Mioshi, E., Burrell, J., Tan, R., Kiernan, M.C., Hodges, J.R., 2014. Frontotemporal Dementia Associated With the *C9ORF72* Mutation: A Unique Clinical Profile. JAMA Neurology 71, 331. doi:10.1001/jamaneurol.2013.6002

Dopper, E.G.P., Rombouts, S.A.R.B., Jiskoot, L.C., Heijer, T. den, de Graaf, J.R.A., Koning, I. de, Hammerschlag, A.R., Seelaar, H., Seeley, W.W., Veer, I.M., van Buchem, M.A., Rizzu, P., van Swieten, J.C., 2013. Structural and functional brain connectivity in presymptomatic familial frontotemporal dementia. Neurology 80, 814–823. doi:10.1212/WNL.0b013e31828407bc

Douaud, G., Jbabdi, S., Behrens, T.E.J., Menke, R.A., Gass, A., Monsch, A.U., Rao, A., Whitcher, B., Kindlmann, G., Matthews, P.M., Smith, S., 2011. DTI measures in crossing-fibre areas: Increased diffusion anisotropy reveals early white matter alteration in MCI and mild Alzheimer's disease. NeuroImage 55, 880–890. doi:10.1016/j.neuroimage.2010.12.008

Downey, L.E., Mahoney, C.J., Rossor, M.N., Crutch, S.J., Warren, J.D., 2012. Impaired self-other differentiation in frontotemporal dementia due to the C9ORF72 expansion. Alzheimers Res Ther 4, 42. doi:10.1186/alzrt145

Drzezga, A., Becker, J.A., Van Dijk, K.R.A., Sreenivasan, A., Talukdar, T., Sullivan, C., Schultz, A.P., Sepulcre, J., Putcha, D., Greve, D., Johnson, K.A., Sperling, R.A., 2011. Neuronal dysfunction and disconnection of cortical hubs in non-demented subjects with elevated amyloid burden. Brain 134, 1635–1646. doi:10.1093/brain/awr066

Du, A.-T., Schuff, N., Chao, L.L., Kornak, J., Ezekiel, F., Jagust, W.J., Kramer, J.H., Reed, B.R., Miller, B.L., Norman, D., Chui, H.C., Weiner, M.W., 2005. White matter lesions are associated with cortical atrophy more than entorhinal and hippocampal atrophy. Neurobiology of Aging 26, 553–559. doi:10.1016/j.neurobiolaging.2004.05.002

Dubois, B., Feldman, H.H., Jacova, C., Dekosky, S.T., Barberger-Gateau, P., Cummings, J., Delacourte, A., Galasko, D., Gauthier, S., Jicha, G., Meguro, K., O'brien, J., Pasquier, F., Robert, P., Rossor, M., Salloway, S., Stern, Y., Visser, P.J., Scheltens, P., 2007. Research criteria for the diagnosis of Alzheimer's disease: revising the NINCDS-ADRDA criteria. Lancet Neurol 6, 734–746. doi:10.1016/S1474-4422(07)70178-3

Eaton-Rosen, Z., Melbourne, A., Orasanu, E., Cardoso, M.J., Modat, M., Bainbridge, A., Kendall, G.S., Robertson, N.J., Marlow, N., Ourselin, S., 2015. Longitudinal measurement of the developing grey matter in preterm subjects using multi-modal MRI. NeuroImage. doi:10.1016/j.neuroimage.2015.02.010

Faria, A.V., Sebastian, R., Newhart, M., Mori, S., Hillis, A.E., 2014. Longitudinal Imaging and Deterioration in Word Comprehension in Primary Progressive Aphasia: Potential Clinical Significance. Aphasiology 28, 948–963. doi:10.1080/02687038.2014.911241

Fazekas, F., Chawluk, J., Alavi, A., Hurtig, H., Zimmerman, R., 1987. MR signal abnormalities at 1.5 T in Alzheimer's dementia and normal aging. American Journal of Roentgenology 149, 351–356. doi:10.2214/ajr.149.2.351

Fellgiebel, A., Dellani, P.R., Greverus, D., Scheurich, A., Stoeter, P., Müller, M.J., 2006. Predicting conversion to dementia in mild cognitive impairment by volumetric and diffusivity measurements of the hippocampus. Psychiatry Res 146, 283–287. doi:10.1016/j.pscychresns.2006.01.006

Filippi, M., Agosta, F., Scola, E., Canu, E., Magnani, G., Marcone, A., Valsasina, P., Caso, F., Copetti, M., Comi, G., Cappa, S.F., Falini, A., 2013. Functional network connectivity

in the behavioral variant of frontotemporal dementia. Cortex 49, 2389–2401. doi:10.1016/j.cortex.2012.09.017

Fletcher, P.D., Warren, J.D., 2011. Semantic Dementia: a specific network-opathy. J Mol Neurosci. doi:10.1007/s12031-011-9586-3

Forman, M.S., Zhukareva, V., Bergeron, C., Chin, S.S.-M., Grossman, M., Clark, C., Lee, V.M.-Y., Trojanowski, J.Q., 2002. Signature Tau Neuropathology in Gray and White Matter of Corticobasal Degeneration. The American Journal of Pathology 160, 2045–2053. doi:10.1016/S0002-9440(10)61154-6

Fox, R.J., Cronin, T., Lin, J., Wang, X., Sakaie, K., Ontaneda, D., Mahmoud, S.Y., Lowe, M.J., Phillips, M.D., 2010. Measuring Myelin Repair and Axonal Loss with Diffusion Tensor Imaging. American Journal of Neuroradiology. doi:10.3174/ajnr.A2238

Freeborough, P.A., Fox, N.C., 1997. The boundary shift integral: an accurate and robust measure of cerebral volume changes from registered repeat MRI. IEEE Trans Med Imaging 16, 623–629. doi:10.1109/42.640753

Freeborough, P.A., Fox, N.C., Kitney, R.I., 1997. Interactive algorithms for the segmentation and quantitation of 3-D MRI brain scans. Comput Methods Programs Biomed 53, 15–25.

Freeman, S.H., Hyman, B.T., Sims, K.B., Hedley-Whyte, E.T., Vossough, A., Frosch, M.P., Schmahmann, J.D., 2009. Adult Onset Leukodystrophy with Neuroaxonal Spheroids: Clinical, Neuroimaging and Neuropathologic Observations. Brain Pathology 19, 39–47. doi:10.1111/j.1750-3639.2008.00163.x

Galantucci, S., Tartaglia, M.C., Wilson, S.M., Henry, M.L., Filippi, M., Agosta, F., Dronkers, N.F., Henry, R.G., Ogar, J.M., Miller, B.L., Gorno-Tempini, M.L., 2011. White matter

damage in primary progressive aphasias: a diffusion tensor tractography study. Brain. doi:10.1093/brain/awr099

Gans, A., 1922. Pick Betrachtungen ü ber Art und Aus- breitung des krankhaften Prozesses in einem Fall von Pickscher Atrophie des Stirnhirns. Ztschr f d ges Neurol U Psychiatr. 80, 10–28.

Garrido, L., Furl, N., Draganski, B., Weiskopf, N., Stevens, J., Tan, G.C.-Y., Driver, J., Dolan, R.J., Duchaine, B., 2009. Voxel-based morphometry reveals reduced grey matter volume in the temporal cortex of developmental prosopagnosics. Brain 132, 3443–3455. doi:10.1093/brain/awp271

Geranmayeh, F., Wise, R.J.S., Mehta, A., Leech, R., 2014. Overlapping networks engaged during spoken language production and its cognitive control. J. Neurosci. 34, 8728–8740. doi:10.1523/JNEUROSCI.0428-14.2014

Geschwind, N., 1965. DISCONNEXION SYNDROMES IN ANIMALS AND MAN. Brain 88, 237–237. doi:10.1093/brain/88.2.237

Ginsberg, S.D., Martin, L.J., 2002. Axonal Transection in Adult Rat Brain Induces Transsynaptic Apoptosis and Persistent Atrophy of Target Neurons. Journal of Neurotrauma 19, 99–109. doi:10.1089/089771502753460277

Goedert, M., Falcon, B., Clavaguera, F., Tolnay, M., 2014. Prion-like Mechanisms in the Pathogenesis of Tauopathies and Synucleinopathies. Current Neurology and Neuroscience Reports 14. doi:10.1007/s11910-014-0495-z

Goll, J.C., Ridgway, G.R., Crutch, S.J., Theunissen, F.E., Warren, J.D., 2012. Nonverbal sound processing in semantic dementia: A functional MRI study. NeuroImage 61, 170–180. doi:10.1016/j.neuroimage.2012.02.045

Gordon, E., Rohrer, J.D., Kim, L.G., Omar, R., Rossor, M.N., Fox, N.C., Warren, J.D., 2010. Measuring disease progression in frontotemporal lobar degeneration: a clinical and MRI study. Neurology 74, 666–673. doi:10.1212/WNL.0b013e3181d1a879

Gorno-Tempini, M.L., Dronkers, N.F., Rankin, K.P., Ogar, J.M., Phengrasamy, L., Rosen, H.J., Johnson, J.K., Weiner, M.W., Miller, B.L., 2004. Cognition and anatomy in three variants of primary progressive aphasia. Ann. Neurol 55, 335–346. doi:10.1002/ana.10825

Gorno-Tempini, M.L., Hillis, A.E., Weintraub, S., Kertesz, A., Mendez, M., Cappa, S.F., Ogar, J.M., Rohrer, J.D., Black, S., Boeve, B.F., Manes, F., Dronkers, N.F., Vandenberghe, R., Rascovsky, K., Patterson, K., Miller, B.L., Knopman, D.S., Hodges, J.R., Mesulam, M.M., Grossman, M., 2011. Classification of primary progressive aphasia and its variants. Neurology 76, 1006–1014. doi:10.1212/WNL.0b013e31821103e6

Greicius, M.D., Srivastava, G., Reiss, A.L., Menon, V., 2004. Default-mode network activity distinguishes Alzheimer's disease from healthy aging: evidence from functional MRI. Proc. Natl. Acad. Sci. U.S.A 101, 4637–4642. doi:10.1073/pnas.0308627101

Grossman, M., 2010. Primary progressive aphasia: clinicopathological correlations. Nat Rev Neurol 6, 88–97. doi:10.1038/nrneurol.2009.216

Grossman, M., Libon, D.J., Forman, M.S., Massimo, L., Wood, E., Moore, P., Anderson, C., Farmer, J., Chatterjee, A., Clark, C.M., Coslett, H.B., Hurtig, H.I., Lee, V.M.-Y., Trojanowski, J.Q., 2007. Distinct antemortem profiles in patients with pathologically defined frontotemporal dementia. Arch. Neurol. 64, 1601–1609. doi:10.1001/archneur.64.11.1601

Hailstone, J.C., Crutch, S.J., Vestergaard, M.D., Patterson, R.D., Warren, J.D., 2010. Progressive associative phonagnosia: a neuropsychological analysis. Neuropsychologia 48, 1104–1114. doi:10.1016/j.neuropsychologia.2009.12.011

Hampel, H., Frank, R., Broich, K., Teipel, S.J., Katz, R.G., Hardy, J., Herholz, K., Bokde, A.L.W., Jessen, F., Hoessler, Y.C., Sanhai, W.R., Zetterberg, H., Woodcock, J., Blennow, K., 2010. Biomarkers for Alzheimer's disease: academic, industry and regulatory perspectives. Nature Reviews Drug Discovery 9, 560–574. doi:10.1038/nrd3115

Han, Z., Ma, Y., Gong, G., Huang, R., Song, L., Bi, Y., 2014. White matter pathway supporting phonological encoding in speech production: a multi-modal imaging study of brain damage patients. Brain Struct Funct. doi:10.1007/s00429-014-0926-2

Hardy, J., Revesz, T., 2012. The Spread of Neurodegenerative Disease. New England Journal of Medicine 366, 2126–2128. doi:10.1056/NEJMcibr1202401

Harsan, L.A., Poulet, P., Guignard, B., Steibel, J., Parizel, N., de Sousa, P.L., Boehm, N., Grucker, D., Ghandour, M.S., 2006. Brain dysmyelination and recovery assessment by noninvasive in vivo diffusion tensor magnetic resonance imaging. J. Neurosci. Res. 83, 392–402. doi:10.1002/jnr.20742

Hartikainen, P., Räsänen, J., Julkunen, V., Niskanen, E., Hallikainen, M., Kivipelto, M., Vanninen, R., Remes, A.M., Soininen, H., 2012. Cortical thickness in frontotemporal dementia, mild cognitive impairment, and Alzheimer's disease. J. Alzheimers Dis. 30, 857–874. doi:10.3233/JAD-2012-112060

Heim, S., Pieperhoff, P., Grande, M., Kuijsten, W., Wellner, B., Sáez, L.E., Schulte, S., Südmeyer, M., Caspers, S., Minnerop, M., Binkofski, F., Huber, W., Amunts, K.,

2014. Longitudinal changes in brains of patients with fluent primary progressive aphasia. Brain Lang 131, 11–19. doi:10.1016/j.bandl.2013.05.012

Henley, S.M.D., Downey, L.E., Nicholas, J.M., Kinnunen, K.M., Golden, H.L., Buckley, A., Mahoney, C.J., Crutch, S.J., 2014. Degradation of cognitive timing mechanisms in behavioural variant frontotemporal dementia. Neuropsychologia 65, 88–101. doi:10.1016/j.neuropsychologia.2014.10.009

Henry, M.L., Gorno-Tempini, M.L., 2010. The logopenic variant of primary progressive aphasia. Curr. Opin. Neurol 23, 633–637. doi:10.1097/WCO.0b013e32833fb93e

Herskowitz, J.H., Seyfried, N.T., Duong, D.M., Xia, Q., Rees, H.D., Gearing, M., Peng, J., Lah, J.J., Levey, A.I., 2010. Phosphoproteomic Analysis Reveals Site-Specific Changes in GFAP and NDRG2 Phosphorylation in Frontotemporal Lobar Degeneration. Journal of Proteome Research 9, 6368–6379. doi:10.1021/pr100666c

Hiji, M., Takahashi, T., Fukuba, H., Yamashita, H., Kohriyama, T., Matsumoto, M., 2008. White matter lesions in the brain with frontotemporal lobar degeneration with motor neuron disease: TDP-43-immunopositive inclusions co-localize with p62, but not ubiquitin. Acta Neuropathologica 116, 183–191. doi:10.1007/s00401-008-0402-2

Horel, J.A., Misantone, L.J., 1974. The Klüver-Bucy syndrome produced by partial isolation of the temporal lobe. Experimental Neurology 42, 101–112. doi:10.1016/0014-4886(74)90010-7

Hornberger, M., Geng, J., Hodges, J.R., 2011. Convergent grey and white matter evidence of orbitofrontal cortex changes related to disinhibition in behavioural variant frontotemporal dementia. Brain 134, 2502–2512. doi:10.1093/brain/awr173

Hornberger, M., Wong, S., Tan, R., Irish, M., Piguet, O., Kril, J., Hodges, J.R., Halliday, G., 2012. In vivo and post-mortem memory circuit integrity in frontotemporal dementia and Alzheimer's disease. Brain 135, 3015–3025. doi:10.1093/brain/aws239

Huang, H., Fan, X., Weiner, M., Martin-Cook, K., Xiao, G., Davis, J., Devous, M., Rosenberg, R., Diaz-Arrastia, R., 2011. Distinctive disruption patterns of white matter tracts in Alzheimer's disease with full diffusion tensor characterization. Neurobiol. Aging. doi:10.1016/j.neurobiolaging.2011.06.027

Hutton, M., Lendon, C.L., Rizzu, P., Baker, M., Froelich, S., Houlden, H., Pickering-Brown, S., Chakraverty, S., Isaacs, A., Grover, A., Hackett, J., Adamson, J., Lincoln, S., Dickson, D., Davies, P., Petersen, R.C., Stevens, M., de Graaff, E., Wauters, E., van Baren, J., Hillebrand, M., Joosse, M., Kwon, J.M., Nowotny, P., Che, L.K., Norton, J., Morris, J.C., Reed, L.A., Trojanowski, J., Basun, H., Lannfelt, L., Neystat, M., Fahn, S., Dark, F., Tannenberg, T., Dodd, P.R., Hayward, N., Kwok, J.B., Schofield, P.R., Andreadis, A., Snowden, J., Craufurd, D., Neary, D., Owen, F., Oostra, B.A., Hardy, J., Goate, A., van Swieten, J., Mann, D., Lynch, T., Heutink, P., 1998. Association of missense and 5'-splice-site mutations in tau with the inherited dementia FTDP-17. Nature 393, 702–705. doi:10.1038/31508

Iaccarino, L., Crespi, C., Della Rosa, P.A., Catricalà, E., Guidi, L., Marcone, A., Tagliavini, F., Magnani, G., Cappa, S.F., Perani, D., 2015. The Semantic Variant of Primary Progressive Aphasia: Clinical and Neuroimaging Evidence in Single Subjects. PLOS ONE 10, e0120197. doi:10.1371/journal.pone.0120197

Irwin, D.J., McMillan, C.T., Suh, E., Powers, J., Rascovsky, K., Wood, E.M., Toledo, J.B., Arnold, S.E., Lee, V.M.-Y., Van Deerlin, V.M., Trojanowski, J.Q., Grossman, M., 2014. Myelin oligodendrocyte basic protein and prognosis in behavioral-variant

frontotemporal dementia. Neurology 83, 502–509. doi:10.1212/WNL.0000000000000668

Jaarsma, D., Haasdijk, E.D., Grashorn, J.A.C., Hawkins, R., van Duijn, W., Verspaget, H.W., London, J., Holstege, J.C., 2000. Human Cu/Zn Superoxide Dismutase (SOD1) Overexpression in Mice Causes Mitochondrial Vacuolization, Axonal Degeneration, and Premature Motoneuron Death and Accelerates Motoneuron Disease in Mice Expressing a Familial Amyotrophic Lateral Sclerosis Mutant SOD1. Neurobiology of Disease 7, 623–643. doi:10.1006/nbdi.2000.0299

Janssen, J.C., Schott, J.M., Cipolotti, L., Fox, N.C., Scahill, R.I., Josephs, K.A., Stevens, J.M., Rossor, M.N., 2005. Mapping the onset and progression of atrophy in familial frontotemporal lobar degeneration. J. Neurol. Neurosurg. Psychiatr. 76, 162–168. doi:10.1136/jnnp.2003.032201

Janssen, J.C., Warrington, E.K., Morris, H.R., Lantos, P., Brown, J., Revesz, T., Wood, N., Khan, M.N., Cipolotti, L., Fox, N.C., Rossor, M.N., 2002. Clinical features of frontotemporal dementia due to the intronic tau 10(+16) mutation. Neurology 58, 1161–1168.

Jbabdi, S., Behrens, T.E.J., Smith, S.M., 2010. Crossing fibres in tract-based spatial statistics. Neuroimage 49, 249–256. doi:10.1016/j.neuroimage.2009.08.039

Jenkinson, M., Smith, S., 2001. A global optimisation method for robust affine registration of brain images. Medical Image Analysis 5, 143–156. doi:10.1016/S1361-8415(01)00036-6

Jensen, J.H., Helpern, J.A., Ramani, A., Lu, H., Kaczynski, K., 2005. Diffusional kurtosis imaging: The quantification of non-gaussian water diffusion by means of magnetic

resonance imaging. Magnetic Resonance in Medicine 53, 1432–1440. doi:10.1002/mrm.20508

Jones, D.K., Knösche, T.R., Turner, R., 2013. White matter integrity, fiber count, and other fallacies: The do's and don'ts of diffusion MRI. NeuroImage 73, 239–254. doi:10.1016/j.neuroimage.2012.06.081

Josephs, K.A., Whitwell, J.L., Dickson, D.W., Boeve, B.F., Knopman, D.S., Petersen, R.C., Parisi, J.E., Jack, C.R., 2008. Voxel-based morphometry in autopsy proven PSP and CBD. Neurobiol. Aging 29, 280–289. doi:10.1016/j.neurobiolaging.2006.09.019

Josephs, K.A., Whitwell, J.L., Knopman, D.S., Boeve, B.F., Vemuri, P., Senjem, M.L., Parisi, J.E., Ivnik, R.J., Dickson, D.W., Petersen, R.C., Jack, C.R., 2009. Two distinct subtypes of right temporal variant frontotemporal dementia. Neurology 73, 1443–1450. doi:10.1212/WNL.0b013e3181bf9945

Katanoda, K., Yoshikawa, K., Sugishita, M., 2001. A functional MRI study on the neural substrates for writing. Hum Brain Mapp 13, 34–42.

Kay, J., 1992. PALPA: psycholinguistic assesments of language processing in aphasia. Psychology Press, Hove.

Keihaninejad, S., Ryan, N.S., Malone, I.B., Modat, M., Cash, D., Ridgway, G.R., Zhang, H., Fox, N.C., Ourselin, S., 2012. The importance of group-wise registration in tract based spatial statistics study of neurodegeneration: a simulation study in Alzheimer's disease. PLoS ONE 7, e45996. doi:10.1371/journal.pone.0045996

Keihaninejad, S., Zhang, H., Ryan, N.S., Malone, I.B., Modat, M., Cardoso, M.J., Cash, D.M., Fox, N.C., Ourselin, S., 2013. An unbiased longitudinal analysis framework for tracking white matter changes using diffusion tensor imaging with application to

Alzheimer's disease. NeuroImage 72, 153–163. doi:10.1016/j.neuroimage.2013.01.044

Keil, C., Prell, T., Peschel, T., Hartung, V., Dengler, R., Grosskreutz, J., 2012. Longitudinal diffusion tensor imaging in amyotrophic lateral sclerosis. BMC Neuroscience 13, 141. doi:10.1186/1471-2202-13-141

Kertesz, A., McMonagle, P., Blair, M., Davidson, W., Munoz, D.G., 2005. The evolution and pathology of frontotemporal dementia. Brain 128, 1996–2005. doi:10.1093/brain/awh598

Kim, E.-J., Sidhu, M., Gaus, S.E., Huang, E.J., Hof, P.R., Miller, B.L., DeArmond, S.J., Seeley, W.W., 2012. Selective frontoinsular von Economo neuron and fork cell loss in early behavioral variant frontotemporal dementia. Cereb. Cortex 22, 251–259. doi:10.1093/cercor/bhr004

Kimonis, V.E., Fulchiero, E., Vesa, J., Watts, G., 2008. VCP disease associated with myopathy, Paget disease of bone and frontotemporal dementia: review of a unique disorder. Biochim. Biophys. Acta 1782, 744–748. doi:10.1016/j.bbadis.2008.09.003

Kipps, C.M., Hodges, J.R., Hornberger, M., 2010. Nonprogressive behavioural frontotemporal dementia: recent developments and clinical implications of the "bvFTD phenocopy syndrome": Current Opinion in Neurology 23, 628–632. doi:10.1097/WCO.0b013e3283404309

Kitamura, S., Kiuchi, K., Taoka, T., Hashimoto, K., Ueda, S., Yasuno, F., Morikawa, M., Kichikawa, K., Kishimoto, T., 2013. Longitudinal white matter changes in Alzheimer's disease: A tractography-based analysis study. Brain Research 1515, 12–18. doi:10.1016/j.brainres.2013.03.052

Klunk, W.E., Engler, H., Nordberg, A., Wang, Y., Blomqvist, G., Holt, D.P., Bergström, M., Savitcheva, I., Huang, G., Estrada, S., Ausén, B., Debnath, M.L., Barletta, J., Price, J.C., Sandell, J., Lopresti, B.J., Wall, A., Koivisto, P., Antoni, G., Mathis, C.A., Långström, B., 2004. Imaging brain amyloid in Alzheimer's disease with Pittsburgh Compound-B. Ann. Neurol. 55, 306–319. doi:10.1002/ana.20009

Knibb, J.A., Xuereb, J.H., Patterson, K., Hodges, J.R., 2006. Clinical and pathological characterization of progressive aphasia. Ann. Neurol 59, 156–165. doi:10.1002/ana.20700

Knopman, D.S., Jack, C.R., Jr, Kramer, J.H., Boeve, B.F., Caselli, R.J., Graff-Radford, N.R., Mendez, M.F., Miller, B.L., Mercaldo, N.D., 2009. Brain and ventricular volumetric changes in frontotemporal lobar degeneration over 1 year. Neurology 72, 1843–1849. doi:10.1212/WNL.0b013e3181a71236

Lam, B.Y.K., Halliday, G.M., Irish, M., Hodges, J.R., Piguet, O., 2014. Longitudinal white matter changes in frontotemporal dementia subtypes. Hum Brain Mapp 35, 3547–3557.

Larsson, E.-M., Englund, E., Sjöbeck, M., Lätt, J., Brockstedt, S., 2004. MRI with Diffusion Tensor Imaging Post-Mortem at 3.0 T in a Patient with Frontotemporal Dementia. Dement Geriatr Cogn Disord 17, 316–319. doi:10.1159/000077162

Lashley, T., Rohrer, J.D., Bandopadhyay, R., Fry, C., Ahmed, Z., Isaacs, A.M., Brelstaff, J.H., Borroni, B., Warren, J.D., Troakes, C., King, A., Al-Saraj, S., Newcombe, J., Quinn, N., Ostergaard, K., Schroder, H.D., Bojsen-Moller, M., Braendgaard, H., Fox, N.C., Rossor, M.N., Lees, A.J., Holton, J.L., Revesz, T., 2011. A comparative clinical,

pathological, biochemical and genetic study of fused in sarcoma proteinopathies. Brain 134, 2548–2564. doi:10.1093/brain/awr160

Lassmann, H., van Horssen, J., Mahad, D., 2012. Progressive multiple sclerosis: pathology and pathogenesis. Nature Reviews Neurology 8, 647–656. doi:10.1038/nrneurol.2012.168

Lee, E.B., Lee, V.M.-Y., Trojanowski, J.Q., 2011. Gains or losses: molecular mechanisms of TDP43-mediated neurodegeneration. Nature Reviews Neuroscience. doi:10.1038/nrn3121

Lieberman, A.P., Trojanowski, J.Q., Lee, V.M.-Y., Balin, B.J., Ding, X.-S., Greenberg, J., Morrison, D., Reivich, M., Grossman, M., 1998. Cognitive, neuroimaging, and pathological studies in a patient with Pick's disease. Annals of Neurology 43, 259–265. doi:10.1002/ana.410430218

Lillo, P., Mioshi, E., Burrell, J.R., Kiernan, M.C., Hodges, J.R., Hornberger, M., 2012. Grey and white matter changes across the amyotrophic lateral sclerosis-frontotemporal dementia continuum. PLoS ONE 7, e43993. doi:10.1371/journal.pone.0043993

Linke, J., King, A.V., Poupon, C., Hennerici, M.G., Gass, A., Wessa, M., 2013. Impaired Anatomical Connectivity and Related Executive Functions: Differentiating Vulnerability and Disease Marker in Bipolar Disorder. Biol. Psychiatry. doi:10.1016/j.biopsych.2013.04.010

Liu, L., Drouet, V., Wu, J.W., Witter, M.P., Small, S.A., Clelland, C., Duff, K., 2012. Trans-Synaptic Spread of Tau Pathology In Vivo. PLoS ONE 7, e31302. doi:10.1371/journal.pone.0031302

Liu, M., Gross, D.W., Wheatley, B.M., Concha, L., Beaulieu, C., 2013. The acute phase of Wallerian degeneration: Longitudinal diffusion tensor imaging of the fornix following temporal lobe surgery. NeuroImage 74, 128–139. doi:10.1016/j.neuroimage.2013.01.069

Liu-Yesucevitz, L., Bilgutay, A., Zhang, Y.-J., Vanderwyde, T., Citro, A., Mehta, T., Zaarur, N., McKee, A., Bowser, R., Sherman, M., Petrucelli, L., Wolozin, B., 2010. Tar DNA Binding Protein-43 (TDP-43) Associates with Stress Granules: Analysis of Cultured Cells and Pathological Brain Tissue. PLoS ONE 5, e13250. doi:10.1371/journal.pone.0013250

Lynch, T., Sano, M., Marder, K.S., Bell, K.L., Foster, N.L., Defendini, R.F., Sima, A.A., Keohane, C., Nygaard, T.G., Fahn, S., 1994. Clinical characteristics of a family with chromosome 17-linked disinhibition-dementia-parkinsonism-amyotrophy complex. Neurology 44, 1878–1884.

Mackenzie, I.R.A., Neumann, M., Baborie, A., Sampathu, D.M., Plessis, D., Jaros, E., Perry, R.H., Trojanowski, J.Q., Mann, D.M.A., Lee, V.M.Y., 2011. A harmonized classification system for FTLD-TDP pathology. Acta Neuropathologica 122, 111–113. doi:10.1007/s00401-011-0845-8

Mackenzie, I.R.A., Neumann, M., Bigio, E.H., Cairns, N.J., Alafuzoff, I., Kril, J., Kovacs, G.G., Ghetti, B., Halliday, G., Holm, I.E., Ince, P.G., Kamphorst, W., Revesz, T., Rozemuller, A.J.M., Kumar-Singh, S., Akiyama, H., Baborie, A., Spina, S., Dickson, D.W., Trojanowski, J.Q., Mann, D.M.A., 2010. Nomenclature and nosology for neuropathologic subtypes of frontotemporal lobar degeneration: an update. Acta Neuropathol. 119, 1–4. doi:10.1007/s00401-009-0612-2

Maguire, E.A., Kumaran, D., Hassabis, D., Kopelman, M.D., 2010. Autobiographical memory in semantic dementia: a longitudinal fMRI study. Neuropsychologia 48, 123–136. doi:10.1016/j.neuropsychologia.2009.08.020

Mahoney, C.J., Beck, J., Rohrer, J.D., Lashley, T., Mok, K., Shakespeare, T., Yeatman, T., Warrington, E.K., Schott, J.M., Fox, N.C., Rossor, M.N., Hardy, J., Collinge, J., Revesz, T., Mead, S., Warren, J.D., 2012a. Frontotemporal dementia with the C9ORF72 hexanucleotide repeat expansion: clinical, neuroanatomical and neuropathological features. Brain 135, 736–750. doi:10.1093/brain/awr361

Mahoney, C.J., Downey, L.E., Ridgway, G.R., Beck, J., Clegg, S., Blair, M., Finnegan, S., Leung, K.K., Yeatman, T., Golden, H., Mead, S., Rohrer, J.D., Fox, N.C., Warren, J.D., 2012b. Longitudinal neuroimaging and neuropsychological profiles of frontotemporal dementia with C9ORF72 expansions. Alzheimers Res Ther 4, 41. doi:10.1186/alzrt144

Mahoney, C.J., Malone, I.B., Ridgway, G.R., Buckley, A.H., Downey, L.E., Golden, H.L., Ryan, N.S., Ourselin, S., Schott, J.M., Rossor, M.N., Fox, N.C., Warren, J.D., 2013. White matter tract signatures of the progressive aphasias. Neurobiol. Aging. doi:10.1016/j.neurobiolaging.2012.12.002

Mahoney, C.J., Ridgway, G.R., Malone, I.B., Downey, L.E., Beck, J., Kinnunen, K.M., Schmitz, N., Golden, H.L., Rohrer, J.D., Schott, J.M., Rossor, M.N., Ourselin, S., Mead, S., Fox, N.C., Warren, J.D., 2014. Profiles of white matter tract pathology in frontotemporal dementia. Hum Brain Mapp 35, 4163–4179. doi:10.1002/hbm.22468

Mandelli, M.L., Caverzasi, E., Binney, R.J., Henry, M.L., Lobach, I., Block, N., Amirbekian, B., Dronkers, N., Miller, B.L., Henry, R.G., Gorno-Tempini, M.L., 2014. Frontal White

Matter Tracts Sustaining Speech Production in Primary Progressive Aphasia. Journal of Neuroscience 34, 9754–9767. doi:10.1523/JNEUROSCI.3464-13.2014

Martin, J.A., Craft, D.K., Su, J.H., Kim, R.C., Cotman, C.W., 2001. Astrocytes degenerate in frontotemporal dementia: possible relation to hypoperfusion. Neurobiol. Aging 22, 195–207.

Maruyama, M., Shimada, H., Suhara, T., Shinotoh, H., Ji, B., Maeda, J., Zhang, M.-R., Trojanowski, J.Q., Lee, V.M.-Y., Ono, M., Masamoto, K., Takano, H., Sahara, N., Iwata, N., Okamura, N., Furumoto, S., Kudo, Y., Chang, Q., Saido, T.C., Takashima, A., Lewis, J., Jang, M.-K., Aoki, I., Ito, H., Higuchi, M., 2013. Imaging of Tau Pathology in a Tauopathy Mouse Model and in Alzheimer Patients Compared to Normal Controls. Neuron 79, 1094–1108. doi:10.1016/j.neuron.2013.07.037

Matsuo, K., Mizuno, T., Yamada, K., Akazawa, K., Kasai, T., Kondo, M., Mori, S., Nishimura, T., Nakagawa, M., 2008. Cerebral white matter damage in frontotemporal dementia assessed by diffusion tensor tractography. Neuroradiology 50, 605–611. doi:10.1007/s00234-008-0379-5

Mechelli, A., Price, C., Friston, K., Ashburner, J., 2005. Voxel-Based Morphometry of the Human Brain: Methods and Applications. Current Medical Imaging Reviews 1, 105–113. doi:10.2174/1573405054038726

Mehta, A., Ghaghada, K.B., Mukundan, S., 2014. Future Clinical Applications of Molecular Imaging: Nanoparticles, Cellular Probes, and Imaging of Gene Expression, in: Pillai, J.J. (Ed.), Functional Brain Tumor Imaging. Springer New York, New York, NY, pp. 225–237.

Menke, R.A.L., Abraham, I., Thiel, C.S., Filippini, N., Knight, S., Talbot, K., Turner, M.R., 2012. Fractional anisotropy in the posterior limb of the internal capsule and

prognosis in amyotrophic lateral sclerosis. Arch. Neurol. 69, 1493–1499. doi:10.1001/archneurol.2012.1122

Mesulam, M.M., 1982. Slowly progressive aphasia without generalized dementia. Ann. Neurol. 11, 592–598. doi:10.1002/ana.410110607

Metzler-Baddeley, C., Jones, D.K., Steventon, J., Westacott, L., Aggleton, J.P., O'Sullivan, M.J., 2012. Cingulum Microstructure Predicts Cognitive Control in Older Age and Mild Cognitive Impairment. Journal of Neuroscience 32, 17612–17619. doi:10.1523/JNEUROSCI.3299-12.2012

Mielke, M.M., Kozauer, N.A., Chan, K.C.G., George, M., Toroney, J., Zerrate, M., Bandeen-Roche, K., Wang, M.-C., Vanzijl, P., Pekar, J.J., Mori, S., Lyketsos, C.G., Albert, M., 2009. Regionally-specific diffusion tensor imaging in mild cognitive impairment and Alzheimer's disease. Neuroimage 46, 47–55. doi:10.1016/j.neuroimage.2009.01.054

Mioshi, E., Hsieh, S., Savage, S., Hornberger, M., Hodges, J.R., 2010. Clinical staging and disease progression in frontotemporal dementia. Neurology 74, 1591–1597. doi:10.1212/WNL.0b013e3181e04070

Mitelman, S.A., Nikiforova, Y.K., Canfield, E.L., Hazlett, E.A., Brickman, A.M., Shihabuddin, L., Buchsbaum, M.S., 2009. A longitudinal study of the corpus callosum in chronic schizophrenia. Schizophr. Res. 114, 144–153. doi:10.1016/j.schres.2009.07.021

Mori, S., Wakana, S., Van Zijl, P.C.M., 2004. MRI atlas of human white matter. Elsevier, Amsterdam, the Netherlands; San Diego, CA.

Mummery, C.J., Patterson, K., Price, C.J., Ashburner, J., Frackowiak, R.S., Hodges, J.R., 2000. A voxel-based morphometry study of semantic dementia: relationship between temporal lobe atrophy and semantic memory. Ann. Neurol 47, 36–45.

Neary, D., Snowden, J.S., Gustafson, L., Passant, U., Stuss, D., Black, S., Freedman, M., Kertesz, A., Robert, P.H., Albert, M., Boone, K., Miller, B.L., Cummings, J., Benson, D.F., 1998. Frontotemporal lobar degeneration: a consensus on clinical diagnostic criteria. Neurology 51, 1546–1554.

Nestor, P.J., Graham, N.L., Fryer, T.D., Williams, G.B., Patterson, K., Hodges, J.R., 2003. Progressive non-fluent aphasia is associated with hypometabolism centred on the left anterior insula. Brain 126, 2406–2418. doi:10.1093/brain/awg240

Neumann, M., Kwong, L.K., Truax, A.C., Vanmassenhove, B., Kretzschmar, H.A., Van Deerlin, V.M., Clark, C.M., Grossman, M., Miller, B.L., Trojanowski, J.Q., Lee, V.M.-Y., 2007. TDP-43-Positive White Matter Pathology in Frontotemporal Lobar Degeneration With Ubiquitin-Positive Inclusions. Journal of Neuropathology and Experimental Neurology 66, 177–183. doi:10.1097/01.jnen.0000248554.45456.58

Neumann, M., Sampathu, D.M., Kwong, L.K., Truax, A.C., Micsenyi, M.C., Chou, T.T., Bruce, J., Schuck, T., Grossman, M., Clark, C.M., McCluskey, L.F., Miller, B.L., Masliah, E., Mackenzie, I.R., Feldman, H., Feiden, W., Kretzschmar, H.A., Trojanowski, J.Q., Lee, V.M.-Y., 2006. Ubiquitinated TDP-43 in frontotemporal lobar degeneration and amyotrophic lateral sclerosis. Science 314, 130–133. doi:10.1126/science.1134108

Newcombe, J., Hawkins, C.P., Henderson, C.L., Patel, H.A., Woodroofe, M.N., Hayes, G.M., Cuzner, M.L., MacManus, D., du Boulay, E.P., McDonald, W.I., 1991. Histopathology of multiple sclerosis lesions detected by magnetic resonance imaging in unfixed postmortem central nervous system tissue. Brain 114 (Pt 2), 1013–1023.

Nichols, T.E., Holmes, A.P., 2002. Nonparametric permutation tests for functional neuroimaging: A primer with examples. Human Brain Mapping 15, 1–25. doi:10.1002/hbm.1058

Noel-Storr, A.H., Flicker, L., Ritchie, C.W., Nguyen, G.H., Gupta, T., Wood, P., Walton, J., Desai, M., Solomon, D.F., Molena, E., Worrall, R., Hayen, A., Choudhary, P., Ladds, E., Lanctôt, K.L., Verhey, F.R., McCleery, J.M., Mead, G.E., Clare, L., Fioravanti, M., Hyde, C., Marcus, S., McShane, R., 2013. Systematic review of the body of evidence for the use of biomarkers in the diagnosis of dementia. Alzheimer's & Dementia 9, e96–e105. doi:10.1016/j.jalz.2012.01.014

Noonan, K.A., Jefferies, E., Visser, M., Lambon Ralph, M.A., 2013. Going beyond inferior prefrontal involvement in semantic control: evidence for the additional contribution of dorsal angular gyrus and posterior middle temporal cortex. J Cogn Neurosci 25, 1824–1850. doi:10.1162/jocn_a_00442

Nowrangi, M.A., Lyketsos, C.G., Leoutsakos, J.-M.S., Oishi, K., Albert, M., Mori, S., Mielke, M.M., 2013. Longitudinal, region-specific course of diffusion tensor imaging measures in mild cognitive impairment and Alzheimer's disease. Alzheimer's & Dementia 9, 519–28. doi:10.1016/j.jalz.2012.05.2186

Nussbaum, J.M., Schilling, S., Cynis, H., Silva, A., Swanson, E., Wangsanut, T., Tayler, K., Wiltgen, B., Hatami, A., Rönicke, R., Reymann, K., Hutter-Paier, B., Alexandru, A., Jagla, W., Graubner, S., Glabe, C.G., Demuth, H.-U., Bloom, G.S., 2012. Prion-like behaviour and tau-dependent cytotoxicity of pyroglutamylated amyloid-β. Nature 485, 651–655. doi:10.1038/nature11060

Oishi, K., Mielke, M.M., Albert, M., Lyketsos, C.G., Mori, S., 2011. The Fornix Sign: A Potential Sign for Alzheimer's Disease Based on Diffusion Tensor Imaging. J Neuroimaging. doi:10.1111/j.1552-6569.2011.00633.x

Orrù, G., Pettersson-Yeo, W., Marquand, A.F., Sartori, G., Mechelli, A., 2012. Using Support Vector Machine to identify imaging biomarkers of neurological and psychiatric disease: A critical review. Neuroscience & Biobehavioral Reviews 36, 1140–1152. doi:10.1016/j.neubiorev.2012.01.004

Parker, G.J.M., Luzzi, S., Alexander, D.C., Wheeler-Kingshott, C.A.M., Ciccarelli, O., Lambon Ralph, M.A., 2005. Lateralization of ventral and dorsal auditory-language pathways in the human brain. Neuroimage 24, 656–666. doi:10.1016/j.neuroimage.2004.08.047

Park, H.-J., Friston, K., 2013. Structural and Functional Brain Networks: From Connections to Cognition. Science 342, 1238411–1238411. doi:10.1126/science.1238411

Paviour, D.C., Price, S.L., Jahanshahi, M., Lees, A.J., Fox, N.C., 2006. Longitudinal MRI in progressive supranuclear palsy and multiple system atrophy: rates and regions of atrophy. Brain 129, 1040–1049. doi:10.1093/brain/awl021

Pereira, J.M.S., Williams, G.B., Acosta-Cabronero, J., Pengas, G., Spillantini, M.G., Xuereb, J.H., Hodges, J.R., Nestor, P.J., 2009a. Atrophy patterns in histologic vs clinical groupings of frontotemporal lobar degeneration. Neurology 72, 1653–1660. doi:10.1212/WNL.0b013e3181a55fa2

Pereira, J.M.S., Williams, G.B., Acosta-Cabronero, J., Pengas, G., Spillantini, M.G., Xuereb, J.H., Hodges, J.R., Nestor, P.J., 2009b. Atrophy patterns in histologic vs clinical groupings of frontotemporal lobar degeneration. Neurology 72, 1653–1660. doi:10.1212/WNL.0b013e3181a55fa2

Phan, K.L., Orlichenko, A., Boyd, E., Angstadt, M., Coccaro, E.F., Liberzon, I., Arfanakis, K., 2009. Preliminary evidence of white matter abnormality in the uncinate fasciculus in generalized social anxiety disorder. Biol. Psychiatry 66, 691–694. doi:10.1016/j.biopsych.2009.02.028

Piao, Y.-S., Tan, C.-F., Iwanaga, K., Kakita, A., Takano, H., Nishizawa, M., Lashley, T., Revesz, T., Lees, A., de Silva, R., Tsujihata, M., Takahashi, H., 2005. Sporadic four-repeat tauopathy with frontotemporal degeneration, parkinsonism and motor neuron disease. Acta Neuropathol. 110, 600–609. doi:10.1007/s00401-005-1086-5

Pick, A., 1904. Über primäre progressive Demenz bei Er- wachsenen. Prag Med Wochenschr. 29, 417–420.

Pick, A., 1892. ÜberdieBeziehungendersenilenHirnat- rophie zur Aphasie. Prag Med Wochenschr. 17, 165–167.

Pievani, M., de Haan, W., Wu, T., Seeley, W.W., Frisoni, G.B., 2011. Functional network disruption in the degenerative dementias. The Lancet Neurology 10, 829–843. doi:10.1016/S1474-4422(11)70158-2

Poudel, G.R., Stout, J.C., Domínguez D, J.F., Churchyard, A., Chua, P., Egan, G.F., Georgiou-Karistianis, N., 2014. Longitudinal change in white matter microstructure in Huntington's disease: The IMAGE-HD study. Neurobiol. Dis. 74C, 406–412. doi:10.1016/j.nbd.2014.12.009

Prakash, N., Hageman, N., Hua, X., Toga, A.W., Perlman, S.L., Salamon, N., 2009. Patterns of fractional anisotropy changes in white matter of cerebellar peduncles distinguish spinocerebellar ataxia-1 from multiple system atrophy and other ataxia syndromes. Neuroimage 47 Suppl 2, T72–81. doi:10.1016/j.neuroimage.2009.05.013

Rademakers, R., Baker, M., Nicholson, A.M., Rutherford, N.J., Finch, N., Soto-Ortolaza, A., Lash, J., Wider, C., Wojtas, A., DeJesus-Hernandez, M., Adamson, J., Kouri, N., Sundal, C., Shuster, E.A., Aasly, J., MacKenzie, J., Roeber, S., Kretzschmar, H.A., Boeve, B.F., Knopman, D.S., Petersen, R.C., Cairns, N.J., Ghetti, B., Spina, S., Garbern, J., Tselis, A.C., Uitti, R., Das, P., Van Gerpen, J.A., Meschia, J.F., Levy, S., Broderick, D.F., Graff-Radford, N., Ross, O.A., Miller, B.B., Swerdlow, R.H., Dickson, D.W., Wszolek, Z.K., 2012. Mutations in the colony stimulating factor 1 receptor (CSF1R) gene cause hereditary diffuse leukoencephalopathy with spheroids. Nat. Genet. 44, 200–205. doi:10.1038/ng.1027

Raff, M.C., Whitmore, A.V., Finn, J.T., 2002. Axonal self-destruction and neurodegeneration. Science 296, 868–871. doi:10.1126/science.1068613

Raj, A., Kuceyeski, A., Weiner, M., 2012. A network diffusion model of disease progression in dementia. Neuron 73, 1204–1215. doi:10.1016/j.neuron.2011.12.040

Rankin, K.P., Salazar, A., Gorno-Tempini, M.L., Sollberger, M., Wilson, S.M., Pavlic, D., Stanley, C.M., Glenn, S., Weiner, M.W., Miller, B.L., 2009. Detecting sarcasm from paralinguistic cues: anatomic and cognitive correlates in neurodegenerative disease. Neuroimage 47, 2005–2015. doi:10.1016/j.neuroimage.2009.05.077

Rascovsky, K., Hodges, J.R., Knopman, D., Mendez, M.F., Kramer, J.H., Neuhaus, J., van Swieten, J.C., Seelaar, H., Dopper, E.G.P., Onyike, C.U., Hillis, A.E., Josephs, K.A., Boeve, B.F., Kertesz, A., Seeley, W.W., Rankin, K.P., Johnson, J.K., Gorno-Tempini, M.-L., Rosen, H., Prioleau-Latham, C.E., Lee, A., Kipps, C.M., Lillo, P., Piguet, O., Rohrer, J.D., Rossor, M.N., Warren, J.D., Fox, N.C., Galasko, D., Salmon, D.P., Black, S.E., Mesulam, M., Weintraub, S., Dickerson, B.C., Diehl-Schmid, J., Pasquier, F., Deramecourt, V., Lebert, F., Pijnenburg, Y., Chow, T.W., Manes, F., Grafman, J.,

Cappa, S.F., Freedman, M., Grossman, M., Miller, B.L., 2011. Sensitivity of revised diagnostic criteria for the behavioural variant of frontotemporal dementia. Brain 134, 2456–2477. doi:10.1093/brain/awr179

Ratnavalli, E., Brayne, C., Dawson, K., Hodges, J.R., 2002. The prevalence of frontotemporal dementia. Neurology 58, 1615–1621.

Renton, A.E., Majounie, E., Waite, A., Simón-Sánchez, J., Rollinson, S., Gibbs, J.R., Schymick, J.C., Laaksovirta, H., van Swieten, J.C., Myllykangas, L., Kalimo, H., Paetau, A., Abramzon, Y., Remes, A.M., Kaganovich, A., Scholz, S.W., Duckworth, J., Ding, J., Harmer, D.W., Hernandez, D.G., Johnson, J.O., Mok, K., Ryten, M., Trabzuni, D., Guerreiro, R.J., Orrell, R.W., Neal, J., Murray, A., Pearson, J., Jansen, I.E., Sondervan, D., Seelaar, H., Blake, D., Young, K., Halliwell, N., Callister, J.B., Toulson, G., Richardson, A., Gerhard, A., Snowden, J., Mann, D., Neary, D., Nalls, M.A., Peuralinna, T., Jansson, L., Isoviita, V.-M., Kaivorinne, A.-L., Hölttä-Vuori, M., Ikonen, E., Sulkava, R., Benatar, M., Wuu, J., Chiò, A., Restagno, G., Borghero, G., Sabatelli, M., Heckerman, D., Rogaeva, E., Zinman, L., Rothstein, J.D., Sendtner, M., Drepper, C., Eichler, E.E., Alkan, C., Abdullaev, Z., Pack, S.D., Dutra, A., Pak, E., Hardy, J., Singleton, A., Williams, N.M., Heutink, P., Pickering-Brown, S., Morris, H.R., Tienari, P.J., Traynor, B.J., 2011. A Hexanucleotide Repeat Expansion in C9ORF72 Is the Cause of Chromosome 9p21-Linked ALS-FTD. Neuron. doi:10.1016/j.neuron.2011.09.010

Ringman, J.M., O'Neill, J., Geschwind, D., Medina, L., Apostolova, L.G., Rodriguez, Y., Schaffer, B., Varpetian, A., Tseng, B., Ortiz, F., Fitten, J., Cummings, J.L., Bartzokis, G., 2007. Diffusion Tensor Imaging in Preclinical and Presymptomatic Carriers of

Familial Alzheimer's Disease Mutations. Brain 130, 1767–1776. doi:10.1093/brain/awm102

Rogalski, E., Cobia, D., Harrison, T.M., Wieneke, C., Thompson, C.K., Weintraub, S., Mesulam, M.-M., 2011. Anatomy of language impairments in primary progressive aphasia. J. Neurosci 31, 3344–3350. doi:10.1523/JNEUROSCI.5544-10.2011

Rogalski, E., Cobia, D., Harrison, T.M., Wieneke, C., Weintraub, S., Mesulam, M.-M., 2011. Progression of language decline and cortical atrophy in subtypes of primary progressive aphasia. Neurology 76, 1804–1810. doi:10.1212/WNL.0b013e31821ccd3c

Rogalski, E., Cobia, D., Martersteck, A., Rademaker, A., Wieneke, C., Weintraub, S., Mesulam, M.-M., 2014. Asymmetry of cortical decline in subtypes of primary progressive aphasia. Neurology 83, 1184–1191. doi:10.1212/WNL.0000000000000824

Rohrer, J.D., Caso, F., Mahoney, C., Henry, M., Rosen, H.J., Rabinovici, G., Rossor, M.N., Miller, B., Warren, J.D., Fox, N.C., Ridgway, G.R., Gorno-Tempini, M.L., 2013. Patterns of longitudinal brain atrophy in the logopenic variant of primary progressive aphasia. Brain and Language 127, 121–126. doi:10.1016/j.bandl.2012.12.008

Rohrer, J.D., Crutch, S.J., Warrington, E.K., Warren, J.D., 2010a. Progranulin-associated primary progressive aphasia: a distinct phenotype? Neuropsychologia 48, 288–297. doi:10.1016/j.neuropsychologia.2009.09.017

Rohrer, J.D., Geser, F., Zhou, J., Gennatas, E.D., Sidhu, M., Trojanowski, J.Q., Dearmond, S.J., Miller, B.L., Seeley, W.W., 2010. TDP-43 subtypes are associated with distinct atrophy patterns in frontotemporal dementia. Neurology 75, 2204–2211. doi:10.1212/WNL.0b013e318202038c

Rohrer, J.D., Guerreiro, R., Vandrovcova, J., Uphill, J., Reiman, D., Beck, J., Isaacs, A.M., Authier, A., Ferrari, R., Fox, N.C., Mackenzie, I.R.A., Warren, J.D., de Silva, R., Holton, J., Revesz, T., Hardy, J., Mead, S., Rossor, M.N., 2009. The heritability and genetics of frontotemporal lobar degeneration. Neurology 73, 1451–1456. doi:10.1212/WNL.0b013e3181bf997a

Rohrer, J.D., Knight, W.D., Warren, J.E., Fox, N.C., Rossor, M.N., Warren, J.D., 2008. Word-finding difficulty: a clinical analysis of the progressive aphasias. Brain 131, 8–38. doi:10.1093/brain/awm251

Rohrer, J.D., McNaught, E., Foster, J., Clegg, S.L., Barnes, J., Omar, R., Warrington, E.K., Rossor, M.N., Warren, J.D., Fox, N.C., 2008. Tracking progression in frontotemporal lobar degeneration: Serial MRI in semantic dementia. Neurology 71, 1445–1451. doi:10.1212/01.wnl.0000327889.13734.cd

Rohrer, J.D., Ridgway, G.R., Crutch, S.J., Hailstone, J., Goll, J.C., Clarkson, M.J., Mead, S., Beck, J., Mummery, C., Ourselin, S., Warrington, E.K., Rossor, M.N., Warren, J.D., 2010b. Progressive logopenic/phonological aphasia: erosion of the language network. Neuroimage 49, 984–993. doi:10.1016/j.neuroimage.2009.08.002

Rohrer, J.D., Ridgway, G.R., Modat, M., Ourselin, S., Mead, S., Fox, N.C., Rossor, M.N., Warren, J.D., 2010c. Distinct profiles of brain atrophy in frontotemporal lobar degeneration caused by progranulin and tau mutations. Neuroimage 53, 1070–1076. doi:10.1016/j.neuroimage.2009.12.088

Rohrer, J.D., Rossor, M.N., Warren, J.D., 2010d. Syndromes of nonfluent primary progressive aphasia: a clinical and neurolinguistic analysis. Neurology 75, 603–610. doi:10.1212/WNL.0b013e3181ed9c6b

Rohrer, J.D., Warren, J.D., Modat, M., Ridgway, G.R., Douiri, A., Rossor, M.N., Ourselin, S., Fox, N.C., 2009. Patterns of cortical thinning in the language variants of frontotemporal lobar degeneration. Neurology 72, 1562–1569. doi:10.1212/WNL.0b013e3181a4124e

Rohrer, J., Lashley, T., Schott, J., 2011. Clinical and neuroanatomical signatures of tissue pathology in fontotemporal lobar degeneration. Brain 134, 2565–81.

Rovaris, M., Filippi, M., Falautano, M., Minicucci, L., Rocca, M.A., Martinelli, V., Comi, G., 1998. Relation between MR abnormalities and patterns of cognitive impairment in multiple sclerosis. Neurology 50, 1601–1608.

Sajjadi, S.A., Patterson, K., Arnold, R.J., Watson, P.C., Nestor, P.J., 2012. Primary progressive aphasia: A tale of two syndromes and the rest. Neurology 78, 1670–1677. doi:10.1212/WNL.0b013e3182574f79

Sakai, K., Piao, Y.-S., Kikugawa, K., Ohara, S., Hasegawa, M., Takano, H., Fukase, M., Nishizawa, M., Kakita, A., Takahashi, H., 2006. Corticobasal degeneration with focal, massive tau accumulation in the subcortical white matter astrocytes. Acta Neuropathologica 112, 341–348. doi:10.1007/s00401-006-0093-5

Salloway, S., Sperling, R., Fox, N.C., Blennow, K., Klunk, W., Raskind, M., Sabbagh, M., Honig, L.S., Porsteinsson, A.P., Ferris, S., Reichert, M., Ketter, N., Nejadnik, B., Guenzler, V., Miloslavsky, M., Wang, D., Lu, Y., Lull, J., Tudor, I.C., Liu, E., Grundman, M., Yuen, E., Black, R., Brashear, H.R., 2014. Two Phase 3 Trials of Bapineuzumab in Mild-to-Moderate Alzheimer's Disease. New England Journal of Medicine 370, 322–333. doi:10.1056/NEJMoa1304839

Sandell, J.H., Peters, A., 2003. Disrupted myelin and axon loss in the anterior commissure of the aged rhesus monkey. The Journal of Comparative Neurology 466, 14–30. doi:10.1002/cne.10859

Sandrine, C., Keith, A., Mark, B., Grazzia, dell'agnello, Michael, H., 2014. Systematic Literature Review and Meta-Analysis of Diagnostic Test Accuracy in Alzheimer's Disease and Other Dementia Using Autopsy as Standard of Truth. Journal of Alzheimer's Disease 169–182. doi:10.3233/JAD-131559

Saur, D., Kreher, B.W., Schnell, S., Kummerer, D., Kellmeyer, P., Vry, M.-S., Umarova, R., Musso, M., Glauche, V., Abel, S., Huber, W., Rijntjes, M., Hennig, J., Weiller, C., 2008. Ventral and dorsal pathways for language. Proceedings of the National Academy of Sciences 105, 18035–18040. doi:10.1073/pnas.0805234105

Saxena, S., Caroni, P., 2007. Mechanisms of axon degeneration: From development to disease. Progress in Neurobiology 83, 174–191. doi:10.1016/j.pneurobio.2007.07.007

Schmahmann, J.D., Pandya, D.N., Wang, R., Dai, G., D'Arceuil, H.E., de Crespigny, A.J., Wedeen, V.J., 2007. Association fibre pathways of the brain: parallel observations from diffusion spectrum imaging and autoradiography. Brain 130, 630–653. doi:10.1093/brain/awl359

Schmahmann, J., Pandya, D., 2008. Disconnection syndromes of basal ganglia, thalamus, and cerebrocerebellar systems. Cortex 44, 1037–1066. doi:10.1016/j.cortex.2008.04.004

Schmierer, K., Wheeler-Kingshott, C.A.M., Boulby, P.A., Scaravilli, F., Altmann, D.R., Barker, G.J., Tofts, P.S., Miller, D.H., 2007. Diffusion tensor imaging of post

mortem multiple sclerosis brain. NeuroImage 35, 467–477. doi:10.1016/j.neuroimage.2006.12.010

Schroeter, M.L., Raczka, K., Neumann, J., von Cramon, D.Y., 2008. Neural networks in frontotemporal dementia—A meta-analysis. Neurobiology of Aging 29, 418–426. doi:10.1016/j.neurobiolaging.2006.10.023

Schroeter, M.L., Raczka, K., Neumann, J., Yves von Cramon, D., 2007. Towards a nosology for frontotemporal lobar degenerations—A meta-analysis involving 267 subjects. NeuroImage 36, 497–510. doi:10.1016/j.neuroimage.2007.03.024

Schwindt, G.C., Graham, N.L., Rochon, E., Tang-Wai, D.F., Lobaugh, N.J., Chow, T.W., Black, S.E., 2011. Whole-brain white matter disruption in semantic and nonfluent variants of primary progressive aphasia. Hum Brain Mapp. doi:10.1002/hbm.21484

Scott, S.K., Blank, C.C., Rosen, S., Wise, R.J., 2000. Identification of a pathway for intelligible speech in the left temporal lobe. Brain 123 Pt 12, 2400–2406.

Seeley, W.W., Crawford, R.K., Zhou, J., Miller, B.L., Greicius, M.D., 2009. Neurodegenerative diseases target large-scale human brain networks. Neuron 62, 42–52. doi:10.1016/j.neuron.2009.03.024

Seeley, W.W., Menon, V., Schatzberg, A.F., Keller, J., Glover, G.H., Kenna, H., Reiss, A.L., Greicius, M.D., 2007. Dissociable intrinsic connectivity networks for salience processing and executive control. J. Neurosci. 27, 2349–2356. doi:10.1523/JNEUROSCI.5587-06.2007

Shaw, L.M., Korecka, M., Clark, C.M., Lee, V.M.-Y., Trojanowski, J.Q., 2007. Biomarkers of neurodegeneration for diagnosis and monitoring therapeutics. Nature Reviews Drug Discovery 6, 295–303. doi:10.1038/nrd2176

Simon, O., Mangin, J.-F., Cohen, L., Le Bihan, D., Dehaene, S., 2002. Topographical Layout of Hand, Eye, Calculation, and Language-Related Areas in the Human Parietal Lobe. Neuron 33, 475–487. doi:10.1016/S0896-6273(02)00575-5

Simons, M., Misgeld, T., Kerschensteiner, M., 2014. A unified cell biological perspective on axon-myelin injury. The Journal of Cell Biology 206, 335–345. doi:10.1083/jcb.201404154

Simonyan, K., Fuertinger, S., 2015. Speech networks at rest and in action: Interactions between functional brain networks controlling speech production. J. Neurophysiol. jn.00964.2014. doi:10.1152/jn.00964.2014

Sj□gren, M., Blomberg, M., Jonsson, M., Wahlund, L.-O., Edman, □, Lind, K., Rosengren, L., Blennow, K., Wallin, A., 2001. Neurofilament protein in cerebrospinal fluid: A marker of white matter changes. Journal of Neuroscience Research 66, 510–516. doi:10.1002/jnr.1242

Skosnik, P.D., Mirza, F., Gitelman, D.R., Parrish, T.B., Mesulam, M.-M., Reber, P.J., 2002. Neural correlates of artificial grammar learning. Neuroimage 17, 1306–1314.

Smith, S.M., Jenkinson, M., Johansen-Berg, H., Rueckert, D., Nichols, T.E., Mackay, C.E., Watkins, K.E., Ciccarelli, O., Cader, M.Z., Matthews, P.M., Behrens, T.E.J., 2006. Tract-based spatial statistics: voxelwise analysis of multi-subject diffusion data. Neuroimage 31, 1487–1505. doi:10.1016/j.neuroimage.2006.02.024

Smith, S.M., Nichols, T.E., 2009. Threshold-free cluster enhancement: addressing problems of smoothing, threshold dependence and localisation in cluster inference. Neuroimage 44, 83–98. doi:10.1016/j.neuroimage.2008.03.061

Snowden, J., Griffiths, H., Neary, D., 1994. Semantic dementia: Autobiographical contribution to preservation of meaning. Cognitive Neuropsychology 11, 265–288. doi:10.1080/02643299408251976

Snowden, J.S., Thompson, J.C., Stopford, C.L., Richardson, A.M.T., Gerhard, A., Neary, D., Mann, D.M.A., 2011. The clinical diagnosis of early-onset dementias: diagnostic accuracy and clinicopathological relationships. Brain 134, 2478–2492. doi:10.1093/brain/awr189

Song, S.-K., Sun, S.-W., Ramsbottom, M.J., Chang, C., Russell, J., Cross, A.H., 2002. Dysmyelination revealed through MRI as increased radial (but unchanged axial) diffusion of water. Neuroimage 17, 1429–1436.

Suarez, J., Tartaglia, M.C., Vitali, P., Erbetta, A., Neuhaus, J., Laluz, V., Miller, B.L., 2009. CHARACTERIZING RADIOLOGY REPORTS IN PATIENTS WITH FRONTOTEMPORAL DEMENTIA. Neurology 73, 1073–1074. doi:10.1212/WNL.0b013e3181b9c8a6

Sun, S.-W., Liang, H.-F., Trinkaus, K., Cross, A.H., Armstrong, R.C., Song, S.-K., 2006. Noninvasive detection of cuprizone induced axonal damage and demyelination in the mouse corpus callosum. Magn Reson Med 55, 302–308. doi:10.1002/mrm.20774

Tartaglia, M.C., Zhang, Y., Racine, C., Laluz, V., Neuhaus, J., Chao, L., Kramer, J., Rosen, H., Miller, B., Weiner, M., 2012. Executive dysfunction in frontotemporal dementia is related to abnormalities in frontal white matter tracts. J. Neurol. 259, 1071–1080. doi:10.1007/s00415-011-6300-x

Teipel, S.J., Meindl, T., Wagner, M., Stieltjes, B., Reuter, S., Hauenstein, K.-H., Filippi, M., Ernemann, U., Reiser, M.F., Hampel, H., 2010. Longitudinal changes in fiber tract

integrity in healthy aging and mild cognitive impairment: a DTI follow-up study. J. Alzheimers Dis. 22, 507–522. doi:10.3233/JAD-2010-100234

Thomason, M.E., Thompson, P.M., 2011. Diffusion Imaging, White Matter, and Psychopathology. Annual Review of Clinical Psychology 7, 63–85. doi:10.1146/annurev-clinpsy-032210-104507

Tyszka, J.M., Readhead, C., Bearer, E.L., Pautler, R.G., Jacobs, R.E., 2006. Statistical diffusion tensor histology reveals regional dysmyelination effects in the shiverer mouse mutant. Neuroimage 29, 1058–1065. doi:10.1016/j.neuroimage.2005.08.037

Vance, C., Al-Chalabi, A., Ruddy, D., Smith, B.N., Hu, X., Sreedharan, J., Siddique, T., Schelhaas, H.J., Kusters, B., Troost, D., Baas, F., de Jong, V., Shaw, C.E., 2006. Familial amyotrophic lateral sclerosis with frontotemporal dementia is linked to a locus on chromosome 9p13.2-21.3. Brain 129, 868–876. doi:10.1093/brain/awl030

Van den Heuvel, M.P., Sporns, O., 2013. Network hubs in the human brain. Trends Cogn. Sci. (Regul. Ed.) 17, 683–696. doi:10.1016/j.tics.2013.09.012

Van den Heuvel, M.P., Sporns, O., 2011. Rich-Club Organization of the Human Connectome. Journal of Neuroscience 31, 15775–15786. doi:10.1523/JNEUROSCI.3539-11.2011

Van der Knaap, L.J., van der Ham, I.J.M., 2011. How does the corpus callosum mediate interhemispheric transfer? A review. Behavioural Brain Research 223, 211–221. doi:10.1016/j.bbr.2011.04.018

Van der Werf, Y.D., Scheltens, P., Lindeboom, J., Witter, M.P., Uylings, H.B.M., Jolles, J., 2003. Deficits of memory, executive functioning and attention following infarction in the thalamus; a study of 22 cases with localised lesions. Neuropsychologia 41, 1330–1344. doi:10.1016/S0028-3932(03)00059-9

Van Eersel, J., Stevens, C.H., Przybyla, M., Gladbach, A., Stefanoska, K., Chan, C.K.-X., Ong, W.-Y., Hodges, J.R., Sutherland, G.T., Kril, J.J., Abramowski, D., Staufenbiel, M., Halliday, G.M., Ittner, L.M., 2015. Early-onset axonal pathology in a novel P301S-Tau transgenic mouse model of frontotemporal lobar degeneration: Early-onset axonal pathology in a transgenic tau mouse model. Neuropathology and Applied Neurobiology n/a–n/a. doi:10.1111/nan.12233

Van Geemen, K., Herbet, G., Moritz-Gasser, S., Duffau, H., 2014. Limited plastic potential of the left ventral premotor cortex in speech articulation: evidence from intraoperative awake mapping in glioma patients. Hum Brain Mapp 35, 1587–1596. doi:10.1002/hbm.22275

Vanhoutte, G., Pereson, S., Delgado y Palacios, R., Guns, P.-J., Asselbergh, B., Veraart, J., Sijbers, J., Verhoye, M., Van Broeckhoven, C., Van der Linden, A., 2013. Diffusion kurtosis imaging to detect amyloidosis in an APP/PS1 mouse model for Alzheimer's disease: Diffusion Kurtosis Imaging in Alzheimer's Disease. Magnetic Resonance in Medicine 69, 1115–1121. doi:10.1002/mrm.24680

Vergara, V.M., Ulloa, A., Calhoun, V.D., Boutte, D., Chen, J., Liu, J., 2014. A three-way parallel ICA approach to analyze links among genetics, brain structure and brain function. NeuroImage 98, 386–394. doi:10.1016/j.neuroimage.2014.04.060

Villain, N., Desgranges, B., Viader, F., de la Sayette, V., Mezenge, F., Landeau, B., Baron, J.-C., Eustache, F., Chetelat, G., 2008. Relationships between Hippocampal Atrophy, White Matter Disruption, and Gray Matter Hypometabolism in Alzheimer's Disease. Journal of Neuroscience 28, 6174–6181. doi:10.1523/JNEUROSCI.1392-08.2008

Vincent, J.L., Kahn, I., Snyder, A.Z., Raichle, M.E., Buckner, R.L., 2008. Evidence for a Frontoparietal Control System Revealed by Intrinsic Functional Connectivity. Journal of Neurophysiology 100, 3328–3342. doi:10.1152/jn.90355.2008

Von Der Heide, R.J., Skipper, L.M., Klobusicky, E., Olson, I.R., 2013. Dissecting the uncinate fasciculus: disorders, controversies and a hypothesis. Brain 136, 1692–707. doi:10.1093/brain/awt094

Wang, Y., Gupta, A., Liu, Z., Zhang, H., Escolar, M.L., Gilmore, J.H., Gouttard, S., Fillard, P., Maltbie, E., Gerig, G., Styner, M., 2011. DTI registration in atlas based fiber analysis of infantile Krabbe disease. NeuroImage 55, 1577–1586. doi:10.1016/j.neuroimage.2011.01.038

Warren, J.D., Rohrer, J.D., Hardy, J., 2012. Disintegrating brain networks: from syndromes to molecular nexopathies. Neuron 73, 1060–1062. doi:10.1016/j.neuron.2012.03.006

Warren, J.D., Rohrer, J.D., Schott, J.M., Fox, N.C., Hardy, J., Rossor, M.N., 2013. Molecular nexopathies: a new paradigm of neurodegenerative disease. Trends in Neurosciences 36, 561–9. doi:10.1016/j.tins.2013.06.007

Warrington, E.K., 1975. The selective impairment of semantic memory. Q J Exp Psychol 27, 635–657. doi:10.1080/14640747508400525

Wechsler, D., 1999. Wechsler Abbreviated Scale of Intelligence. Psychological Corporation, Sa.

Weiner, M.W., Veitch, D.P., Aisen, P.S., Beckett, L.A., Cairns, N.J., Green, R.C., Harvey, D., Jack, C.R., Jagust, W., Liu, E., Morris, J.C., Petersen, R.C., Saykin, A.J., Schmidt, M.E., Shaw, L., Siuciak, J.A., Soares, H., Toga, A.W., Trojanowski, J.Q., Alzheimer's Disease Neuroimaging Initiative, 2012. The Alzheimer's Disease Neuroimaging

Initiative: a review of papers published since its inception. Alzheimers Dement 8, S1–68. doi:10.1016/j.jalz.2011.09.172

Wheeler-Kingshott, C.A.M., Cercignani, M., 2009. About "axial" and "radial" diffusivities. Magn Reson Med 61, 1255–1260. doi:10.1002/mrm.21965

Whitwell, J.L., Avula, R., Senjem, M.L., Kantarci, K., Weigand, S.D., Samikoglu, A., Edmonson, H.A., Vemuri, P., Knopman, D.S., Boeve, B.F., Petersen, R.C., Josephs, K.A., Jack, C.R., 2010. Gray and white matter water diffusion in the syndromic variants of frontotemporal dementia. Neurology 74, 1279–1287. doi:10.1212/WNL.0b013e3181d9edde

Whitwell, J.L., Jack, C.R., Parisi, J.E., Knopman, D.S., Boeve, B.F., Petersen, R.C., Ferman, T.J., Dickson, D.W., Josephs, K.A., 2006. Rates of cerebral atrophy differ in different degenerative pathologies. Brain 130, 1148–1158. doi:10.1093/brain/awm021

Whitwell, J.L., Josephs, K.A., 2012. Neuroimaging in frontotemporal lobar degeneration—predicting molecular pathology. Nature Reviews Neurology 8, 131–142. doi:10.1038/nrneurol.2012.7

Whitwell, J.L., Josephs, K.A., Rossor, M.N., Stevens, J.M., Revesz, T., Holton, J.L., Al-Sarraj, S., Godbolt, A.K., Fox, N.C., Warren, J.D., 2005. Magnetic resonance imaging signatures of tissue pathology in frontotemporal dementia. Arch. Neurol. 62, 1402–1408. doi:10.1001/archneur.62.9.1402

Whitwell, J.L., Przybelski, S.A., Weigand, S.D., Ivnik, R.J., Vemuri, P., Gunter, J.L., Senjem, M.L., Shiung, M.M., Boeve, B.F., Knopman, D.S., Parisi, J.E., Dickson, D.W., Petersen, R.C., Jack, C.R., Jr, Josephs, K.A., 2009. Distinct anatomical subtypes of

the behavioural variant of frontotemporal dementia: a cluster analysis study. Brain 132, 2932–2946. doi:10.1093/brain/awp232

Whitwell, J.L., Weigand, S.D., Boeve, B.F., Senjem, M.L., Gunter, J.L., DeJesus-Hernandez, M., Rutherford, N.J., Baker, M., Knopman, D.S., Wszolek, Z.K., Parisi, J.E., Dickson, D.W., Petersen, R.C., Rademakers, R., Jack, C.R., Jr, Josephs, K.A., 2012. Neuroimaging signatures of frontotemporal dementia genetics: C9ORF72, tau, progranulin and sporadics. Brain 135, 794–806. doi:10.1093/brain/aws001

WHO, 1993. WHO International Programme on Chemical Safety. Biomarkers and Risk Assessment: Concepts and Principles.

Wider, C., Dachsel, J.C., Farrer, M.J., Dickson, D.W., Tsuboi, Y., Wszolek, Z.K., 2010. Elucidating the genetics and pathology of Perry syndrome. J. Neurol. Sci. 289, 149–154. doi:10.1016/j.jns.2009.08.044

Wilson, S.M., Galantucci, S., Tartaglia, M.C., Rising, K., Patterson, D.K., Henry, M.L., Ogar, J.M., DeLeon, J., Miller, B.L., Gorno-Tempini, M.L., 2011. Syntactic processing depends on dorsal language tracts. Neuron 72, 397–403. doi:10.1016/j.neuron.2011.09.014

Wilson, S.M., Henry, M.L., Besbris, M., Ogar, J.M., Dronkers, N.F., Jarrold, W., Miller, B.L., Gorno-Tempini, M.L., 2010. Connected speech production in three variants of primary progressive aphasia. Brain 133, 2069–2088. doi:10.1093/brain/awq129

Winkler, A.M., Ridgway, G.R., Webster, M.A., Smith, S.M., Nichols, T.E., 2014. Permutation inference for the general linear model. NeuroImage 92, 381–397. doi:10.1016/j.neuroimage.2014.01.060

Wong, F.C.K., Chandrasekaran, B., Garibaldi, K., Wong, P.C.M., 2011. White Matter Anisotropy in the Ventral Language Pathway Predicts Sound-to-Word Learning

Success. Journal of Neuroscience 31, 8780–8785. doi:10.1523/JNEUROSCI.0999-11.2011

Zhang, H., Schneider, T., Wheeler-Kingshott, C.A., Alexander, D.C., 2012. NODDI: Practical in vivo neurite orientation dispersion and density imaging of the human brain. NeuroImage 61, 1000–1016. doi:10.1016/j.neuroimage.2012.03.072

Zhang, H., Yushkevich, P., Alexander, D., Gee, J., 2006. Deformable registration of diffusion tensor MR images with explicit orientation optimization. Medical Image Analysis 10, 764–785. doi:10.1016/j.media.2006.06.004

Zhang, Y., Schuff, N., Ching, C., Tosun, D., Zhan, W., Nezamzadeh, M., Rosen, H.J., Kramer, J.H., Gorno-Tempini, M.L., Miller, B.L., Weiner, M.W., 2011. Joint Assessment of Structural, Perfusion, and Diffusion MRI in Alzheimer's Disease and Frontotemporal Dementia. International Journal of Alzheimer's Disease 2011, 1–11. doi:10.4061/2011/546871

Zhang, Y., Schuff, N., Du, A.-T., Rosen, H.J., Kramer, J.H., Gorno-Tempini, M.L., Miller, B.L., Weiner, M.W., 2009. White matter damage in frontotemporal dementia and Alzheimer's disease measured by diffusion MRI. Brain 132, 2579–2592. doi:10.1093/brain/awp071

Zhang, Y., Tartaglia, M.C., Schuff, N., Chiang, G.C., Ching, C., Rosen, H.J., Gorno-Tempini, M.L., Miller, B.L., Weiner, M.W., 2013. MRI signatures of brain macrostructural atrophy and microstructural degradation in frontotemporal lobar degeneration subtypes. J. Alzheimers Dis. 33, 431–444. doi:10.3233/JAD-2012-121156

Zhou, J., Gennatas, E.D., Kramer, J.H., Miller, B.L., Seeley, W.W., 2012. Predicting regional neurodegeneration from the healthy brain functional connectome. Neuron 73, 1216–1227. doi:10.1016/j.neuron.2012.03.004

Zhou, J., Greicius, M.D., Gennatas, E.D., Growdon, M.E., Jang, J.Y., Rabinovici, G.D., Kramer, J.H., Weiner, M., Miller, B.L., Seeley, W.W., 2010. Divergent network connectivity changes in behavioural variant frontotemporal dementia and Alzheimer's disease. Brain 133, 1352–1367. doi:10.1093/brain/awq075

Zhukareva, V., Joyce, S., Schuck, T., Van Deerlin, V., Hurtig, H., Albin, R., Gilman, S., Chin, S., Miller, B., Trojanowski, J.Q., Lee, V.M.-Y., 2006. Unexpected abundance of pathological tau in progressive supranuclear palsy white matter. Annals of Neurology 60, 335–345. doi:10.1002/ana.20916

9. Division of Labour

Chapter 3

The author conceived, designed and recruited individuals for this study. Clinical and neuropsychological evaluations were carried out by the author; with additional support provided by Ms Aisling Buckley, Dr Laura Downey and Ms Hannah Golden. The author collected all DNA samples with laboratory analysis of DNA co-ordinated by Dr Simon Mead and Dr Jon Beck. The author performed analysis of DTI data using TBSS analysis with additional technical support in running this pipeline provided by Dr Ian Malone. The author performed statistical analysis and interpretation of all data.

Chapter 4

The author conceived, designed and recruited individuals for this study. Dr Shiva Keihaninijad developed the longitudinal DTI analysis pipeline. The study author performed longitudinal DTI image analysis with additional technical advice from Dr Ivor Simpson. Whole brain volumetric analysis was co-ordinated by Ms. Shona Clegg. The author performed statistical analysis with additional advice from Dr Jennifer Nicholas.

Chapter 5

The author conceived, designed and recruited individuals for this study. Clinical and neuropsychological evaluations were carried out by the author; with additional support provided by Ms Aisling Buckley, Dr Laura Downey and Ms Hannah Golden. The author performed analysis of DTI data using TBSS analysis with additional technical support in running this pipeline provided by Dr Ian Malone. The author performed statistical analysis and interpretation of all data.

Chapter 6

The author conceived, designed and recruited individuals for this study. The author performed longitudinal DTI image analysis with additional technical support from Dr Ivor Simposon. Whole brain volumetric analysis was co-ordinated by Ms. Shona Clegg. The author performed statistical analysis and interpretation of the data.

10. Acknowledgments

Thank you to all the participants who made this study possible, in particular to the carers and families of the patient's who were unwavering in their support. Thank you to my supervisors, Professor Jason Warren and Professor Nick Fox, for their wisdom, support and encouragement over the last few years. These studies were possible due to funding from the Medical Research Council. Finally I would like to thank all my colleagues at the Dementia Research Centre, who have not only been colleagues but have become good friends, as well as my friends and family for their constant support and encouragement over the last few years.

11. Publications arising from this thesis

Chapter 3 – Cross sectional profiles of white matter pathology in bvFTD

- Profiles of white matter tract pathology in frontotemporal dementia. Mahoney CJ, Ridgway GR, Malone IB, Downey LE, Beck J, Kinnunen KM, Schmitz N, Golden HL, Rohrer JD, Schott JM, Rossor MN, Ourselin S, Mead S, Fox NC, Warren JD. Hum Brain Mapp. 2014 Aug;35(8):4163-79
- Frontotemporal dementia with the C9ORF72 hexanucleotide repeat expansion: clinical, neuroanatomical and neuropathological features. Mahoney CJ, Beck J, Rohrer JD, Lashley T, Mok K, Shakespeare T, Yeatman T, Warrington EK, Schott JM, Fox NC, Rossor MN, Hardy J, Collinge J, Revesz T, Mead S, Warren JD. Brain. 2012 Mar;135(Pt 3):736-50

Chapter 4 – Longitudinal profiles of white matter pathology in bvFTD

- Longitudinal diffusion tensor imaging in frontotemporal dementia. Mahoney CJ, Simpson IJ, Nicholas JM, Fletcher PD, Downey LE, Golden HL, Clark CN, Schmitz N, Rohrer JD, Schott JM, Zhang H, Ourselin S, Warren JD, Fox NC. Ann Neurol. 2015 Jan;77(1):33-46
- Longitudinal neuroimaging and neuropsychological profiles of frontotemporal dementia with C9ORF72 expansions. Mahoney CJ, Downey LE, Ridgway GR, Beck J, Clegg S, Blair M, Finnegan S, Leung KK, Yeatman T, Golden H, Mead S, Rohrer JD, Fox NC, Warren JD. Alzheimers Res Ther. 2012 Sep 24;4(5):41.

Chapter 5 – Cross sectional profiles of white matter pathology in PPA

- White matter tract signatures of the progressive aphasias. Mahoney CJ, Malone IB, Ridgway GR, Buckley AH, Downey LE, Golden HL, Ryan NS, Ourselin S, Schott JM, Rossor MN, Fox NC, Warren JD. Neurobiol Aging. 2013 Jun;34(6):1687-99

Chapter 6 - Longitudinal profiles of white matter pathology in PPA

- Longitudinal diffusion tensor imaging in the primary progressive aphasias. Mahoney CJ, Simpon IJ, Golden HL, Downey LE, Fletcher PF, Fox NC, Warren JD. Neurology (In submission).